MALAYSIAN JOURNAL OF SCIENCE

MJS

ISSN 1394-3065

Malaysian Journal of Science

Vol 44 | No 4 | December 2025

MJS in indexed in Scopus, Google Scholar, Chemical Abstracts Service Database, ASEAN Citation Index (ACI), & MyCite.

MALAYSIAN JOURNAL OF SCIENCE
MJS
ISSN 1394-3065

Regular Issue

Malaysian Journal of Science 44 (4): 1-9 (December 2025) https://mjs.um.edu.my

Evaluating The Suitability of Sunflowers as Companion Plants in an Intercropping System with Tomatoes

Ratna Yuniati*, Siti Zahrotul Karimah and Niarsi Merry Hemelda

Abstract: The intercropping system involves growing multiple crop species simultaneously on the same land to reduce the risk of crop failure. One such example is the co-cultivation of sunflowers and tomatoes, where sunflowers function as living mulch. However, studies on the function and impact of sunflower–tomato intercropping systems, particularly in relation to weed management and productivity enhancement in Indonesia, remain limited. This study aims to evaluate the suitability of sunflower plants as companion and living mulch species in intercropping systems with tomatoes, and to assess the performance of both crops when grown individually or together. A randomized block design with two replications per treatment was employed using raised beds. Both crops were transplanted simultaneously in alternating arrangements for 13 weeks at a 1:1 ratio. Results showed that intercropping effectively suppressed weed growth and reduced pest and disease incidence. The Mann–Whitney test ($P < 0.05$) revealed significantly lower sunflower yields in the intercropping system than in monocropping. A Land Equivalent Ratio (LER) of 0.65 (<1) indicated higher productivity under monocropping, due to intense belowground interspecific competition and rhizosphere interactions. Competition analysis showed that tomatoes dominated the system (Aggressiveness, A = +0.165; Competition Ratio, CR = 1.677). Therefore, sunflower and tomato plants can be effectively intercropped, provided that planting times are staggered to minimize competition and aggressiveness between species.

Keywords: *Intercropping, monocropping, sunflower, tomato, weed.*

1. Introduction

Tomato cultivation frequently encounters challenges associated with weed interference, leading farmers to adopt diverse control methods such as herbicide application and plastic mulching. While herbicides are convenient and cost-effective, they may harm non-target plants and pose environmental and health risks due to chemical residues contaminating soil and water (Jurado et al., 2011). Plastic mulch, on the other hand, effectively suppresses weed growth by blocking sunlight (Freitas et al., 2021), but its use can contribute to plastic waste accumulation and soil degradation (Wu et al., 2020). Consequently, sustainable and environmentally friendly alternatives, such as the use of living mulch within intercropping systems, have gained increasing attention.

Intercropping involves planting multiple types of crops together in one area, offering benefits beyond weed reduction, including decreased crop failure risk, improved soil and water conservation, and reduced pest populations. Intercropping promotes plant diversity by incorporating multiple plant species into the same area, thereby supporting a broader range of flora and fauna. This increased diversity facilitates more efficient resource use, can reduce damage caused by diseases and pests as interactions among diverse species enhance the overall health and productivity of the system. (Boudreau, 2013). Many plants can be effectively used as companion plants in intercropping systems, including legumes (beans, peas), marigolds, basil, corn, and sunflowers, which are commonly employed in such systems (Makoi & Ndakidemi, 2012).

Sunflowers are commonly integrated into intercropping systems with various primary crops such as soybeans (Saudy & El-Metwally, 2008), sorghum, and cotton (Kandhro et al., 2014). The sunflower-soybean, sunflower-sorghum, and sunflower-cotton intercropping systems, as reported by Saudy and El-Metwally (2008) and Kandhro et al. (2014), have demonstrated abilities to suppress weed growth and enhance plant characteristics such as height, sunflower diameter, fresh weight, and seed yield. Another benefit highlighted in research by Kestha & El-Baz (2004) conducted in Giza, Egypt during the summer season indicates that sunflower and tomato intercropping can improve tomato fruit quality by providing shade and enhancing land use efficiency. Land use often involves optimizing the use of resources such as water, nutrients, and space. When resources are used efficiently, plants can grow more healthily, which can lead to higher fruit quality. The primary determinant of a viable intercropping system is the compatibility of crops. Therefore, the effectiveness of any intercropping setup relies on carefully selecting crop species that minimize competition for light, space, moisture, and nutrients between them (Fukai & Trenbath, 1993). In Indonesia, tomatoes are generally cultivated with chillies, soybeans, winged beans, lettuce, cauliflower and Chinese broccoli to reduce pest attacks such as the cabbage leaf-eating Diamondback moth (*Plutella xylostella*) (Asare-Bediako et al., 2010). However, research evaluating the suitability of sunflowers as companion plants in intercropping systems with tomatoes in Indonesia in controlling weeds and increasing productivity is still limited. In addition, until

Authors information:
[a]Department of Biology, Faculty of Mathematics and Natural Sciences, Universitas Indonesia, Depok, INDONESIA. E-mail: ratnayuniati@sci.ui.ac.id[1]; zahrotulkarimah07@gmail.com[2]; merry.hemelda@sci.ui.ac.id[3]
*Corresponding Author: mailto:ratnayuniati@sci.ui.ac.id

Received: April, 2024
Accepted: July, 2024
Published: December, 2025

DOI:https//doi.org/10.22452/mjs.vol44no4.1
Malaysian Journal of Science 44(4): 1-9 (December 2025)

now, the intensity of competition between component plants in the intercropping system is still unclear.

The objective of this study is to evaluate the compatibility of sunflower plants as companion plants and living mulch, and to assess the performance of sunflower and tomato plants when grown individually or intercropped. This will be achieved by evaluating competitive interactions between intercrop components and their impact on yield quality.

2. Methodology

Experimental Site

The experiment was conducted between May and September 2020, in the Tanjung Barat District of South Jakarta, situated at an altitude of approximately 26.2 meters above sea level. The average rainfall, according to Meteorological Climatological and Geophysical Agency (BMKG) ranges from 21 to 50 mm, and the soil pH is 6.5. During the experiment, temperatures fluctuated between 28 and 32 °C, with average relative humidity levels ranging from 69% to 90%,

Planting Pot Preparation

The experimental setup employed a randomized block design comprising three treatments: (i) a tomato monocrop featuring only tomato plants; (ii) a sunflower monocrop consisting solely of sunflower plants; and (iii) a sunflower-tomato intercropping system, where tomato and sunflower were planted alternately in a 1:1 ratio (3 tomato plants : 3 sunflower plants) according to the following planting arrangement (Figure 1).

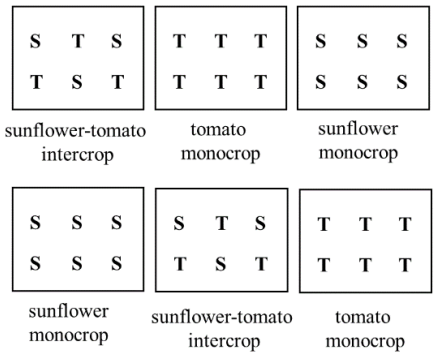

Figure 1. Planting arrangement of sunflower and tomato plants (S= sunflower, T=tomato)

Each treatment was replicated twice, resulting in six-bed plots with six plants in each plot. The plants were spaced 20 cm apart. The seeds used were the New Mutiara F1 hybrid tomato (Jawara Superior Seed) and the Giant Single Sunflower variety.

Preparation of planting plots involved land clearing, plowing, and bed setup. Land clearing aimed to remove weeds and plant residues that could harbor bacteria or fungi (Panth et al., 2020). Plowing was done to a depth of 30-40 cm. The beds were constructed with a height of approximately 10 cm, and above them, plant plots made of wood reaching 40 cm in height were installed (Naika et al., 2019). Both the sunflower and tomato plots were filled with commercial substrate (CV Tani Tangguh Perkasa), composed of topsoil, burnt husks, and manure. Each individual plant received five grams of NPK 16:16:16 fertilizer (Rawal et al., 2022). The plant plots were left exposed to sunlight and air exchange for two weeks before further proceedings.

Germination and Seedling Preparation

The seeds were sown at different intervals, with tomato seeds planted 28 days before sunflower seeds. This discrepancy in seeding times is based on the duration each plant requires to reach the generative growth phase. Sunflower plants typically require approximately 80-95 days to produce seeds (Dagustu et al., 2012) while tomato plants need 100-140 days to bear fruit (Hossain et al., 2014). Both tomato and sunflower seeds were sown in a 54 x 28 x 5 cm seedling tray containing 50 holes. Each hole was filled with commercial planting media composed of a mixture of topsoil, burnt rice husks, and cow manure. Following sowing, the seed germination tray was sprayed with tap water, and a thin layer of rice husk was applied over the seeds to retain moisture.

Three weeks-old tomato seedlings, were transplanted into 15 x 15 cm polybags, whereas sunflower seedlings were transferred to polybags 15 days after sowing (Kestha & El-Baz, 2004). A total of 36 individuals from both the sunflower and tomato seedlings, exhibiting uniform morphology and height, were selected for transplantation into the bed plots.

Plant Transplantation and Maintenance

Tomato seedlings were transplanted three weeks after sowing, maintaining a 20 cm spacing between plants, which falls within the recommended range (NCPS, 2015). Plant maintenance, includes irrigation, fertilization, and the application of fungicides. Watering is performed twice daily to ensure adequate moisture levels for the plants. Fertilization entails the application of NPK 16:16:16 fertilizer at a dosage of 5 g per 0.5 L of water every two weeks for each treatment plot. Fungicide application treatment with Antracol (2 g/L) is administered only during the 3rd and 4th weeks after transplantation. The fungicide solution is applied by spraying the leaves of plants infected with fungi, particularly targeting powdery mildew.

Data Collection Process

Data were collected from both abiotic and biotic parameters. The abiotic parameters monitored encompassed pH, temperature, and soil moisture. The biotic parameters examined included tomato plants, sunflower plants, and weeds. Sunflowers and tomatoes were both harvested 13 weeks after planting.

Abiotic (Environmental) Parameter

In this study, soil abiotic parameters such as pH, temperature, and soil moisture were recorded weekly over a 13-week period, with three repetitions. Soil moisture observations were conducted by drying 20 g soil samples from a depth of 10 cm on the soil surface. Subsequently, drying was performed using an oven set at a temperature of 40°C until the soil's dry weight remained constant (Owodoyin, 2007). The results obtained were

DOI:https//doi.org/10.22452/mjs.vol44no4.1
Malaysian Journal of Science 44(4): 1-9 (December 2025)

then calculated using the soil moisture percentage formula (Teame et al. 2017), as outlined below:

$$Soil\ moisture\ (\%) = \frac{Wet\ soil\ weight - Dry\ soil\ weight}{Dry\ soil\ weight} \times 100\%$$

Soil pH observations involved placing soil samples obtained from a depth of 10 cm into distilled water with a neutral pH. Subsequently, pH strip paper was immersed into a mixture of distilled water and soil, and the color of the pH paper was compared with the color on the pH scale to determine the pH level. Meanwhile, soil temperature measurements were conducted by inserting a thermometer to a depth of 10 cm below the soil surface (Nkansah et al., 2003).

2.4.2. Intercropping system and weed control

Weed density was observed by counting and identifying each weed present in every plot. Weeds were categorized into three groups: broadleaf weeds, grasses, and sedges. The number and density of weeds were determined using the formula outlined by Lukitasari (2018).

$$Density\ (individual/m2) = \frac{Number\ of\ weeds}{Area\ of\ observation\ plot}$$

Plant Growth and Plant Productivity Parameters

Both sunflower and tomato plant growth parameters were observed, including various growth and productivity metrics. For tomato plants, these metrics encompassed plant height, chlorophyll content, number of fruits per plant, and fruit weight. Sunflower plant metrics included plant height, chlorophyll content, number of flowers per plant, flower diameter, and yield per plant.

The method used to measure total chlorophyll in tomato and sunflower leaves was adapted from the research conducted by Zhao et al. (2019), with modifications to the leaf disk sample size and centrifugation speed. The absorbance values obtained were then calculated using the total chlorophyll formulation provided by Wintermans & de Mots (1965), as outlined below:

Total chlorophyll (mg/mL) = 20.0 × OD649 + 6.1 × OD665

Evaluation of Competitive Intensity

Plant competitive intensity in the intercropping system is assessed based on research conducted by Gitari et al. (2020), utilizing the Land Equivalency Ratio (LER) formulation. LER is defined as the land requirement in a monocropping system to produce the same crop yield as in the intercropping system. The LER value > 1 indicates that the intercropping system produces more profitable crops than monocropping. Conversely, if LER value < 1 suggests that intercropping is less profitable than monocropping, while an LER value equal to 1 indicates that the results of intercropping are equivalent to those of monocropping.

The LER formula, according to Chipomho (2015), is as follows:

$$LER = \frac{intercrop\ 1}{monocrop\ 1} + \frac{intercrop\ 2}{monocrop\ 2}$$

The evaluation of competition between sunflower and tomato in the intercropping system involves assessing the aggressiveness value and competition ratio, as outlined by Machiani et al (2018). Plant aggressiveness in the intercropping system is calculated to gauge the impact of interspecific competition between tomato and sunflower within the intercropping setup. The aggressiveness index is computed by comparing the yields of plants in the intercropping system with those in the monocropping system, along with considering the proportion of land utilized in the intercropping system. The aggressiveness formulation (A) as used by Islam et al. (2016) is presented as follows:

$$Ahi = \frac{Yhi}{Yhh - Zhi} - \frac{Yti}{Ytt - Zti}$$

$$Ati = \frac{Yti}{Ytt - Zti} - \frac{Yhi}{Yhh - Zhi}$$

Where A_{hi} and A_{ti} are aggressivity of sunflower and tomato respectively, Y_{hi} and Y_{ti} are are yield of sunflower and tomato in the intercrop respectively; Y_{hh} and Y_{tt} yield of sunflower and tomato in monocrop plot respectively; Z_{hi} and Z_{ti} are the proportions of sunflower and tomato in the intercrop respectively.

Data Analysis

Data analysis was conducted using SPSS version 26. The tomato and sunflower plant parameter data were analyzed using the T-test with a significance level of 99%. The T-test was employed to ascertain the significant effects between the monocropping and intercropping systems.

3. Result and Discussion

Abiotic Parameter

In comparison to intercropped plots, the mean soil temperature in monocropped sunflower plots was notably the highest, at 27.65 ± 1.16 °C, indicating that the intercropping system effectively lowered soil temperatures. The higher soil water content observed at 0–30 cm depth in the soil of intercropping plots correlates with the shade provided by the canopy of sunflower plants, which have wide leaf types, thereby minimizing soil evaporation. Intercropping plots exhibited the highest soil moisture percentage, whereas the soil pH was almost the same across all plots (Table 1).

DOI:https//doi.org/10.22452/mjs.vol44no4.1
Malaysian Journal of Science 44(4): 1-9 (December 2025)

Table 1. Soil parameter observation

Treatment	Soil Parameter		
	pH	Temperature (°C)	Moisture (%)
Intercrop	6 ± 0.37	27.27 ± 1.12	66.05 ± 15.85
Tomato Monocrop	6 ± 0.44	27.28 ± 0.96	62.50 ± 13.38
Sunflower Monocrop	6 ± 0.40	27.65 ± 1.16	60.82 ± 14.39

These findings are consistent with visual soil assessments, which revealed that the soil in intercropping plots had a looser structure compared to monocropping plots. Soil physical properties is influenced by various factors, including constituents and concentration of the soil components porosity, and soil moisture content (Doran & Zeiss, 2000). The increased shade generated by plants can indeed lower soil temperature, subsequently increasing groundwater viscosity and leading to elevated soil moisture levels around the shaded area (Onwuka et al., 2018). Hence, this phenomenon is believed to be the reason behind the high soil moisture observed in the intercropping system. However, the lower soil moisture in monocropping systems does not necessarily cause faster leaf aging and drying. This is because the soil moisture levels in the monocropping system are within the range of ideal soil moisture for tomato plant growth, which is typically around 60% - 70% (Liu et al., 2009)

Intercropping System and Weed Control

The intercropping system significantly reduced weed density compared to the monocropping systems of either sunflower or tomato (Table 2). This suppression likely results from competition for light, water, and nutrients at both surface and subsurface levels, as well as allelopathic effects from sunflower roots. Sunflowers produce secondary metabolites such as sesquiterpene lactones and helinunol, which act as natural bioherbicides that inhibit weed growth (Makoi & Ndakidemi, 2012). Additionally, the dense sunflower canopy in the intercropping system reduces solar radiation reaching the soil surface, further limiting weed germination and development.

Table 2. The effectiveness of intercropping and monocropping as weed control

Treatment	Total	Average number/plot			Density (individual/m^2)		
		Grasses	Sedges	Broadleaves	Grasses	Sedges	Broadleaves
Intercrop	9	0.5	0	4	2.09	0	16.67
Sunflower	24	0.5	0.5	11	2.09	2.09	45.80
Tomato	19	1	0.5	8	4.17	2.09	33.35

The canopy architecture in the intercropping system determines the distribution of sunlight, as noted by Gao et al. (2010). The broad leaf type of sunflower plants grows vertically with various lamina and petiole tilt angles in the upper and lower canopy layers. Leaves in the upper canopy tend to lean upwards, while those in the lower canopy lean downwards, resulting in decreased light interception efficiency in the lower canopy layers (Hernandez, 2010). The obstruction of sunlight by the leaf canopy of sunflowers in intercropping plots is believed to hinder the interception of solar radiation reaching the soil surface, thereby inhibiting weed growth.

Weeds with vegetative reproduction are generally easier to control during soil tillage compared to weeds that produce seeds. This difference arises because the vegetative reproductive organs of weeds typically have lower tolerance to environmental changes, while seeds possess high dispersal ability and resistance to environmental fluctuations (Sastroutomo, 1990). As a result, the prevalence of broad-leaved weeds is believed to be primarily due to weed seeds being transported during land processing.

Based on the mechanism of weed photosynthesis, sedges and grasses are typically classified as C4 class weeds, which have a high requirement for light during the photosynthesis process, while broadleaf weeds are categorized as C3 class weeds, which have a lower need for light during photosynthesis (Marsal et al., 2015). The high density of broadleaf weeds observed in each treatment plot (Table 2) is likely due to the shade provided by each plant in both the intercropping and monocropping systems. Additionally, the research area being a plantation surrounded by large trees contributes to the dominance of broadleaf weeds, with limited growth of sedges and grasses. According to Marsal et al. (2015) suboptimal light intensity hampers the growth of sedges and grasses, while broadleaf weeds can thrive and survive better under such conditions.

The sunflower and tomato intercropping system effectively reduces the growth of broadleaf weeds compared to the monocropping system. This is attributed to the more optimal canopy architecture formed by the intercropping system, which minimizes light interception on the ground surface. Consequently, not only is the growth of sedges and grasses inhibited, but the growth of broadleaf weeds is also significantly suppressed. The canopy created by the intercropping system exhibits strong chlorophyll absorption capacity, thereby reducing photon flux across all photosynthetically active wavelengths in the 400-700 nm (PAR) spectrum, which in turn suppresses physiological processes and weed development (Bilalis, 2010).

Additional parameters were also observed on both tomato and

DOI:https//doi.org/10.22452/mjs.vol44no4.1
Malaysian Journal of Science 44(4): 1-9 (December 2025)

sunflower plants to assess the impact of intercropping and monocropping systems on pest and disease management. Findings revealed a higher incidence of pest and disease infestations in the monocropping system as opposed to the intercropping system (Table 3). Specifically, pests such as Liriomyza huidobrensis, responsible for leaf miner disease, Bemisia tabaci, causing leaf curl disease and the caterpillar pest Spodoptera litura were identified as common threats to tomato.

Table 3. Pest and diseases attack

Treatment	Plant	% total infection of all plants			
		Leaf miner	Bemisia tabaci	Spodoptera litura	Homeosoma electellum
Intercropping	Tomato	50	25	0	0
	Sunflower	16.67	0	0	0
Monocropping	Tomato	50	25	0	0
	Sunflower	0	0	16.67	8.33

Among all the tomato plants observed, the incidence of infestation by the leaf miner disease-causing pest Liriomyza huidobrensis, was higher in monocropping tomato plants compared to those in intercropping plots. Conversely, infestation by the pest Bemisia tabaci showed similar percentages in both monocropping and intercropping tomato plants. Caterpillar pests Spodoptera litura and Homeosoma electellum were exclusively detected on sunflowers. In monocropping sunflower plots, the incidence of S. litura and H. electellum caterpillar infestations was greater than in intercropping sunflower plots. This phenomenon is believed to result from the partitioning of populations between the main crop and companion plants. Population partitioning reduces the intensity of pest attacks on the main crop through the transmission of visual and chemical signals that alter insect behavior (González-Chang et al., 2019). Consequently, it is believed that the concurrent cultivation of tomato and sunflower plants in an intercropping system may reduce the incidence of caterpillar infestations on sunflower plants. Additionally, beneficial insects like various bee species acting as pollinators and natural pest predators such as coleoptera, dragonflies, and spiders were frequently observed on sunflowers in both intercropping and monocropping systems.

Furthermore, intercropping settings create physical barriers that impede pest movement between plants and offer floral resources that attract natural enemies of pests (Smith and McSorley, 2000). Similar findings were reported by Degri and Samaila (2014) in the context of tomato-corn intercropping systems. The plant partitions established by the tomato-corn intercropping system were effective in reducing the population of the Helicoverpa armigera borer pest on tomatoes compared to monocropping systems. This reduction is attributed to changes in the microclimate of the plant canopy, increased plant diversity, and greater spacing between similar plants. Consequently, the partitions created by corn plants effectively limit the spread of borer pests on tomato plants. In this study, sunflower plants serve a similar role.

Plant growth parameters

Based on the independent samples T test analysis, plant height (0.681>0.01), fresh weight (0.083>0.01) and total chlorophyll (0.104>0.01) of tomato plant in the intercropping and monocropping systems were not significantly different. The average of all tomato plant growth parameters in the intercropping system is higher compared to monocropping (Table 4).

Table 4. Growth parameter of tomato plant

Treatment	Growth Parameter		
	Plant height (cm)	Fresh weight (g)	Chlorophyll (mg/mL)
Intercropping	143.33 ± 23.39[a]	168.67± 25.36[a]	1.71 ±1.76[a]
Monocropping	139.17 ± 18.15[a]	123.08 ± 20.83[a]	0.69±0.24[a]

Parameters of plant height and total chlorophyll of sunflower plants in the intercropping system are higher than those in the monocropping system, while the fresh weight of plants in the intercropping system is lower because sunflower plants in the intercropping system have thin stems and leaves that are much smaller than sunflower in monocropping (Table 5).

DOI:https//doi.org/10.22452/mjs.vol44no4.1
Malaysian Journal of Science 44(4): 1-9 (December 2025)

Table 5. Growth parameter of sunflower plant

Treatment	Growth parameter		
	Plant height (cm)	Fresh weight (g)	Chlorophyll (mg/L)
Intercropping	138.17 ± 19.27[a]	150.5± 19.38[a]	2.43 ±2.3[a]
Monocropping	132.5 ± 9.98[a]	155.17±29.13[a]	1.15±0.8[a]

The sunflower-tomato intercropping system results in tomato plants exhibiting higher average values for vegetative growth parameters such as fresh weight, plant height, and total chlorophyll compared to the monocropping system. This outcome is attributed to the interspecific competition effects observed in the intercropping system. The observed root structures of tomato plants reveal numerous and long lateral roots with a branched and fibrous tap root system, whereas sunflowers possess fewer lateral roots with a single large tap root. Consequently, it is presumed that tomato plants have a higher nutrient absorption capacity compared to sunflowers, thereby facilitating better growth of the tomato plants.

The vegetative growth parameters of tomato plants, including fresh weight, plant height, and total chlorophyll (Table 5), demonstrated higher average values in the intercropping system compared to the monocropping system. This phenomenon is believed to be influenced by the interspecific competition occurring within the intercropping system. Similar results were reported by Cunha-Chiamolera (2017) in an intercropping system of tomatoes with lettuce. Tomatoes exhibit better tolerance and nutrient absorption than lettuce, thus enhancing nutrient absorption efficiency and preventing reduced lettuce yields.

In the monocropping system, tomato leaves experienced a faster period of senescence and drying compared to the intercropping system by week 12. This is attributed to high exposure to direct sunlight, which accelerates leaf senescence, resulting in lower total chlorophyll levels in both tomato and sunflower plants. Consequently, the total chlorophyll in the intercropping system is higher than in the monocropping system. El-Mehy and Mohamed (2018) reported similar findings in a tomato-maize intercropping system, where reduced leaf aging of tomatoes and increased ear leaf area of maize were observed due to optimal shading on the soil surface. Additionally, shading by rows of maize plants can stimulate internode growth and plant height, thereby increasing the wet weight and dry weight of the plants.

Plant Productivity Parameters

According to the T-test results, the number of tomato fruits, diameter, and fruit weight did not exhibit a significant difference between the two systems (Table 6). However, tomatoes in the monocropping system produced more fruit with larger sizes and weights.

Table 6. Tomato plant productivity

Treatment	Fruit parameter			
	Number/plant	Diameter (cm)	Weight (g)	Cracked (%)
Intercropping	5.67 ± 3.56[a]	3.45 ± 0.69[a]	24.91 ± 13.10[a]	2.9
Monocropping	7.4 ± 5.9[a]	3.81± 0.55[a]	24.91 ± 13.10[a]	12

Additionally, based on morphological observations, tomatoes in the monocropping system tend to have an oval shape, whereas those in the intercropping system tend to have a rounded shape (Figure 2).

DOI:https//doi.org/10.22452/mjs.vol44no4.1
Malaysian Journal of Science 44(4): 1-9 (December 2025)

Figure 2. Harvested tomatoes (a) and (b) monocropping (c) and (d) intercropping.

Based on the Mann-Whitney test results, there was no significant difference between the number of flowers and the diameter of sunflowers per individual plant in the two cropping systems. However, the yield per individual in the intercropping system was significantly different from the monocropping system (Table 7).

Table 7. Sunflower plant productivity

Treatment	Flower parameter		
	Number /plant	diameter (cm)	Weight (g) /plant
Intercropping	1 ± 0^{a}	12.99 ± 1.60^{a}	12.17 ± 1.17^{a}
Monocropping	1.17 ± 0.58^{a}	13.52 ± 1.44^{a}	21.00 ± 14.57^{b}

The sunflower and tomato intercropping system effectively creates an optimal canopy, inhibiting excessive sunlight and reducing the occurrence of tomato fruit cracking. According to Jones (2002), tomato fruit cracking is caused by high differences in day and night temperatures and rapid water absorption during fruit ripening, which reduces the elasticity of the fruit exocarp (outer skin).

Evaluation of Competitive Intensity Result

The relationship between the yield obtained and intraspecific competition between sunflower plants and tomato plants in the intercropping system was evaluated by assessing the Land Equivalent Ratio (LER) ratio, aggressiveness values and competition ratios (Table 8).

Table 8. Yield evaluation

Plant	Treatment	Yields (g/2400 cm^2)	Individual LER	LER	Aggressiveness	Competition Ratio
Sunflower	Intercropping	29				
	Monocropping	119	0.24	0.650	-0.165	0.596
Tomato	Intercropping	385				
	Monocropping	942	0.41		0.165	1.677

The resulting LER ratio value of 0.650 in sunflower-tomato intercropping shows that plant productivity using the intercropping system reaches 65% of the yield from a single crop. A LER ratio of less than one means that productivity with a monocropping system is higher per unit area. The aggressiveness value and competition ratio in sunflower and tomato intercropping explain why this happens. Narwal and Malik (1985) also found similar results in various intercropping systems involving sunflowers and other plants, unless when the two plants were planted at different ages. Kestha & El-Baz (2004) stated that planting sunflowers when tomato plants have entered the flowering and fruiting phase can increase the LER value>1, while planting sunflowers when transplanting tomato plants results LER value <1.

The observations of intercropped sunflowers and tomatoes indicate that tomatoes dominate when associated with sunflowers. This conclusion is based on the negative aggressiveness value obtained by sunflower plants (A = -0.165) and the positive aggressiveness value obtained by tomato plants (A = 0.165). Additionally, the plant aggressiveness is reinforced by the competition ratio results, which serve as indicators for evaluating the plant's ability to acquire resources both vertically and horizontally. The competition ratio for tomato yields (1.677) exceeds the ratio for sunflower (0.596). Therefore, both the competition ratio and aggressiveness provide strong evidence of interspecific competition in the sunflower-tomato intercropping system, with tomato plants emerging as the strongest competitors in resource acquisition. Based on observations, tomato plants have many and long lateral roots with a branched and fibrous tap root structure (Jones 2007) while sunflower plants have fewer lateral roots with a single, large tap root structure (Gregory 2006). Thus, the absorption of nutrients in tomato plants

DOI:https//doi.org/10.22452/mjs.vol44no4.1
Malaysian Journal of Science 44(4): 1-9 (December 2025)

is thought to be higher than in sunflower plants.

Based on the results of a comprehensive evaluation, the recommendation that can be given is to pay attention to the difference in age of the two plants in the intercropping system and use inappropriate planting distances so as to minimize overlapping root systems but still accommodate the ability of sunflower plants as living mulch to inhibit weed growth.

4. Conclusion

This study demonstrates that sunflowers can serve as effective companion plants for tomatoes in intercropping systems. However, simultaneous planting of both species increases interspecific competition, resulting in overall productivity reaching only 65% of monocropped yields. Tomatoes exhibited a higher aggressiveness index and competition ratio, indicating dominance in resource acquisition. Nevertheless, sunflower plants function efficiently as living mulch, substantially reducing weed growth. Future studies should investigate optimized planting intervals and spatial arrangements to minimize competition and maximize intercropping benefits.

5. Acknowledgement

The authors acknowledge the financial support provided by the Hibah Publikasi Terindeks Internasional (PUTI) Prosiding 2020 No.: NKB-3584/UN2.RST/HKP.05.00/2020, which contributed to funding the author's research.

6. References

Asare-Bediako E, Addo-Quaye AA, Mohammed A. (2010). Control of Diamondback Moth (*Plutella xylostella*) on cabbage (*Brassica oleracea* var. *capitata*) using intercropping with non-host crops. *American Journal of Food Tecnology*, 5(4): 269-274.

Bilalis D, Papastylianou P, Konstantas A, Patsiali S, Karkanis A, Efthimiadou A. (2010). Weed-suppressive effects of maize-legume intercropping in organic farming. *International Journal of Pest Management* 56(2): 173—181

Boudreau MA. (2013). Diseases in intercropping systems. *Annual Review of Phytopathology* 51: 499–519

Chipomho J, Mapope N, Masuka B, Ngezimana W, Chipomho C. (2015) The influence of cropping system and maize-bean intercrop spatial patterns on companion crop yield weed density and biomass. *International Journal of Agriculture and Crop Sciences* 8(5): 697—705.

Cunha-Chiamolera TPL. (2017). Agronomic and economic feasibility of tomato and lettuce intecropping in a soilless system as a function of electrical conductivity of the nutrient solution. *HortScience* 52(9): 1195—1200

Dagustu N, Bayram G, Sincik M, Bayraktaroglu M. (2012). The short breeding cycle protocol effective on diverse genotypes of sunflower (*Helianthus annuus* L.) *Turkish Journal of Field Crops*, 17(2):124-128

Degri MM, Samaila AE. (2014). Impact of intercropping tomato and maize on the infestation of tomato fruit borer [*Helicoverpa armigera* (Hubner)] *Journal of Agricultural and Crop Research* 2(8) 160-164.

Doran JW, Zeiss MR. (2000). Soil health and sustainability: managing the biotic component of soil quality. *Appl Soil Ecol*. 15: 3–11.

El-Mehy AA, Mohamed MHM. (2018). Yield and economic evaluation of maize and tomato as effected by cropping systems and some growth stimulants. *Middle East Journal of Applied* 8(1): 209 — 222.

Freitas AR, De Freitas FCL, de Souza CM, J.C. Zanuncio et al. (2021) Biodegradable mulch controls weeds and increases water use efficiency in lettuce crops. *Horticultura Brasileira*, 39(3): 330-334

Fukai S, Trenbath BR. (1993). Processes determining intercrop productivity and yields of component crops. *Field Crop Research*, 34: 247-271

Gitari HI, Nyawade SO, Kamau S, Karanja NN, Gachene CKK, Raza MA, Maitra S, Schulte-Geldermann E. (2020). Revisiting intercropping indices with respect to potato-legume intercropping systems *Field Crops Research* 258: 107957

Gao Y, Duan AW, Qiu XQ, Liu ZG, Sun JS, Zhang JP. (2010). Distribution and use efficiency of photosynthetically active radiation in strip intercropping of maize and soybean. *Journal of Agriculture* 102: 1149—1157.

Gonzalez-Chang M, Tiwari S, Sharma S, Wratten AD. (2019). Habitat management for pest management: Limitations and Prospects. *Annals of Entomological Society of America* 20(10): 1—16.

Gregory PJ. (2006). *Plant Roots Growth, Activity and Interaction with Soils*. Blackwell Publishing Ltd. Oxford

Hernandez LF. (2010). Leaf angle and light interception in sunflower (*Helianthus annuus* L.) role of the petiole's mechanical and anatomical properties. *International Journal of Experimental Botany* 79: 109—115.

Hossain MF, Ara N, Uddin MS, Islam MR, Kaisar MO. (2014). Effect of sowing dates on flowering, fruit setting and yield of tomato genotypes. *J. Agric. Res*., 52(4)

Islam MR, Molla MSH, Main MAK. (2016). Productivity and profitability of intercropping sesame with turmeric at marginal farmers level of Bangladesh. *SAARC J. Agri*. 14(1): 47-58

DOI:https//doi.org/10.22452/mjs.vol44no4.1
Malaysian Journal of Science 44(4): 1-9 (December 2025)

Jones Jr JB. (2002). *Tomato plant culture in the field, greenhouse, and home garden*. 1st ed. CRC Press

Jones Jr JB. (2007). *Tomato plant culture in the field, greenhouse, and home garden*, 2nd ed. CRC Press

Jurado AS, Fernandes MAS, Videira RA, Peixoto FP, Vicente JAF. (2011). Herbicides: the face and the reverse of the coin. an in vitro approach to the toxicity of herbicides in non-target organisms. *In*: Kortekamp, A. (eds). 2011. *Herbicides and Environment*. InTech, Rijeka: 3—44.

Kandhro MN, Tunio S, Rajpar I, Chachar Q. (2014). Allelopathic impact of sorghum and sunflower intercropping on weed management and yield enhancement in cotton.*Journal of Agriculture* 30(2): 312—318.

Kestha MM, El-Baz MG. (2004). Studies on sunflower-tomato intercropping. *Field Crops Research Institute* 16: 243—249.

Liu H, Gao Y, Sun JS, Liang YY. (2009). Effect of soil moisture regime on greenhouse tomato yield and its formation under drip irrigation. *Journal of Applied Ecology*20(11): 2699—2704.

Lukitasari M. (2018). Mengenal tumbuhan lumut (Bryophyta): Deskripsi, klasifikasi, potensi dan cara mempelejarinya. Media Grafika, Magetan.

Machiani MA, Javanmarda A, Morshedloo MA, Maggi F. (2018). Evaluation of competition, essential oil quality and quantity of peppermint intercropped with soybean. *Ind. Crops Prod*. 111: 743–754.

Makoi JHJR, Ndakidemi PA. (2012). Allelopathic as protectant, defence, and growth stimulants in legume cereal mixed culture systems. *Journal of Crop and Horticultural Science* 40(3):1—26

Marsal D, Wicaksono KP, Widaryanto E. (2015). Dinamika perubahan komposisi gulma pada tanaman tebu keprasan di lahan sistem reynoso dan tegalan. *Jurnal Produksi Tanaman* 3(1) :81—90.

Naika S, van Lidt de Jeude J, de Goffau M, Hilmi M, van Dam B. (2005). Cultivation of tomato production, processing and marketing Agrodok-series No. 17 Agromisa Foundation and CTA, Wageningen

Narwal SS, Malik DS. (1985). Influence of intercropping on the yield and food value of rainfed sunflower and companion legumes. *Agricultural Journal* 21: 395-401.

Nkansah GO., Owusu EO, Bonsu KO, Dennis EA. (2003). Effect of mulch types on growth, yields, and fruit quality of tomato (*Lycopersicon esculentum Mill.*). *Ghana Journal of Horticulture* 5: 55—64.

NPCS Board of Consultants & Engineers. (2015) The complete book on tomato & tomato products manufacturing (cultivation & processing). Asia Pacific Business Press, India:

Onwuka B, Mang B. (2018). Effect of soil temperature on some soil properties and plant growth. *Advances in Plants and Agriculture Research* 8(1): 34—37.

Owodoyin RO, Ogbeide FI, Oluwole O. (2007). Effect of three mulch types on the growth and Yield of tomato (*Lycopersicon esculentum* Mill) and weed suppression in Ibadan, Rainforest-savanna transition zone of Nigeria. *Tropical Agricultural Research and Extention* **10**: 53—60.

Panth M, Hassler SC, Baysal-Gurel F (2020) Methods for Management of Soilborne Diseases in Crop Production. *Agriculture*, 10: 16

Rawal N, Pande KR, Shrestha R, Vista SP (2022). Nutrient use efficiency (NUE) of wheat (*Triticum aestivum* L.) as affected by NPK fertilization. *PLos ONE* 17(1): e0262771

Sastroutomo SS (1990) *Ekologi gulma*. Gramedia Pustaka Indonesia, Jakarta: 141—167

Saudy HS, El-Metwally IM. (2008) Weed management under different patterns of sunflower-soybean intercropping. *Journal Central European Agriculture*. 10(1): 41—52.

Smith, HA, McSorley R (2000) Intercropping and pest management: a review of major concepts. *Journal of Entomology* 46: 154—161.

Teame G, Tsegay S, Abrha B. (2017). Effect of organic mulching on soil moisture, yield, and yield contributing component of sesame (*Sesamum indicum* L.). *Journal of Agronomy*: 1—6

Wintermans JFGM, De Mots A. (1965). Spectrophotometric characteristics of chlorophylls alpha and beta and their pheophytins in ethanol. *Biochimica Et Biophysica ACTA* 109: 448—453

Wu C, Ma Y, Wang D, Shan Y, Song X, Hu, H, Ren X, Ma X, Cui J, Ma Y (2022) Integrated microbiology and metabolomics analysis reveal plastic mulch film residue affects soil microorganisms and their metabolic functions. *Journal of Hazardous Materials,* 423: 127258

Zhao Y, Yan C, Lu S, Wang P, Qiu GY, Li R. (2019). Estimation of chlorophyll content in intertidal mangrove leaves with different thickness using hyperspectral data. *Ecological Indicator,* 106(105511): 1—13.

DOI:https//doi.org/10.22452/mjs.vol44no4.1
Malaysian Journal of Science 44(4): 1-9 (December 2025)

MALAYSIAN JOURNAL OF SCIENCE
MJS
ISSN 1394-3065

Regular Issue

Malaysian Journal of Science 44 (4): 10-17 (December 2025) https://mjs.um.edu.my

Chemical and Sensory Properties of Spontaneous Fermented Red Rice Vinegar with Fermentation Time Variation

Lidya Puspita Sumino Putri[1a] and Viera Nu'riza Pratiwi[2a]*

Abstract: Red rice is a variety of Indonesian rice that contains anthocyanins, which are antioxidant compounds that can neutralize free radicals. Red rice is used as another valuable food source, specifically for vinegar. The fermentation duration determines the quality of vinegar in terms of chemical and sensory characteristics. The purpose of this study was to examine the effect of fermentation time on the chemical properties and sensory attributes of red rice vinegar made by spontaneous fermentation. Red rice vinegar was produced through a spontaneous fermentation process at 30- and 60-day fermentation periods. The pH, alcohol content, acetic acid, antioxidant activity, and total phenolic content were measured. Red rice vinegar produced after 30 and 60 days of fermentation had an acetic acid concentration of 73.02±4.91 mg GAE/G. The alcohol content differed significantly between 30 and 60 day fermentation treatments ($p<0.05$). The fermentation time has no effect on the sensory qualities (aroma, taste, and colour) of the product. The yeast aroma, slightly sweet, bitter flavour, and brownish yellow colour were the best treatments based on sensory evaluation.

Keywords: *Chemical, fermentation time, red rice, sensory properties, vinegar, spontaneous fermentation*.

1. Introduction

Red rice is a variety of rice cultivated in Indonesia. The red colour of this rice originates from aleurone, which contains genes that produce anthocyanin, a pigment that imparts a red colour while also functioning as an antioxidant. Quality red rice is characterised by the grain's surface being coated in a dark red colour and remaining intact (Deng et al., 2013). Rice's colour is associated with antioxidant activity, particularly anthocyanins (Sompong et al., 2011). Red rice contains antioxidants, as indicated by an IC50 value ranging from 85.69 to 290.54 ppm (Pangerang, 2022). Red rice contains various bioactive compounds such as polyphenols and vitamins, including vitamin E, which serves as an antioxidant. This component is what makes red rice popular as a functional food. Red rice exhibits the highest antioxidant activity (95.05%) compared with white rice and brown rice (Azis et al., 2015). Currently, red rice is being investigated as a functional meal. One study on rice crackers utilized red rice (*Oryza nivara*) flour and *Moringa oleifera* leaf powder as a functional food (Malibun Fais Bintang, Husain Syam, 2019), and also milk with the main ingredient of red rice, revealing the potential of red rice milk as a functional beverage with antioxidants (Wijaya & Romulo, 2021). One example of a processed rice product that can become a functional food is vinegar.

Vinegar is an organic sour solution derived from sugar-rich substances like apples, grapes, rice, and black sticky rice that undergo fermentation (Kim et al., 2021). Vinegar is commonly employed as a spice, flavouring, preservative, and product for daily usage (Hidalgo et al., 2010). Vinegar is a liquid fermented product containing at least 4% acetic acid. The process of producing vinegar is commonly referred to as "vinegaring." There are many types of raw materials that may be used to produce vinegar, including fruits (e.g., apples, grapes, dates, figs, plums, cherries, persimmons, etc.), grains (e.g., rice, sorghum, barley, malt, wheat, corn, rye), cane sugar, honey, coconut, roots and tubers (e.g., sweet potato), and other materials containing fermentable or hydrolyzable carbohydrates (Kandylis, 2019). Vinegar fermentation consists of two stages: anaerobic fermentation, where sugar is converted into ethanol, and aerobic fermentation, where ethanol is transformed into acetic acid. Vinegar fermentation is typically carried out by combining the yeast *Saccharomyces cerevisiae* and *Acetobacter acetii* (Yuan et al., 2017).

Vinegar fermentation can occur spontaneously and be initiated by back-slopping or starters in both small- and large-scale operations (Ghosh et al., 2012). Spontaneous fermentation occurs naturally, without the use of any starter, using microorganisms that grow inherently in the medium and conditioning the medium such that specific microbes responsible for fermentation can develop adequately (Antoniewicz et al., 2021). The benefits of spontaneous fermentation include high economic value and easy, affordable processing (Jayus et al., 2020). The duration of the fermentation process influences the physical and chemical characteristics of kombucha made from Sargassum sp, affecting its overall quality in terms of both chemical and sensory properties (Pratiwi & Aryawati, 2012). The characteristics and quality of vinegar products are affected by various raw materials, microbial environments, and fermentation techniques. These factors influence the dynamic changes in chemical properties (e.g., pH, total acid, amino acid nitrogen, reducing sugar, acetic acid, and free amino acids) and sensory properties (including aroma and taste) of vinegar (Gong et al.,

Authors information:
[a]Department of Nutrition, Faculty of Health, Universitas Nahdlatul Ulama Surabaya, Surabaya 60237, INDONESIA. E-mail: vieranpratiwi@unusa.ac.id[1]; lidyapuspita054.gz19@student.unusa.ac.id[2]
*Corresponding Author: vieranpratiwi@unusa.ac.id

Received: May, 2024
Accepted: November, 2024
Published: December, 2025

DOI: https//doi.org/10.22452/mjs.vol44no4.2
Malaysian Journal of Science 44(4): 10-17 (December 2025)

2021). Rice vinegar products have not become as popular as expected. There are currently no red rice vinegar products in Indonesia, and the objective of this study is to examine the effect of fermentation time on the chemical properties and sensory aspects of red rice vinegar produced by spontaneous fermentation.

2. Materials and Methods

Materials and Reagents

N790 brand red rice, Aek Sibundong variety, was collected from Malang Regency, along with mineral water, distilled water, phenolphthalein indicator, 0.1 N NaOH, DPPH (Diphenyl Picrylhydrazyl), ascorbic acid, methanol, gallic acid, Folin Ciocalteu, and Na_2CO_3.

Rice Preparation

Milled red rice was produced by placing 200 grams of washed red rice and 840 ml of water in a glass jar, soaking at room temperature (27°C–28°C) overnight. Next, the water was separated, and the rice was ground (semi-coarse) using a blender. Cooked red rice was prepared by washing 400 grams of red rice three times in running water, then placing it in a pan and adding 1.2 L of water. The red rice was cooked at 80°C for 15 min until the water was reduced.

Vinegar Fermentation Process

Ground rice and cooked red rice were mixed in a sterile glass jar, with 560 ml of water added and stirred well. The jar was covered with a cloth and fermented for 30 and 60 days at room temperature. The mixture was stirred once a week during the fermentation process. The vinegar was strained using cheesecloth once fermentation was complete. The filtered liquid was fermented again at room temperature for 30 days. Next, the vinegar was filtered with several layers of filter cloth.

pH and Alcohol Analysis

pH measurements were carried out with a pH meter (HP 9000) (Laily et al., 2019). A mixture of 25 ml of red rice vinegar and 100 ml of distilled water was placed into a distillation flask. The mixture was distilled until the distillate yield was exactly 25 ml. The pycnometer, whose weight was known, was filled with the distillate mixture and weighed at a specific temperature, such as 28°C. The weight of the distillate was calculated from the weight of the pycnometer containing the sample minus the weight of the empty pycnometer. Alcohol content was determined using a conversion table for the specific gravity of alcohol and its temperature (Ernawangtyas & Yudhayanti, 2017).

Acetic Acid Analysis

Acetic acid level analysis followed the method of Laily et al. (2019). Ten milliliters of red rice vinegar were diluted to 100 ml and placed in an Erlenmeyer flask. A 25 ml sample was taken and placed in an Erlenmeyer flask, followed by the addition of 2–3 drops of phenolphthalein indicator. The sample was titrated with 0.1 N NaOH until the color changed to pink. The acetic acid content was calculated by multiplying the percentage of total acid by the acetic acid molecular weight 60, and the formula for calculating acetic acid is:

$$\% \text{ Acetic acid } = \frac{(\text{titrated volume NaOH (mL) x N NaOH x Greek acetic acid})}{\text{volume of sample (mL)}}$$

Total Phenolic Content Analysis

Analysis of total phenolic content using a gallic acid standard curve and Folin Ciocalteu reagent. The standard solution of gallic acid (concentrations 0, 10, 20, 30, 40, 50, and 60 ppm) was measured in 200 µl of each concentration and placed into a test tube, then 1.5 ml of Folin Ciocalteu reagent (10x dilution) was added and mixed with a vortex until homogeneous. A mixture of gallic acid and Folin Ciocalteu reagent followed by 1.5 ml Na_2CO_3 (prepared from 75 g/L) was added and stirred until homogeneous. The mixed solution was incubated for 180 minutes at room temperature under dark conditions. The absorbance value was measured with a spectrophotometer at λ= 765 nm. A linear regression equation curve was generated using the absorbance value of the standard gallic acid solution. Testing of the total phenol content of samples was conducted in the same manner as the standard curve, namely by replacing 200 µl of gallic acid solution with the sample extract (Zhou et al., 2014).

Antioxidant Analysis

Antioxidant activity testing was conducted with DPPH, and the antioxidant activity value was expressed as IC50 according to the method used in prior work (Rubiati, 2021). Ascorbic acid was used as a control at concentrations of 6 ppm, 8 ppm, 10 ppm, and 12 ppm. Red rice vinegar samples were prepared at concentrations of 5, 10, 15, and 20 ppm. The sample was treated with 0.2 ml of a 0.4 mM DPPH solution and methanol. The solution was incubated in the dark for 60 minutes before analysis with a spectrophotometer at 517 nm. DPPH standards were prepared at concentrations of 5, 10, 15, 20, and 25 ppm. Vinegar samples were prepared at 5, 10, 15, and 20 ppm concentrations, followed by the addition of 0.2 ml of 0.4 mM DPPH and methanol.

Sensory Analysis

Analysis of the sensory properties of vinegar used a hedonic quality test to determine the panelists' impressions of the sensory characteristics of red rice vinegar, including aroma, taste, and color. The sensory test involved 25 panelists aged between 19 and 21 years, all of whom were non-smokers and free from any impairments affecting their five senses. Panelists received an initial briefing on perceptual alignment before testing and underwent primary taste recognition. Panelists were given a closed questionnaire containing answer scores ranging from 1 to 5 for each sensory attribute (Eshak, 2016). The research passed ethical clearance with certificate number 0030/EC/KEPK/UNUSA/2023.

Statistic Analysis

Data were analyzed using one-way analysis of Variance (ANOVA) for chemical tests ($p < 0.05$) between fermentation times. Sensory

DOI: https//doi.org/10.22452/mjs.vol44no4.2
Malaysian Journal of Science 44(4): 10-17 (December 2025)

test data were analyzed using the Kruskal-Wallis test in SPSS 27.0. Data for all measurements were obtained in triplicate and expressed as mean ± SD.

3. Result and Discussion

Figure 1 shows the properties of the red rice vinegar created in this investigation. Different fermentation times result in red rice vinegars with similar colour characteristics, particularly yellow.

30 days 60 days

Figure 1. Red rice vinegar with different spontaneous fermentation times

pH and Alcohol

After 30 days of fermentation, the pH is 3.7 ± 0.11, whereas after 60 days of fermentation, it is 3.2 ± 0.22. There was a drop in pH, with the 30-day fermentation treatment having a higher pH than the 60-day fermentation treatment. The pH of red rice vinegar with spontaneous fermentation was significantly influenced by fermentation time ($p<0.05$) (Table 1). As the fermentation time increases, the acid content of the product rises due to bacteria breaking down alcohol, making the fermentation conditions acidic and causing the pH to decline. The pH decrease is caused by H+ ions released from acetic acid produced during the acetate fermentation process. Therefore, the more acetic acid formed, the lower the pH (Zubaidah & Veronica, 2014). The degree of acidity, or pH, is a vital component in fermentation because it affects microbe proliferation and product synthesis (Fadilah et al., 2018). Vinegar's pH level defines its quality based on the amount or strength of acid in the vinegar (Suwardiyono et al., 2014). Previous research by Rahayu et al. (2017) on cocoa vinegar showed that changing pH has the opposite effect on acetic acid levels. Cocoa vinegar with the greatest pH value of 3.8 produces acetic acid levels of 1.55%, while the lowest pH value of 3.3 yields the highest acetic acid levels of 2.64%.

As shown in Table 1, the alcohol content of red rice vinegar had not yet developed by the 30th day of fermentation. The result was 0. Meanwhile, on day 60 of fermentation, the alcohol concentration was 1.48%. The alcohol content of red rice vinegar differed significantly between 30 and 60 days of treatment ($p<0.05$). The fermentation period influences the chemical parameters (alcohol content) of red rice vinegar made through spontaneous fermentation (Table 1). The alcohol percentage of red rice vinegar after a 30-day fermenting period is low. This is due to the low sugar content of the components, which is necessary for microbial growth as food. However, the alcohol level of red rice vinegar in the 60-day treatment was higher because bacterial activity to convert sugar into alcohol had already developed and was more effective. This is because acetic acid fermentation is affected by alcoholic fermentation; therefore, if the alcohol fermentation process has not yet produced alcohol, the amount of acetic acid formed will be reduced. Low alcohol content is closely related to the sugar content that is transformed through alcoholic fermentation (Pohan et al., 2019). The rise in alcohol content corresponds to increased fermentation time induced by yeast growth and metabolism to generate alcohol. In the fermentation process, yeast aids the conversion of pyruvic acid from the glycolysis process (the conversion of lactose into glucose) into alcohol (Lestari et al., 2018).

Acetic Acid

Table 1 showed that after 30 days of fermentation, red rice vinegar had an acetic acid level of 1.08±0.04%. After 60 days, the acetic acid content increased to 1.22±0.05%, and acetic acid levels vary considerably with fermentation time ($p<0.05$). Acetic acid levels were determined using the titration method. The length of fermentation influences the acetic acid concentration in red rice vinegar made through spontaneous fermentation. This can occur because a shorter fermentation time results in less acetic acid since the substrate is not fully decomposed. Vinegar fermented for 60 days contains more acetic acid, probably due to the higher alcohol content produced compared to vinegar fermented for 30 days. Acetic acid is formed during the fermentation process of red rice vinegar, which converts alcohol to acetic acid. The longer the fermentation, the greater the amount of acetic acid produced. Acetobacter bacteria performed more efficiently in converting alcohol into acid, resulting in an increase in total acid (Arnata, 2015).

Total Phenolic Content

Red rice vinegar, after 30 days of fermentation, had a phenolic acid concentration of 73.02±4.91 mg GAE/G. In the 60-day fermentation treatment, the phenolic compound content was 83.02±14.14 mg GAE/G. The results demonstrate that the quantities of phenolic compounds in red rice vinegar increased from 30 to 60 days of fermentation. The total phenol content increased with increasing fermentation time. Table 1 shows that fermentation time has a significant effect ($p < 0.05$) on the total phenolic content of red rice vinegar. There are numerous types of microorganisms from the bacteria and yeast groups that can metabolize to create flavonoid compounds via enzymatic processes, influencing the overall amount of phenol. The length of fermentation might affect the amount of phenolic compounds produced since microbial activity can continue over time, producing more phenolic compounds. Phenolic compounds are chemical components that influence the antioxidant activity of a substance. The majority of antioxidants in components produced

DOI: https//doi.org/10.22452/mjs.vol44no4.2
Malaysian Journal of Science 44(4): 10-17 (December 2025)

from plants are phenolic chemicals (Hardoko et al., 2019). Fermentation time significantly affects the chemical properties and bioactive compounds in fruit vinegars (Hammouda et al., 2023). Research indicates that fermentation time and storage conditions significantly influence the antioxidant activity and total phenolic content of apple vinegars, peaking at week 3 (Budak, 2021).

The fermentation process increases the amount of phenolic compounds because there is a decarboxylation process of cinnamic acid components, such as trans-4-hydroxy-methoxycinnamic acid (ferulic acid (FA)) and trans-4-hydroxycinnamic acid (p-coumaric acid (PCA)), to form phenolic compounds, namely 4-vinylguaiacol (4-VG) and 4-vinylphenol (4-VP), by microorganisms (Coelho et al., 2017). Yeast decarboxylates cinnamic acid into vinyl phenol by the activity of the enzyme phenol reductase. Phenolic chemicals are closely associated with antioxidant activity. The capacity of phenolic compounds to release protons, form chelates, and produce radical dismutase contributes to their antioxidant properties. Phenolic substances donate hydrogen atoms from the hydroxyl groups to radical molecules, resulting in stable phenoxy radical compounds. Therefore, the assessment of total phenolic compounds is highly significant in determining the antioxidant activity of plant extracts (Aksoy et al., 2013).

Table 1. Chemical analysis red rice vinegar with different spontaneous fermentation time

Analysis	Fermentation Time (day)		p-value
	30	60	
pH	3,7±0,11	3,2±0,22	0,006*
Acetic acid (%)	1,08±0,04	1,22±0,05	0,001*
Alcohol (%)	0,00±0,00	1,48±0,35	0,013*
Total Phenolic content (mg GAE/g)	73,02±4,91	83,02±14,14	0,009*
Antioxidant activity (IC50)	87,78±1,81	47,63±1,55	0,021*

Data are displayed as average and standard deviation (n=3), and analyzed using One Way Anova (p<0.05)

Antioxidant Activity

Red rice vinegar fermented for 30 days has an antioxidant activity value (IC50) of 87.78±1.81, while vinegar fermented for 60 days has an IC50 value of 47.63±1.55. Red rice vinegar fermented for 60 days has greater antioxidant activity, with an IC50 value of less than 50. Table 1 shows that fermentation time has a significant effect ($p < 0.05$) on antioxidant activity. The time of fermentation influences the chemical properties, namely the antioxidant activity of red rice vinegar with spontaneous fermentation. The increased antioxidant activity results from vinegar culture bacteria metabolism during the fermentation process. As fermentation time increases, microorganisms will remain active and perform biotransformation activities, converting raw material components into molecules with improved antioxidant potential. This process can increase the antioxidant content of fermented products. The total phenolic content and antioxidant activity may increase with fermentation time (Hapsari et al., 2021). Fermentation can enhance antioxidant activity in plant-based products (Yan et al., 2019). The increase in antioxidant activity was mediated by free phenols produced during the fermentation process. Higher levels of total phenolics and flavonoids correspond to stronger antioxidant and antibacterial effects (Sartini et al., 2019). Vinegar contains various amounts of antioxidants, one of which depends on the raw materials used to produce it (Laily et al., 2019). Vinegar's phenolic content also affects its antioxidant activity (Taweekasemsombut et al., 2021). Researchers have identified a connection between total phenolic content and antioxidant activity. This phenolic component is found in rice grains that are fermented into rice vinegar (Wijaya & Romulo, 2021).

Sensory Analysis

Aroma

The aroma of red rice vinegar after 30 and 60 days of fermentation was more likely to be yeasty compared to the panellists' judgement (Figure 3A), and there was no difference since the majority of the panellists agreed that red rice vinegar had a yeast aroma. The statistical test results revealed no significant difference (Table 2) in the scent of red rice vinegar ($p > 0.05$). Additionally, spontaneous fermentation involves a mixture of microorganisms that could reach a balanced state early on, preventing further noticeable changes in scent. Yeast typically contains bacteria that assist the fermentation process and serve as a culture medium for these microorganisms. Acetobacter is one of the microorganisms found in yeast, along with other types of bacteria and mould. Acetobacter is a bacterium that produces acetic acid and can convert ethanol into vinegar. This study supports previous research on Wuluh starfruit vinegar, indicating that the yeast scent is associated with the presence of ethanol and CO_2 in the product. As is known, in fermentation, yeast works to convert sugar and produce metabolites in the form of alcohol and carbon dioxide (Laily et al., 2019).

Table 2. Statistic analysis of sensory red rice vinegar with different spontaneous fermentation time

Fermentation Time (days)	Aroma	Taste	Color
30	3,04±1,36	3,28±1,02	2,52±1,32
60	2,76±1,50	3,64±1,38	2,56±1,22
p-value	0,480	0,215	0,928

Data are displayed as average and standard deviation (n=3), and analyzed using Kruskal Wallis (p<0,05)

DOI: https//doi.org/10.22452/mjs.vol44no4.2
Malaysian Journal of Science 44(4): 10-17 (December 2025)

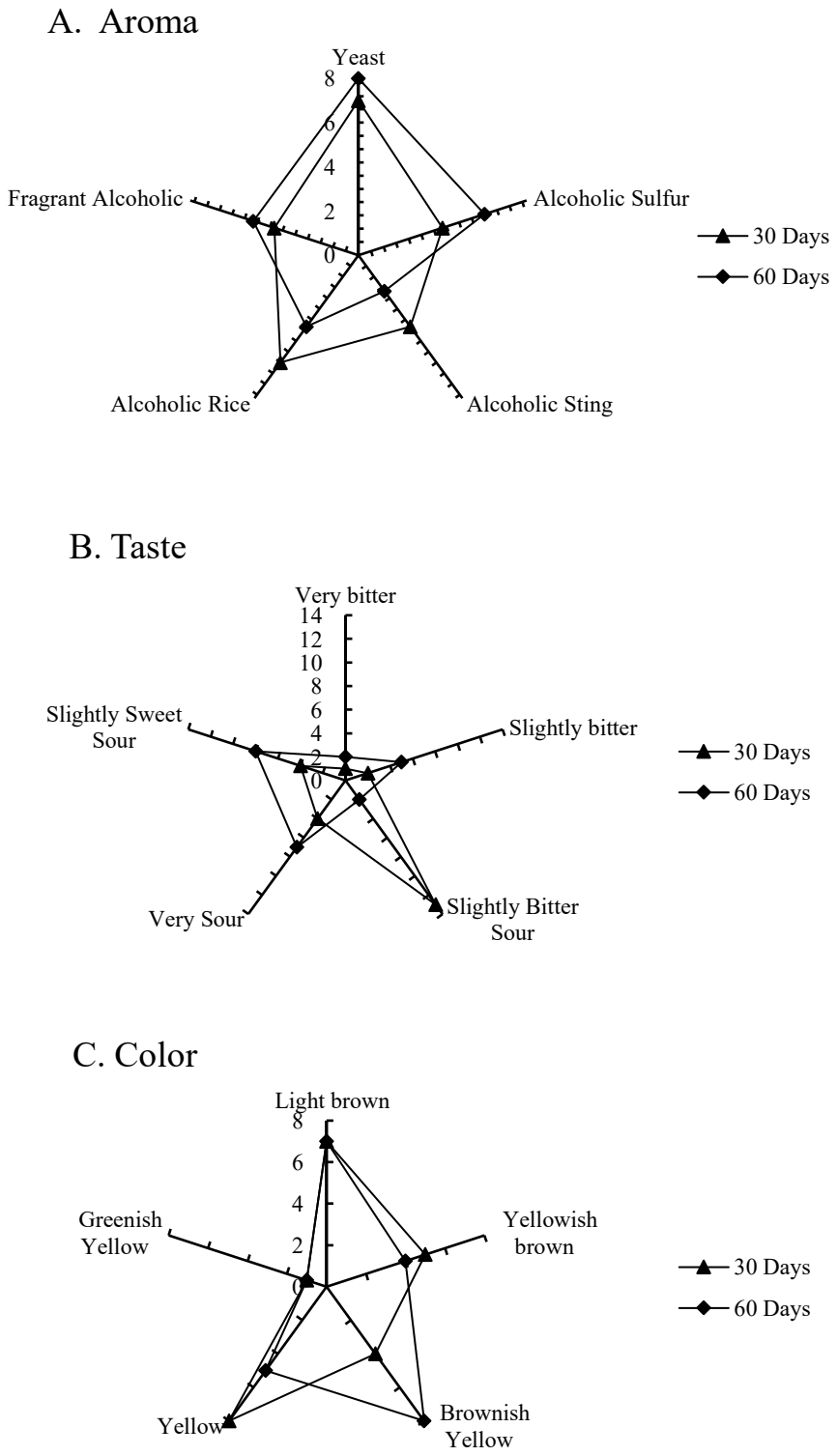

Figure 3. Sensory evaluation of aroma (A), taste (B), and color (C) in red rice vinegar with different spontaneous fermentation time.

Taste

Red rice vinegar treated for 30 days has a slightly bitter, sour flavor (Figure 3B). According to Table 1, there is no significant difference in the flavor of red rice vinegar after 30 or 60 days of fermentation ($p>0.05$). The duration of fermentation has no effect on the sensory qualities (taste) of spontaneously produced red rice vinegar. The bitter taste is likely due to the pH being higher than during the 60-day fermentation. Bitter taste in vinegar is typically caused by acetic acid, which forms during alcoholic fermentation by Acetobacter bacteria. Acetobacter bacteria then convert alcohol to acetic acid, producing vinegar. The 60-day treatment had a slightly sweet sour flavor; this sweet

DOI: https//doi.org/10.22452/mjs.vol44no4.2
Malaysian Journal of Science 44(4): 10-17 (December 2025)

taste was associated with the phenolic content, and it was known that the phenolic content of red rice vinegar after 60 days was higher than after 30 days of fermentation. The sour taste of red rice vinegar after 30 or 60 days of treatment is most likely due to its high acetic acid content. Additionally, the alcohol content may influence the vinegar's sour taste. This is because alcohol concentration affects the progression of acetic acid fermentation. Meanwhile, the taste of red rice vinegar is unaffected by its antioxidant activity or phenolic compounds. Phenolic compounds in vinegar, such as phenolic and polyphenolic substances, can contribute flavor and aroma, but their relationship to bitterness is usually indirect. Phenolics often impart a sour, sweet, or astringent taste but do not produce substantial bitterness (Praja, 2015). The fermentation time can affect the sugar content in vinegar because microorganisms convert sugar in the raw material into acetic acid during alcoholic fermentation.

Color

According to the results of the colour sensory test in Figure 2C, the majority of panellists agreed that the red rice vinegar produced after 30 days of vinegar treatment was yellow, whereas the red rice vinegar produced after 60 days of vinegar treatment tended to become brownish yellow. The colour shift is induced by changes in fermentation time, which result from the microbial consortium's ability to break down colour. Table 1 demonstrates that there is no significant difference in the colour of red rice vinegar between 30 and 60 days of fermentation ($p > 0.05$). The colour of red rice vinegar produced through spontaneous fermentation is unaffected by variations in fermentation time. The findings of this study are consistent with previous research that found honey pineapple vinegar to be brownish yellow. The brownish colour results from the browning process. The brownish colour results from the Maillard process, which occurs when amino acids in sugar condensate and rearrange themselves. A browning process in vinegar can occur during fermentation, especially if fermentation is conducted over a long period of time (Mizrotun, 2020). Colour is the primary characteristic of a food or beverage product that can influence the panellists' subsequent evaluation. Colour is also a highly essential part of visual assessment and can affect the analysis of other sensory components (Lemmetti et al., 2014).

4. Conclusion

With spontaneous fermentation, the chemical parameters of red rice vinegar (acetic acid content, pH, alcohol content, antioxidant activity, and phenolic compounds) are influenced by fermentation time. However, fermentation time has no effect on the sensory qualities (aroma, taste, and colour) of red rice vinegar with spontaneous fermentation. Red rice vinegar fermented for 60 days contained higher amounts of acetic acid, phenolic compounds, and antioxidant activity than vinegar fermented for 30 days. A prolonged fermentation treatment of 60 days produced red rice vinegar with a yeast scent, slightly sweet bitter flavour, and brownish yellow colour, which was the best treatment based on sensory qualities. Future study should focus on the utilisation of microorganisms in fermentation to enhance the functional qualities of red rice vinegar.

5. Acknowledgement

The author is grateful to Universitas Nahdlatul Ulama Surabaya for their support during this research.

6. References

Aksoy, L., Kolay, E., Ağılönü, Y., Aslan, Z., & Kargıoğlu, M. (2013). Free radical scavenging activity, total phenolic content, total antioxidant status, and total oxidant status of endemic Thermopsis turcica. *Saudi Journal of Biological Sciences*, *20*(3), 235–239. https://doi.org/10.1016/j.sjbs.2013.02.003

Antoniewicz, J., Jakubczyk, K., Kwiatkowski, P., Maciejewska-markiewicz, D., Kochman, J., Rębacz-Maron, E., & Janda-Milczarek, K. (2021). Analysis of antioxidant capacity and antimicrobial properties of selected polish grape vinegars obtained by spontaneous fermentation. *Molecules*, *26*(16). https://doi.org/10.3390/molecules26164727

Arnata, M. P. A. N. M. W. I. W. (2015). Pengaruh Lama Fermentasi Alami Secara Aerob Cairan Pulpa Hasil Samping Fermentasi Biji Kakao Terhadap Karakteristik Cuka Fermentasi. *Jurnal Rekayasa Dan Manajemen Agroindustri*, *3*(3), 82–94. https://ojs.unud.ac.id/index.php/jtip/article/view/18687/12169

Azis, A., Izzati, M., Biologi, S. H.-J. A., & 2015, U. (2015). Antioxidant Activity and Nutritional Value of Several Types of Rice and Millet as Indonesian Functional Food Ingredients. *Jurnal Biologi*, *4*(1), 45–61. https://ejournal3.undip.ac.id/index.php/biologi/article/view/19400

Budak, H. N. (2021). Alteration of antioxidant activity and total phenolic content during the eight-week fermentation of apple cider vinegar. *Horticultural Studies*, *38*(1), 39–45. https://doi.org/10.16882/hortis.882469

Coelho, E., Genisheva, Z., Oliveira, J. M., Teixeira, J. A., & Domingues, L. (2017). Vinegar production from fruit concentrates: effect on volatile composition and antioxidant activity. *Journal of Food Science and Technology*, *54*(12), 4112–4122. https://doi.org/10.1007/s13197-017-2783-5

Deng, G. F., Xu, X. R., Zhang, Y., Li, D., Gan, R. Y., & Li, H. Bin. (2013). Phenolic Compounds and Bioactivities of Pigmented Rice. *Critical Reviews in Food Science and Nutrition*, *53*(3), 296–306. https://doi.org/10.1080/10408398.2010.529624

Ernawangtyas, E., & Yudhayanti, D. (2017). Penetapan Kadar Alkohol pada Arak Jowo yang Beredar di Ponorogo dengan Metode Destilasi. *Jurnal Edunursing*, *1*(2), 57–63.

DOI: https//doi.org/10.22452/mjs.vol44no4.2
Malaysian Journal of Science 44(4): 10-17 (December 2025)

http://journal.unipdu.ac.id/index.php/edunursing/article/view/1089

Eshak, N. S. (2016). Sensory evaluation and nutritional value of balady flat bread supplemented with banana peels as a natural source of dietary fiber. *Annals of Agricultural Sciences*, *61*(2), 229–235. https://doi.org/10.1016/j.aoas.2016.07.002

Fadilah, U., Wijaya, I. M. M., & Antara, N. S. (2018). Studi Pengaruh pH Awal Media dan Lama Fermentasi pada Proses Produksi Etanol dari Hidrolisat Tepung Biji Nangka dengan Menggunakan Saccharomycess cerevisiae. *Jurnal Rekayasa Dan Manajemen Agroindustri*, *6*(2), 92–102. https://doi.org/10.24843/JRMA.2018.v06.i02.p01

Ghosh, S., Chakraborty, R., Chatterjee, G., & Raychaudhuri, U. (2012). Study on fermentation conditions of palm juice vinegar by Response Surface Methodology and development of a kinetic model. *Brazilian Journal of Chemical Engineering*, *29*(3), 461–472. https://doi.org/10.1590/S0104-66322012000300003

Gong, M., Zhou, Z., Liu, S., Zhu, S., Li, G., Zhong, F., & Mao, J. (2021). Dynamic changes in physico-chemical attributes and volatile compounds during fermentation of Zhenjiang vinegars made with glutinous and non-glutinous japonica rice. *Journal of Cereal Science*, *100*, 103246. https://doi.org/https://doi.org/10.1016/j.jcs.2021.103246

Hammouda, M. Ben, Castro, R., Durán-Guerrero, E., Attia, H., & Azabou, S. (2023). Vinegar production via spontaneous fermentation of different prickly pear fruit matrices: changes in chemical composition and biological activities. *Journal of the Science of Food and Agriculture*, *103*(11), 5221–5230. https://doi.org/10.1002/jsfa.12605

Hapsari, M., Rizkiprilisa, W., & Sari, A. (2021). Pengaruh lama fermentasi terhadap aktivitas antioksidan minuman fermentasi kombucha lengkuas merah (Alpinia purpurata). *AGROMIX*, *12*(2), 146–149. https://doi.org/https://doi.org/10.35891/agx.v12i2.2647

Hardoko, Prihanto, N. H., & Sasmito, B. B. (2019). Aktivitas Antioksidan Dan Karakteristik Cuka Buah Mangrove Pedada (Sonneratia alba). *JFMR-Journal of Fisheries and Marine Research*, *3*(3), 322–330. https://doi.org/10.21776/ub.jfmr.2019.003.03.6

Hidalgo, C., Mateo, E., Cerezo, A. B., Torija, M. J., & Mas, A. (2010). Technological process for production of persimmon and strawberry vinegars. *International Journal of Wine Research*, *2*(1), 55–61. https://doi.org/10.2147/ijwr.s8741

Jayus, J., Rosyidawati, E. H., & Purnomo, B. H. (2020). Acceleration of Moromi Production Using Inoculum of Pediococcus halophilus FNCC 0033 and Zygosaccharomyces rouxii FNCC 3008 Jay. *Jurnal Agroteknologi*, *13*(02), 148. https://doi.org/10.19184/j-agt.v13i02.9061

Kandylis, P. (2019). *Advances in Vinegar Production* (A. Bekatorou (ed.); 1st ed.). CRC Press. https://doi.org/https://doi.org/10.1201/9781351208475

Kim, E. J., Cho, K. M., Kwon, S. J., Seo, S. H., Park, S. E., & Son, H. S. (2021). Factors affecting vinegar metabolites during two-stage fermentation through metabolomics study. *Lwt*, *135*(May 2020), 110081. https://doi.org/10.1016/j.lwt.2020.110081

Laily, I., Santy, W. H., & Pratiwi, V. N. (2019). Effect of mixed cultures in alcoholic fermentation on the physicochemical and sensory properties of bilimbi vinegar (Averrhoa bilimbi L.). *Jurnal Pangan Dan Agroindustri*, *7*(3), 9–18. https://doi.org/https://doi.org/10.21776/ub.jpa.2019.007.03.2

Lemmetti, F., Solieri, L., Bonciani, T., Zanichelli, G., & Giudici, P. (2014). Sensory analysis of traditional balsamic vinegars: current state and future perspectives. *Acetic Acid Bacteria*, *3*(1), 1–6. https://doi.org/10.4081/aab.2014.4619

Lestari, M. W., Priyo Bintoro, V., & Rizqiati, H. (2018). Pengaruh Lama Fermentasi terhadap Tingkat Keasaman, Viskositas, Kadar Alkohol, dan Mutu Hedonik Kefir Air Kelapa Effect of Fermentation Time on Acidity, Viscosity, Alcohol Concentration, and Hedonic Quality of Coconut (Cocos nucifera) Water Kefir. *Jurnal Teknologi Pangan*, *2*(1), 8–13. https://doi.org/https://doi.org/10.14710/jtp.2018.20750

Malibun Fais Bintang, Husain Syam, A. S. (2019). Making Rice Crackers With Addition To Red Rice (Oryza nivara) And A Powder Of Kelor Leaves (Moringa oleifera) As A Functional Food. *Jurnal Pendidikan Teknologi Pertanian*, *5*(2), 1–13. https://doi.org/https://doi.org/10.26858/jptp.v5i2.9621

Mizrotun, N. (2020). Uji Aktivitas Antibakteri Cuka Buah Nanas Madu (Ananas comosus L) Merr) Terhadap Bakteri. In *Tugas Akhir Politeknik Harapan Bersama Tegal*. Politeknik Harapan Bersama Tegal.

Pangerang, F. (2022). Nutritional Content and Antioxidant Activity of Local Field Rice (Red and and Black Rice) from Bulungan Regency, North Kalimantan Province. *Journal of Tropical AgriFood*, *3*(2), 93. https://doi.org/10.35941/jtaf.3.2.2021.8475.93-100

Pohan, A., Maliza, N. O., Sulaiman, M. I., & Yunita, D. (2019). Initial study of vinegar production made from low quality rice using a batch type fermenter. *Jurnal Bioleuser*, *3*(1), 1–4. https://doi.org/https://doi.org/10.24815/j.%20bioleuser.v0i0.18814

Praja, D. I. (2015). *Zat Aditif Makanan : Manfaat dan Bahayanya*. Garudhawaca.

DOI: https//doi.org/10.22452/mjs.vol44no4.2
Malaysian Journal of Science 44(4): 10-17 (December 2025)

Pratiwi, A., & Aryawati, R. (2012). *Pengaruh Waktu Fermentasi Terhadap Sifat Fisik dan Kimia pada Pembuatan Minuman Kombucha dari Rumput Laut Sargasssum sp*. *04*, 131–136. https://doi.org/https://doi.org/10.56064/maspari.v4i1.1438

Rahayu, N. M. M. S., Putra, G. P. G., & Suwariani, N. P. (2017). *Pengaruh Laju Aliran Udara Dan Lama Fermentasi Cairan Pulpa*. *5*(2), 58–67.

Rubiati, S. (2021). Determination of phenolic compounds and antioxidant activity test on fermented rice bran by Saccharomyces cerevisiae. In *Universitas Islam Indonesia*. https://dspace.uii.ac.id/handle/123456789/30424%0Ahttps://dspace.uii.ac.id/bitstream/handle/123456789/30424/16612083 Sri Rubiati.pdf?sequence=1&isAllowed=y

Sartini, S., Djide, M. N., & Nainu, F. (2019). Correlation Phenolic Concentration to Antioxidant and Antibacterial Activities of Several Ethanolic extracts from Indonesia. *Journal of Physics: Conference Series*, *1341*(7), 072009. https://doi.org/10.1088/1742-6596/1341/7/072009

Sompong, R., Siebenhandl-Ehn, S., Linsberger-Martin, G., & Berghofer, E. (2011). Physicochemical and antioxidative properties of red and black rice varieties from Thailand, China and Sri Lanka. *Food Chemistry*, *124*(1), 132–140. https://doi.org/10.1016/j.foodchem.2010.05.115

Suwardiyono, Harianingsih, B. Nugroho, & Wijnarko, R. (2014). Model Pendekteksi pH pada Proses Fermentasi Acetobacter Xylinum Menggunakan Sensor SEN0161. *Prosiding SNST*, 10–14.

Taweekasemsombut, S., Tinoi, J., Mungkornasawakul, P., & Chandet, N. (2021). Thai rice vinegars: Production and biological properties. *Applied Sciences (Switzerland)*, *11*(13), 1–18. https://doi.org/10.3390/app11135929

Wijaya, C., & Romulo, A. (2021). Proximate Analysis and Antioxidant Activity of Red Rice (Oryza sativa L.) Milk. *Journal of Physics: Conference Series*, *2049*(1), 012012. https://doi.org/10.1088/1742-6596/2049/1/012012

Yan, Y., Zhang, F., Chai, Z., Liu, M., Battino, M., & Meng, X. (2019). Mixed fermentation of blueberry pomace with L. rhamnosus GG and L. plantarum-1: Enhance the active ingredient, antioxidant activity and health-promoting benefits. *Food and Chemical Toxicology*, *131*(May), 110541. https://doi.org/10.1016/j.fct.2019.05.049

Yuan, H. W., Tan, L., Chen, H., Sun, Z. Y., Tang, Y. Q., & Kida, K. (2017). Vinegar production from post-distillation slurry deriving from rice shochu production with the addition of caproic acid-producing bacteria consortium and lactic acid bacterium. *Journal of Bioscience and Bioengineering*, *124*(6), 653–659. https://doi.org/10.1016/j.jbiosc.2017.06.011

Zhou, X.-J., Yan, L.-L., Yin, P.-P., Shi, L.-L., Zhang, J.-H., Liu, Y.-J., & Ma, C. (2014). Structural characterisation and antioxidant activity evaluation of phenolic compounds from cold-pressed Perilla frutescens var. arguta seed flour. *Food Chemistry*, *164*, 150–157. https://doi.org/https://doi.org/10.1016/j.foodchem.2014.05.062

Zubaidah, E., & Veronica, C. (2014). Studi Aktivitas Antioksidan Cuka Berbasis Buah Anggur Bali (Vitis Vinifera) Utuh dan Tanpa Kulit. *Jurnal Teknologi Hasil Pertanian*, *7*(2), 95–103. https://doi.org/10.20961/jthp.v0i0.13012

DOI: https//doi.org/10.22452/mjs.vol44no4.2
Malaysian Journal of Science 44(4): 10-17 (December 2025)

MALAYSIAN JOURNAL OF SCIENCE
MJS
ISSN 1394-3065

Regular Issue

Malaysian Journal of Science 44 (4): 18-30 (December 2025) https://mjs.um.edu.my

Enhancing Multispectral Land Use and Land Cover Classification with Transfer Learning and 3D ResNet

Farah Adila Ahmad Marzuki[1a], Helmi Zulhaidi Mohd Shafri[2a*], Siti Nur Aliaa Roslan[3a], Yuhao Ang[4a], Mohammed Mustafa Al-Habshi[5a], Yang Ping Lee[6b], Shahrul Azman Bakar[7b], Haryati Abidin[8b], Hwee San Lim[9c] and Rosni Abdullah[10d]

Abstract: Recent advances in land use and land cover (LULC) classification with remote sensing imagery are driven by state-of-the-art models such as Convolutional Neural Networks (CNNs). Advanced CNN architecture like ResNet can enhance overall classification performance by incorporating residual skip connections. The integration of 3D feature extraction and ResNet architecture suggests a potential improvement in classification tasks. This paper explores the potential of the 3D ResNet model for LULC classification, comparing it with baseline approaches (Support Vector Machine, Random Forest, XGBoost, 1D CNN, 3D CNN) and state-of-the-art 3D models (3D VGG, 3D DenseNet) using WorldView-2 satellite imagery. The 3D ResNet-18 model, fine-tuned via transfer learning on multispectral images, demonstrates significant improvements in classification performance over machine learning models. It achieves the highest Overall Accuracy (OA) of 99.66% and Kappa Accuracy (KA) of 99.39% on the primary dataset. Despite having slightly lower performance on the external validation dataset (OA:82.89%, KA:80.05%) than 3D DenseNet, it is highly efficient with processing times of 490.2 minutes and 3.6 minutes for both datasets respectively. McNemar's test results show 3D ResNet and 3D DenseNet have significant differences in classification performance ($p<0.05$) against other models consistently for both datasets.

Keywords: *Convolutional neural network, deep learning, LULC, multispectral, transfer learning.*

1. Introduction

Land use and land cover (LULC) classification serves an important function as it can be used to identify different types of natural and economic operations which are later used to facilitate better decision-making (Wang et al., 2022). LULC data extracted from remote sensing images are commonly used nowadays due to increasing number of multispectral and hyperspectral satellites along with publicly available dataset. They can be very useful for urban planning and agricultural management (Shaharum et al., 2020). The distinct spectral characteristics of various land cover types across multiple spectral bands are effectively captured by multispectral satellite data or imagery, making it a common choice for LULC classification, which enables more precise classification.

Conventional machine learning (ML) models like Support Vector Machine (SVM), Random Forest (RF) and Extreme Gradient Boost (XGBoost) have been employed extensively throughout the years since they have lower computational complexity and higher interpretability (Sheykhmousa et al., 2020). These models can produce reliable results without much hyperparameter tuning. Contradicting results were reported by several research when comparing these models for LULC classification. Previous studies showed that SVM was able to get a higher accuracy than RF and XGBoost by using Sentinel-2 (Abdi, 2020) satellite imagery. However, findings from another research indicated that RF outperformed SVM for large area mapping using a WorldView-2 image (Jombo et al., 2020). Another research has also shown that XGBoost achieved higher accuracy over SVM and RF for both aerial image and WorldView-2 image (Jozdani et al., 2019).

Deep learning (DL) approaches, particularly Convolutional Neural Networks (CNN), have gained attention for their ability to capture complex patterns in remote sensing images. Deeper CNN networks can learn more intricate details, but this does not always lead to higher accuracy due to the vanishing gradient problem which can hinder training convergence (Noh, 2021). Advanced CNN architectures like Residual Network (ResNet) are later introduced to address this limitation of regular CNN models (He et al., 2015). ResNet has shown exceptional performance in LULC classification using multispectral images (Tong et al., 2020). Complex architectures like ResNet are often used with transfer learning, allowing knowledge from one task to be applied to another. This helps improve model generalization and reduces training time.

Authors information:
[a]Department of Civil Engineering and Geospatial Information Science Research Centre (GISRC), Faculty of Engineering, Universiti Putra Malaysia (UPM), 43400 Serdang, Selangor, MALAYSIA. Email: frhdila13@gmail.com[1], helmi@upm.edu.my[2], aliaa_roslan@upm.edu.my[3], vincentangkhun@gmail.com[4], alhabshi3k@gmail.com[5]
[b]Geoinformatics Unit, FGV R&D Sdn Bhd, FGV Innovation Centre, PT23417, Lengkuk Teknologi, 71760 Bandar Enstek, Negeri Sembilan, MALAYSIA. Email: yangp.lee@fgvholdings.com[6], shahrul.b@fgvholdings.com[7], haryati.a@fgvholdings.com[8]
[c]School of Physics, Universiti Sains Malaysia (USM), 11800 Gelugor, Penang, MALAYSIA. Email: hslim@usm.my[9]
[d]School of Computer Sciences, Universiti Sains Malaysia (USM), 11800 Gelugor, Penang, MALAYSIA. Email: rosni@usm.my[10]
*Corresponding Author: helmi@upm.edu.my

Received: July, 2024
Accepted: June, 2025
Published: December, 2025

DOI:https//doi.org/10.22452/mjs.vol44no4.3
Malaysian Journal of Science 44(4): 18-30 (December 2025)

Recent research has shown the effectiveness of 3D ResNet models for various applications like medical imaging informatics (Ebrahimi et al., 2020). By harnessing the benefits of 3D feature extraction and residual skip connections, 3D ResNet models offer promising results for accurate land cover classification. Hence, various studies have employed 3D ResNet models for LULC classification with hyperspectral images (Firat et al., 2023). To the extent of research conducted, it is believed that there is no other existing research on the application of 3D ResNet models for multispectral LULC classification.

In summary, the objectives of this paper are:

- To investigate the potential application of deep residual model, 3D ResNet-18 in LULC classification of WorldView-2 multispectral satellite imagery. The model performance was compared against several baseline models including RF, SVM, XGBoost, 1D CNN, and 3D models (3D CNN, 3D VGG and 3D DenseNet).
- To demonstrate the benefits of transfer learning by fine-tuning a pre-trained 3D ResNet-18 model on multispectral satellite imagery.
- To employ WorldView-2 spectral ground truth dataset that provides additional bands that capture detailed spectral information beyond the visible spectrum.

2. Materials and Methods

Study Area

The study was conducted on two oil palm regions (Figure 1) situated in Jerantut, Pahang. The dataset features a broad range of land cover types and oil palm trees at multiple growth stages, which was suitable for testing model robustness. The image (10790 x 10351 pixels) was obtained using WorldView-2, a multispectral satellite imagery. Due to its spectral range of 450 to 800 nm and spatial resolution of 0.3 m post-pansharpening, the image offers a more detailed perspective on land cover features.

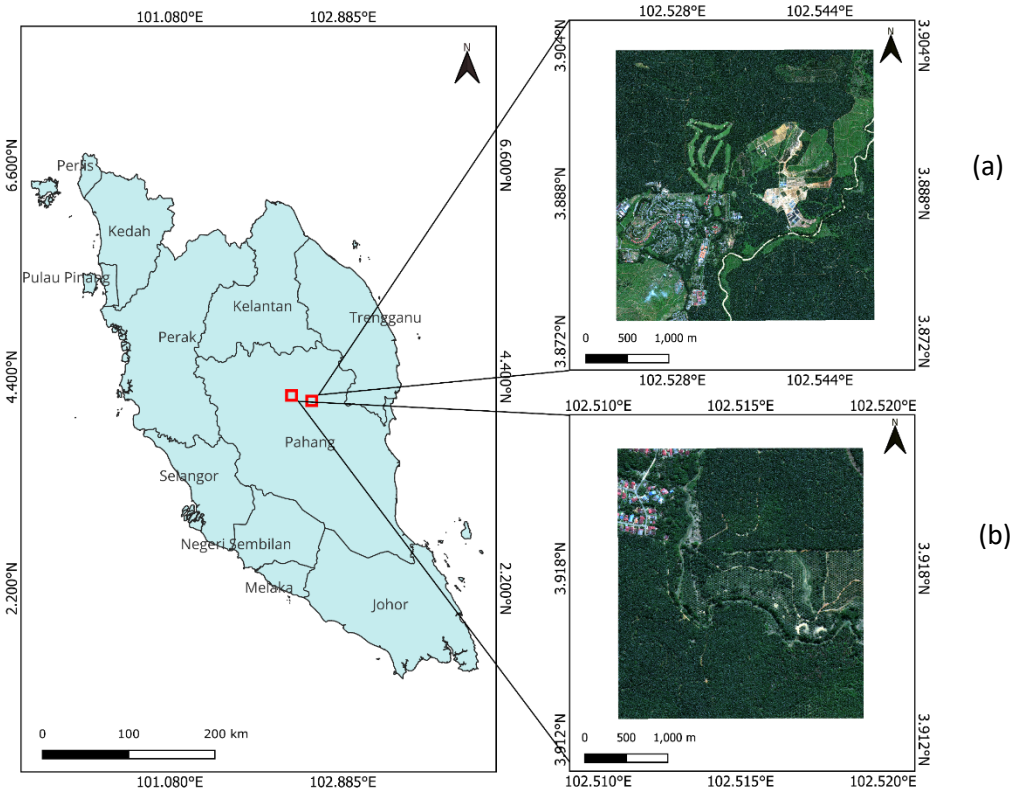

Figure 1. WorldView-2 satellite image of the oil palm plantation located in Jerantut, Pahang, Malaysia, (a) Primary dataset; (b) External validation dataset.

Design of Study

The experiment followed the methodology in Figure 2. Multispectral satellite images were acquired, and seven map classes were defined for classification. A total of 3476175 samples (primary dataset) and 24113 samples (validation dataset) were collected through ground truthing using QGIS software. Stratified k-fold cross-validation (SKCV) was used for data sampling. Three ML models (SVM, RF, XGBoost) and five DL models (1D CNN, 3D CNN, 3D VGG, 3D DenseNet, 3D ResNet) were chosen for LULC classification. Model training and hyperparameter tuning identified the best parameters for each model. Model performance was evaluated using Overall Accuracy (OA), Kappa Accuracy (KA), Precision, Recall, and F1-score.

DOI:https//doi.org/10.22452/mjs.vol44no4.3
Malaysian Journal of Science 44(4): 18-30 (December 2025)

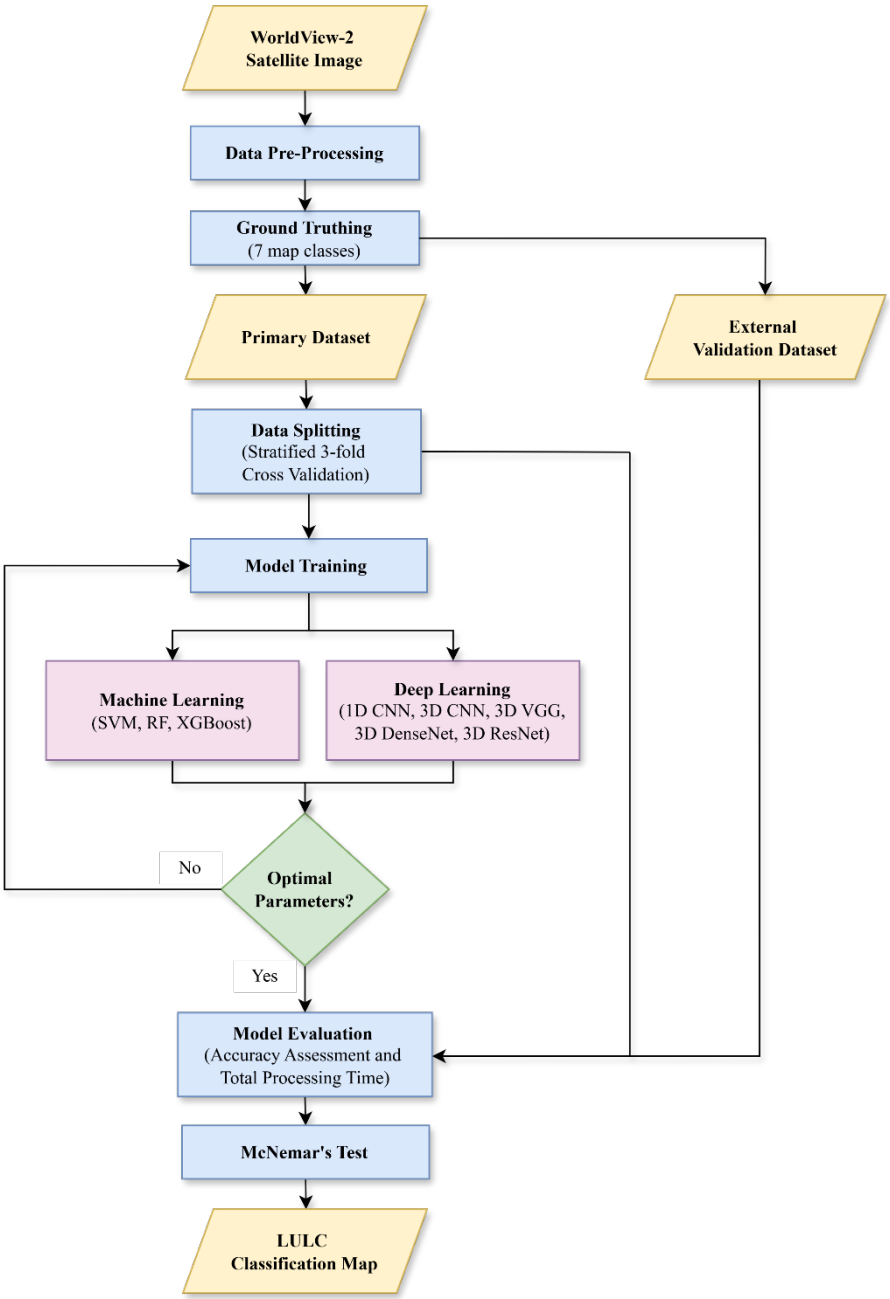

Figure 2. Methodology flowchart.

Sampling Strategy

This study used stratified random sampling and SKCV approach was applied due to the dataset imbalance in Table 1. The SKCV approach is a modified version of normal k-fold cross validation. In the normal k-fold, it splits the dataset randomly into k equal parts. However, the SKCV ensures the same class distribution in every fold like the original dataset; thus, reducing bias during model evaluation. Research performed by Thölke et al. (2023) has shown that SKCV is less sensitive to imbalanced data compared to normal k-fold as it prevents any fold from containing only one class, resulting in a fairer model evaluation.

DOI:https//doi.org/10.22452/mjs.vol44no4.3
Malaysian Journal of Science 44(4): 18-30 (December 2025)

Table 1. Data distribution for primary dataset and external validation dataset.

Class ID	Land Cover Class	Class Description	Number of pixels	
			Primary Dataset	Validation Dataset
1	Water bodies	Natural and artificial water bodies	104052	3734
2	Built-up	Man-made infrastructure	192764	3273
3	Bare soil	Minimal or no vegetation	338023	3748
4	Forest	Open and closed canopy forest	236787	3517
5	Grass	Herbaceous plant cover	237140	3027
6	Oil palm	Oil palm trees of various ages	2222685	3243
7	Other vegetations	Includes other plants like pandan coconut and durian trees	144724	3571
		TOTAL	3476175	24113

Model Architectures

The introduction of ResNet architecture leads to significant improvement in land cover classification as they can utilize skip connections, allowing the training of much deeper models and reducing the optimization difficulty (Tong et al., 2020). By incorporating 3D convolutional filters, 3D ResNet models can be developed to extract spectral-spatial data from remote sensing images. The network depth of 18 layers provides a good balance between the model complexity and computational cost, which makes it a suitable choice.

To reduce overfitting in the 3D ResNet-18 model, we used transfer learning with Dimension Expansion Weight Transfer (DEWT) technique. DEWT is a simple yet effective method, where pre-trained 2D weights are transferred by replicating them across the third dimension. By fine-tuning the model with pre-trained ImageNet weights and adding a new classification layer for the seven classes shown in Figure 3, 3D ResNet-18 model performance and generalizability can be improved. The implementation code is available on GitHub: https://github.com/russelrk/Pre_Trained_3D_CNN. To assess its performance, other state-of-the-art 3D models including 3D VGG-16 (Simonyan & Zisserman, 2015) and 3D DenseNet-121 (G. Huang et al., 2018) were also incorporated in this study. The same type of weight transfer was also used for these models.

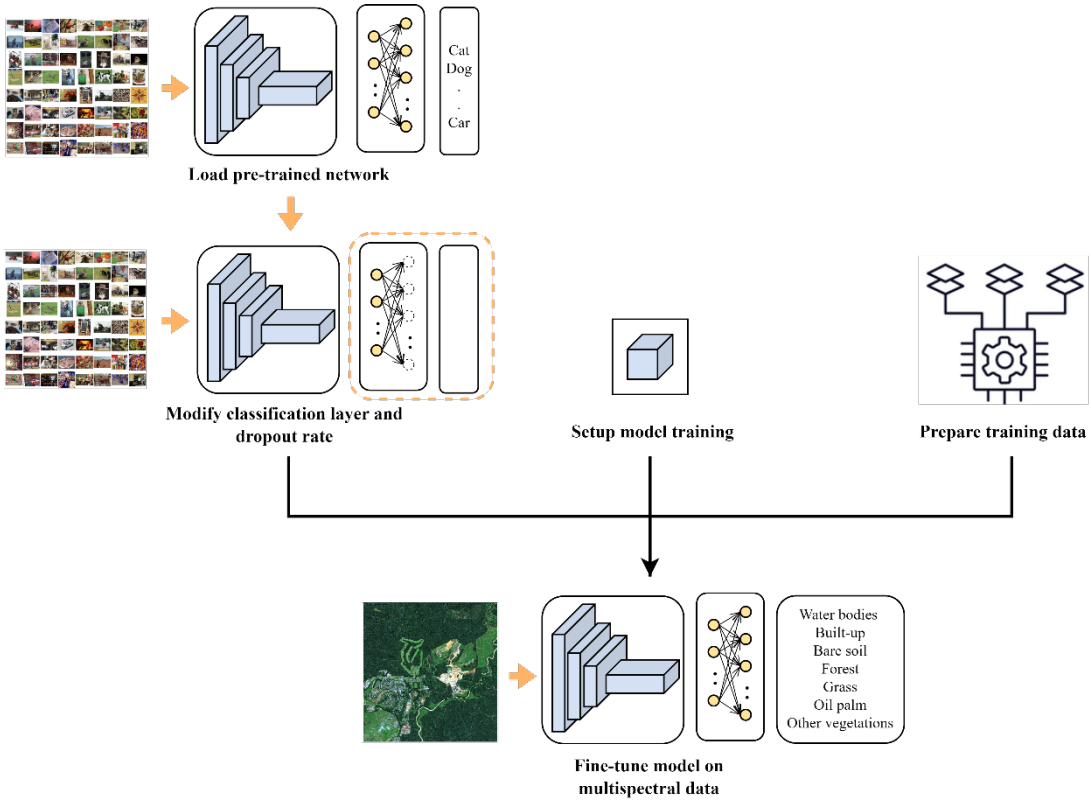

Figure 3. Process of fine-tuning 3D ResNet model.

DOI:https//doi.org/10.22452/mjs.vol44no4.3
Malaysian Journal of Science 44(4): 18-30 (December 2025)

SVM is a popular classifier for LULC classification, especially with small datasets (Vali et al., 2020). It aims to find the best decision boundary that separates target classes by solving a quadratic optimization problem (Sheykhmousa et al., 2020). Due to limited computational resources, linear SVM was used in this study. RF is an ensemble method that improves accuracy by combining multiple decision trees. It performs effectively with high-dimensional data and less prone to overfitting. Like RF, XGBoost uses ensemble learning. It is an improved version of the gradient boosting machine (GBM) algorithm, enhancing both performance and speed (Abdi, 2020). It builds a sequential model with shallow decision trees, optimizing a loss function, while adding regularization to reduce overfitting.

Model Training and Hyperparameter Tuning

All experiments were implemented in Google Colab Pro+ with Python. The processing for ML models was performed on CPU whereas the processing for DL models was performed on A100 GPU NVIDIA with 40 GB of RAM. Hyperparameter tuning was conducted using coarse grid search to determine the best parameters for each model as shown in Table 2. By using PyTorch framework, each DL model was trained in batches of 256 for 100 epochs per fold, with a learning rate of 0.0001. Regularization techniques like using dropout rate of 0.2 and early stopping rounds of 5 were applied to reduce overfitting. The Adam optimizer was used for faster convergence, and a 5x5 pixels patch size was chosen for computational efficiency.

Table 2. Best model parameters after hyperparameter tuning.

Classifier	Parameters
SVM (Linear)	C = 1
RF	n_estimators = 300 max_depth = 30 min_samples_leaf = 1 min_samples_split= 2
XGBoost	n_estimators = 500 max_depth = 7 min_child_weight = 3 subsample = 0.7
1D CNN 3D CNN 3D VGG 3D DenseNet 3D ResNet	learning_rate = 0.0001 batch_size = 256 epochs = 100

Performance Evaluation

Model evaluation was conducted in terms of accuracy and processing times. OA is the proportion of accurately classified instances relative to the overall number of reference instances. KA is measure of agreement between reference data and classifier with the range of -1 to 1. Although these metrics are significant in model evaluation, it can show misleading results in cases of class imbalance; hence, additional metrics were also applied. Precision, as shown in Eq. (1) represents the proportion of correctly classified instances relative to the overall number of instances classified, where TP, FP, and FN represent the number of true positives, false positives, and false negatives respectively.

$$\text{Precision} = \frac{\text{TP}}{(\text{TP}+\text{FP})} \quad (1)$$

Recall in Eq. (2), is the proportion of correctly classified instances to the actual instances.

$$\text{Recall} = \frac{\text{TP}}{(\text{TP}+\text{FN})} \quad (2)$$

F1-score, shown in Eq. (3) is the harmonic mean of Precision and Recall, an indicator of the predictive ability of the model.

$$\text{F1} - \text{score} = 2\left[\frac{(\text{Precision}\,.\,\text{Recall})}{(\text{Precision}+\text{Recall})}\right] \quad (3)$$

McNemar's test was also performed to inspect the statistical significance of difference in the classification performance between models. A 2 x 2 contingency matrix was constructed and calculated to determine the value of chi-square and p-value. The calculation for McNemar's test value is shown in Eq. (4), where f_{12} and f_{21} represent the quantity of accurately classified and misclassified samples respectively. A significance threshold (α=0.05) was fixed before computing the p-value. The null hypothesis (H_0) assumes equal classification performance between models, while the alternative hypothesis (H_1) suggests a difference. H0 is rejected if the p-value is below the threshold.

$$\chi^2 = \frac{(|f_{12}-f_{21}|-1)^2}{(f_{12}+f_{21})} \quad (4)$$

DOI:https//doi.org/10.22452/mjs.vol44no4.3
Malaysian Journal of Science 44(4): 18-30 (December 2025)

3. Results and Discussion

Accuracy Assessment and Processing Time

Based on Figure 4, while the loss curve of the 3D ResNet-18 generally stabilizes, slight fluctuations can be observed in the validation loss. This may result from Adam optimizer's adaptive nature (Kingma & Ba, 2017) and minor imbalances in feature distribution. Experimenting with different optimizers could help address these fluctuations. Despite this, the minimal divergence between training and validation losses indicates no overfitting.

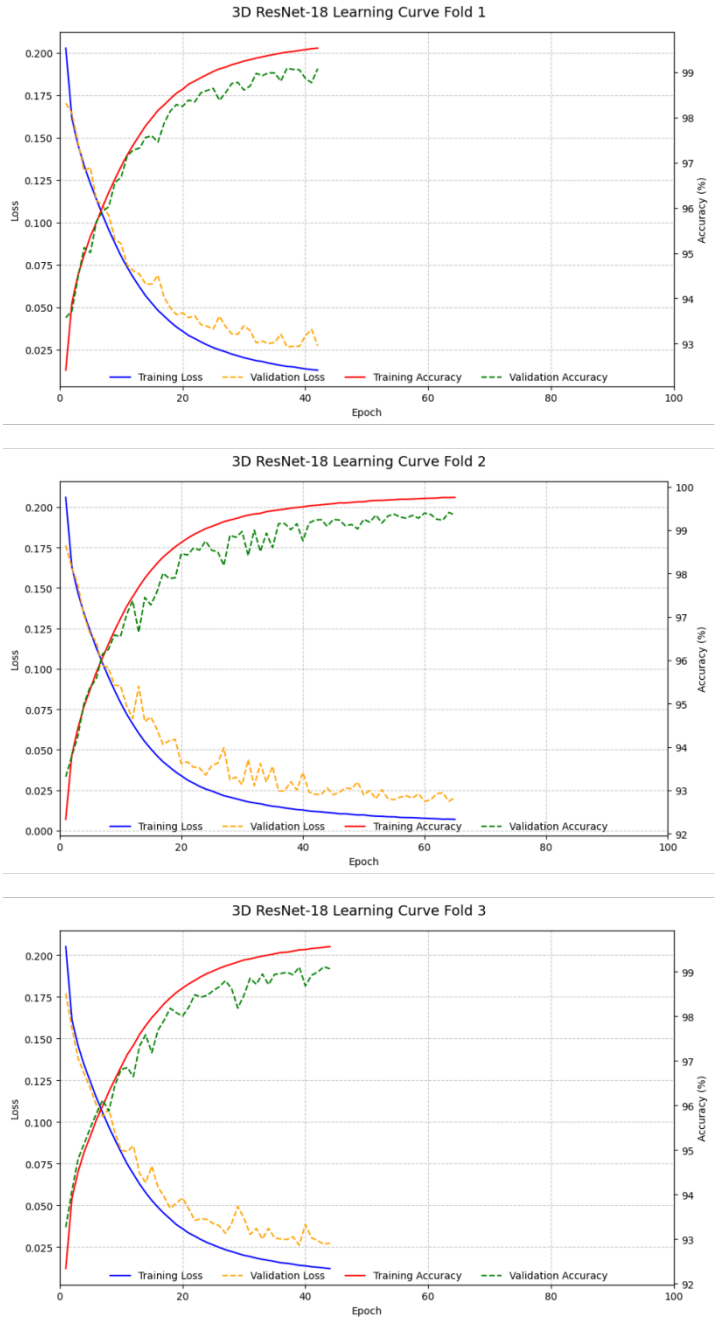

Figure 4. Loss and accuracy learning curves for 3D ResNet.

Overall, 3D ResNet-18 outperformed the other models by achieving a high OA of 99.66% and KA of 99.39% on the primary dataset as shown in Figure 5. Although 3D ResNet-18 has similar ability to 3D CNN in extracting spectral-spatial features, it incorporates residual skip connections which allows it to preserve important information and gradient. The skip connections in ResNet provide a direct path from the input of one layer to the output of deeper layers, allowing for better feature retention in the model. The skip connections also enabled more effective gradient flow as it can bypass certain intermediate layers during backpropagation, addressing the vanishing gradient problem and ensuring more effective weight updates. This is aligned with previous research involving comparison between traditional CNN architecture and ResNet architecture (D & Bhavani, 2023).

DOI:https//doi.org/10.22452/mjs.vol44no4.3
Malaysian Journal of Science 44(4): 18-30 (December 2025)

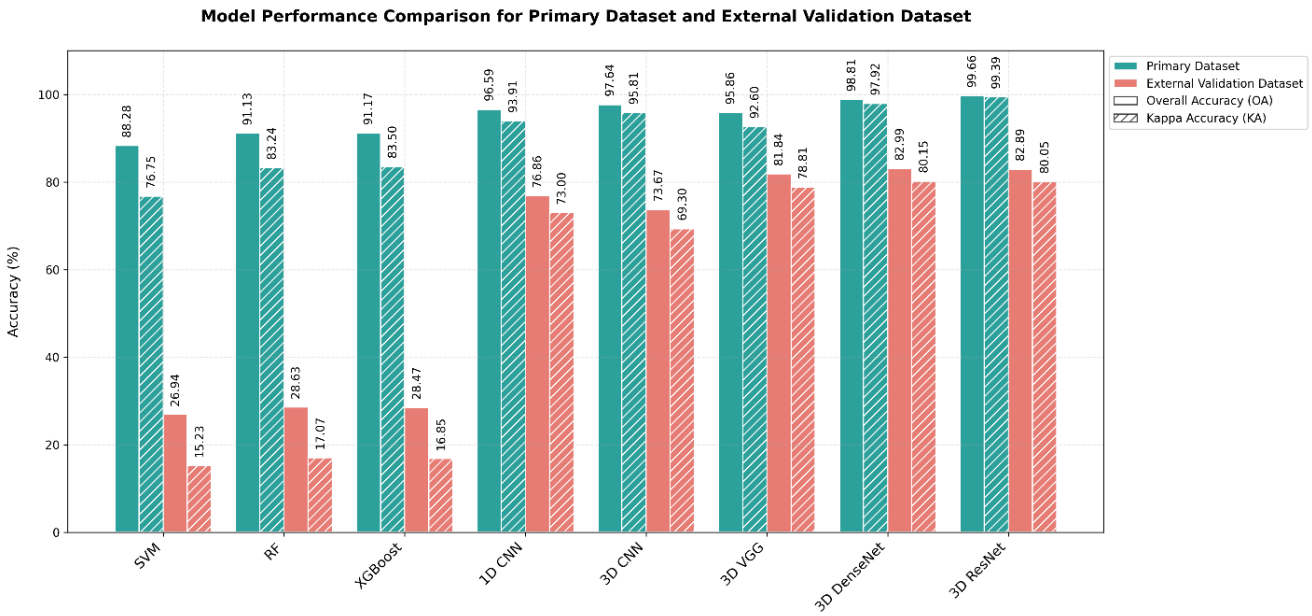

Figure 5. Comparison of model performance (OA and KA) for primary dataset and external validation dataset.

Although 3D ResNet model outperformed both ML models and DL models on the primary dataset, it achieved slightly lower OA (82.89%) and KA (80.05%) than 3D DenseNet for the external validation dataset. Based on the results, the generalizability of the models is clearly impacted when evaluated on the external validation dataset, as seen by the decrease in performance across most models in terms of KA. It also suggests that while DL models like 3D ResNet offer high accuracy, they may require additional strategies such as domain adaptation for better generalization to new areas.

In line with theoretical predictions, 1D CNN has a slightly lower OA and KA than 3D CNN for primary dataset since it only has the ability of capturing the spectral features. Similar results were also reported in other research involving LULC classification using Indian Pines and Wuhan University datasets (Liu et al., 2023). However, 1D CNN has better generalization capability compared to 3D CNN which is probably due to its simpler architecture. There is a significant difference between the classification performance of SVM compared to the other classifiers which is probably due to severe effects of imbalanced datasets to the SVM margin computation.

For primary dataset, all models performed well on most classes with high precision, recall and F1-score (Table 3). However, ML models struggled with forest and other vegetation classes, displaying significant misclassifications. This suggests that ML models may have difficulty differentiating between spectrally similar vegetation types, possibly due to overlapping spectral or spatial characteristics. In contrast, DL models demonstrated improved performance across all classes, especially for challenging vegetation features, indicating their ability to capture more complex feature representations.

DOI:https//doi.org/10.22452/mjs.vol44no4.3
Malaysian Journal of Science 44(4): 18-30 (December 2025)

Table 3. Comparison of model performance (Precision, Recall, F1-score) for primary dataset.

		Classifier							
Metric	**Map Class**	**SVM**	**RF**	**XGBoost**	**1D CNN**	**3D CNN**	**3D VGG**	**3D Dense Net**	**3D ResNet**
Precision	Water bodies	0.997	**1.000**	**1.000**	**1.000**	**1.000**	0.999	**1.000**	**1.000**
	Built-up	0.964	0.998	0.998	**1.000**	**1.000**	**1.000**	**1.000**	**1.000**
	Bare soil	0.964	0.999	0.999	**1.000**	**1.000**	0.999	**1.000**	**1.000**
	Forest	0.028	0.760	0.720	0.897	0.916	0.900	0.918	0.986
	Grass	0.962	0.992	0.995	**1.000**	**1.000**	0.998	**1.000**	**1.000**
	Oil palm	0.852	0.893	0.899	0.967	0.977	0.962	0.995	0.997
	Other vegetations	0.000	0.661	0.611	0.839	0.916	0.749	0.933	0.989
Recall	Water bodies	0.944	**1.000**	**1.000**	**1.000**	**1.000**	**1.000**	**1.000**	**1.000**
	Built-up	0.962	0.997	0.997	0.999	**1.000**	0.998	**1.000**	**1.000**
	Bare soil	0.983	0.999	0.999	**1.000**	**1.000**	**1.000**	**1.000**	**1.000**
	Forest	0.000	0.315	0.342	0.766	0.844	0.703	0.971	0.982
	Grass	0.986	0.994	0.996	**1.000**	**1.000**	**1.000**	**1.000**	**1.000**
	Oil palm	0.996	0.983	0.976	0.985	0.989	0.981	0.987	0.998
	Other vegetations	0.000	0.275	0.330	0.795	0.852	0.785	0.958	0.975
F1-score	Water bodies	0.970	**1.000**	**1.000**	**1.000**	**1.000**	**1.000**	**1.000**	**1.000**
	Built-up	0.963	0.997	0.998	**1.000**	**1.000**	0.999	**1.000**	**1.000**
	Bare soil	0.973	0.999	0.999	**1.000**	**1.000**	**1.000**	**1.000**	**1.000**
	Forest	0.000	0.445	0.464	0.826	0.879	0.789	0.944	0.984
	Grass	0.974	0.993	0.996	**1.000**	**1.000**	0.999	**1.000**	**1.000**
	Oil palm	0.918	0.936	0.936	0.976	0.983	0.971	0.991	0.997
	Other vegetations	0.000	0.388	0.429	0.817	0.883	0.767	0.945	0.982

Based on the validation results in Table 4, ML model performance dropped significantly across most classes, indicating the struggle with generalization to new geographic areas and environmental conditions. In contrast, DL models achieved strong generalization for all classes with only a slight decrease in accuracy. This highlights the importance for model robustness in different geographical settings.

DOI:https//doi.org/10.22452/mjs.vol44no4.3
Malaysian Journal of Science 44(4): 18-30 (December 2025)

Table 4. Comparison of model performance (Precision, Recall, F1-score) for external validation dataset.

		Classifier							
Metric	**Map Class**	**SVM**	**RF**	**XGBoost**	**1D CNN**	**3D CNN**	**3D VGG**	**3D Dense Net**	**3D ResNet**
Precision	Water bodies	**1.000**	0.000	0.000	0.715	0.733	0.821	**1.000**	**1.000**
	Built-up	**1.000**	0.586	0.583	0.915	0.882	0.953	0.960	0.957
	Bare soil	0.303	0.091	0.139	0.943	0.693	0.950	0.983	0.977
	Forest	0.000	0.698	0.639	0.907	0.920	0.923	0.935	0.970
	Grass	0.062	0.630	0.000	0.998	0.971	0.998	0.985	0.971
	Oil palm	0.192	0.201	0.206	0.512	0.489	0.551	0.487	0.483
	Other vegetations	0.000	0.015	0.011	0.738	0.772	0.767	0.697	0.795
Recall	Water bodies	0.017	0.000	0.000	0.994	0.780	**1.000**	**1.000**	0.999
	Built-up	0.577	0.527	0.493	0.998	**1.000**	**1.000**	**1.000**	**1.000**
	Bare soil	0.336	0.095	0.153	0.541	0.583	0.709	0.915	0.923
	Forest	0.000	0.541	0.515	0.819	0.748	0.773	0.782	0.673
	Grass	0.015	0.010	0.000	0.692	0.727	0.797	0.735	0.738
	Oil palm	**1.000**	0.891	0.883	0.904	0.922	0.926	0.837	0.940
	Other vegetations	0.000	0.001	0.001	0.454	0.441	0.542	0.528	0.526
F1-score	Water bodies	0.033	0.000	0.000	0.831	0.756	0.902	**1.000**	0.999
	Built-up	0.731	0.555	0.534	0.955	0.937	0.976	0.980	0.978
	Bare soil	0.318	0.093	0.146	0.687	0.633	0.812	0.947	0.949
	Forest	0.000	0.609	0.570	0.861	0.825	0.841	0.852	0.794
	Grass	0.024	0.019	0.000	0.817	0.832	0.886	0.842	0.839
	Oil palm	0.322	0.328	0.334	0.653	0.639	0.691	0.615	0.638
	Other vegetations	0.000	0.001	0.003	0.562	0.561	0.636	0.600	0.633

In Table 5, ML models had significantly shorter processing times compared to DL models, with SVM taking only 1.8 minutes for primary dataset and 0.2 minutes for external dataset. In contrast, 3D models require much longer processing times, with 3D DenseNet being the most computationally expensive (1642.8 minutes for primary dataset). These results highlight the trade-off between model complexity and computational efficiency, where more complex 3D models demand more resources. In comparison to 3D VGG and 3D DenseNet, 3D ResNet was the most computationally efficient in LULC mapping for both primary dataset (490.2 minutes) and validation dataset (3.6 minutes).

Table 5. Total processing time for primary dataset and external validation dataset.

	Total Processing Time (min)	
Model	**Primary Dataset**	**External Validation Dataset**
SVM	1.8	0.2
RF	385.2	17.4
XGBoost	41.4	20.2
1D CNN	444.0	1.4
3D CNN	403.2	1.2
3D VGG	1101.6	11.6
3D DenseNet	1642.8	23.3
3D ResNet	490.2	3.6

DOI:https//doi.org/10.22452/mjs.vol44no4.3
Malaysian Journal of Science 44(4): 18-30 (December 2025)

Land Cover Classification Map

Based on Figure 6 and Figure 7, all models are capable of classifying land cover classes like water bodies, built-up regions, bare soil, and grass with high accuracy due to their distinct spectral signatures. Despite both rivers and ponds being categorized under the same class, the ML models could only classify rivers accurately and not ponds. Misclassifications often occurred between ponds and built-up areas, likely due to the similar spectral signatures of herbaceous vegetation in the ponds and features of the built-up areas, as well as their proximity to each other. It appears that 3D ResNet and 3D DenseNet have the least misclassifications between ponds and built-up areas, signifying their greater ability in capturing the subtle variations in spectral and spatial features.

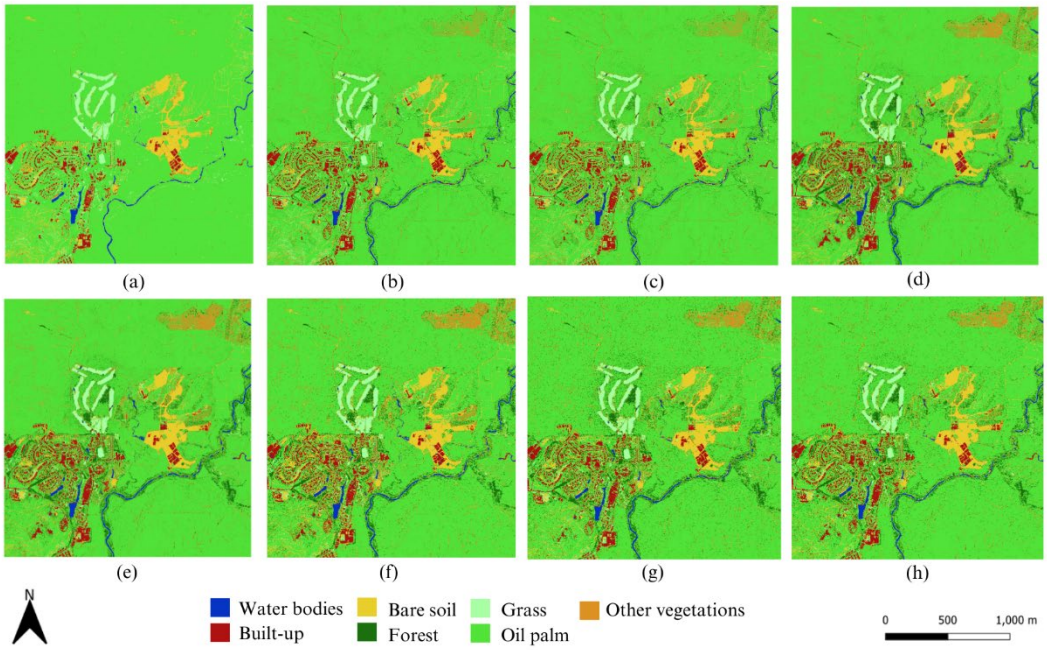

Figure 6. Classification results of primary dataset with (a) SVM; (b) RF; (c) XGBoost; (d) 1D CNN; (e) 3D CNN; (f) 3D VGG; (g) 3D DenseNet; (h) 3D ResNet.

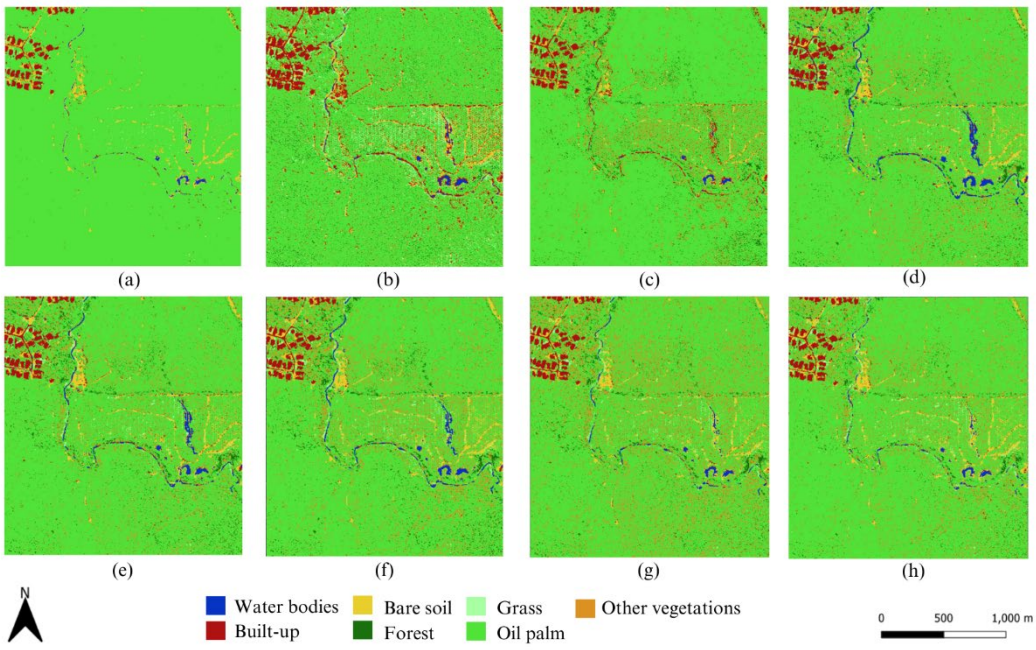

Figure 7. Classification results of external validation dataset with (a) SVM; (b) RF; (c) XGBoost; (d) 1D CNN; (e) 3D CNN; (f) 3D VGG; (g) 3D DenseNet; (h) 3D ResNet.

DOI:https//doi.org/10.22452/mjs.vol44no4.3
Malaysian Journal of Science 44(4): 18-30 (December 2025)

High intra-class variation was observed in built-up, oil palm, and other vegetation samples. Built-up areas varied due to material and structural differences, while oil palm variation resulted from planting density and age, affecting spectral and textural patterns. All models classified built-up and oil palm samples well, but other vegetation samples were more challenging due to mixed patterns. Accurate classification of other vegetation was achieved with 3D ResNet and 3D DenseNet. Despite good intra-class similarity, classifying forest samples was challenging for ML models, which struggled to distinguish forest from oil palm. DL models, especially 3D ResNet and 3D DenseNet performed better as CNNs can extract vegetation features effectively.

McNemar's Test

McNemar's test revealed critical insights into model robustness for primary dataset (Table 6) and external validation dataset (Table 7). 3D ResNet and 3D DenseNet demonstrated consistent superiority (p<0.05) over ML models across datasets, outperforming other DL models. While 1D CNN showed significant advantages over ML models (p<0.05), its generalizability was less robust on external data compared to 3D ResNet and 3D DenseNet. Similarly, both 3D CNN and 3D VGG displayed inconsistencies in model performance across datasets. The variability observed in simpler (1D CNN) or less optimized 3D architectures (3D CNN, 3D VGG) further emphasizes the critical role of architectural design in ensuring generalizability. 3D ResNet evidently achieved comparable classification performance to 3D DenseNet (p = 1.000) with shorter processing times. These findings highlighted the reliability and practical efficiency of 3D ResNet, making it suitable for LULC applications in resource-constrained environments.

Table 6. McNemar's test results for primary dataset.

	SVM	RF	XGBoost	1D CNN	3D CNN	3D VGG	3D DenseNet	3D ResNet
SVM	-	0.134	0.248	0.023*	0.013*	0.023*	0.001*	0.004*
RF		-	0.248	0.044*	0.041*	0.617	0.041*	0.023*
XGBoost			-	0.041*	0.023*	0.074	0.001*	0.004*
1D CNN				-	0.48	0.480	0.074	0.134
3D CNN					-	0.077	0.248	0.248
3D VGG						-	0.023*	0.023*
3D DenseNet							-	1.000
3D ResNet								-

Table 7. McNemar's test results for external validation dataset.

	SVM	RF	XGBoost	1D CNN	3D CNN	3D VGG	3D DenseNet	3D ResNet
SVM	-	0.724	0.724	0.027*	0.039*	0.006*	0.003*	0.001*
RF		-	0.773	0.009*	0.027*	0.003*	0.023*	0.001*
XGBoost			-	0.027*	0.070	0.008*	0.016*	0.009*
1D CNN				-	0.617	0.617	0.617	0.617
3D CNN					-	0.480	0.480	0.248
3D VGG						-	1.000	1.000
3D DenseNet							-	1.000
3D ResNet								-

Limitations and Challenges

The superiority of 3D ResNet model comes with computational trade-offs, which may limit real-time or deployment for large-scale LULC mapping. To overcome this, transfer learning from pre-trained 2D models via DEWT technique was integrated to reduce training time. Although this approach alleviated some computational burden, the reliance on powerful hardware highlights the possible limited accessibility to powerful GPUs. These computational demands influenced model selection as more complex architectures could improve accuracy but with the cost of increased processing time and resource requirements.

Further optimization like model pruning and quantization could further reduce computational demands. While these methods were not explored in this study, they represent practical ways to balance accuracy and efficiency. Aside from that, cloud-based distributed computing could enable scalable model training across multiple devices, improving accessibility for resource-constrained environments. Techniques like knowledge distillation (Hinton et al., 2015) or mixed-precision training (Micikevicius et al., 2018) could also enhance computational efficiency. Alternative setups such as edge computing could provide a practical solution for deploying DL models in large-scale applications. Future research could explore these strategies to improve the feasibility and scalability of 3D models for LULC mapping.

Dataset imbalances were addressed partially via SKCV but it remains a concern, especially for models like SVM which are sensitive to imbalanced data. While SKCV ensures that each fold

DOI:https//doi.org/10.22452/mjs.vol44no4.3
Malaysian Journal of Science 44(4): 18-30 (December 2025)

represents the class distribution, this may not fully mitigate bias in model evaluation. Other technique like oversampling is a common approach in which the minority classes are replicated randomly until a balanced dataset distribution is achieved. On the other hand, undersampling reduces instances from the majority classes. As for cost-sensitive learning, this works by placing a higher misclassifying cost for the minority classes without altering the original dataset distribution. Moreover, synthetic data generation like Synthetic Minority Oversampling Technique (SMOTE) could create new samples for the minority classes, further improving model generalization. Combining these techniques with SKCV could potentially enhance model performance and reduce bias.

The lack of interpretability in DL models also poses significant challenges in domains like LULC classification. Understanding how a model arrives at its predictions is vital for enhancing interpretability (Li et al., 2022). Methods like Class Activation Mapping (CAM) and SHapley Additive exPlanations (SHAP) can aid in prediction explanation and visualizations. Future work could focus on integrating these techniques to improve transparency in DL applications for LULC classification.

Future research could also focus on utilizing deeper 3D variants of ResNet (e.g. 3D ResNet-50) architectures to enhance classification results. Deeper 3D ResNet model could potentially work more effectively than the current 3D ResNet-18 model since it will be able to capture more intricate details from the features. Although recently developed hybrid models like Vision Transformer (ResNet-ViT) is not widely adopted in remote sensing field, it also shows great potential as it can capture both local and global information from the image. Due to cost and data availability constraints, we validated our model using an existing dataset from the same satellite system but with a different location. Future work can also focus on model generalizability to a completely different geographical area or satellite dataset such as Sentinel-2. This would help with evaluation of model transferability while considering cost-effective alternatives.

4. Conclusion

In this research, the possible application of pre-trained 3D ResNet for multispectral land use and land cover (LULC) classification is highlighted by its great capability of capturing spectral-spatial features with high accuracy. The results showed that 3D ResNet outperformed other models by achieving the highest OA of 99.66% and KA of 99.39% on the primary dataset. While its performance on the external validation dataset (OA: 82.89%, KA: 80.05%) was slightly lower than that of the 3D DenseNet, it showed great efficiency with processing times of 490.2 minutes for primary dataset and only 3.6 minutes for validation dataset. McNemar's test results further showed consistent significant statistical differences (p<0.05) in classification performance between 3D ResNet and 3D DenseNet with the other models. Overall, this research contributes to the improvement of multispectral LULC classification in terms of accuracy and efficiency using advanced DL model integrated with transfer learning technique.

5. Acknowledgement

The researchers would like to thank the Ministry of Higher Education (MOHE), Malaysia for its support and resources through the Long-Term Research Grant Scheme (LRGS) of the Malaysian Research University Network (MRUN). This project is being undertaken under the research programme: 'A Big Data Analytics Platform for Optimizing Oil Palm Yield Via Breeding by Design (Grant No: 203.PKOMP.6770007)' with specific project: 'Geoinformatics Data for Palm Oil Yield Prediction Using Machine Learning (Vote No: 6300268-10801)'. Also, the authors wish to acknowledge the expertise provided by the team from FGV R&D Sdn Bhd.

6. References

Abdi, A. M. (2020). Land cover and land use classification performance of machine learning algorithms in a boreal landscape using Sentinel-2 data. *GIScience & Remote Sensing*, *57*(1), 1–20. https://doi.org/10.1080/15481603.2019.1650447

Cervantes, J., Garcia-Lamont, F., Rodríguez-Mazahua, L., & Lopez, A. (2020). A comprehensive survey on support vector machine classification: Applications, challenges and trends. *Neurocomputing*, *408*, 189–215. https://doi.org/10.1016/j.neucom.2019.10.118

D, E., & Bhavani, N. P. G. (2023). An Effective DNN Based ResNet Approach for Satellite Image Classification. *2023 4th International Conference on Smart Electronics and Communication (ICOSEC)*, 1055–1062. https://doi.org/10.1109/ICOSEC58147.2023.10276330

Ebrahimi, A., Luo, S., & Chiong, R. (2020). Introducing Transfer Learning to 3D ResNet-18 for Alzheimer's Disease Detection on MRI Images. *2020 35th International Conference on Image and Vision Computing New Zealand (IVCNZ)*, 1–6. https://doi.org/10.1109/IVCNZ51579.2020.9290616

Firat, H., Asker, M. E., Bayindir, M. İ., & Hanbay, D. (2023). 3D residual spatial–spectral convolution network for hyperspectral remote sensing image classification. *Neural Computing and Applications*, *35*(6), 4479–4497. https://doi.org/10.1007/s00521-022-07933-8

He, K., Zhang, X., Ren, S., & Sun, J. (2015). *Deep Residual Learning for Image Recognition* (arXiv:1512.03385). arXiv. https://doi.org/10.48550/arXiv.1512.03385

Hinton, G., Vinyals, O., & Dean, J. (2015). Distilling the Knowledge in a Neural Network (arXiv:1503.02531). arXiv. https://doi.org/10.48550/arXiv.1503.02531

Huang, G., Liu, Z., Maaten, L. van der, & Weinberger, K. Q. (2018). *Densely Connected Convolutional Networks* (arXiv:1608.06993). arXiv. https://doi.org/10.48550/arXiv.1608.06993

DOI:https//doi.org/10.22452/mjs.vol44no4.3
Malaysian Journal of Science 44(4): 18-30 (December 2025)

Jombo, S., Adam, E., Byrne, M. J., & Newete, S. W. (2020). Evaluating the capability of Worldview-2 imagery for mapping alien tree species in a heterogeneous urban environment. *Cogent Social Sciences*, *6*(1), 1754146. https://doi.org/10.1080/23311886.2020.1754146

Jozdani, S. E., Johnson, B. A., & Chen, D. (2019). Comparing Deep Neural Networks, Ensemble Classifiers, and Support Vector Machine Algorithms for Object-Based Urban Land Use/Land Cover Classification. *Remote Sensing*, *11*(14), Article 14. https://doi.org/10.3390/rs11141713

Kingma, D. P., & Ba, J. (2017). Adam: A Method for Stochastic Optimization (arXiv:1412.6980). arXiv. https://doi.org/10.48550/arXiv.1412.6980

Micikevicius, P., Narang, S., Alben, J., Diamos, G., Elsen, E., Garcia, D., Ginsburg, B., Houston, M., Kuchaiev, O., Venkatesh, G., & Wu, H. (2018). Mixed Precision Training (arXiv:1710.03740). arXiv. https://doi.org/10.48550/arXiv.1710.03740

Li, X., Xiong, H., Li, X., Wu, X., Zhang, X., Liu, J., Bian, J., & Dou, D. (2022). Interpretable deep learning: Interpretation, interpretability, trustworthiness, and beyond. Knowledge and Information Systems, 64(12), 3197–3234. https://doi.org/10.1007/s10115-022-01756-8

Liu, J., Wang, T., Skidmore, A., Sun, Y., Jia, P., & Zhang, K. (2023). Integrated 1D, 2D, and 3D CNNs Enable Robust and Efficient Land Cover Classification from Hyperspectral Imagery. *Remote Sensing*, *15*(19), Article 19. https://doi.org/10.3390/rs15194797

Noh, S.-H. (2021). Performance Comparison of CNN Models Using Gradient Flow Analysis. *Informatics*, *8*(3), 53. https://doi.org/10.3390/informatics8030053

Shaharum, N. S. N., Shafri, H. Z. M., Ghani, W. A. W. A. K., Samsatli, S., Al-Habshi, M. M. A., & Yusuf, B. (2020). Oil palm mapping over Peninsular Malaysia using Google Earth Engine and machine learning algorithms. Remote Sensing Applications: Society and Environment, 17, 100287. https://doi.org/10.1016/j.rsase.2020.100287

Sheykhmousa, M., Mahdianpari, M., Ghanbari, H., Mohammadimanesh, F., Ghamisi, P., & Homayouni, S. (2020). Support Vector Machine Versus Random Forest for Remote Sensing Image Classification: A Meta-Analysis and Systematic Review. *IEEE Journal of Selected Topics in Applied Earth Observations and Remote Sensing*, *13*, 6308–6325. IEEE Journal of Selected Topics in Applied Earth Observations and Remote Sensing. https://doi.org/10.1109/JSTARS.2020.3026724

Simonyan, K., & Zisserman, A. (2015). *Very Deep Convolutional Networks for Large-Scale Image Recognition* (arXiv:1409.1556). arXiv. https://doi.org/10.48550/arXiv.1409.1556

Tong, X.-Y., Xia, G.-S., Lu, Q., Shen, H., Li, S., You, S., & Zhang, L. (2020). Land-cover classification with high-resolution remote sensing images using transferable deep models. *Remote Sensing of Environment*, *237*, 111322. https://doi.org/10.1016/j.rse.2019.111322

Thölke, P., Mantilla-Ramos, Y.-J., Abdelhedi, H., Maschke, C., Dehgan, A., Harel, Y., Kemtur, A., Mekki Berrada, L., Sahraoui, M., Young, T., Bellemare Pépin, A., El Khantour, C., Landry, M., Pascarella, A., Hadid, V., Combrisson, E., O'Byrne, J., & Jerbi, K. (2023). Class imbalance should not throw you off balance: Choosing the right classifiers and performance metrics for brain decoding with imbalanced data. NeuroImage, 277, 120253. https://doi.org/10.1016/j.neuroimage.2023.120253

Vali, A., Comai, S., & Matteucci, M. (2020). Deep Learning for Land Use and Land Cover Classification Based on Hyperspectral and Multispectral Earth Observation Data: A Review. *Remote Sensing*, *12*(15), 2495. https://doi.org/10.3390/rs12152495

Wang, J., Bretz, M., Dewan, M. A. A., & Delavar, M. A. (2022). Machine learning in modelling land-use and land cover-change (LULCC): Current status, challenges and prospects. *Science of The Total Environment*, *822*, 153559. https://doi.org/10.1016/j.scitotenv.2022.153559

DOI:https//doi.org/10.22452/mjs.vol44no4.3
Malaysian Journal of Science 44(4): 18-30 (December 2025)

MALAYSIAN JOURNAL OF SCIENCE
MJS
ISSN 1394-3065

Regular Issue

Malaysian Journal of Science 44 (4): 31-39 (December 2025) https://mjs.um.edu.my

Sustainability of Agricultural Land Management in Critical Areas in Malang Regency, Indonesia

Anisa Zairina[1ab]*, Soemarno[2c], Arief Rachmansyah[3d], Bagyo Yanuwiadi[4e], Gettik Andri Purwanti[5b], Amin Setyo Leksono[6e], Saiful Arif Abdullah[7ef]

Abstract: This study aims to analyze the status of sustainable management of agricultural land in Pujon and Ngantang, East Java. This research was conducted in Pujon and Ngantang Subdistricts, Malang Regency, East Java, Indonesia. Data was obtained from a social survey by distributing questionnaires to 125 respondents. Respondents were purposely selected from locations prone to landslides. Of the 125 questionnaires distributed, 101 contained valid data. Respondents in this study consisted of farmers, landowners, and communities around landslide-prone lands. Data were analyzed using multidimensional scaling analysis. The sustainability status of landslide-prone land management on the social dimension was 80-100%, indicating very sustainable, while the sustainability index for other dimensions was 50-70% (moderately sustainable). The sustainability index for the ecological and technological dimensions had an exact value of 63.44%, whereas the economic dimension had a value of 63.23%. Attributes of the ecological dimension that significantly affect the sustainability of this dimension were the level of pest attacks on agricultural land, the influence of vegetation, and the slope of the land; for the economic dimension, attributes include opportunities for other sources of income, the stability of crop prices, and the availability of places to sell produce, while the attributes of the technological dimension include knowledge of water management, agricultural land technology, and landslide determination.

Keywords: *Critical land, sustainability, ecological dimension, social dimension, economic dimension, technological dimension.*

1. Introduction

Nearly half of the total terrestrial land in Indonesia undergoes land degradation. Natural events and human activities can affect land degradation. Unfavorable physical factors in the region, such as heavy rainfall, steep slopes, and soil prone to erosion, are among the key natural factors affecting land degradation (Kubangun et al., 2014; Leksono & Zairina, 2022). Anthropogenic pressures, such as converting forests into agriculture and residential areas, may lead to land degradation. A previous study shows that population growth and behavior are important factors driving anthropogenic pressure (Iswahyudi, 2017). Critical land experiences significant degradation, losing its ability to function as a productive agricultural area or as a vital part of the environment. It is characterized by a decline in physical, chemical, and biological soil properties, often resulting from unsustainable land management approaches. This degradation can cause reduced agricultural productivity, environmental harm, and even affect water management (Leksono & Zairina, 2022).

Critical land has lost its ability to support the hydrological cycle and land productivity. It can disrupt the balance of the watershed and soil ecosystem. Land degradation can negatively affect soil fertility, decrease the amount of water available during the dry season, and increase the risk of flooding during the rainy season (Rosyada et al., 2015). Reduced soil quality can affect agricultural output and food supply (Hossain et al., 2020; AbdelRahman et al., 2022). Land degradation can progress to critical land if land use management neglects soil and water conservation.

In some areas with limited land availability for agricultural purposes, critical land is inevitably used for agroforestry or agricultural cultivation due to rapidly decreasing arable land resources. Utilizing critical land requires appropriate methods and technology. The development of community forest farming with an agroforestry pattern can be implemented on land with a reasonably steep slope, ranging from 15% to 25%. Adopting an agroforestry system may be the best method to maintain land stability. Therefore, the community should enhance its knowledge and understanding regarding efforts to manage its critical lands to reduce production risks.

Critical land control necessitates appropriate prevention and mitigation strategies. These plans must be supported by thorough studies of restrictions on land use for cultivating agricultural crops, re-vegetation using environmentally friendly technology, and community involvement in sustainable land management. The community is the primary actor in handling and controlling potentially degraded soil. The community's capacity to hold and

Authors information:
[a]Environmental Science Program, Postgraduate School, Brawijaya University, Malang, INDONESIA. E-mail: anisa.zairina85@gmail.com[1]
[b]Institut Pertanian Malang, Malang, INDONESIA, E-mail: anisa.zairina85@gmail.com[1], getikandri1976@gmail.com[5]
[c]Department of Soil Science, Faculty of Agriculture, Brawijaya University, Malang, INDONESIA. E-mail: smno@ub.ac.id[2]
[d]Department of Civil Engineering, Faculty of Engineering, Brawijaya University, Malang, INDONESIA. E-mail: ariefftub@yahoo.com[3]
[e]Department of Biology, Faculty of Mathematics and Natural Sciences, Brawijaya University, Malang, INDONESIA. E-mail: yanuwiadi@ub.ac.id[4]; amin28@ub.ac.id[6]; saiful@ukm.edu.my[7]
[f]Institut Alam Sekitar dan Pembangunan (Lestari), Universiti Kebangsaan Malaysia, MALAYSIA. E-mail: saiful@ukm.edu.my[7]
*Corresponding Author: anisa.zairina85@gmail.com

Received: March, 2024
Accepted: April, 2024
Published: December, 2025

DOI:https//doi.org/10.22452/mjs.vol44no4.4
Malaysian Journal of Science 44(4): 31-39 (December 2025)

control potentially degraded lands determine success in landslide mitigation. Thus, community knowledge and skills in sustainable land management are crucial in preventing and mitigating landslides (Holcombe et al., 2013).

Sustainable land management, by integrating ecological, technological, social, and economic dimensions, can protect land and preserve soil quality. The balance of all existing dimensions can improve land use efficiency to support the provision of food sources, community income, and economic development (Liu et al., 2020). Research on the sustainable management of landslide-prone lands still needs to be conducted. Previous studies have focused on safety, risk assessment, monitoring and developing map for land degradation mitigation (McGowran & Donovan, 2021; Baczynski & Bar, 2017; Masruroh et al., 2023). Sustainable disaster risk management research often attempts to integrate technical and social aspects. In contrast, this research intends to identify the status of sustainable management using ecological, technological, social, and economic dimensions. Therefore, this study aims to analyze the status of sustainable management of landslide-prone lands in Pujon and Ngantang, East Java.

2. Materials and Methods

This research was conducted in the Pujon and Ngantang sub-regencies (112° 22' 9'' to 122°28' 92'' E and latitude 7° 49' 37" to 7°56' 03" S), Malang Regency, East Java, Indonesia. The study sites were included on the slopes of the Arjuno volcanic complex (Noronha & Arifianto, 2019; Rachmansyah et al., 2021). The research location has an altitude of 870 to 1,100 above sea level. Over 35% of the area is prone to landslides.

Data Collection

Two villages with a high incidence of landslides were selected from the research area. The two villages have 2611 households. Research data was obtained from a social survey by distributing questionnaires. Respondents in this study consisted of farmers, landowners, and communities around landslide-prone lands. Respondents were selected using snowball sampling, starting from village officials, community leaders, the heads of farmer groups, and farmer representatives. The number of respondents is determined using the Slovin formula as follows.

$$n = \frac{N}{1 + N(e))^2}$$

Where n = samples
N = population
e = 0.1

with a population of 2611, the results of the Slovin formula calculation yielded a sample of 96 respondents. The questionnaires were distributed to 125 respondents to meet the minimum sample size. The questions in the questionnaire were categorized into ecological, economic, social, and technological aspects (dimensions). Before being used to collect data, the questionnaire was administered to 30 respondents to assess the validity of the questions. The initial questionnaire contained 56 questions, consisting of 14 questions for each dimension. The test results showed nine invalid questions, including seven in ecological, eight in economic, two in social, and seven in technological dimensions. Therefore, those invalid questions were removed from the questionnaire. The final questionnaire consisted of seven ecological aspects, six economic aspects, 12 social aspects, and seven technological aspects (Table 1).

DOI:https//doi.org/10.22452/mjs.vol44no4.4
Malaysian Journal of Science 44(4): 31-39 (December 2025)

Table 1. List of valid questions among ecology, economy, social and technology

Dimensions	Attributes
Ecology	1. The degree of influence of the slope level of the land on the vulnerability of managed land
	2. The degree of influence of the steep slope of the land on agricultural production
	3. The influence of ground movement on the vulnerability of agricultural land
	4. The level of influence of landslides on the vulnerability of agricultural land
	5. The level of pest attacks on agricultural land
	6. The influence of vegetation on landslides
	7. The rainfall affects landslides
Economy	1. Stability the product price of the harvest
	2. The source of farming capital
	3. The existence of a market to sell produce
	4. The opportunities for getting additional income
	5. The harvest sales system
	6. The availability of financial institutions
Social	1. The socio-cultural values enforcement
	2. The existence of farmer groups
	3. The role of agricultural extension officers
	4. The counseling frequency
	5. The role of community leaders
	6. The community harmony
	7. The role of government institutions
	8. The role of private institutions
	9. The role of NGOs
	10. NGO oversight
	11. Government oversight
	12. The role of village institutions (village-owned enterprises, social institutions)
Technology	1. Understanding landslide risk
	2. Understanding slope repair
	3. Understanding slope monitoring
	4. Understanding water pumping
	5. Understanding water management
	6. Understanding the availability of agricultural land management technology
	7. Understanding the availability of pest control technology

Furthermore, the valid questionnaire was distributed to 125 participants. Of the 125 questionnaires distributed, 115 were returned, and 101 had valid data. Responses from participants were classified based on a Likert scale, with a score of 1 = strongly disagree, 2 = disagree, 3 = neutral, 4 = agree, 5 = strongly agree. To develop recommended strategies to improve the sustainability of agricultural land management in risky areas, a focus group discussion was convened. This discussion was attended by experienced farmers and the head of the neighborhood association. The discussion was held to formulate strategies based on current shortcomings and determine strategic priorities.

Data Analysis

Response data from respondents were analyzed using Multidimensional Scaling (MDS) analysis. The MDS is a rapid assessment method that allows for multidisciplinary evaluation. It is a multivariate statistical technique used to describe the structure of relationships between data objects based on their graphical similarities in a multidimensional space. The MDS is also a technique that can help researchers identify the key dimensions underlying the evaluation of objects from respondents. The final result of this analysis is a kite diagram that can describe the position of each dimension. Data analysis starts with validity and reliability tests. The R-squared value is the reliability coefficient of the calculation results. The minimum requirement is reliability if the R-squared value is higher than the R-squared from the table. The value of r is calculated with an error rate of 5%. The reliability test was performed using the product-moment correlation formula from Pearson. It was processed using multidisciplinary rapid assessment by the RAPFISH method (RAPFISH version 3.1). In the sustainability analysis, the measured dimensions are then used on a continuous to intermittent scale. The measure of sustainability regarding the position of the dimensions studied is determined based on the goodness of fit, with an indicator of stress ≤ 0.25. In addition, the analysis results were categorized into four groups based on the sustainability condition: 0-25 was not sustainable, 26-50 was less sustainable, 51-75 was moderately sustainable, and 76-100 was sustainable.

DOI:https//doi.org/10.22452/mjs.vol44no4.4
Malaysian Journal of Science 44(4): 31-39 (December 2025)

3. Result

Most respondents were between 30 and 50 years old (more than 80%). This age group was considered productive. The gender distribution was nearly equal, consisting of 52.48% males and 47.52% females. This proportion indicated that gender participation in this study was balanced. Most respondents held a secondary school education level (Table 2).

Table 2. Respondent Characteristics in Pujon and Ngantang, Malang Regency

Characteristics		N (%)
Age (year)	20–30	15.84
	30-40	40.59
	40-50	40.59
	>50	2.97
Gender	Male	52.48
	Female	47.52
Education	Elementary School	27.72
	Secondary School	62.38
	Bachelor/Diploma	9.90

Sustainability Analysis

The results of the MDS-Rapfish sustainability analysis of four dimensions, including Ecology, Economy, Social, and Technology, were presented in Table 2. Stress values for all dimensions ranged between 0.132 and 0.162, less than 0.25. Furthermore, R-Square values for all dimensions also showed values exceeding 0.90. These results indicated that the MDS analysis satisfies the goodness-of-fit criteria. Therefore, further analysis can be conducted using the available data (Table 3).

Table 3. Summary of MDS-Rapfish Analysis Results

Dimensions	*Stress (S)*	*R-Square (R)*
Ecology	0.161	0.939
Economy	0.162	0.943
Social	0.132	0.956
Technology	0.161	0.939

Ecological Dimension

The value of all attributes' ordination in MDS RAPFISH in the ecological dimension showed a score of 63.44%. The score fell within the range of 50-75, indicating it was moderately sustainable (Figure 1).

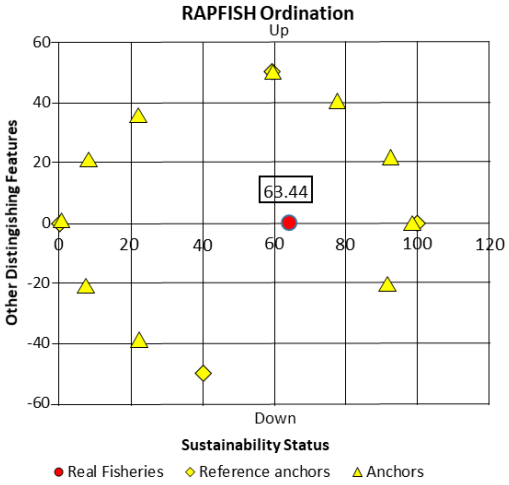

Figure 1. Ecological Dimension Sustainability Status

The ecological attributes that most significantly influence sustainability include the degree of pest infestation on agricultural land, vegetation cover, and land slope. These attributes exhibited higher influence values compared to others, indicating their critical role in sustainable land management. In contrast, attributes with relatively low impact included the perceived effect of land slope on the vulnerability of managed land, the influence of steep slopes on agricultural productivity, and the impact of ground movement on the susceptibility of agricultural land.

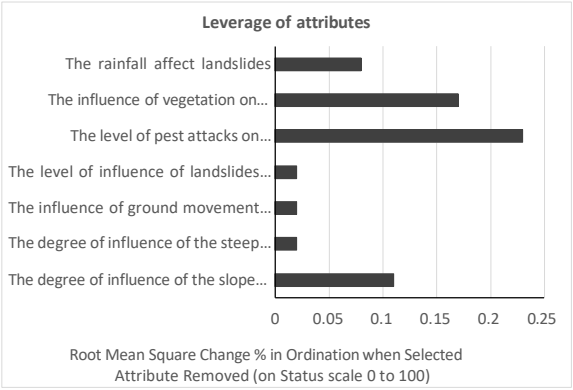

Figure 2. Ecological Dimension Attribute Sensitivity

DOI:https//doi.org/10.22452/mjs.vol44no4.4
Malaysian Journal of Science 44(4): 31-39 (December 2025)

Economic Dimension

The value of all attributes' ordination in MDS RAPFISH in the economic dimension demonstrated a score of 63.23%. The score was 50-75, which means it was moderately sustainable (Figure 3).

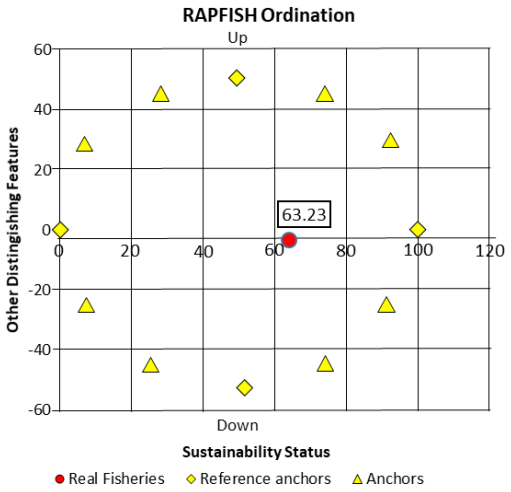

Figure 3. Economic Dimension Attribute Sensitivity

Based on Figure 4, the economic dimension's attributes that significantly affected this dimension's sustainability are opportunities to obtain alternative sources of income and the stability of the selling price of crops. This was indicated by the leverage value of these attributes, which was greater than that of the other attributes. In contrast, economic attributes that had low impacts were the harvest sales system and the source of farming capital.

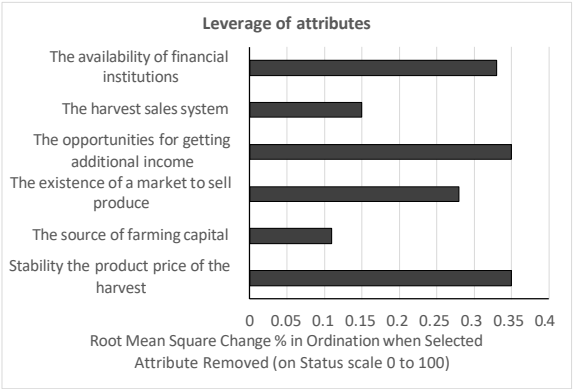

Figure 4. Attribute Sensitivity of the Economic Dimension

Social Dimension

MDS RAPFISH in the social dimension demonstrated a score of 87.18%. The score was in the range of 75-100, which means it was sustainable (Figure 5).

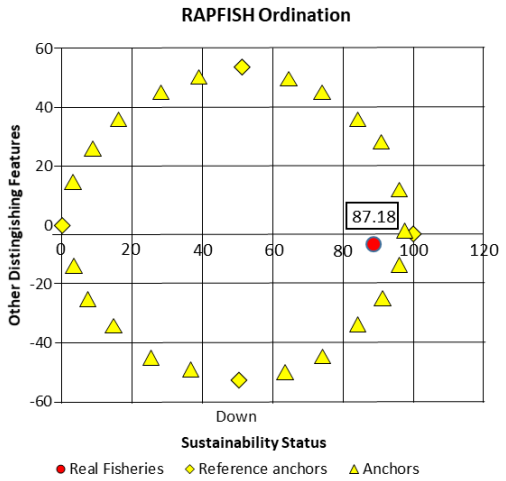

Figure 5. Social Dimension Sustainability Status

The social dimension attributes that greatly influence this dimension's sustainability include the frequency of outreach and the role of private institutions. This attribute has the highest influence values among the others (Figure 6). In contrast, social attributes that had low impacts were the existence of farmer groups and the role of agricultural extension officers.

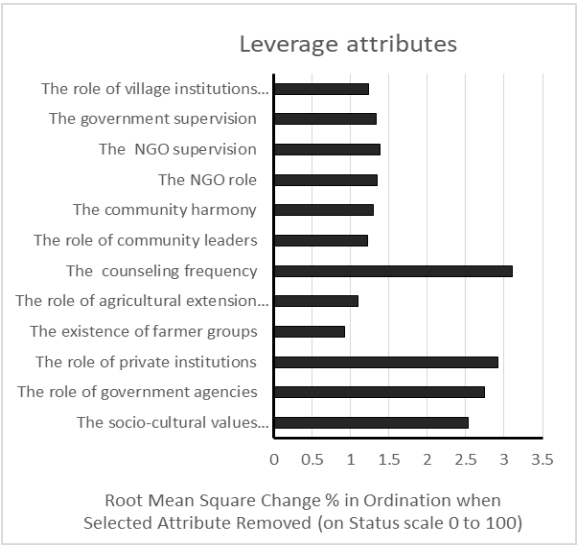

Figure 6. Attribute Sensitivity of the Social Dimension

Technology Dimension

The value of all attribute's ordination in MDS RAPFISH in the technological dimension demonstrated a score of 63.44%. The score was in the range of 50-75, which means it was moderately sustainable (Figure 7).

DOI:https//doi.org/10.22452/mjs.vol44no4.4
Malaysian Journal of Science 44(4): 31-39 (December 2025)

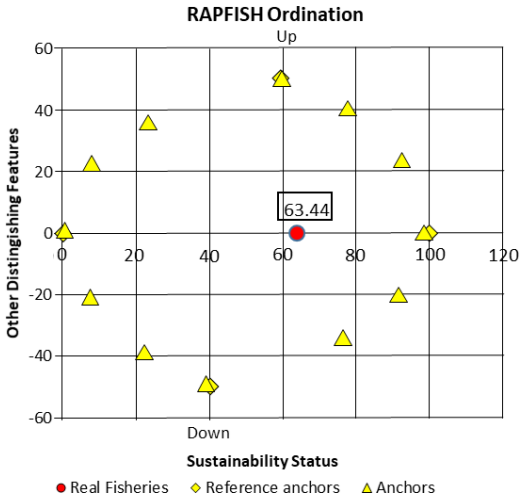

Figure 7. Sustainability Status of the Technology Dimension

Based on Figure 8, the attribute of the technology dimension that significantly influences the sustainability of this dimension is the comprehension of water handling. This is indicated by the impact value of this attribute, which is greater than that of the other attributes. In contrast, technology attributes that had low effects were understanding slope improvement, slope monitoring, and the water pumping system.

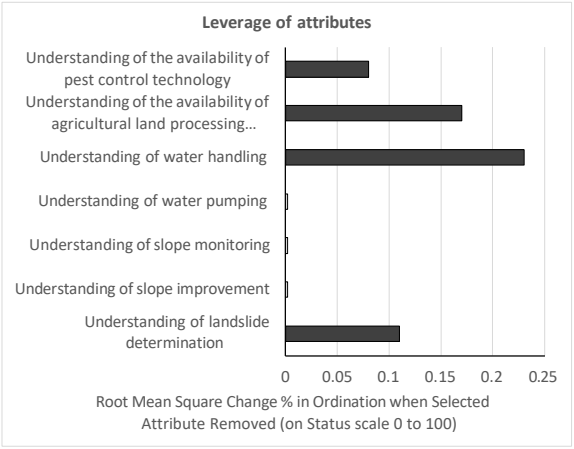

Figure 8. Attribute Sensitivity of the Technology Dimension

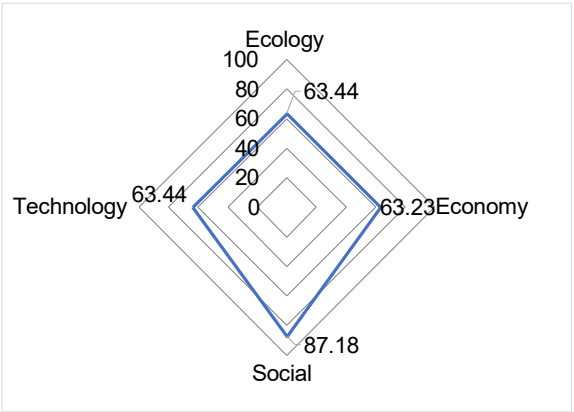

Figure 9. Sustainability Status Flyer Chart

Figure 9 shows a combination of the four dimensions of sustainability examined. Of the four existing dimensions, the social dimension had the highest value, while the economic dimension had the lowest. On average, the sustainability index value of all these dimensions was 69.32. This value suggests that there was still room for improving sustainable land management in landslide-prone areas (50–75). According to this diagram, the sustainability status improved if the index approached 100; on the other hand, if it approached or fell below 0, the sustainability status declined.

Based on the results, this study suggests four strategies as follows. These consist of enhancing farmers' knowledge and skills in managing and improving steep land areas through targeted training programs and the adoption of appropriate technologies to prevent and reduce land degradation; strengthening farmers' understanding of agricultural capital and marketing systems through training and collaborative initiatives, such as village cooperatives; establishing and supporting farmer groups to encourage knowledge sharing, collaboration, and collective action; and improving agricultural extension services by promoting best practices, including the selection of suitable crop varieties, effective cultivation techniques, and the application of post-harvest technologies (Table 4).

Table 4. Strategies to improve sustainability of agricultural land management in risky area

No	Strategies	Rank
1	Enhance farmers' knowledge and skills in managing and improving steep land areas through targeted training programs and the adoption of appropriate technologies to prevent and mitigate land degradation.	3
2	Strengthen farmers' understanding of agricultural capital and marketing systems through training and collaborative initiatives, such as village cooperatives.	4
3	Establish and support farmer groups to encourage knowledge sharing, collaboration, and collective action.	1
4	Improve agricultural extension services by promoting best practices, including the selection of suitable crop varieties, effective cultivation techniques, and the application of post-harvest technologies.	2

DOI:https//doi.org/10.22452/mjs.vol44no4.4
Malaysian Journal of Science 44(4): 31-39 (December 2025)

4. Discussion

The results suggest that the status of sustainable management of landslide-prone land in Malang Regency across all dimensions was 69.32. This value indicated that the management of landslide-prone land was moderately sustainable. However, there was an imbalance among the dimensions examined. The social dimension has the highest score (87.18), meaning it was sustainable. In contrast, the sustainability index for other dimensions ranges from 50 to 70% (moderately sustainable). The sustainability index of the ecological and technological dimensions has the same value of 63.44%, while the economic dimension has a value of 63.23%. The results indicated that several ecological attributes significantly influence the ecosystem. Those attributes were identified as the level of pest attacks on agricultural land, the influence of vegetation, and the slope of the land. The high level of public perception regarding the relationship between vegetation, land slope, and landslides shows that the public pays considerable attention to these factors. Apart from the two attributes above, pest attacks on agricultural land also cause concern among people. These results demonstrated that agricultural land is essential in supporting farmers' lives (livelihoods). Some attributes have small values, meaning that farmers still pay little attention to other attributes, for example, the influence of land slope on agricultural production, the influence of land movement on the vulnerability of agricultural land, the influence of landslides on the vulnerability of agricultural land, and the influence of rainfall on landslides. Weak public attention to those attributes may relate to three things. First, these do not directly influence people's lives. Second, these cannot be sensed directly (for example, the influence of ground movements). Third, these occur naturally, including rainfall and other physical factors.

The economic dimension is critical in supporting the community's capabilities in managing the potential of their resources, including land. Among the economic attributes, three have essential roles: the opportunity to obtain other sources of income, the stability of the selling price of agricultural products, and the availability of a place to sell the products that receive special attention from the community. Those attributes may directly influence the economic level of society. Other attributes, such as the source of farming capital, the harvest sales system, and the availability of financial institutions, have garnered less people's attention. There are three possible reasons for the lack of people's attention. First, financial institutions that can support capital are not accessible to the public. Farmers generally use agricultural business credit services at low interest rates. This kind of credit is available and accessible easily. Second, a harvest sales system has been established, so this is no longer a problem for farmers. Third, the community can manage the agricultural system with their capital.

In general, all attributes in the social dimension have high leverage scores. It means that the local community is satisfied with the attribute's performance. Questions related to social aspects were easy for respondents to understand. This relates to their daily lives, which require less external provision of information.

Attributes in the technological dimension that receive particular attention from the community include understanding water management, agricultural land technology, and identifying landslides. People consider this attribute to have a significant role in supporting their land management efforts. In contrast, some attributes that received low scores include understanding slope repair, slope monitoring, water pumping, and the availability of pest control technology. The technological dimension received a moderate sustainability score. To increase the value of this dimension, people's understanding of those attributes with low scores needs enhancement.

Land management activities include planning, controlling, and evaluating land use and natural resource performance (Izakovičová et al., 2018). Land management aims to adjust the optimal use of land resources, obtain maximum results, and maintain the sustainability of land resources (Anarbayev et al., 2023). Local people must implement appropriate agricultural and non-agricultural land management in landslide-prone areas. On agricultural land, good management practices include crop rotation, cover crops, strip planting, double planting, high-density planting, mulching, reforestation, and agroforestry. The density level requires attention because high density can increase the mechanical load on the slope, thereby increasing the risk of landslides (Suryatmojo & Soedjoko, 2008). In some places, mechanical actions are needed, including minimal tillage, tillage according to contours, making canals and channels according to contours, constructing terraces, and making water channels. Non-agricultural land management consists of improving natural or artificial carrying capacity, cutting water channel slopes, and enhancing water saturation. Land modifications, such as cutting slopes for road construction, housing, agriculture, and stone and sand mining, should be avoided (Hosenuzzaman et al., 2022).

Our findings indicate that key attributes across the three identified dimensions require improvement to enhance land management in the study region. To promote the sustainability of critical land use, this study proposes four strategic recommendations. First, the establishment and support of farmer groups should be prioritized to encourage knowledge sharing, collaboration, and collective action. These groups can expedite the dissemination of skills and best practices among farmers. Second, agricultural extension services must be strengthened by promoting best practices such as selecting suitable crop varieties, effective cultivation techniques, and adopting post-harvest technologies. Improving these services will empower farmers to adopt appropriate technologies and enhance land productivity. Third, farmers' capacity to manage and rehabilitate steep or degraded land should be strengthened through targeted training and the introduction of effective methods. This includes techniques to prevent erosion and landslides, such as terracing, contour farming, strategic vegetation planting, constructing concrete supports, and optimizing irrigation systems. In areas affected by landslides, revegetation with suitable plant species is vital for recovery. Fourth, farmers' understanding of agricultural finance and market access should be enhanced through training

DOI:https//doi.org/10.22452/mjs.vol44no4.4
Malaysian Journal of Science 44(4): 31-39 (December 2025)

and cooperative models, such as village cooperatives. Many farmers encounter challenges in accessing capital and securing fair returns from their agricultural activities.

Collectively, these four strategies aim to equip communities with the knowledge, tools, and support systems necessary to implement sustainable land management practices, contributing to environmentally sound and economically viable agricultural systems. This implementation aligns with efforts to achieve sustainable development goals (SDGs) through sustainable landscape management. Another study suggests that sustainable landscape management is based on a multifunctional land use system that fosters harmony between production and conservation objectives often faced (Wang et al., 2022). In hilly rural areas, agroforestry systems are considered to reverse land degradation by increasing efficiency through soil quality conservation (Sileshi et al., 2020). An agroforestry system is a landscape unit comprising land uses that combine agricultural and forestry components, including using trees for agriculture (Van Noordwijk, 2021). They represent prominent examples of agroecological land use systems. They represent unique examples of agroecological land use systems. Currently, agroforestry systems attract significant interest from local communities and are recognized as playing an important role in future land management. This system represents a suitable land management model as a form of agricultural transformation toward achieving the SDGs (Waldron et al., 2017), especially regarding climate change mitigation and adaptation (Mosquera-Losada et al., 2018).

Previous research suggests various options to address farmers' vulnerability, including improving rural infrastructure and facilities, designing effective and responsive institutional arrangements, and reducing long-term exposure to disaster risk (Ziadat et al., 2022). Unsustainable land use management is among the primary drivers of land degradation. Resource management that overlooks these factors causes land degradation and vulnerability. Furthermore, extreme climatic conditions will exacerbate land quality decline. Therefore, it is essential to promote more sustainable management efforts, such as selecting suitable land use types, managing drainage systems, conserving sloping land, and implementing sustainable land and water management practices that will increase land sustainability and resilience (Ziadat et al., 2022).

5. Conclusion

This study assessed the sustainability status of landslide-prone land management, yielding an overall score of 69.32, indicating a moderate degree of sustainability. However, the results revealed an imbalance across the evaluated dimensions. The social dimension achieved a high sustainability index of 87.18%, placing it in the "sustainable" category (80–100%). In contrast, the ecological, technological, and economic dimensions all fell within the "moderately sustainable" range (50–70%). Specifically, the ecological and technological dimensions each scored 63.44%, while the economic dimension scored 63.23%. Key ecological factors affecting sustainability included the level of pest infestations, vegetation cover, and land slope. For the economic dimension, critical attributes were access to alternative income sources, price stability of agricultural products, and the availability of local markets. The technological dimension was shaped by knowledge of water management, the use of agricultural land technologies, and the identification of landslide- prone areas.

6. Acknowledgement

The authors thank the Dean of Graduate School Universitas Brawijaya for supporting the research. The authors also thank the field assistant for helping with the sampling.

7. References

AbdelRahman, MA., Metwaly, MM., Afifi, AA., D'Antonio, P., & Scopa, A. (2022). Assessment of soil fertility status under soil degradation rate using geomatics in West Nile Delta. *Land*, 11(8), 1256.

Anarbayev, Y., Pentaev, T., & Rakhimzhanova, G. (2023). Economic Efficiency of Using Internal Land Management Based on Agro-Industrial Enterprises. *Regional Science Policy & Practice*.

Baczynski, N., & Bar, N. (2017). Landslide monitoring and management challenge in remote Papua New Guinea. In *Workshop on World Landslide Forum* (pp. 343-354). Cham: Springer International Publishing.

Hadmoko, DS., Lavigne, F., Sartohadi, J., Hadi, P., & Winaryo. (2010). Landslide hazard and risk assessment and their application in risk management and landuse planning in eastern flank of Menoreh Mountains, Yogyakarta Province, Indonesia. *Natural Hazards*, 54, 623-642.

Holcombe, E., Anderson, M., & Holm-Nielsen, N. (2013). Learning by doing: Community based landslide risk reduction. Landslide Science and Practice: Volume 7: Social and Economic Impact and Policies, 297-302.

Hosenuzzaman, M., Kibria, M. G., Sarkar, R., & Abedin, M. A. (2022). Landslide, agricultural vulnerability, and community initiatives: A case study in Southeast part of Bangladesh. *Impact of climate change, land use and land cover, and socio-economic dynamics on landslides*, 123-145.

Hossain, A., Krupnik, TJ., Timsina, J., Mahboob, MG., Chaki, AK., Farooq, M., ... & Hasanuzzaman, M. (2020). Agricultural land degradation: processes and problems undermining future food security. In Environment, climate, plant and vegetation growth (pp. 17-61). Cham: Springer International Publishing.

Iswahyudi, I. (2017). Sustainable management of critical land in the Bukit Batabuh Protected Forest. *Jurnal Penelitian Agrosamudra*, 4(1), 91-99. (In Indonesian)

DOI:https//doi.org/10.22452/mjs.vol44no4.4
Malaysian Journal of Science 44(4): 31-39 (December 2025)

Izakovičová, Z., Špulerová, J., & Petrovič, F. (2018). Integrated approach to sustainable land use management. *Environments*, *5*(3), 37.

Kubangun, SH., Haridjaja, O., & Gandasasmita, K. (2014). Spatial Model of Critical Land Hazard at Bogor, Cianjur and Sukabumi Regencies. *Majalah Ilmiah Globe*, 16(2). (In Indonesian)

Leksono, A. S., & Zairina, A. (2022). A Review on the Direction of Future Studies on Biocultural Landscapes in Forest and Agroforestry Systems in Indonesia. In Conserving Biocultural Landscapes in Malaysia and Indonesia for Sustainable Development, 207-221.

Liu, J., Jin, X., Xu, W., Gu, Z.., Yang, X., Ren, J., ... & Zhou, Y. (2020). A new framework of land use efficiency for the coordination among food, economy and ecology in regional development. *Science of the Total Environment*, 710, 135670.

Masruroh, H., Leksono, A. S., & Kurniawan, S. (2023). Developing landslide susceptibility map using Artificial Neural Network (ANN) method for mitigation of land degradation. *Journal of Degraded & Mining Lands Management*, *10*(3), 4479-4494.

McGowran, P., & Donovan, A. (2021). Assemblage theory and disaster risk management. *Progress in Human Geography*, 45(6), 1601-1624.

Mosquera-Losada, MR., Santiago-Freijanes, JJ., Rois-Díaz, M., Moreno, G., den Herder, M., Aldrey-Vázquez, JA., ... & Rigueiro-Rodríguez, A. (2018). Agroforestry in Europe: A land management policy tool to combat climate change. *Land use policy*, 78, 603-613.

Rachmansyah, A., Baroto, A., & Rahmawati, IMP. (2021). Landslide Hazard Mapping Using the Analytical Hierarchy Process Method in Arjuno Welirang, East Java. *Rekayasa Sipil*, 15(1), 69-77. (In Indonesian)

Rosyada, M., Prasetyo, Y., & Haniah, H. (2015). Landslide Hazard Mapping Using the Analytical Hierarchy Process Method in Arjuno Welirang, East Java. *Jurnal Geodesi Undip*, 4(1), 85-94. (In Indonesian)

Sileshi, GW., Mafongoya, PL., & Nath, AJ. (2020). Agroforestry systems for improving nutrient recycling and soil fertility on degraded lands. *Agroforestry for Degraded Landscapes: Recent Advances and Emerging Challenges*-Vol. 1, 225-253.

Suryatmojo, H., & Soedjoko, SA. (2008). Vegetation Selection for Landslide Control. *Jurnal Kebencanaan Indonesia*, *1*(5), 374-382. (In Indonesian)

van Noordwijk, M. (2021). Agroforestry-Based ecosystem services: Reconciling values of humans and nature in sustainable development. *Land,* 10(7), 699.

Waldron, A., Garrity, D., Malhi, Y., Girardin, C., Miller, DC., & Seddon, N. (2017). Agroforestry can enhance food security while meeting other sustainable development goals. *Tropical Conservation Science*, *10*, 1940082917720667.

Waluyo, MRE., Saputra, PY., & Dien, HE. (2020). Klasterisasi Wilayah Tanah Longsor Berdasarkan Dampak Wilayah dan Geografis Menggunakan Metode K-Means (Studi Kasus: Kabupaten dan Kota di Jawa Timur). In *Seminar Informatika Aplikatif Polinema*. (In Indonesian)

Wang, Q., Wang, H., Zeng, H., Chang, R., & Bai, X. (2022). Understanding relationships between landscape multifunctionality and land-use change across spatiotemporal characteristics: Implications for supporting landscape management decisions. *Journal of Cleaner Production*, 377, 134474.

Ziadat, FM., Zdruli, P., Christiansen, S., Caon, L., Monem, MA., & Fetsi, T. (2021). An overview of land degradation and sustainable land management in the Near East and North Africa. *Sustainable Agriculture Research*, 11(1), 11-24.

DOI:https//doi.org/10.22452/mjs.vol44no4.4
Malaysian Journal of Science 44(4): 31-39 (December 2025)

MALAYSIAN JOURNAL OF SCIENCE
MJS
ISSN 1394-3065

Regular Issue

Malaysian Journal of Science 44 (4): 40-52 (December 2025) https://mjs.um.edu.my

High-Performance Liquid Chromatography Analysis of Caffeine and Trigonelline in Instant Coffee: A Malaysian Market Study

Yen Mae Lee[1a], Cherlyn Cheng Chen Xi[2a] and Lai Chun Wong[3a]*

Abstract: Caffeine and trigonelline are key alkaloids in coffee that significantly influence its quality and effects on human well-being. However, exceeding the recommended intake can produce negative effects. Yet, instant coffee products often lack their content labelling. This study addresses this gap by quantifying these compounds in 15 instant coffee products marketed in Malaysia. A reverse-phase high-performance liquid chromatography method was developed and validated for the simultaneous analysis of black, two-in-1, and three-in-1 instant coffee products. Separation was achieved on a C18 column with gradient elution using water and methanol, with heptafluorobutyric acid as the ion pairing agent. Caffeine content ranged from 2.02 to 47.54 mg/g, and trigonelline from 0.37 to 11.00 mg/g. Per serving, this corresponded to 36.43–183.33 mg of caffeine and 6.70–41.41 mg of trigonelline. Caffeine levels per serving met safety recommendations, but multiple servings would exceed the advised daily limits of 400 mg for adults and 200 mg for pregnant women. Seven products exceeded the 100 mg/day limit for adolescents in just one serving. Additionally, one product contained only 50.5% of its declared caffeine content. In conclusion, this study underscores the need for accurate labelling and informed consumer decisions regarding instant coffee consumption.

Keywords: *Caffeine, trigonelline, instant coffee, high-performance liquid chromatography.*

1. Introduction

Coffee, a globally embraced beverage, has attracted significant scientific interest due to its potential health benefits. Notably, Malaysia, traditionally a tea-drinking country, has seen a remarkable increase in coffee consumption in recent years (Ali & Ramanathan, 2021). This shift is important, given the association between coffee consumption and reduced risks of fatty liver disease, type 2 diabetes, cardiovascular diseases, and various metabolic and neurological disorders (Kolb et al., 2021; Safe et al., 2023). These health benefits can be linked to specific bioactive compounds in coffee, with caffeine and trigonelline being the most notable. Besides their health benefits, trigonelline and caffeine also play a key role in determining coffee flavour quality (Ogutu et al., 2022). Figure 1 presents their chemical structures.

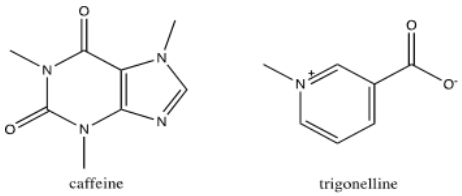

Figure 1. Chemical structures of caffeine and trigonelline analyzed in this study.

Authors information:
[a]School of Pharmacy, Department of Pharmaceutical Chemistry, IMU University, 57000 Kuala Lumpur, MALAYSIA. E-mail: leeyenmae@gmail.com[1]; cherlynchengchenxi@gmail.com[2]; wlaichun@yahoo.com[3]
*Corresponding Author: wlaichun@yahoo.com

Caffeine is the primary alkaloid in coffee and contributes to the signature bitterness of the beverage (Seninde & Chambers, 2020). It is recognized for its stimulant effects and potential health benefits, including enhanced cognitive function, mood regulation, and reduced risk of certain chronic diseases (Açıkalın & Sanlier, 2021; Fiani et al., 2021; Rodak et al., 2021). However, excessive intake can pose risks, including elevated risk of miscarriage and adverse effects on the gastrointestinal, liver, cardiovascular, renal, bone, and reproductive systems (Cornelis, 2019; Depaula & Farah, 2019). Chronic consumption may also influence mood, sleep, and behavior (van Dam et al., 2020). Hence, current guidelines recommend limiting daily caffeine intake to 400 mg for adults (European Food Safety Authority (EFSA), 2015).

Trigonelline is the second most abundant coffee alkaloid. It is found in green coffee beans (Saud & Salamatullah, 2021), with levels up to 34.2 g/kg. It contributes to the appealing aroma of coffee through roasting-induced formation of alkylpyridiniums. At the same time, its strong correlation with pH suggests its significant role as a major flavor precursor, influencing taste and aroma. Beyond its sensory contributions, trigonelline offers various health benefits, including potential blood glucose reduction, support for liver autophagy, and decreased risk of neurological diseases and heart conditions. It also exhibits sedative, anticarcinogenic, antimigraine, antidiabetic, antibacterial, and antiviral properties (Mohamadi et al., 2018). Recent findings suggest it helps reduce dental caries by inhibiting *Streptococcus mutans* (de Almeida et al., 2021; Narayan Biswal et

Received: June, 2023
Accepted: June, 2024
Published: December, 2025

DOI:https//doi.org/10.22452/mjs.vol44no4.5
Malaysian Journal of Science 44(4): 40-52 (December 2025)

al., 2020). Despite some concerns regarding its potential health effects, a 2023 risk assessment concluded that both acute and chronic exposure to trigonelline is safe for human health (Konstantinidis et al., 2023), resulting in no established safe consumption limit.

Given the rise in coffee consumption in Malaysia, there is an urgent need for accurate quantification of these compounds, not only for consumer knowledge but also for ensuring the quality and consistency of coffee products. Despite the extensive consumption of instant coffee, there is a notable lack of comprehensive studies that specifically quantify and compare the caffeine and trigonelline content across different brands available in the Malaysian market. Hence, this work aims to develop and validate a high-performance liquid chromatography (HPLC) method for the simultaneous measurement of these compounds in instant coffee products sold in the country. HPLC, recognized for its high precision, offers a broad dynamic linear range, selective separation, and superior sensitivity, making it suitable for this purpose.

We hypothesize that the caffeine and trigonelline content in these products per serving do not exceed the recommended guidelines. Moreover, we hypothesize variability in the caffeine and trigonelline content among different instant coffee products in Malaysia, which could result from differences in coffee bean origin, processing methods, and formulation techniques used by various manufacturers (Olechno et al., 2021).

2. Materials and Methods

Chemicals and Reagents

Caffeine (Sigma-Aldrich, Merck Peruana, Lima), trigonelline (Sigma-Aldrich, Merck Peruana, Lima), HPLC-grade methanol (Merck KGaA, Germany), and heptafluorobutyric acid (Alfa Aesar, Thermo Fisher Scientific, Great Britain) were used in this study. Ultrapure water (UPW) was prepared using a Sartorius AG model H2OPRO-VF-T system and utilized for all experimental procedures.

Instant Coffee Products

Instant coffee products in powder form were obtained from supermarkets in Malaysia. Products placed at the eye level of the shelves were selected for analysis in this study. Coffee samples were classified into black coffee (BC), two-in-one coffee (2I1C), and three-in-one coffee (3I1C), with five different brands chosen for each group.

Preparation of Stock and Working Standard Solutions

Stock standard solutions of caffeine and trigonelline (200 µg/mL) were prepared in UPW and sonicated for 15 minutes using an ultrasonic bath (Model FB 15061, Fisher Scientific, UK). Working standard solutions were prepared by diluting the stock solutions with UPW. All solutions were filtered through a 0.22 µm nylon syringe filter (Thermoline) prior to HPLC injection.

Preparation of Coffee Samples

BC coffee powder samples were prepared by dissolving 0.3 g of coffee powder in 100 mL UPW, stirring at 100°C until fully dissolved, cooling to room temperature, and filtering through qualitative filter paper. For 2I1C and 3I1C samples, 0.5 g of coffee powder was dissolved in the same way. Each filtrate was filtered using a 0.22 µm nylon syringe filter and stored at 4°C until analysis.

Determination of Maximum Wavelength Absorbance (λ_{max})

UV absorbance spectra of 10 µg/mL caffeine and trigonelline standard solutions were recorded between 200 and 400 nm using a Shimadzu UV-1800 spectrophotometer, with UPW as the blank solution. The λmax was identified as the wavelength at which the maximum absorption occurs.

Chromatographic Conditions

Chromatographic analysis was performed using an Agilent 1260 Infinity HPLC system, including a quaternary pump (G1311C), an autosampler (G1329B), and a diode array detector (DAD) (G1315D). Data processing was performed using Agilent OpenLAB CDS ChemStation software. A GraceSmart reverse phase C18 analytical column (150 mm x 4.6 mm, 5 µm) was utilized for chromatographic separation at room temperature. The mobile phase consisted of UPW with 5 mM HFBA (mobile phase A) and methanol with 5 mM HFBA (mobile phase B). A gradient method was applied, starting with 5% B and increasing to 70% B over 8 minutes. The mobile phase composition returned to 5% B within 2 minutes, followed by a 6-minute equilibration period. The flow rate was 0.8 mL/min, with an injection volume of 20 µL. Caffeine and trigonelline were detected at wavelengths of 273 nm and 264 nm, respectively. The autosampler temperature was held at 4°C.

System Suitability Test

A system suitability test was performed to ensure the HPLC system and method could generate valid results. The parameters evaluated were repeatability, plate number, resolution, and symmetry.

Repeatability

Repeatability assesses the HPLC system's performance consistency when the same sample or standard is injected multiple times under the same conditions. It was assessed by determining the peak area and retention time consistency of 7 replicate injections of a mixed working standard solution containing 20 µg/mL each of caffeine and trigonelline. Percentage relative standard deviation (% RSD) values under 2% were considered acceptable, calculated using Equation (1).

$$\% \text{ RSD} = \frac{\text{Standard deviation of peak area}}{\text{Mean of peak area}} \text{ x } 100\% \qquad (1)$$

DOI:https//doi.org/10.22452/mjs.vol44no4.5
Malaysian Journal of Science 44(4): 40-52 (December 2025)

Plate Number

Plate number, N, indicates the efficiency of the column. A higher plate number corresponds to improved separation efficiency. Injection of a mixed working standard solution containing 20 µg/mL each of caffeine and trigonelline was conducted. The plate number was calculated using Equation (2). Plate number values greater than 2000 were considered acceptable.

$$N = 5.54 \left(\frac{t_R}{w_{0.5}}\right)^2 \quad (2)$$

where t_R is the retention time of caffeine and trigonelline peaks and $w_{0.5}$ the width of their respective peak at half of the height.

Resolution

Resolution, Rs measures the degree of separation between the caffeine and trigonelline peaks. A resolution value of 1.5 or above indicates baseline resolution between the two peaks. Resolution was evaluated by injection of a mixed working standard solution containing 20 µg/mL each of caffeine and trigonelline. The resolution was calculated using Equation (3). Resolution values of 1.5 or above were considered acceptable.

$$Rs = 1.18 \text{ x } \frac{(t_2 - t_1)}{(w_{0.5}1 + w_{0.5}2)} \quad (3)$$

where t_2 and t_1 are the retention times for caffeine and trigonelline, respectively, while $w_{0.5}1$ and $w_{0.5}2$ are the peak widths measured at half the peak height for caffeine and trigonelline, respectively.

Symmetry Factor

The symmetry factor is a coefficient that indicates the degree of peak symmetry. It was determined with a mixed working standard solution containing 20 µg/mL each of caffeine and trigonelline. Symmetry values of no more than two were considered acceptable (Ravisankar et al., 2015).

HPLC Method Validation

The optimised HPLC method underwent validation according to the International Council for Harmonisation (ICH) guidelines, focusing on linearity and range, precision, accuracy, limit of detection (LOD), and limit of quantification (LOQ) (ICH, 2005).

Linearity and Range

The linearity curve for caffeine and trigonelline was assessed at five concentration levels ranging from 1 to 200 µg/mL. Each solution underwent triplicate injections into the HPLC system, and a calibration curve was constructed using the mean values. The acceptance criterion for the linearity test was a correlation coefficient (R^2) value equal to or greater than 0.9999.

Precision

Precision was determined as % RSD for intra-day precision (repeatability) and inter-day precision (intermediate precision). Intra-day precision was evaluated by performing seven determinations of mixed working standard solutions at 20 µg/mL on the same day. Inter-day precision was assessed by repeating the intra-day precision procedure over three days. The acceptance criterion for precision was % RSD of the peak area not exceeding 2%, calculated using Equation (1).

LOD and LOQ

The LOD, the minimum analyte concentration detectable by the analytical method, was established by identifying the lowest concentration at which the analytes could be detected. This involved measuring individual working standard solutions of the analytes until the concentration reached a level distinguishable from background noise. The LOQ, defined as the lowest analyte concentration reliably quantified by the analytical method, was determined by establishing the lowest analyte concentration at which the analytes can be consistently and reliably quantified with acceptable precision (% RSD of peak area < 20%) and accuracy (% Recovery ± 20%).

Accuracy

Accuracy was evaluated through nine determinations across three concentration levels, each including three replicates. Decaffeinated coffee samples were spiked with low (10 µg/mL), medium (100 µg/mL), and high (190 µg/mL) concentrations of the analytes. The % Recovery values were calculated by dividing the experimentally measured concentration of each analyte spiked into the blank by its theoretical amount (as per Equation (4)). Acceptable accuracy was defined as % Recovery falling within the 90% to 110% range.

$$\% \text{ Recovery} = \frac{\text{Experimental concentration of analyte}}{\text{Theoretical concentration of analyte}} \text{ x } 100\% \quad (4)$$

Robustness

The method's robustness was evaluated by calculating the % RSD of peak areas for caffeine and trigonelline in a 100 µg/mL mixed standard solution, following intentional minor variations in flow rate (± 0.1 mL/min) and detection wavelength (± 2 nm).

Stability

The stability of caffeine and trigonelline working standard solutions at 100 µg/mL was assessed at ambient temperature and 4 °C for 24, 48, and 72 hours to confirm stability for autosampler and storage conditions. Stability assessment involved comparing the concentration of each analyte in a freshly prepared solution ($Conc_{theoretical}$) with its concentration after specified time points ($Conc_{measured}$), as per Eq. (5).

$$\% \text{ Relative error (\% RE)} = \frac{Conc_{measured} - Conc_{theoretical}}{Conc_{theoretical}} \text{ x } 100\% \quad (5)$$

Caffeine and Trigonelline in Coffee Samples

A calibration curve (peak areas versus concentrations) was established for each analyte within 1–200 µg/mL. The regression equation derived from these calibration curves was used to

DOI:https//doi.org/10.22452/mjs.vol44no4.5
Malaysian Journal of Science 44(4): 40-52 (December 2025)

calculate the caffeine and trigonelline amounts in the coffee samples based on their peak areas. Each coffee sample was analyzed in triplicate, and the mean concentration of each analyte was reported.

3. Results and Discussion

HPLC Method Development

An analytical technique for measuring caffeine and trigonelline simultaneously in instant coffee products was developed using HPLC-DAD. The DAD wavelength was set to the maximum absorbance peaks of trigonelline (264 nm) and caffeine (273 nm). The mobile phase consisted of methanol and water with HFBA as the ion pairing reagent. The optimized method involved gradient elution with a runtime of 10 minutes and a flow rate of 0.8 mL/min. Under these conditions, caffeine and trigonelline standards showed distinct retention times of 3.332 and 6.369 minutes, respectively (Figures 2(A) and 2(B)). Complete separation was confirmed by injecting a mixed standard solution of caffeine and trigonelline, resulting in baseline separation (Figure 2(C)).

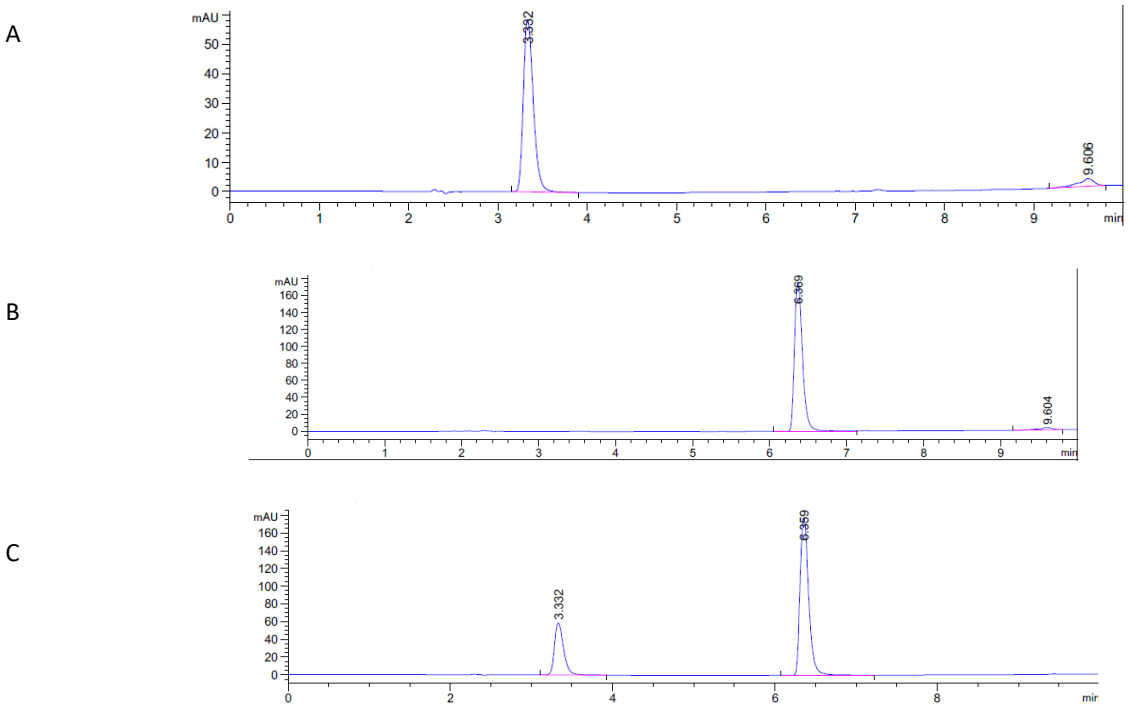

Figure 2. HPLC chromatograms illustrating (A) standard trigonelline at concentration 20 µg/mL, (B) standard caffeine at concentration 20 µg/mL, and (C) a mixed standard solution (20 µg/mL), displaying baseline-resolved peaks for both trigonelline and caffeine.

System Suitability Test

Before validating the method, a system suitability test was conducted to evaluate the HPLC system's performance for analyzing caffeine and trigonelline. A system suitability test is a series of checks performed to ensure that the HPLC system and method can produce accurate results. These tests are essential in confirming that the chromatographic system is functioning correctly before the analysis of samples begins. The main objective is to verify that the system performance satisfies the necessary criteria for the analysis to be dependable. Using a mixed working standard solution (20 µg/mL), the test assessed column efficiency, peak resolution, symmetry, and repeatability (Table 1). All measured parameters complied with the predefined acceptance criteria outlined in the methodology chapter (Section 2.7). This confirmed that the HPLC system is functioning correctly and is suitable for the intended analysis.

Table 1. Results of system suitability.

Parameter	Caffeine	Trigonelline	Acceptance limit
Repeatability of retention time (% RSD)[a]	0.05	0.23	< 2.0%
Repeatability of peak area (% RSD)[a]	0.04	0.06	< 2.0%
Plate number, N	18157	4466	> 2000
Resolution, Rs	15.53	15.53	≥ 1.5
Symmetry, S	0.74	0.68	< 2.0

[a]Repeatability was reported as the % RSD of seven injections.

DOI:https//doi.org/10.22452/mjs.vol44no4.5
Malaysian Journal of Science 44(4): 40-52 (December 2025)

Method Validation

Linearity and Range

The linearity of the HPLC method was evaluated across a concentration range of 1-200 µg/mL for both caffeine and trigonelline. This parameter assesses the method's ability to generate responses directly proportional to the analyte concentration within this specified range. Figure 3 illustrates a strong linear relationship between peak area and concentration, with correlation coefficients exceeding 0.999. The regression equations were y = 61.023x + 37.257 for caffeine and y = 28.05x + 3.9441 for trigonelline. These results demonstrate the precision of the method in quantifying these compounds within the defined concentration range.

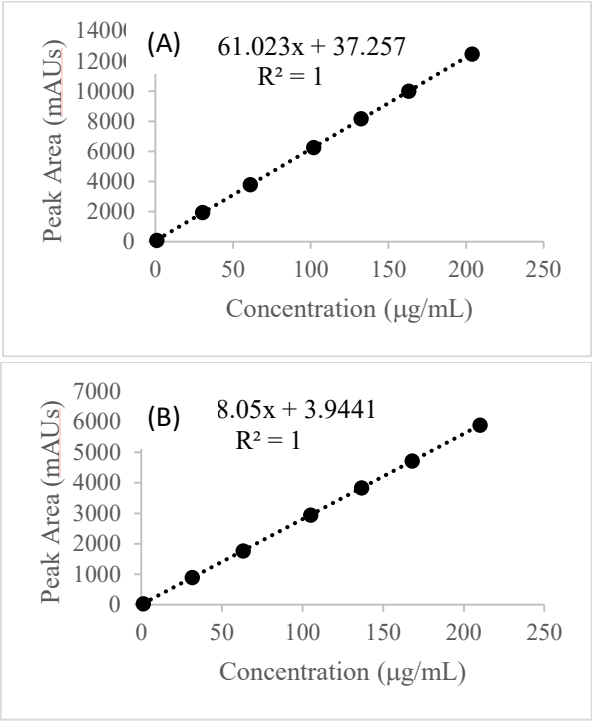

Figure 3. Calibration curves for (A) caffeine and (B) trigonelline. Each data point represents the mean ± standard deviation (SD) of three injections.

LOD and LOQ

LOD and LOQ were determined for both caffeine and trigonelline to establish method sensitivity. Individual standard solutions at estimated LOD levels indicated LOD values of 0.1 µg/mL for caffeine and 0.2 µg/mL for trigonelline (Figure 4). The LOQ values were defined as 0.2 µg/mL for caffeine and 0.3 µg/mL for trigonelline. To confirm the validity of the established LOQ values, accuracy and precision assessments were conducted at LOQ concentrations. At the LOQ, the % Recovery values for caffeine and trigonelline were 97.00% and 113.87%, respectively, while the % RSD peak area (n=3) for caffeine and trigonelline were 8.19% and 3.48%, respectively. Therefore, the accuracy and precision assessments at LOQ confirmed the method's validity, meeting the predefined acceptance criteria of % Recovery within ±20%, and % RSD below 20%.

DOI:https//doi.org/10.22452/mjs.vol44no4.5
Malaysian Journal of Science 44(4): 40-52 (December 2025)

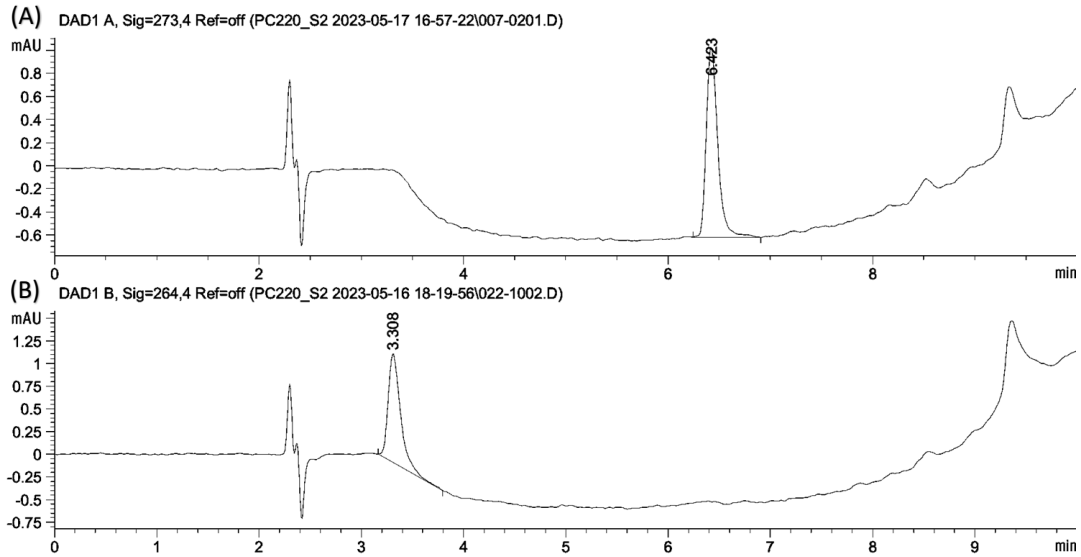

Figure 4. HPLC chromatograms of (A) standard caffeine (0.1 µg/mL) with elution at 6.423 mins and (B) standard trigonelline (0.2 µg/mL) with elution at 3.308 mins.

Precision

The precision of the HPLC method was assessed by evaluating repeatability (intra-day) and reproducibility (inter-day) of the peak area and retention time for both compounds. Seven replicate injections of a 20 µg/mL mixed working standard solution were analyzed on the same day and over three consecutive days. The calculated % RSD values for peak area and retention time remained consistently below 2.0% (Table 2). Therefore, the method is demonstrated to be repeatable and capable of producing consistent results within and across multiple days.

Accuracy

Accuracy measures how closely the measured concentration reflects the true value of the analyte in the sample. To evaluate accuracy, we determined the % Recovery at low quality control (LQC), mid quality control (MQC), and high quality control (HQC) concentration levels. The % Recovery values ranging from 93.92% to 109.09% were within the acceptable range (Table 2), confirming the method's reliable quantification of caffeine and trigonelline in instant coffee samples. However, the % Recovery values for caffeine were lower than those for trigonelline. This difference may be due to several factors related to the chemical properties of the compounds. The lower solubility and stability of caffeine in the extraction solvent compared with those of trigonelline may have influenced the efficiency of its extraction and subsequent quantification. Additionally, interactions between caffeine and the coffee matrix components might have caused variations in recovery rates. For instance, a study by other researchers using hot water extraction of instant coffee also reported lower % Recovery of caffeine compared to trigonelline when spiked at concentrations between 0.02-0.08 g/100g (Liu et al., 2012).

Table 2. Precision and accuracy assessment of the HPLC method.

Analyte	Accuracy		Intra-day precision		Inter-day precision	
	Spike level (µg/mL)	% Recovery[a]	% RSD of retention time (n=7)	% RSD of peak area (n = 7)	% RSD of retention time (n=7)	% RSD of peak area (n = 7)
Caffeine	10	93.92 ± 2.14	0.05	0.04	0.21	1.41
	100	96.09 ± 0.08				
	190	97.18 ± 0.14				
Trigonelline	10	101.20 ± 0.18	0.23	0.06	0.55	0.19
	100	108.37 ± 0.01				
	190	109.09 ± 0.12				

[a]Recovery values are expressed as the mean ± SD of triplicate injections.

DOI:https//doi.org/10.22452/mjs.vol44no4.5
Malaysian Journal of Science 44(4): 40-52 (December 2025)

Robustness

In ICH Q2 (R1), "the robustness of an analytical procedure is a measure of its ability to remain unaffected by small, but deliberate variations in method parameters and provides an indication of its reliability during normal usage." ICH Q2 (R1) also states that the robustness assessment "should demonstrate the reliability of an analysis with respect to deliberate variations in method parameters." If measurements are susceptible to variations in analytical conditions, the analytical conditions should be properly controlled, or a precautionary statement should be included in the procedure. We validated the robustness of our method by varying the mobile phase flow rate and detector wavelength. These parameters are frequently studied in robustness tests of HPLC methods (Epshtein et al., 2018). We varied the flow rate by ±0.1 mL/min and the wavelength by ±2 nm. These variations are common in the literature for HPLC robustness experiments (Epshtein et al., 2018).

A % RSD of less than 2% for peak area was established as the acceptable limit. This implies the analysis remains reliable if, after deliberate changes in the method parameters, the % RSD of the peak areas remains below 2%. As shown in Table 3, the % RSD for all parameters examined was found to be less than 2%. Other reported HPLC methods used to quantify caffeine and trigonelline in instant coffee products have not evaluated robustness with respect to changes in flow rate and wavelength (Arai et al., 2015; Gant et al., 2015; Syamimi et al., 2022).

Table 3. Results of the robustness study were determined using a 100 µg/mL mixed working standard solution.

Parameter	% RSD of peak area	
	Caffeine	Trigonelline
Flow rate (mL/min)		
0.70	0.02	0.04
0.80*	0.03	0.03
0.90	0.03	0.05
Wavelength (nm)		
271	0.04	-
273*	0.04	-
275	0.04	-
Wavelength (nm)		
262	-	0.05
264*	-	0.06
266	-	0.06

*normal chromatography condition

Stability of Caffeine and Trigonelline Solution

The stability of caffeine and trigonelline solutions was assessed over three days at room temperature and under refrigeration (4–8°C). These conditions were selected because the solutions were prepared at room temperature, while storage and autosampler temperatures were maintained at 4–8°C during the study. Evaluating stability under these conditions ensures the compounds remain stable throughout the experimental processes. The % RE was employed to monitor any concentration fluctuations. Trigonelline solutions exhibited excellent stability under both conditions, with % RE values between 0.00% and 0.11% (Table 4). In contrast, caffeine solutions showed higher % RE values, especially at room temperature (0.35%–4.19%) compared to refrigerated storage (0.02%–1.48%).

Caffeine, an alkaloid, is thermally stable during coffee bean roasting (Wei et al., 2012). In aqueous solution, caffeine is generally stable at moderate temperatures and pH. However, its degradation in the environment is affected by factors such as UV radiation (Edwards et al., 2015). In this study, caffeine solutions stored at room temperature were kept in clear vials, unprotected from light, potentially leading to faster degradation due to exposure to environmental factors such as light and oxygen. Conversely, caffeine solutions stored in the refrigerator were less exposed to light, as the refrigerator lacks built-in light. Thus, the stability of caffeine solutions was better maintained under refrigerated conditions. Nevertheless, the stability of the caffeine stock and working solutions in this study was preserved because these solutions were promptly stored at refrigerated temperatures shortly after their preparation at the bench. For future routine analysis, it is advisable to store caffeine solutions under refrigeration and protect them from light to maintain accurate quantification and reduce stability-related issues.

Table 4. Stability assessment of 100 µg/mL mixed working standard solution at room temperature and 4°C after 72 hours.

Analyte	Storage Conditions (°C)	% RE[a] Day 1	Day 2	Day 3
Caffeine	Room temperature	0.35 ± 0.05	4.43 ± 0.02	4.19 ± 0.02
	4–8	0.02 ± 0.50	1.31 ± 0.08	1.48 ± 0.04
Trigonelline	Room temperature	0.00 ± 0.04	0.08 ± 0.02	0.09 ± 0.03
	4–8	0.06 ± 0.09	0.11 ± 0.02	0.04 ± 0.03

[a] % RE values are expressed as the mean ± SD of triplicate injections.

Caffeine Content in Instant Coffee Products

Fifteen commercially available instant coffee products from various brands sold in Malaysia were analyzed for caffeine and trigonelline content. Using the validated HPLC-DAD method, simultaneous quantification of these compounds was achieved, and the results are presented in Table 5 with manufacturer-declared values. Chromatograms of BC, 2I1, and 3I1 products are shown in Figure 5.

DOI:https//doi.org/10.22452/mjs.vol44no4.5
Malaysian Journal of Science 44(4): 40-52 (December 2025)

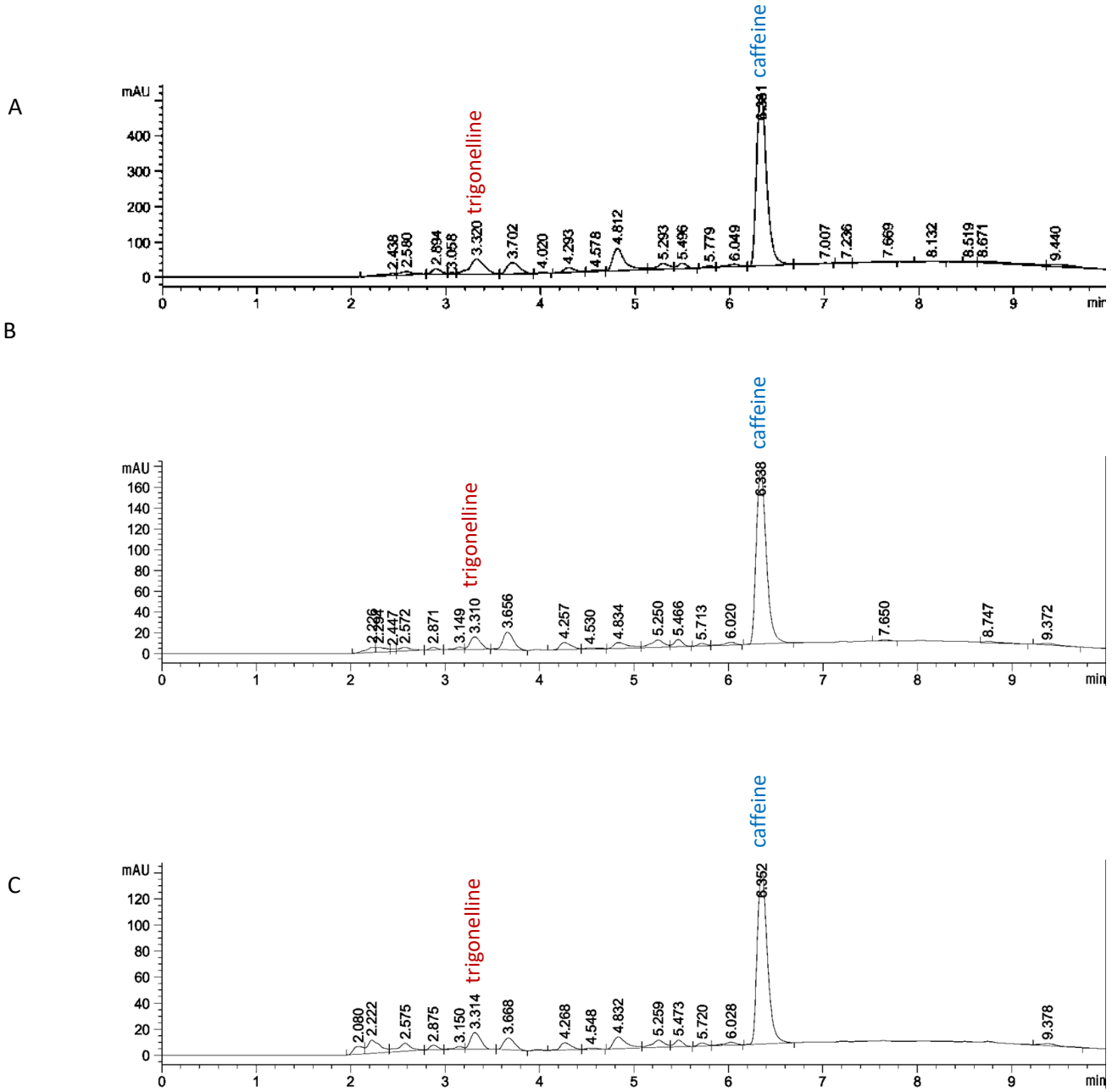

Figure 5. HPLC chromatograms of instant coffee products analyzed by the validated HPLC method showing caffeine and trigonelline peaks: (A) BC-3, (B) 2I1C-3, and (C) 3I1C-1.

DOI:https//doi.org/10.22452/mjs.vol44no4.5
Malaysian Journal of Science 44(4): 40-52 (December 2025)

Table 5. Quantification of caffeine and trigonelline in instant coffee products using the validated HPLC-DAD method.

Instant coffee products[a]	Serving size (g)[b]	Amount detected (mg/g)[c]		Manufacturer declared amount (mg/g)		Calculated amount per serving (mg)[c]		Calculated amount in 2.38 servings (mg)[c]	
		Caffeine	Trigonelline	Caffeine	Trigonelline	Caffeine	Trigonelline	Caffeine	Trigonelline
BC-1 (Arabica and Robusta mixture)	02.0	37.76 ± 0.04	11.00 ± 0.04	25–45	Not declared (n.d)	75.52 ± 0.07	21.99 ± 0.07	179.73 ± 0.17	52.35 ± 0.17
BC-2 (Arabica)	02.0	31.78 ± 0.08	9.67 ± 0.00	n.d	n.d	63.56 ± 0.16	19.35 ± 0.01	151.28 ± 0.37	46.04 ± 0.02
BC-3 (Arabica)	01.8	24.50 ± 0.01	5.43 ± 0.02	n.d	n.d	44.11 ± 0.02	9.77 ± 0.03	104.97 ± 0.05	23.26 ± 0.07
BC-4 (Arabica and Robusta mixture)	02.0	47.54 ± 0.01	10.38 ± 0.00	n.d	n.d	95.09 ± 0.02	20.75 ± 0.01	226.31 ± 0.04	49.39 ± 0.02
BC-5 (Arabica)	01.6	26.48 ± 0.01	9.68 ± 0.04	n.d	n.d	42.37 ± 0.02	15.49 ± 0.06	100.83 ± 0.05	36.86 ± 0.15
2I1C-1	25.0	5.23 ± 0.00	1.05 ± 0.00	n.d	n.d	130.87 ± 0.05	26.16 ± 0.05	311.48 ± 0.12	62.27 ± 0.13
2I1C-2	30.0	6.11 ± 0.01	1.38 ± 0.00	n.d	n.d	183.33 ± 0.20	41.41 ± 0.03	436.31 ± 0.46	98.55 ± 0.07
2I1C-3	30.0	4.90 ± 0.00	0.62 ± 0.00	5	n.d	146.89 ± 0.10	18.63 ± 0.04	349.59 ± 0.23	44.34 ± 0.09
2I1C-4	16.0	3.85 ± 0.00	0.68 ± 0.00	n.d	n.d	61.63 ± 0.02	10.88 ± 0.03	146.68 ± 0.04	25.88 ± 0.07
2I1C-5	25.0	6.35 ± 0.00	0.77 ± 0.00	n.d	n.d	158.63 ± 0.08	19.30 ± 0.03	377.53 ± 0.18	45.93 ± 0.06
3I1C-1	40.0	3.22 ± 0.00	0.70 ± 0.00	n.d	n.d	128.68 ± 0.15	28.02 ± 0.03	306.27 ± 0.35	66.68 ± 0.07
3I1C-2	38.0	3.47 ± 0.00	0.69 ± 0.00	n.d	n.d	131.70 ± 0.03	26.25 ± 0.05	313.45 ± 0.06	62.49 ± 0.11
3I1C-3	18.0	2.67 ± 0.00	0.38 ± 0.00	n.d	n.d	47.99 ± 0.06	6.88 ± 0.01	114.21 ± 0.14	16.38 ± 0.03
3I1C-4	18.0	2.02 ± 0.00	0.37 ± 0.00	4	n.d	36.43 ± 0.04	6.70 ± 0.02	86.70 ± 0.09	15.95 ± 0.04
3I1C-5	38.0	4.17 ± 0.00	0.91 ± 0.00	n.d	n.d	158.65 ± 0.08	34.46 ± 0.04	377.58 ± 0.19	82.00 ± 0.09

[a]BC: black coffee; 2I1C: two-in-one coffee; 3I1C: three-in-one coffee.

[b]Values indicated on the product label.

[c]Values are expressed as the mean ± SD of triplicate injection

DOI:https//doi.org/10.22452/mjs.vol44no4.5
Malaysian Journal of Science 44(4): 40-52 (December 2025)

Caffeine concentrations varied among different types of instant coffee products, with BC containing the highest amount per gram (average 33.61 mg/g), followed by 2I1C products (average 5.29 mg/g), and the lowest in 3I1C products (average 3.11 mg/g). Instant BC products typically consist solely of instant coffee powder and roasted ground coffee, which likely explains their greater caffeine content. In contrast, 2I1C and 3I1C products include additional components such as creamer, sugar, and additives, which reduce the concentration of caffeine.

Moreover, variability within similar product types was also observed. In BC products, caffeine content ranged from 24.50 to 47.54 mg/g, while for 2I1C and 3I1C products, it varied between 3.85 and 6.35 mg/g and 2.02 to 4.17 mg/g, respectively. These differences within product types can be attributed to factors such as coffee bean variety, origin, degree of roasting, and processing methods (Olechno et al., 2021). For example, in our study, BC samples containing a blend of Arabica and Robusta coffee (BC-4 and BC-1) exhibited higher caffeine concentrations than samples consisting solely of Arabica coffee. This finding corresponds with previous research indicating that Robusta coffee generally contains more caffeine than Arabica coffee (Nyoro et al., 2018).

Only three of the 15 coffee products tested (BC-1, 2I1C-3, and 3I1C-4) provided information on their caffeine content (Table 5). Product 2I1C-3 closely matched its declared caffeine content, meeting 98.0% of the specified amount on the label. Similarly, the caffeine content in product BC-1 (37.76 mg/g) was within the manufacturer's claim of 50–90 mg/2 g as published on its website. However, product 3I1C-4 met only 50.5% of its label claim, highlighting potential inconsistencies and misinformation in food labelling practices (da Costa et al., 2022; Duffy et al., 2021).

According to the Malaysian Standard MS1360 (1994), it is assumed that all coffee species contain an average of 0.9% (w/w) caffeine, equivalent to 9 mg/g (Standards & Industrial Research Institute of Malaysia, 1994). In our study, the measured caffeine levels in BC (24.50 to 47.54 mg/g) generally exceeded this standard. The measured caffeine content in our study is generally consistent with other findings in the literature (Table 6). The closest study to ours is by Nyoro et al., who quantified caffeine in seven locally available coffee products in Malaysia using chloroform extraction and ATR-FTIR analysis (Nyoro et al., 2018). The average caffeine content reported was 0.55% (5.5 mg/g), with Arabica coffee exhibiting lower caffeine levels compared to Robusta coffee. The lower caffeine content reported by Nyoro compared to our study could be ascribed to differences in solvent type, extraction method, and analytical techniques employed in their study.

Table 6. Comparison of caffeine content in instant coffee powder determined in this study and the past 10 years of literature.

Type of instant coffee powder	Caffeine content	Analytical method used	Reference (Past 10 years)
Black coffee (This study)	24.50 – 47.54 mg/g	HPLC	-
2I1 coffee (This study)	3.85 – 6.35 mg/g	HPLC	-
3I1 coffee (This study)	2.02 – 4.17 mg/g	HPLC	-
Commercial regular coffee	1.7 – 9.8 mg/g	FTIR	(Nyoro et al., 2018)
Commercial regular coffee	0.49 – 9.64 mg/g	HPLC	(Gonzales-Yépez et al., 2023)
Commercial regular coffee	28.8 – 35.0 mg/g	HPLC	(Arai et al., 2015)
Seven different types	65 – 1503 (µg, w/w%) in 2.5 mg/ml of coffee	HPLC	(Syamimi et al., 2022)

To assess consumer caffeine intake per serving, the caffeine content per serving was calculated based on the specified serving size on the product packaging (Table 5). Among different coffee types, 2I1C exhibited the highest caffeine content per serving (average 136.27 mg/serving), followed by 3I1C (average 100.69 mg/serving), with the lowest in BC (average 64.13 mg/serving). Within the 15 tested products, 2I1C-2 contained the greatest caffeine amount per serving (183.33 mg).

Considering the average daily coffee consumption of 2.38 cups among Malaysians (UKEssays, 2018), 2.38 servings of 2I1C-2 would exceed the FDA recommended daily allowance of 400 mg for adults. This scenario highlights the alarming ease with which recommended daily intake limits can be surpassed, particularly for frequent coffee consumers. Exceeding these limits has been associated with a twofold higher risk of anxiogenic effects (Jahrami et al., 2020). Adolescents and children, who are especially vulnerable to even moderate caffeine doses, should not exceed 100 mg/day and 2.5 mg/kg per day, respectively (Seifert et al., 2011). Pregnant women should also avoid consuming multiple servings of instant coffee daily to remain within the recommended limit of 200 mg/day (European Food Safety Authority (EFSA), 2015). According to our analysis, 8 out of 15 products contained more than 200 mg of caffeine in 2.38 servings (products BC-4, 2I1C-1, 2I1C-2, 2I1C-3, 2I1C-5, 3I1C-1, 3I1C-2, and 3I1C-5). This demonstrates the critical importance of monitoring caffeine intake, especially among specific demographic groups, to reduce potential health risks.

Trigonelline Content in Instant Coffee Products

The concentration of trigonelline in instant coffee products showed a strong correlation with caffeine concentrations. Similar to caffeine, BC exhibited the highest trigonelline content (average value of 9.23 mg/g), followed by 2I1C (average value of 0.9 mg/g) and 3I1BC (average value of 0.61 mg/g). These values are consistent with existing literature (Arai et al., 2015). In our study, the highest trigonelline content per gram of product was

DOI:https//doi.org/10.22452/mjs.vol44no4.5
Malaysian Journal of Science 44(4): 40-52 (December 2025)

recorded in BC-1 (11.00 mg/g), while 2I1C-2 contained the highest trigonelline content per serving (41.41 mg/serving).

Despite its potential health benefits, toxicological data on trigonelline remain limited, and no recommended limits have been identified. However, an oral LD50 of 5000 mg/kg bw from rat studies provides a threshold for acute oral toxicity (Konstantinidis et al., 2023). Extrapolating these data to the Benchmark Dose Lower Confidence Limit (BMDL10) suggests a daily intake of 34.3 g for an individual weighing 70 kg. Considering Malaysia's average daily coffee consumption of 2.38 cups, reaching this amount would require consuming approximately 828 servings of product 2I1C-2 in a single day, exceeding any reasonable consumption pattern. Therefore, instant coffee beverages are a safe source of dietary trigonelline, and no toxic or adverse effects are expected upon acute oral exposure to trigonelline when consuming multiple servings of the instant coffee products tested in this study.

4. Conclusion

This study quantified the caffeine and trigonelline content in 15 instant coffee products sold in Malaysia using HPLC-DAD. The developed HPLC method was validated and exhibited precision, accuracy, reliability, and linearity within the specified concentration range. On average, the highest concentration (per gram) of caffeine was observed in BC (33.61 mg/g), followed by 2I1C (5.29 mg/g), and the lowest in 3I1BC (3.11 mg/g). However, when considering content per serving, the order changed to 2I1C (136.27 mg/serving), 3I1C (100.69 mg/serving), and BC (64.13 mg/serving). Consuming one serving per day of any tested product complies with the FDA's recommended daily caffeine limit of 400 mg for adults. However, consuming more than 2.38 cups per day (the average cups of coffee consumed by Malaysians) of product 2I1C-2 would surpass this limit, emphasizing the need for moderation. For pregnant women, 2.38 cups of products BC-4, 2I1C-1, 2I1C-2, 2I1C-3, 2I1C-5, 3I1C-1, 3I1C-2, and 3I1C-3 would exceed the recommended daily caffeine limit of 200 mg. Regarding label accuracy, one product failed to meet its declared caffeine content by 50.5%, highlighting discrepancies that could mislead consumers. Trigonelline content per gram and per serving varied similarly with caffeine, with the highest in BC (9.23 mg/g), followed by 2I1C (0.90 mg/g), and the lowest in 3I1BC (0.61 mg/g). Per serving, the amount was 23.28 mg/serving in 2I1C, 20.46 mg/serving in 3I1C, and 17.47 mg/serving in BC. Unlike caffeine, trigonelline poses no overdose risk even with multiple daily servings. In conclusion, the findings in this study emphasize the importance of accurate labelling and transparent information for consumers to make informed decisions about their coffee consumption. Adults are advised to limit instant coffee intake to no more than two servings daily, especially for 2I1C and 3I1C products, to avoid caffeine overdose. Adolescents should avoid consuming instant coffee, as one serving daily would exceed the recommended limit of 100 mg/day in seven out of the 15 products tested.

5. References

Açıkalın, B., & Sanlier, N. (2021). Coffee and its effects on the immune system. *Trends in Food Science and Technology*, *114*, 625–632. https://doi.org/10.1016/j.tifs.2021.06.023

Ali, N., & Ramanathan, R. (2021). Coffee consumption and the sustainability of the coffee industry in Malaysia. *Trends in Undergraduate Research*, *4*(2), 91–10. https://doi.org/10.33736/tur.1911.2021

Arai, K., Terashima, H., Aizawa, S., Taga, A., Yamamoto, A., Tsutsumiuchi, K., & Kodama, S. (2015). Simultaneous determination of trigonelline, caffeine, chlorogenic acid and their related compounds in instant coffee samples by HPLC using an acidic mobile phase containing octanesulfonate. *Analytical Sciences*, *31*, 831–835.

Cornelis, M. C. (2019). The impact of caffeine and coffee on human health. *Nutrients*, *11*(2), 416. https://doi.org/10.3390/nu11020416

da Costa, B. R. B., El Haddad, L. P., Freitas, B. T., Marinho, P. A., & De Martinis, B. S. (2022). Pre-workout supplements marketed in Brazil: Caffeine quantification and caffeine daily intake assessment. *Drug Testing and Analysis*, *14*(3), 567–577. https://doi.org/10.1002/dta.3043

de Almeida, S. A., Ferracane, J. L., da Silva, E. M., Mushashe, A. M., Merritt, J., Rocha, A. A., Noronha-Filho, J. D., de Almeida, R. V., & Poskus, L. T. (2021). Antimicrobial potential of resin matrices loaded with coffee compounds. *Journal of Biomedical Materials Research - Part B Applied Biomaterials*, *109*(3), 428–435. https://doi.org/10.1002/jbm.b.34711

Depaula, J., & Farah, A. (2019). Caffeine consumption through coffee: Content in the beverage, metabolism, health benefits and risks. *Beverages*, *5*(2), 37. https://doi.org/10.3390/beverages5020037

Duffy, E. W., Hall, M. G., Dillman Carpentier, F. R., Musicus, A. A., Meyer, M. L., Rimm, E., & Smith Taillie, L. (2021). Nutrition claims on fruit drinks are inconsistent indicators of nutritional profile: A content analysis of fruit drinks purchased by households with young children. *Journal of the Academy of Nutrition and Dietetics*, *121*(1), 36-46.e4. https://doi.org/10.1016/j.jand.2020.08.009

Edwards, Q. A., Kulikov, S. M., & Garner-O'Neale, L. D. (2015). Caffeine in surface and wastewaters in Barbados, West Indies. *SpringerPlus*, *4*(57), 1–12. https://doi.org/10.1186/s40064-015-0809-x

DOI:https//doi.org/10.22452/mjs.vol44no4.5
Malaysian Journal of Science 44(4): 40-52 (December 2025)

Epshtein, N. A., Sevastianova, V. L., & Koroleva, A. I. (2018). Investigation of robustness at validation of HPLC and UPLC methods: A modern approach including risk analysis. *Drug Development & Registration Journal (Russia)*, *1*(22), 96–109.

European Food Safety Authority (EFSA). (2015). Scientific opinion on the safety of caffeine. *EFSA Journal*, *13*(5), 4102. https://doi.org/10.2903/j.efsa.2015.4102

Fiani, B., Zhu, L., Musch, B. L., Briceno, S., Andel, R., Sadeq, N., & Ansari, A. Z. (2021). The neurophysiology of caffeine as a central nervous system stimulant and the resultant effects on cognitive function. *Cureus*, *13*(5), e15032. https://doi.org/10.7759/cureus.15032

Gant, A., Leyva, V. E., Gonzalez, A. E., & Maruenda, H. (2015). Validated HPLC-diode array detector method for simultaneous evaluation of six quality markers in coffee. *Journal of AOAC International*, *98*(1), 98–102. https://doi.org/10.5740/jaoacint.14-113

Gonzales-Yépez, K. A., Vilela, J. L., & Reátegui, O. (2023). Determination of caffeine, theobromine, and theophylline by HPLC-DAD in beverages commonly consumed in Lima, Peru. *International Journal of Food Science*, 4323645. https://doi.org/https://doi.org/10.1155/2023/4323645

ICH. (2005). *ICH harmonised tripartite guideline. Validation of analytical procedures-text and methodology Q2(R1)*.

Jahrami, H., Al-Mutarid, M., Penson, P. E., Al-Islam Faris, M., Saif, Z., & Hammad, L. (2020). Intake of caffeine and its association with physical and mental health status among university students in Bahrain. *Foods*, *9*(4), 473. https://doi.org/10.3390/foods9040473

Kolb, H., Martin, S., & Kempf, K. (2021). Coffee and lower risk of type 2 diabetes: Arguments for a causal relationship. *Nutrients*, *13*(4), 1144. https://doi.org/10.3390/nu13041144

Konstantinidis, N., Franke, H., Schwarz, S., & Lachenmeier, D. W. (2023). Risk assessment of trigonelline in coffee and coffee by-products. *Molecules*, *28*(8), 3460. https://doi.org/10.3390/molecules28083460

Liu, H., Shao, J., Li, Q., Li, Y., Yan, H. M., & He, L. (2012). Determination of trigonelline, nicotinic acid, and caffeine in yunnan arabica coffee by microwave-assisted extraction and HPLC with two columns in series. *Journal of AOAC International*, *95*(4), 1138–1141. https://doi.org/10.5740/jaoacint.11-275

Mohamadi, N., Sharififar, F., Pournamdari, M., & Ansari, M. (2018). A review on biosynthesis, analytical techniques, and pharmacological activities of trigonelline as a plant alkaloid. *Journal of Dietary Supplements*, *15*(2), 207–222. https://doi.org/10.1080/19390211.2017.1329244

Narayan Biswal, B., Narayan Das, S., Kumar Das, B., & Rath, R. (2020). Can coffee combat caries? An in vitro study. *Journal of Oral and Maxillofacial Pathology*, *24*(1), 64–67. https://doi.org/10.4103/jomfp.JOMFP

Nyoro, F. D., Sim, S. F., & Jeffrey Kimura, A. L. (2018). Estimation of caffeine content in coffee of Malaysian market using Fourier Transform Infrared (FTIR) spectroscopy. *Trends in Undergraduate Research*, *1*(1), a16-22. https://doi.org/10.33736/tur.1137.2018

Ogutu, C., Cherono, S., Ntini, C., Wang, L., & Han, Y. (2022). Comprehensive analysis of quality characteristics in main commercial coffee varieties and wild Arabica in Kenya. *Food Chemistry: X*, *14*, 100294. https://doi.org/10.1016/j.fochx.2022.100294

Olechno, E., Puścion-Jakubik, A., Zujko, M. E., & Socha, K. (2021). Influence of various factors on caffeine content in coffee brews. *Foods*, *10*(6), 1208. https://doi.org/10.3390/foods10061208

Ravisankar, P., Naga Navya, C., Pravallika, D., & Navya, D. (2015). A review on step-by-step analytical method validation. *IOSR Journal of Pharmacy*, *5*(10), 7–19. www.iosrphr.org

Rodak, K., Kokot, I., & Kratz, E. M. (2021). Caffeine as a factor influencing the functioning of the human body—friend or foe? *Nutrients*, *13*(9), 3088. https://doi.org/10.3390/nu13093088

Safe, S., Kothari, J., Hailemariam, A., Upadhyay, S., Davidson, L. A., & Chapkin, R. S. (2023). Health benefits of coffee consumption for cancer and other diseases and mechanisms of action. *International Journal of Molecular Sciences*, *24*(3), 2706. https://doi.org/10.3390/ijms24032706

Saud, S., & Salamatullah, A. M. (2021). Relationship between the chemical composition and the biological functions of coffee. *Molecules*, *26*(24), 7634. https://doi.org/10.3390/molecules26247634

Seifert, S. M., Schaechter, J. L., Hershorin, E. R., & Lipshultz, S. E. (2011). Health effects of energy drinks on children, adolescents, and young adults. *Pediatrics*, *127*(3), 511–528. https://doi.org/10.1542/peds.2009-3592

DOI:https//doi.org/10.22452/mjs.vol44no4.5
Malaysian Journal of Science 44(4): 40-52 (December 2025)

Seninde, D. R., & Chambers, E. (2020). Coffee flavor: A review. *Beverages*, *6*(3), 44. https://doi.org/10.3390/beverages6030044

Standards & Industrial Research Institute of Malaysia. (1994). *Malaysian Standard MS 1360. Penentuan untuk kopi campuran*.

Syamimi, W., Zaman, W. K., Loh, S. P., & Mohd Esa, N. (2022). Quantification of selected bioactive compounds in instant coffee and their effect on gastric release using HGT-1 cells. *Malaysian Journal of Medicine and Health Sciences*, *18*(1), 257–267.

UKEssays. (2018, January). *Coffee culture in malaysia marketing essay*. https://www.ukessays.com/essays/marketing/coffee-culture-in-malaysia-marketing-essay.php

van Dam, R. M., Hu, F. B., & Willett, W. C. (2020). Coffee, caffeine, and health. *New England Journal of Medicine* , *383*(4), 369–378. https://doi.org/10.1056/nejmra1816604

Wei, F., Furihata, K., Koda, M., Hu, F., Miyakawa, T., & Tanokura, M. (2012). Roasting process of coffee beans as studied by nuclear magnetic resonance: Time course of changes in composition. *Journal of Agricultural and Food Chemistry*, *60*(4), 1005–1012. https://doi.org/10.1021/jf205315r

DOI:https//doi.org/10.22452/mjs.vol44no4.5
Malaysian Journal of Science 44(4): 40-52 (December 2025)

MALAYSIAN JOURNAL OF SCIENCE
MJS
ISSN 1394-3065

Regular Issue

Malaysian Journal of Science 44 (4): 53-64 (December 2025) https://mjs.um.edu.my

Extraction of Flavonoid from Rice Straw: The Study of Total Phenolic Content (TPC), Total Flavonoid Content (TFC) and Antibacterial Activity

Siti Lestari[1a]*, Tri Sunaryo[2a] and Rizky Ibnufaatih Arvianto[3b]

Abstract: The combustion of rice straw results in air pollution and a decrease in soil fertility. This research aims to extract flavonoids from rice straw and evaluate their antibacterial properties. The extraction of flavonoids from rice straw was conducted using Soxhlet, reflux, and maceration methods. These extraction techniques were subsequently compared based on the Total Phenolic Content (TPC) and Total Flavonoid Content (TFC). The optimal extraction method for rice straw involved ethanol solvents with concentrations of 0%, 25%, 70%, and 96%. This same optimal method was used to extract rice straw at various time intervals, specifically 12 hours, one day, and three days. A comparative analysis of ethanol concentration and extraction duration was performed based on the Total Phenolic Content (TPC) and Total Flavonoid Content (TFC). The rice straw extract underwent the disc diffusion method for antibacterial tests against gram-positive (Staphylococcus aureus) and gram-negative (Escherichia coli) bacteria. The antibacterial efficacy of rice straw extract was evaluated based on its ability to inhibit the growth of these microorganisms. The maceration method proved to be the most effective for extracting rice straw due to its significantly greater total flavonoid content (TFC) value compared to the reflux and Soxhlet extraction methods. Increasing the ethanol concentration from 0% to 96% and extending the extraction time from 12 hours to 3 days led to a proportional increase in total phenolic content (TPC) and TFC. Ethanol at a concentration of 96% was the most appropriate solvent for extracting rice straw due to its highest total flavonoid content (TFC) value relative to other ethanol concentrations. A three-day extraction period was optimal, yielding a significantly higher TFC value than 12-hour and one-day extractions. Furthermore, it is noteworthy that rice straw extract exhibits greater inhibition of gram-negative bacteria (Escherichia coli) than gram-positive bacteria (Staphylococcus aureus). The antibacterial activity of rice straw extract correlated with the flavonoid content in the sample.

Keywords: *Rice straw, phenolic, flavonoid, anti-bacterial.*

1. Introduction

Indonesia is an agrarian nation where various agricultural products, including rice, cassava, and corn, are cultivated. Indonesia is the world's third-largest rice producer, behind China and India (Indonesian Ministry of Home Affairs, 2004). The elevated rice production levels result in a proportional increase in waste generation. In 2021, rice production was estimated to have reached 55.27 million tons of GKG, marking a rise of 620.42 thousand tons or 1.14 percent compared to the 2020 rice production figure, which stood at 54.65 million tons of GKG (BPS-Indonesian Statistics, 2021). The rise in rice production results in a growth in agricultural waste, notably straw. Generally, this waste is collected and subsequently burned, thereby contributing to air pollution through the emission of several hazardous gases, including sulfur dioxide (SO_2), carbon monoxide (CO), volatile organic compounds (VOC), polycyclic aromatic hydrocarbons (PAHs), as well as various greenhouse gases, such as methane (CH_4), nitrous oxide (N_2O), and carbon dioxide (CO_2) (Gadde et al., 2009; Romasanta et al., 2017). The increase in greenhouse gases leads to global warming and Earth's climate change (Gadde et al., 2009). Burning straw also results in a decline in soil quality characterized by the loss of essential nutrients and organic matter, the depletion of soil-fertilizing bacteria, and an increased vulnerability to soil erosion (Kumar et al., 2019). Rice straw waste must be used carefully to prevent further pollution.

Rice straw contains secondary metabolites in the form of phenolic compounds, particularly flavonoids (Elzaawely et al., 2017; Karimi et al., 2014). These phenolic compounds show potent antibacterial activity. The extract from *Crataegus azarolus L. var. Aronia callus* contained high levels of flavonoids. These compounds showed antibacterial activity against both gram-positive and gram-negative bacteria, including *Staphylococcus aureus* (ATCC 29213), *Staphylococcus epidermidis* (NCIMB 8853), *Escherichia coli* (ATCC 35218), *Pseudomonas aeruginosa* (ATCC 27853), *Micrococcus luteus* (NCIMB 8166), and *Salmonella typhimurium* (Bahri-Sahloul et al., 2014). Bergamot seed extract (Citrus bergamia Risso) contains flavonoids that give it antibacterial capabilities against gram-positive bacteria, including Listeria innocua, Bacillus subtilis, Staphylococcus aureus, and Lactococcus lactis (Mandalari et al., 2007). Mandarin orange seed extract (Citrus reticulata Blanco) contains the highest concentration of flavonoids. These compounds show antibacterial activity against *Bacillus subtilis* and *Klebsiella pneumoniae* (Balaky et al., 2020). Numerous previous studies have demonstrated the strong antibacterial properties of flavonoid compounds.

The flavonoid extraction process is influenced by several factors.

Authors information:
[a]Nursing Department, Politeknik Kesehatan Kementrian Kesehatan Surakarta, Jl. Letjen Sutoyo Mojosongo Jebres Surakarta 57127 INDONESIA. E-mail: lestaristi68@gmail.com[1]; tri_sunaryo@yahoo.com[2]
[b]Petrochemical Industry Technology Process Study Program, Petrochemical Industry Politechnic Banten, Jalan Raya Karang Bolong, Cikoneng, Anyar, Kab. Serang, Banten 42166, INDONESIA. E-mail: rizky.ibnufaatih@poltek-petrokimia.ac.id[3]
*Corresponding Author: lestaristi68@gmail.com

Received: June, 2023
Accepted: June, 2024
Published: December, 2025

DOI:https//doi.org/10.22452/mjs.vol44no4.6
Malaysian Journal of Science 44(4): 53-64 (December 2025)

Extraction methods

Flavonoid extraction methods can be conducted through reflux, Soxhlet, or maceration. Reflux involves extraction with a solvent at its boiling point for a specified time, maintaining a constant solvent volume due to the presence of a condenser (Chua et al., 2016). Soxhlet extraction shows similarities to reflux. A Soxhlet flask is placed between the condenser and the round-bottom flask, acting as a solid sample holder. This extraction method is used for non heat-resistant samples, preventing direct contact between the solid sample and boiling solvent during extraction (Redfern et al., 2014). Meanwhile, maceration involves immersing the material in a solvent without or with minimal heating (Rabiu & Haque, 2017; Tambun et al., 2021).

Solvent Concentration

Solvent concentration is related to solvent polarity, and flavonoids should exhibit similar polarity to the solvent (Yusof et al., 2020). Furthermore, concentration reflects the quantity of solvent molecules, and an increase in the number of particles results in a higher frequency of collisions during the extraction process (Cui et al., 2021).

Extraction Time

Extraction time is correlated with dwelling time, as a longer extraction time leads to a prolonged period of solvent contact with the sample during extraction (Dewi et al., 2019).

The total phenolic content (TPC) analysis in samples was performed using the Folin-Ciocalteu method. Phenolic compounds react with the Folin-Ciocalteu reagent under alkaline conditions to produce a blue complex compound (Blainski et al., 2013). Meanwhile, the colorimetric method was employed to analyze the total flavonoid content (TFC) of the sample (Martono et al., 2019; Shraim et al., 2021). This method used aluminum chloride (AlCl3), which forms stable complex compounds with flavonoid compounds. AlCl3 creates a stable complex compound by interacting with the ketone group at C4 and the OH group at C3 or C5 (Martono et al., 2019). AlCl3 also forms an acid-labile complex with the orthodihydroxyl group on the flavonoid ring (Martono et al., 2019). This complex compound causes a shift in wavelength toward visible light so that the solution changes color to yellow (Fadillah et al., 2007; Martono et al., 2019). The absorbance of the color changes in the sample can be measured using a UV-visible spectrophotometer at specific wavelengths. This absorbance value is directly proportional to the total phenolic and flavonoid content in the sample (Mekonnen & Desta, 2021; Zhu et al., 2010).

The present study focused on isolating flavonoids from rice straw using the procedures of reflux, Soxhlet, or maceration. The optimal flavonoid extraction method was determined based on the Total Flavonoid Content (TFC) and Total Phenolic Content (TPC). The solvent concentration and extraction duration influence on TPC and TFC was assessed using the selected extraction method. Subsequently, using the disc diffusion method, rice straw extracts with varying solvent concentrations were assessed for their antibacterial activity against Staphylococcus aureus (gram-positive) and *Escherichia coli* (gram-negative). The antibacterial efficacy of the rice straw extract was evaluated based on the clear zone diameter against these bacteria.

2. Materials and Methods

Material

In this study, various materials were employed, such as 96% ethanol, distilled water, sodium bicarbonate, gallic acid, rice straw, glass wool, Whatman paper, *Staphylococcus aureus* and *Escherichia coli cultures*, Muller-Hinton medium, Nutrient Agar, and Nutrient Broth.

Methods

Straw Powder Production

A kilogram of rice straw underwent an 8-hour drying procedure conducted in direct sunlight. The drying process involved enveloping the rice straw with a black mesh. After a drying duration of 8 hours, the straw was sliced into small pieces.

Total Flavonoid Content (TFC) Analysis

Determination of Standard Curve

The samples' flavonoid content was quantified using quercetin as the standard. A mixture was prepared by combining 10.0 mg of quercetin, 0.3 mL of a 5% sodium nitrite solution, 0.6 mL of a 10% aluminum chloride solution, and 2 mL of a 1 M sodium hydroxide solution in a glass beaker. The resulting quercetin solution was diluted with distilled water to a final volume of 10 mL using a volumetric flask. The quercetin stock solution, obtained at a concentration of 1000 ppm, was diluted to concentrations of 0.5 ppm, 1 ppm, 2 ppm, 5 ppm, 10 ppm, 25 ppm, 50 ppm, 75 ppm, and 100 ppm, as shown in Table 1. Subsequently, the absorbance of each solution was measured using a UV-Vis spectrophotometer at a wavelength of 510 nm. The linearity equation was obtained from a standard curve plotting absorbance versus concentration. This equation was used to determine the flavonoid content in the extract samples.

Table 1. Dilution of quercetin stock solution (1000 ppm)

Concentration (ppm)	0.5	1	2	5	10	25	50	75	100
Stock solution (mL)	0.005	0.010	0.020	0.050	0.100	0.250	0.500	0.750	1.000
Aquades (mL)	9.995	9.990	9.980	9.950	9.900	9.750	9.500	9.250	9.000
Final volume (mL)	10	10	10	10	10	10	10	10	10

DOI:https//doi.org/10.22452/mjs.vol44no4.6
Malaysian Journal of Science 44(4): 53-64 (December 2025)

TFC Determination of Rice Straw Extract

The colorimetric assay measured the total flavonoid content (Shraim et al., 2021). Two milliliters of a sodium hydroxide solution (1 M) and two milliliters of a 10% aluminum chloride solution were added to 0.2 milliliters of rice straw extract and 0.3 milliliters of 5% sodium nitrite. The extract solution was then diluted using a measuring flask until it reached a final volume of 10 mL. Subsequently, a UV-Vis spectrophotometer was used to measure the extract solution's absorbance at a wavelength of 510 nm. Using a linear equation, we determined the total flavonoid concentration of the rice straw extract.

Total Phenolic Content (TPC) Analysis

Determination of Standard Curve

A glass beaker combined 10 mg of gallic acid, 0.5 mL of Folin-Ciocalteu reagent, 1.5 mg of 20% sodium carbonate, and 7.5 mL of distilled water (aquabides). The resulting gallic acid solution was heated in a water bath at 40 °C for 20 minutes and rapidly cooled on ice. The original stock solution of gallic acid (1000 ppm) was subsequently diluted to various concentrations ranging from 0.5 ppm to 100 ppm. The absorbance of each of these dilutions was measured using a UV-Vis spectrophotometer, with readings taken at a wavelength of 760 nm. A standard curve established the linearity equation by plotting absorbance against concentration. This linear equation provides an essential basis for calculating the phenolic content in the extract samples.

Table 2. Dilution of gallic acid stock solution (1000 ppm)

Concentration (ppm)	0.5	1	2	5	10	25	50	75	100
Stock solution (mL)	0.005	0.010	0.020	0.050	0.100	0.250	0.500	0.750	1.000
Aquades (mL)	9.995	9.990	9.980	9.950	9.900	9.750	9.500	9.250	9.000
Final volume (mL)	10	10	10	10	10	10	10	10	10

TPC Determination of Rice Straw Extract

In a glass beaker, 0.2 mL of rice straw extract, 0.5 mL of Folin-Ciocalteu reagent, 1.5 mL of 20% sodium carbonate, and 7.5 mL of distilled water (aquabides) were combined. The extract solution was adjusted to a final volume of 10 mL using a volumetric flask. Subsequently, the absorbance of the extract solution was measured using a UV-Vis spectrophotometer at a wavelength of 760 nm. The total flavonoid content within the extract solution was determined employing the linearity equation.

Effect of Extraction Method on TPC and TFC

Reflux Extraction

In total, 50 grams of rice straw were placed into a round-bottom flask. 300 mL of 70% ethanol was added to the round-bottom flask. The rice straw underwent reflux for a duration of 2 hours at 70℃. Following this step, the filtrate and residue were separated using a Buchner vacuum filter. The filtrate was evaporated using a distillator to remove the ethanol solvent. The resulting rice straw extract was then analyzed for TFC (Total Flavonoid Content) and TPC (Total Phenolic Content).

Soxhlet Extraction

A Soxhlet flask was filled with fifty grams of rice straw. The round-bottom vial was subsequently filled with 300 mL of 70% ethanol. The Soxhlet extraction was conducted for a period of two hours. The sample was then filtered using a Buchner vacuum filter. The ethanol solvent was removed by evaporating the resulting filtrate with a distillator. Ultimately, the rice straw extract was analyzed for TFC (Total Flavonoid Content) and TPC (Total Phenolic Content).

Maceration

For 15 hours at room temperature, fifty grams of rice straw were submerged in 300 mL of 70% ethanol. The filtrate and residue were separated using a Buchner vacuum filter after 24 hours. The ethanol solvent was subsequently removed from the filtrate by evaporating it with a distillator. Ultimately, the rice straw extract was analyzed for TFC (Total Flavonoid Content) and TPC (Total Phenolic Content).

Effect of Ethanol Concentration and Extraction Time on TPC and TFC

The extraction procedure was carried out according to the optimum method specified in section 2.2.4 of the paper. Ethanol concentrations were adjusted to 0%, 25%, 70%, and 96%. The extraction times were set to durations of 12 hours, one day, and three days. An investigation was conducted on each rice straw extract, which varied in ethanol concentrations and extraction times, to determine its Total Flavonoid Content (TFC) and Total Phenolic Content (TPC).

Anti-bacterial Activity Test

Testing was performed to evaluate the antibacterial activity of the most effective rice straw extraction technique, as outlined in section 2.2.4. Antibacterial tests employed *Escherichia coli* (gram-negative) and *Staphylococcus aureus* (gram-positive) bacterial strains. A single dose of culture from Nutrient Agar (NA) was suspended in Nutrient Broth (NB) medium and incubated for 24 hours. In a petri dish, 1 mL of Nutrient Broth (NB) culture was mixed with 9 mL of Mueller Hinton (MH) medium. The mixture was agitated and left undisturbed briefly to allow solidification. Paper discs soaked in 1000 mg of chloroform were placed evenly within the solidified medium. The plate was incubated at 37 ℃ for 24 hours, and measurements were taken by assessing the Inhibitory Zone Diameter.

DOI:https//doi.org/10.22452/mjs.vol44no4.6
Malaysian Journal of Science 44(4): 53-64 (December 2025)

3. Result and Discussion

Total Phenolic Content (TPC) Analysis

The standard curve for total phenolic analysis is depicted in Figure 1. The graph demonstrates that the concentration of gallic acid is directly proportional to the absorbance (Mayerhöfer & Popp, 2019). The structure of the linear equation is as follows: y = 0.0081x + 0.0005 (where "x" and "y" represent the phenolic concentration and absorbance, respectively). Therefore, the phenolic concentration in straw extract can be calculated using equation (1).

$$\text{Concentration} = \frac{\text{Absorbance}}{0{,}0081} - 0{,}0005 \qquad (1)$$

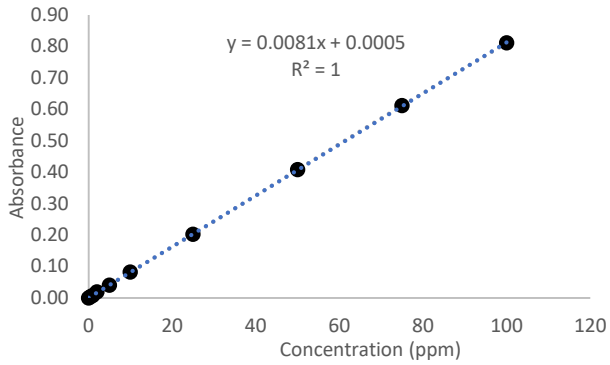

Figure 1. Standard Curve of TPC Analysis

Phenolics were compounds characterized by aromatic rings that could bind one or more hydroxyl groups (Tsao, 2010; Vuolo et al., 2019). Numerous studies have demonstrated that gallic acid is the reference for quantifying total phenolics in various samples (Blainski et al., 2013; Elzaawely et al., 2017; Karimi et al., 2014). When gallic acid and Folin-Ciocalteu reagent were combined in an alkaline environment, they formed a blue complex compound (Martono et al., 2019). The addition of Na_2CO_3 into the sample created an alkaline environment. Na_2CO_3 enabled the dissociation of protons in gallic acid, forming gallic acid phenolate ions (Karimi et al., 2014; Martono et al., 2019). Subsequently, the hydroxyl group within the gallic acid phenolate ions reacted with the Folin-Ciocalteu reagent, resulting in the formation of a blue molybdenum-tungsten complex (Abdelkader et al., 2014; Agbor et al., 2014; Martono et al., 2019). The gallic acid phenolate ion acted as a reducing agent in this reaction, converting Mo^{6+} to Mo^{5+}. Simultaneously, molybdenum oxidizes the hydroxyl group within the gallic acid phenolate ion, transforming it into a ketone group (Shi et al., 2022). The process for the formation of the molybdenum-tungsten complex was illustrated in Figure 2.

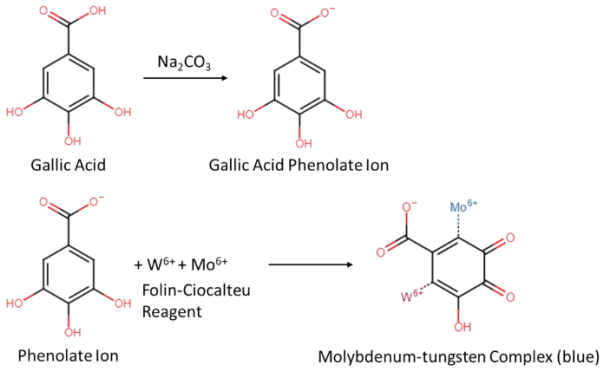

Figure 2. Formation of molybdenum-tungsten complex (Martono et al., 2019; Shi et al., 2022).

The absorbance of the blue molybdenum-tungsten complex was measured using a UV-visible spectrophotometer (Zhu et al., 2010). The absorbance is directly proportional to the concentration of the substance (Mayerhöfer & Popp, 2019). Gallic acid was prepared at different concentrations to create a standard curve (Bhaigyabati et al., 2015). A linear equation was derived from this curve, which was then used to determine the phenolic compound content in rice straw extract.

Total Flavonoid Content (TFC) Analysis

The total flavonoid concentration in rice straw extract was quantified using the same methods applied for the total phenolic analysis, using quercetin as the reference compound. Figure 3 presents the standard curve for the analysis of total flavonoids. The plot shows the direct relationship between the concentration of quercetin and the absorbance, as cited in the literature (Mayerhöfer & Popp, 2019). The result of the regression equation is y = 0.0032x - 0.0026 (“x” and "y” respectively represent the flavonoid concentration and absorbance). Therefore, the concentration of flavonoids in the straw extract could be calculated utilizing equation (2).

$$\text{Concentration} = \frac{\text{Absorbance}}{0{,}0032} + 0{,}0026 \qquad (2)$$

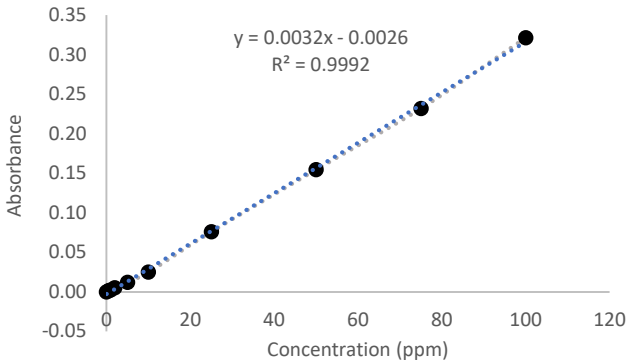

Figure 3. Standard Curve of TFC Analysis

DOI:https//doi.org/10.22452/mjs.vol44no4.6
Malaysian Journal of Science 44(4): 53-64 (December 2025)

A series of investigations have shown that quercetin is a flavonoid that can be used to determine the total flavonoid content (Alide et al., 2020; Bhaigyabati et al., 2015; Chun et al., 2003; Rammohan et al., 2019). Figure 4 illustrates the formation of an Al(III)-quercetin complex resulting from the interaction between AlCl3 and quercetin in an alkaline environment. The complex formed by Al(III) with quercetin is shaded yellow (Rammohan et al., 2019).

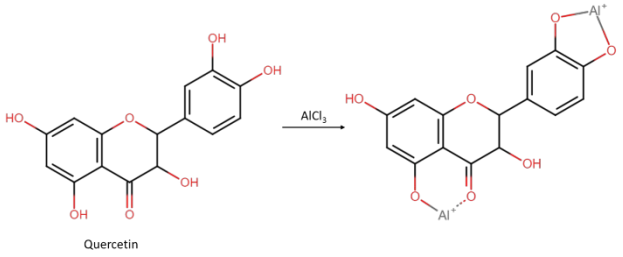

Figure 4. Formation of the Al(III)-quercetin complex (Martono et al., 2019)

Effect of Extraction Method on TPC and TFC

A comparison of extraction methods for rice straw was conducted to ascertain the most efficient technique for flavonoid extraction, as measured by TPC and TFC values. The employed methods included Soxhlet extraction, reflux, and maceration, using a 70% ethanol solvent. Figure 6 shows that maceration yielded a substantially higher flavonoid content than Soxhlet or reflux methods. These results were consistent with the research conducted by Vifta et al. (2019). The extraction of Clitoria ternatea flowers using the maceration method produced a TFC value of 53.127 mg QE/g. This value was significantly higher than that obtained through reflux extraction (24.527 mg QE/g) and Soxhlet (21.06 mg QE/g) methods (Vifta et al., 2022). Maceration was conducted at room temperature without heating, whereas reflux and Soxhlet extractions were performed at the boiling point of ethanol using heating. According to the literature, flavonoids are polyphenolic compounds easily degraded by heat exposure (Anukam et al., 2014; Vifta et al., 2022). Several studies also support this finding. The extraction of flavonoids from garlic using ethanol as a solvent exhibited a decrease in TFC from 414.98 ± 20.16 mg QE/g to 69.10 ± 6.03 mg QE/g as the extraction temperature rose from 25 ℃ to 150 ℃ (Alide et al., 2020). Flavonoids undergo degradation with increasing extraction temperatures. A reduction in flavonoid content also occurred during the black rice extraction process, decreasing from 450 mg/100g to 350 mg/100g due to elevating the extraction temperature from 40 ℃ to 100 ℃ (Lang et al., 2019). The decline in TFC can be attributed to the degradation or damage of flavonoids with increasing temperature (Gao et al., 2022).

The phenolics extracted through reflux exhibit the highest values compared with those obtained through Soxhlet and maceration techniques (Figure 6). Some literature suggests that phenolic compounds have higher thermal degradation thresholds than flavonoids. On the other hand, reflux allows the sample to be subjected to more intense heat than Soxhlet or maceration. Thus, reflux extraction causes the release of phenolic compounds due to heat breakdown of flavonoid compounds. In grape seed flour samples, phenolic compounds degraded when exposed to temperatures above 180 ℃, whereas flavonoids began to degrade at 120 ℃ (Ross et al., 2011). The high TPC and low TFC values observed during reflux extraction indicate the extraction of other phenolic compounds, including tannins, stilbenes, phenolic acids, and lignin. These compounds possess a higher thermal degradation threshold than flavonoids (Tambun et al., 2021; Widiyastuti et al., 2020). Figure 7 illustrates that flavonoids were transformed into various phenolic compounds when exposed to high temperatures (Chaaban et al., 2017). As a result, the TPC obtained through the reflux method typically exceeded that obtained through maceration.

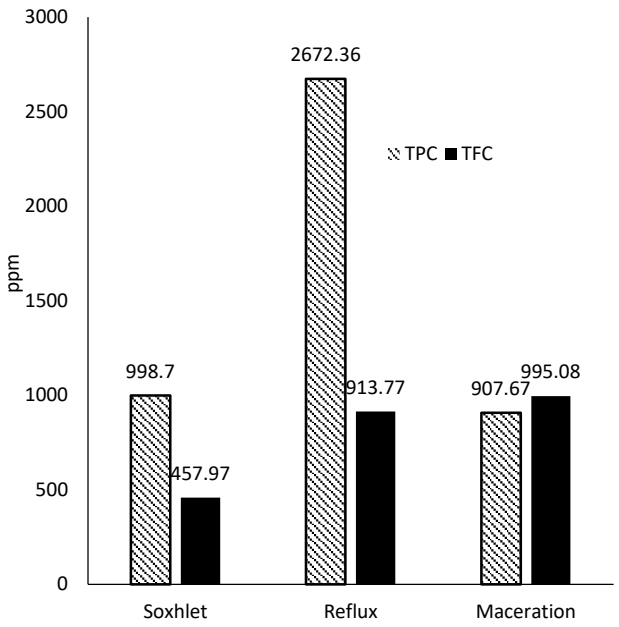

Figure 4. TPC and TFC of rice straw extracts using various methods

DOI:https//doi.org/10.22452/mjs.vol44no4.6
Malaysian Journal of Science 44(4): 53-64 (December 2025)

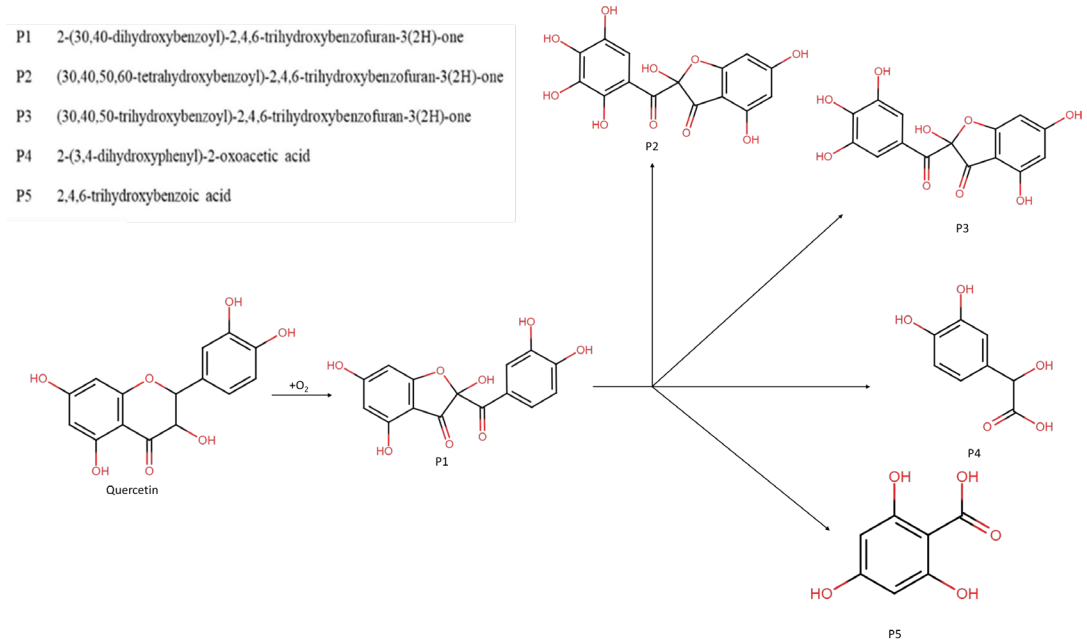

Figure 5. Scheme of the reaction of flavonoid degradation into other phenolics (non-flavonoids) (Chaaban et al., 2017)

The color of the rice straw extract is depicted in Figure 7. Existing literature indicates that flavonoid compounds typically exhibit a pale yellow hue (Iwashina, 2015; Stavenga et al., 2021). The maceration method for extracting rice straw results in a pale yellow color, confirming the presence of the highest flavonoid content. This finding is further supported by the higher TFC observed in macerated rice straw extract compared to reflux and Soxhlet extractions, as illustrated in Figure 5. The increasing darkness observed from maceration to reflux and Soxhlet extraction indicates an elevated concentration of other phenolic compounds (non-flavonoids) (Ge et al., 2021). This result aligns with Figure 5, which shows the highest TPC value for reflux compared to Soxhlet and maceration.

(a) (b) (c)

Figure 6. The color of rice straw extract: (a) soxhlet, (b) reflux, and (c) maceration

According to the literature, flavonoids were recognized as active compounds with antibacterial properties (Biharee et al., 2020; Cushnie & Lamb, 2005; Donadio et al., 2021). Consequently, the selection of an effective extraction method hinged on achieving the highest TFC. As depicted in Figure 5, maceration emerged as the most effective method for extracting rice straw. The optimization of ethanol concentration and contact time during the rice straw extraction process was carried out using the maceration method.

Effect of Ethanol Concentration on TPC and TFC

A comparison of ethanol concentrations was conducted to determine the optimal solvent concentration for extracting flavonoids, which were recognized for their antibacterial properties. Ethanol concentrations were varied at 0%, 25%, 70%, and 96% to evaluate the effect of solvent concentration on TPC and TFC. Notably, 96% ethanol yielded the highest TPC (1288.56 ppm) and TFC (1000.16 ppm), as shown in Figure 8. Consequently, the TPC and TFC exhibited a proportional decline with the reduction in ethanol concentration. According to the literature, the increase of ethanol concentration from 20% to 80% in the *Malaysian Propolis* extraction raised the TFC value from 0.010 ± 0.19 mg QE/ml to 0.034 ± 0.1875 mg QE/ml. TPC also rose from 1,456 ± 0.0025 mg GAE/ml to 8,898 ± 0.008 mg GAE/ml (Yusof et al., 2020). Comparable findings in other studies indicate that increasing the ethanol content from 50% to 70% in the extraction

DOI:https//doi.org/10.22452/mjs.vol44no4.6
Malaysian Journal of Science 44(4): 53-64 (December 2025)

of A. bilimbi resulted in an increase in TFC (62.74 ± 1.16 to 64.81 ± 1.85 mg RTE/g) and TPC (103.79 ± 3.19 to 119.47 ± 1.76 mg GAE/g) (Rahardhian et al., 2019). An increase in ethanol content led to a decrease in the polarity of the solvent. In contrast, flavonoids have relatively low polarity (Wang et al., 2022). As a result, flavonoids were more readily dissolved and extracted when the ethanol concentration was high (Rahardhian et al., 2019; Wang et al., 2022; Yusof et al., 2020). The extraction process was enhanced by the solvent's rapid penetration of the solid matrix of the sample, which was aided by the similarity in polarity (Yusof et al., 2020). Furthermore, the increase in concentration resulted in more ethanol particles in the solution. A higher concentration of ethanol particles led to a greater frequency of contacts between the sample and the solvent (Cui et al., 2021).

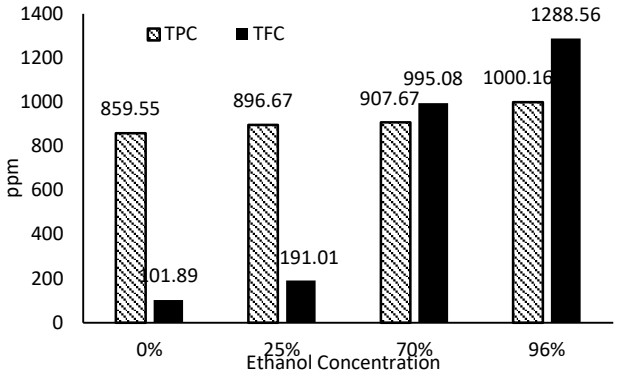

Figure 7. TPC and TFC of rice straw extracts with various ethanol concentrations

Differences in ethanol concentration influenced the color of rice straw extract, as shown in Figure 9. A decrease in color darkness occurred in direct proportion to the increase in ethanol concentration, ranging from 0% to 98% (shifting from dark yellow to pale yellow). This result provided evidence of increased flavonoid content (Iwashina, 2015; Stavenga et al., 2021), as illustrated in Figure 8. Conversely, the dark color of the rice straw extract indicated a high non-flavonoid phenolic content (Ge et al., 2021).

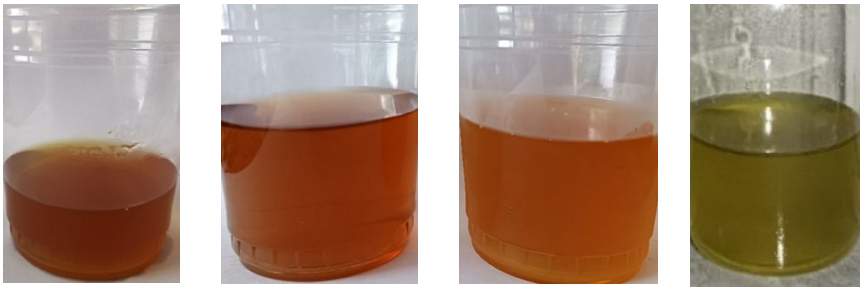

(a) (b) (c) (d)

Figure 8. TPC and TFC of rice straw extracts with various ethanol concentrations

The ethanol concentration was directly proportional to the flavonoid content. Flavonoids have been demonstrated to possess the ability to disrupt bacterial cell walls (Xie et al., 2014). Therefore, 96% ethanol is the most appropriate solvent for rice straw extraction.

Effect of Time Extraction on TPC and TFC

A comparative analysis of extraction time was conducted to determine the most effective period for obtaining flavonoids from rice straw. Extraction times were adjusted to 12 hours, one day, and three days. The data shown in Figure 10 demonstrates that extending the extraction time resulted in an increase in total phenolic content (TPC) and total flavonoid content (TFC). This result is similar to the literature by Diniyah et al. (2023), where increasing the extraction time of *Mucuna pruriens L.* at room temperature from 2 hours to 6 hours caused an increase in TPC (20.79 mg QE/100 g to 26.02 mg QE/100 g) and TFC (0.77 mg QE/100 g to 1.09 mg QE/100 g) (Diniyah et al., 2023). The extended extraction time increases the contact duration between the sample and the solvent (Dewi et al., 2019; Diniyah et al., 2023).

Extending the extraction time resulted in a shift towards a pale yellow color in the extracted solution. These findings indicated increased flavonoid concentration within the extract (Iwashina, 2015; Stavenga et al., 2021). Conversely, the shortest extraction period (12 hours) yielded a darker hue due to the high total phenolic content (TPC), as depicted in Figure 13 (Ge et al., 2021).

DOI:https//doi.org/10.22452/mjs.vol44no4.6
Malaysian Journal of Science 44(4): 53-64 (December 2025)

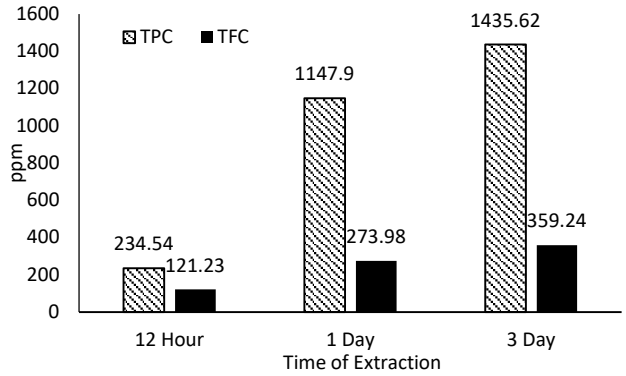

Figure 9. TPC and TFC of rice straw extract with various extraction times

(a) (b) (c)

Figure 10. The color of rice straw extract varies depending on the duration of the extraction process: (a) 12 hours, (b) 1 day, (c) 3 days

Anti-bacterial Activity

Flavonoids are phenolic compounds that exhibit antibacterial capabilities through various mechanisms. Numerous studies have demonstrated that flavonoids can impede energy metabolism, disrupt cytoplasmic membrane function, and inhibit nucleic acid synthesis (Biharee et al., 2020; Donadio et al., 2021; Górniak et al., 2019; Xie et al., 2014). Additionally, flavonoids show the ability to reduce adhesion and biofilm formation, regulate membrane permeability, affect porins on cell membranes, and decrease pathogenicity, which are all critical for bacterial proliferation (Biharee et al., 2020; Donadio et al., 2021; Xie et al., 2014).

Antibacterial testing was performed in this investigation with both gram-negative and gram-positive microorganisms. Gram-negative bacteria are enclosed by a lipopolysaccharide outer membrane and a thin peptidoglycan cell wall, whereas gram-positive bacteria have a thicker peptidoglycan layer and lack an outer membrane (Silhavy et al., 2010). Specifically, *Escherichia coli* served as the representative gram-negative bacterium, and *Staphylococcus aureus* was chosen as the gram-positive counterpart.

The extraction procedure was performed with ethanol concentrations of 96% (sample A), 70% (sample B), and 25% (sample C). Antibacterial testing was conducted by measuring the presence of clear zones (inhibitory zones). Figure 12 shows clear zones were observed in the *Escherichia coli* and *Staphylococcus aureus* tests during the first and second repetitions. These clear zones provided evidence of the antibacterial activity of the rice straw extract. Sample A, shown in Figure 13, exhibited the greatest clear zone width for *Escherichia coli* and *Staphylococcus aureus*. This result is related to the high ethanol content (96%). As shown in Figure 8, 96% ethanol contains the greatest flavonoid concentration (1288.56 ppm), indicating that sample A has better antibacterial effects than samples B and C. These results are consistent with previous studies by Bacon et al. (2017), where increasing the percentage of methanol solvent from 75% to 95% in *jalapeño pepper* extractions improves antibacterial activity against Escherichia coli (leading to a larger clear zone width from 7.4 to 8 mm) (Bacon et al., 2017). The clear zone diameter increased from 9 mm to 12 mm and from 10 mm to 13 mm, respectively, indicating that increasing the methanol concentration from 7.5 mg/ml to 15 mg/ml in the extraction of *Dipcadi viride (L.)* also led to enhanced antibacterial activity against *Escherichia coli* and *Staphylococcus aureus* (Al Farraj et al., 2020). Table 3 presents the classification of clear zones based on the literature. Sample A, classified as "very strong" and "strong," significantly reduced the development of Staphylococcus aureus and Escherichia coli, as shown in Figure 13.

DOI:https//doi.org/10.22452/mjs.vol44no4.6
Malaysian Journal of Science 44(4): 53-64 (December 2025)

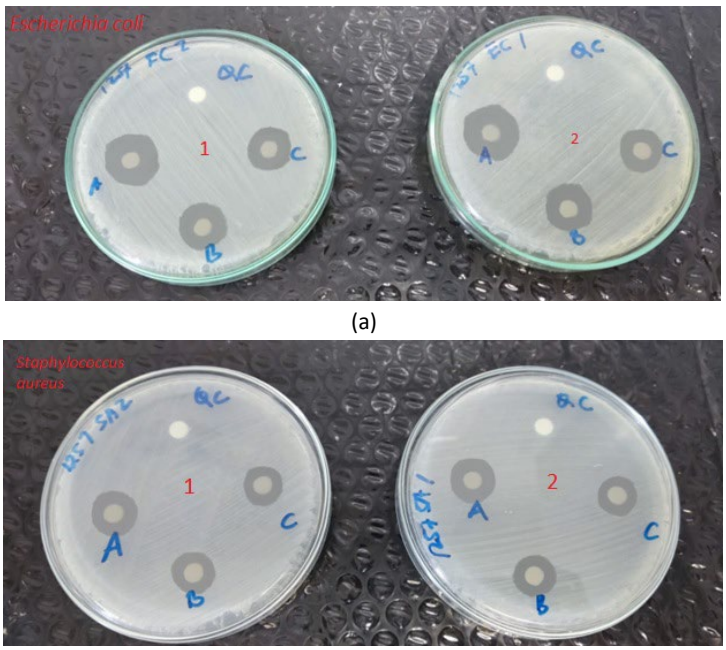

(a)

(b)

Figure 11. Antibacterial test of rice straw extract: (a) *Escherichia coli* dan (b) *Staphylococcus aureus*

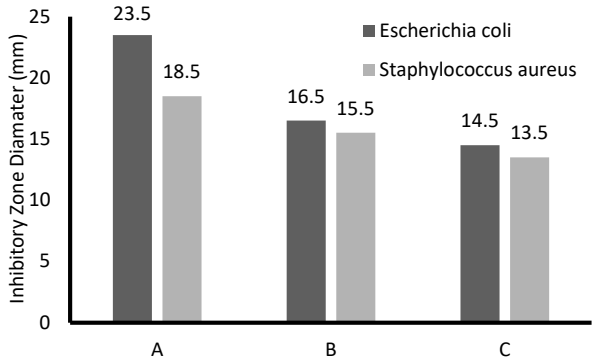

Figure 12. Average Inhibitory Zone Diamater for each straw extract

Table 3. Classification of Inhibitory Zone Diameter (Indriani et al., 2020)

Inhibitory Zone Diamater (mm)	Category
>20	Very Strong
10-20	Strong
5-10	Intermediate
<5	Weak

Figure 12 illustrates that flavonoids extracted from rice straw tend to display superior antibacterial activity against gram-negative bacteria (*Escherichia coli*) compared to gram-positive bacteria (*Staphylococcus aureus*). Several research studies show that flavonoids derived from bergamot orange seeds exhibit stronger antibacterial effects against gram-negative bacteria (*Escherichia coli*, *Pseudomonas putida*, *Salmonella enterica*) than gram-positive bacteria (*Listeria innocua*, *Bacillus subtilis*, *Staphylococcus aureus*, *Lactococcus lactis*) (Mandalari et al., 2007). A similar trend is observed in the flavonoid activity derived from the leaves of Bugis Ginseng (*Talinum paniculatum Gaertn.*). The efficacy of this extract in inhibiting gram-negative bacteria (*Escherichia coli*) is demonstrated by a clear zone measurement of 7.27 mm, which exceeds its impact on gram-positive bacteria (*Staphylococcus aureus*) at 7.04 mm (Emelda et al., 2021).

4. Conclusion

The study findings indicate that maceration is the most efficient approach for extracting flavonoids from rice straw compared to Soxhlet or reflux extraction methods. A direct correlation was observed between the increase in ethanol content and the corresponding rise in TPC and TFC. Significantly, the TPC and TFC values were higher following a three-day extraction period than 12 hours or 1 day. Comparative antibacterial testing demonstrated that the straw extract had greater inhibitory effectiveness against *Escherichia coli* than *Staphylococcus aureus*. The antibacterial activity exhibited a clear association with the TFC of the rice straw extract.

DOI:https//doi.org/10.22452/mjs.vol44no4.6
Malaysian Journal of Science 44(4): 53-64 (December 2025)

5. Acknowledgement

We thank Politeknik Kesehatan Kementerian Kesehatan for supporting this research under DIPA 2023 scheme with contract number DIPA-024.12.2.632259/2023.

6. References

Abdelkader, M., Ahcen, B., Rachid, D., Hakim, H., & Materiel, A. P. (2014). Phytochemical Study and Biological Activity of Sage. *International Journal of Biological, Biomolecular, Agricultural, Food and Biotechnological Engineering*, *8*(11), 1227–1231.

Agbor, G. A., Vinson, J. A., & Donnelly, P. E. (2014). Folin-Ciocalteau Reagent for Polyphenolic Assay. *Int. J. Food Sci. Nutr. Diet.*, *3*(801), 147–156. https://doi.org/10.19070/2326-3350-1400028

Al Farraj, D. A., Gawwad, M. R. A., Mehmood, A., Alsalme, A., Darwish, N. M., Al-Zaqri, N., & Warad, I. (2020). In-vitro antimicrobial activities of organic solvent extracts obtained from Dipcadi viride (L.) Moench. *J. King Saud Univ. Sci.*, *32*(3), 1965–1968. https://doi.org/10.1016/j.jksus.2020.01.007

Alide, T., Wangila, P., & Kiprop, A. (2020). Effect of cooking temperature and time on total phenolic content, total flavonoid content and total in vitro antioxidant activity of garlic. *BMC Res. Notes*, *13*(1), 1–7. https://doi.org/10.1186/s13104-020-05404-8

Anukam, A., Mamphweli, S., Meyer, E., & Okoh, O. (2014). Computer Simulation of the Mass and Energy Balance during Gasification of Sugarcane Bagasse. *J. Energy*, *2014*, 1–9. https://doi.org/10.1155/2014/713054

Bacon, K., Boyer, R., Denbow, C., O'Keefe, S., Neilson, A., & Williams, R. (2017). Evaluation of different solvents to extract antibacterial compounds from jalapeño peppers. *Food Sci. Nutr.*, *5*(3), 497–503. https://doi.org/10.1002/fsn3.423

Bahri-Sahloul, R., Fredj, B. R., Boughalleb, N., Shriaa, J., Saguem, S., Hilbert, J. L., Trotin, F., Ammar, S., Bouzid, S., & Harzallah-Skhiri, F. (2014). Phenolic composition and antioxidant and antimicrobial activities of extracts obtained from Crataegus azarolus L. var. aronia (Willd.) Batt. ovaries calli. *J. Bot.*, *2014*. https://doi.org/10.1155/2014/623651

Balaky, H. H., Galali, Y., Osman, A. A., Karaoğul, E., Altuntas, E., Uğuz, M. T., Galalaey, A. M. K., & Alma, M. H. (2020). Evaluation of antioxidant and antimicrobial activities of mandarin peel (Citrus reticulata blanco) with microwave assisted extract using two different solvents. *Asian J. Plant Sci.*, *19*(3), 223–229. https://doi.org/10.3923/ajps.2020.223.229

Bhaigyabati, T., Bag, G. C., & Grihanjali Devi, P. (2015). Assessment of total flavonoid content and antioxidant activity of methanolic rhizome extract of three Hedychium species of Manipur valley. *Int. J. Pharm. Sci. Rev. Res.*, *30*(1), 154–159.

Biharee, A., Sharma, A., Kumar, A., & Jaitak, V. (2020). Antimicrobial flavonoids as a potential substitute for overcoming antimicrobial resistance. *Fitoterapia*, *146*, 104720. https://doi.org/10.1016/j.fitote.2020.104720

Blainski, A., Lopes, G. C., & De Mello, J. C. P. (2013). Application and analysis of the folin ciocalteu method for the determination of the total phenolic content from limonium brasiliense L. *Molecules*, *18*(6), 6852–6865. https://doi.org/10.3390/molecules18066852

BPS-Indonesian Statistics. (2021). Luas Panen dan Produksi Padi di Indonesia 2021. In *Berita Resmi Statistik* (Vol. 2021, Issue 77).

Chaaban, H., Ioannou, I., Chebil, L., Slimane, M., Gérardin, C., Paris, C., Charbonnel, C., Chekir, L., & Ghoul, M. (2017). Effect of heat processing on thermal stability and antioxidant activity of six flavonoids. *J. Food Process. Preserv.*, *41*(5). https://doi.org/10.1111/jfpp.13203

Chua, L. S., Latiff, N. A., & Mohamad, M. (2016). Reflux extraction and cleanup process by column chromatography for high yield of andrographolide enriched extract. *J. Appl. Res. Med. Aromat. Plants*, *3*(2), 64–70. https://doi.org/10.1016/j.jarmap.2016.01.004

Chun, O. K., Kim, D. O., & Lee, C. Y. (2003). Superoxide Radical Scavenging Activity of the Major Polyphenols in Fresh Plums. *J. Agric. Food Chem.*, *51*(27), 8067–8072. https://doi.org/10.1021/jf034740d

Cui, X., Lamborg, C. H., Hammerschmidt, C. R., Xiang, Y., & Lam, P. J. (2021). The Effect of Particle Composition and Concentration on the Partitioning Coefficient for Mercury in Three Ocean Basins. *Front. Env. Chem.*, *2*(May), 1–16. https://doi.org/10.3389/fenvc.2021.660267

Cushnie, T. P. T., & Lamb, A. J. (2005). Antimicrobial activity of flavonoids. *Int. J. Antimicrob. Agents*, *26*(5), 343–356. https://doi.org/10.1016/j.ijantimicag.2005.09.002

Dewi, A. L., Siregar, V. D., & Kusumayanti, H. (2019). Effect of Extraction Time on Tannin Antioxidant Level and Flavonoid on Pandan Wangi Leaf (Pandanusamary llifolius Roxb) Using Hydrothermal Extractor. *J. Phys. Conf. Ser.*, *1295*(1). https://doi.org/10.1088/1742-6596/1295/1/012066

Diniyah, N., Bulgis, U. M., & Novi Marchianti, A. C. (2023). Antioxidant activity and phytochemical compositions of Mucuna pruriens L. in different conditions of time and temperature extraction. *IOP Conf. Ser.: Earth Environ. Sci.*, *1177*(1), 012042. https://doi.org/10.1088/1755-1315/1177/1/012042

DOI:https//doi.org/10.22452/mjs.vol44no4.6
Malaysian Journal of Science 44(4): 53-64 (December 2025)

Donadio, G., Mensitieri, F., Santoro, V., Parisi, V., Bellone, M. L., De Tommasi, N., Izzo, V., & Piaz, F. D. (2021). Interactions with microbial proteins driving the antibacterial activity of flavonoids. *Pharmaceutics*, *13*(5). https://doi.org/10.3390/pharmaceutics13050660

Elzaawely, A. A., Maswada, H. F., El-Sayed, M. E. A., & Ahmed, M. E. (2017). Phenolic Compounds and Antioxidant Activity of Rice Straw Extract. *Int. Lett. Nat. Sci.*, *64*, 1–9. https://doi.org/10.18052/www.scipress.com/ilns.64.1

Emelda, A., Fitriana, & Adnan, R. S. (2021). Antibacterial Activity of Ethanol Extract and Ethyl Acetate of Ginseng Bugis (*Talinum Panicullatum Gaertn.*) Leaves against Staphylococcus Aureus and Escherichia coli Bacteria. *J. Phys. Conf. Ser.*, *1899*(1). https://doi.org/10.1088/1742-6596/1899/1/012007

Fadillah, A., Rahmadani, A., & Rijai, L. (2007). Analysis of total flavonoid and antioxidant activity of Passion leaves (*Passiflora foetida L.*). *Proceeding of the 5th Mulawarman Pharmaceuticals Conference*, *April*, 23–24.

Gadde, B., Bonnet, S., Menke, C., & Garivait, S. (2009). Air pollutant emissions from rice straw open field burning in India, Thailand and the Philippines. *Environ. Pollut.*, *157*(5), 1554–1558. https://doi.org/10.1016/j.envpol.2009.01.004

Gao, Y., Xia, W., Shao, P., Wu, W., Chen, H., Fang, X., Mu, H., Xiao, J., & Gao, H. (2022). Impact of thermal processing on dietary flavonoids. *Curr. Opin. Food Sci.*, *48*, 100915. https://doi.org/10.1016/j.cofs.2022.100915

Ge, X., Jing, L., Zhao, K., Su, C., Zhang, B., Zhang, Q., Han, L., Yu, X., & Li, W. (2021). The phenolic compounds profile, quantitative analysis and antioxidant activity of four naked barley grains with different color. *Food Chem.*, *335*, 127655. https://doi.org/10.1016/j.foodchem.2020.127655

Górniak, I., Bartoszewski, R., & Króliczewski, J. (2019). Comprehensive review of antimicrobial activities of plant flavonoids. *Phytochem. Rev.*, *18*(1), 241–272. https://doi.org/10.1007/s11101-018-9591-z

Indonesian Ministry of Home Affairs. (2004). *Rice Commodity Profile*. https://ews.kemendag.go.id/file/commodity/120116_ANK_PKM_DSK_Jagung Rev 1.4.pdf

Indriani, V., Chiuman, L., Wijaya, L. L., Lister, G., & Grandis, L. (2020). Antibacterial Effect of Curcuma zedoaria Extract on Bacillus cereus and Staphylococcus epidermidis. *Althea Med. J.*, *7*(1), 6–10. https://doi.org/10.15850/amj.v7n1.1886

Iwashina, T. (2015). Contribution to flower colors of flavonoids including anthocyanins: A review. *Nat. Prod. Commun.*, *10*(3), 529–544. https://doi.org/10.1177/1934578x1501000335

Karimi, E., Mehrabanjoubani, P., Keshavarzian, M., Oskoueian, E., Jaafar, H. Z., & Abdolzadeh, A. (2014). Identification and quantification of phenolic and flavonoid components in straw and seed husk of some rice varieties (*Oryza sativa L.*) and their antioxidant properties. *J. Sci. Food Agric.*, *94*(11), 2324–2330. https://doi.org/10.1002/jsfa.6567

Kumar, A., Kushwaha, K. K., Singh, S., Shivay, Y. S., Meena, M. C., & Nain, L. (2019). Effect of paddy straw burning on soil microbial dynamics in sandy loam soil of Indo-Gangetic plains. *Environ. Technol. Innov.*, *16*, 100469. https://doi.org/10.1016/j.eti.2019.100469

Lang, G. H., Lindemann, I. da S., Ferreira, C. D., Hoffmann, J. F., Vanier, N. L., & de Oliveira, M. (2019). Effects of drying temperature and long-term storage conditions on black rice phenolic compounds. *Food Chem.*, *287*, 197–204. https://doi.org/10.1016/j.foodchem.2019.02.028

Mandalari, G., Bennett, R. N., Bisignano, G., Trombetta, D., Saija, A., Faulds, C. B., Gasson, M. J., & Narbad, A. (2007). Antimicrobial activity of flavonoids extracted from bergamot (Citrus bergamia Risso) peel, a byproduct of the essential oil industry. *J. Appl. Microbiol.*, *103*(6), 2056–2064. https://doi.org/10.1111/j.1365-2672.2007.03456.x

Martono, Y., Yanuarsih, F. F., Aminu, N. R., & Muninggar, J. (2019). Fractionation and determination of phenolic and flavonoid compound from Moringa oleifera leaves. *J. Phys. Conf. Ser.*, *1307*(1). https://doi.org/10.1088/1742-6596/1307/1/012014

Mayerhöfer, T. G., & Popp, J. (2019). Beer's Law – Why Absorbance Depends (Almost) Linearly on Concentration. *Chem. Phys. Chem.*, *20*(4), 511–515. https://doi.org/10.1002/cphc.201801073

Mekonnen, A., & Desta, W. (2021). Comparative study of the antioxidant and antibacterial activities of Rumex abyssinicus with commercially available Zingiber officinale and Curcuma longa in Bahir Dar city, Ethiopia. *Chem. Biol. Technol. Agric.*, *8*(1), 1–11. https://doi.org/10.1186/s40538-020-00198-0

Rabiu, A., & Haque, M. (2017). Preparation of Medicinal Plants: Basic Extraction and Fractionation Procedures for Experimental Purposes Article. *Asian J. Pharm. Clin. Res.*, *7*(10), 1–5. https://doi.org/10.4103/jpbs.JPBS

Rahardhian, M. R. R., Murti, B. T., Wigati, D., Suharsanti, R., & Putri, C. N. (2019). Solvent concentration effect on total flavonoid and total phenolic contents of Averrhoa bilimbi leaf extract. *Pharmaciana*, *9*(1), 137. https://doi.org/10.12928/pharmaciana.v9i1.8793

Rammohan, A., Bhaskar, B. V., Venkateswarlu, N., Rao, V. L.,

DOI:https//doi.org/10.22452/mjs.vol44no4.6
Malaysian Journal of Science 44(4): 53-64 (December 2025)

Gunasekar, D., & Zyryanov, G. V. (2019). Isolation of flavonoids from the flowers of Rhynchosia beddomei Baker as prominent antimicrobial agents and molecular docking. *Microb. Pathog.*, *136*, 1–7. https://doi.org/10.1016/j.micpath.2019.103667

Redfern, J., Kinninmonth, M., Burdass, D., & Verran, J. (2014). Tips & Tools Using Soxhlet Ethanol Extraction to Produce and Test Plant. *J. Microbiol. Biol. Educ.*, *15*(1), 45–46.

Romasanta, R. R., Sander, B. O., Gaihre, Y. K., Alberto, M. C., Gummert, M., Quilty, J., Nguyen, V. H., Castalone, A. G., Balingbing, C., Sandro, J., Correa, T., & Wassmann, R. (2017). How does burning of rice straw affect CH_4 and N_2O emissions? A comparative experiment of different on-field straw management practices. *Agric. Ecosyst. Environ.*, *239*, 143–153. https://doi.org/10.1016/j.agee.2016.12.042

Ross, C. F., Hoye, C., & Fernandez-Plotka, V. C. (2011). Influence of Heating on the Polyphenolic Content and Antioxidant Activity of Grape Seed Flour. *J. Food Sci.*, *76*(6), 884–890. https://doi.org/10.1111/j.1750-3841.2011.02280.x

Shi, L., Zhao, W., Yang, Z., Subbiah, V., & Suleria, H. A. R. (2022). Extraction and characterization of phenolic compounds and their potential antioxidant activities. *Environ. Sci. Pollut. Res.*, *29*(54), 81112–81129. https://doi.org/10.1007/s11356-022-23337-6

Shraim, A. M., Ahmed, T. A., Rahman, M. M., & Hijji, Y. M. (2021). Determination of total flavonoid content by aluminum chloride assay: A critical evaluation. *Lwt*, *150*, 111932–111943. https://doi.org/10.1016/j.lwt.2021.111932

Silhavy, T. J., Kahne, D., & Walker, S. (2010). The Bacterial Cell Envelope. *Cold Spring Harb. Perspect. Biol.*, *2*(5), 1–16. https://doi.org/doi: 10.1101/cshperspect.a000414

Stavenga, D. G., Leertouwer, H. L., Dudek, B., & van der Kooi, C. J. (2021). Coloration of Flowers by Flavonoids and Consequences of pH Dependent Absorption. *Front. Plant Sci.*, *11*, 1–11. https://doi.org/10.3389/fpls.2020.600124

Tambun, R., Alexander, V., & Ginting, Y. (2021). Performance comparison of maceration method, soxhletation method, and microwave-assisted extraction in extracting active compounds from soursop leaves (*Annona muricata*): A review. *IOP Conf. Ser.: Mater. Sci. Eng.*, *1122*(1), 1–7. https://doi.org/10.1088/1757-899x/1122/1/012095

Tsao, R. (2010). Chemistry and biochemistry of dietary polyphenols. *Nutrients*, *2*(12), 1231–1246. https://doi.org/10.3390/nu2121231

Vifta, R. L., Trinadi, K. S., & Suratno, S. (2022). Potential of Flavonoid Content from Clitoria ternatea Flowers Extract as Natural Antioxidant Candidate and Its Correlation. *Proceedings of Conference on Health Universitas Ngudi Waluyo*, *1*, 53–60.

Vuolo, M. M., Lima, V. S., & Maróstica Junior, M. R. (2019). Phenolic Compounds: Structure, Classification, and Antioxidant Power. In *Bioactive Compounds: Health Benefits and Potential Applications*. Elsevier Inc. https://doi.org/10.1016/B978-0-12-814774-0.00002-5

Wang, Z., Yang, S., Gao, Y., & Huang, J. (2022). Extraction and purification of antioxidative flavonoids from Chionanthus retusa leaf. *Frontiers in Bioengineering and Biotechnology*, *10*(December), 1–8. https://doi.org/10.3389/fbioe.2022.1085562

Widiyastuti, W., Rois, M. F., Setyawan, H., Machmudah, S., & Anggoro, D. (2020). Carbonization of lignin extracted from liquid waste of coconut coir delignification. *Indones. J. Chem.*, *20*(4), 842–849. https://doi.org/10.22146/ijc.46484

Xie, Y., Yang, W., Tang, F., Chen, X., & Ren, L. (2014). Antibacterial Activities of Flavonoids: Structure-Activity Relationship and Mechanism. *Curr. Med. Chem.*, *22*(1), 132–149. https://doi.org/10.2174/0929867321666140916113443

Yusof, N., Abdul Munaim, M. S., & Veloo Kutty, R. (2020). The effects of different ethanol concentration on total phenolic and total flavonoid content in *Malaysian Propolis*. *IOP Conf. Ser.: Mater. Sci. Eng.*, *991*(1), 5–10. https://doi.org/10.1088/1757-899X/991/1/012033

Zhu, H., Wang, Y., Liu, Y., Xia, Y., & Tang, T. (2010). Analysis of flavonoids in Portulaca oleracea L. by UV-vis spectrophotometry with comparative study on different extraction technologies. *Food Anal. Methods*, *3*(2), 90–97. https://doi.org/10.1007/s12161-009-9091-2

DOI:https//doi.org/10.22452/mjs.vol44no4.6
Malaysian Journal of Science 44(4): 53-64 (December 2025)

MALAYSIAN JOURNAL OF SCIENCE
MJS
ISSN 1394-3065

Regular Issue

Malaysian Journal of Science 44 (4): 65-76 (December 2025) https://mjs.um.edu.my

Coalbed Methane Potential of The Muara Enim Formation in The South Sumatera Basin as a Source of Natural Gas

Yulfi Zetra[1a], Muhamad Nur Khozin[2a], R.Y. Perry Burhan[3a]*, Shindy Eka Fittriani[4a], Zjahra Vianita Nugrahaeni[5a], Rizka Berliana Putri[6a] and Husnul Rohma[7a]

Abstract: Identification of aromatic hydrocarbon fraction by biomarker analysis was carried out to determine the geochemical characteristics of the coal samples from the Muara Enim formation in the South Sumatra basin for potential coalbed methane (CBM) exploration and production. Biomarker analysis using gas chromatography-mass spectrometry (GC-MS) shows the distribution of naphthalene, phenanthrene, and pentacyclic polyaromatic triterpenoid compound groups. The high abundance of 1,2,5- and 1,2,7-trimethylnaphthalene (TMN) compounds indicates that the organic matter in the coal samples mostly originated from higher Angiosperm plants that were deposited in a terrestrial and oxic environment. This terrestrial depositional environment was also indicated by the dominance of the 1,6- and 1,7- dimethylphenanthrene (DMP) compounds. The low maturity of the analyzed coal was indicated by the dominance of less stable isomers over more stable isomers. The identification of 2- and 1- methylphenanthrene (MP) biomarkers that are associated with type II and type III kerogens in relatively high abundance indicates that the analyzed coal samples tend to produce oil and gas. However, the lower abundance value of 2,7-dimethyl-1,2-(isopropylpenteno)-1,2,3,4-tetrahydrochrysene compared to 1,2,4a,9-tetramethyl-1,2,3,4,4a ,5,6,14b-octahydropicene indicates that the coal samples from the Muara Enim formation possess a higher potential to produce gas than oil. In addition, the high vitrinite content in the samples is related to type III kerogen, which shows that the coal is more gas-prone than oil-prone. The obtained methylphenanthrene index (MPI) value of 0.99 indicates moderate maturity of coal. These implicatons show that the analyzed coal can be exploited for its CBM gas content.

Keywords: *Coalbed methane, coal, biomarker, aromatic hydrocarbon, GC-MS analysis, Muara Enim.*

1. Introduction

Coalbed methane (CBM) is a rare natural gas found in coal seams. This gas is trapped in the coal matrix in the form of bubbles or dissolved in water and released into the surrounding sediment during compaction at shallow depths and low temperatures (Gao et al., 2020). A ton of coal typically produces 250–500 cubic feet of methane gas but can produce 250,000–500,000 Btu when burned. This energy potential makes CBM suitable for use as a fuel (Gao et al., 2020). Furthermore, CBM can be extracted from coal deposits without having to conduct coal mining. CBM is an environmentally friendly fuel because it does not produce sulfur oxides, nitrogen, or other toxic materials. The carbon dioxide gas emissions produced by CBM are less than those produced by the direct combustion of conventional coal fossil fuels in steam power plants. The development of CBM by the coal mining industry in Indonesia has a positive impact on the environment by reducing in-situ gas content during the exploitation process, which can also improve industrial safety conditions (Huang et al., 2019).

Indonesia has the largest coal reserves in the Asia-Pacific region and is one of the largest coal-producing countries in the world. As of 2020, the total coal resources in Indonesia reached 143.73 billion tons, with coal reserves reaching up to 38.80 billion tons (ESDM, 2020), which accounts for 3.7% of the world's reserves. Most Indonesian coal is low- and medium-calorie, which posses a lower economic value than high-calorie coal (Nugroho, 2017). Furthemore, many of the largest coal reserves are located in the South Sumatra Basin. This basin is a tertiary basin that includes the Lahat, Lemat, Talang Akar, Baturaja, Gumai, Lower Palembang, Kasai and Muara Enim formations. The Muara Enim formation has coal bearings that were formed in the Late Miocene to Early Pliocene eras (Amijaya et al., 2006; Darman, 2000; Kim et al., 2017; Stanford, 2013; Yasin et al., 2021).

Knowledge on the origin of CBM is a prerequisite for formulating an effective and successful CBM exploration strategy (Martini et al., 2008; Scott et al., 1994). Biogenic CBM is produced through microbial decomposition of organic matter in coal at low temperatures (usually less than 56 °C). In contrast, thermogenic CBM is produced from thermal decomposition of organic matter in coal, primarily at temperatures above 100 °C at which methanogenic microbial activity becomes biochemically impossible (Hunt, 1979; Rice & Claypool, 1981). The exploration of biogenic CBM should be focused on shallow and thermally immature coal seams that possess larger fractures which can result in a faster gas extraction process. In contrast, thermogenic CBM is more likely to accumulate in deeper and more thermally mature coal seams, where the network of open fractures are

Authors information:
[a]Department of Chemistry, Sepuluh Nopember Institute of Technology, Surabaya, INDONESIA. E-mail: yzetra@chem.its.ac.id[1]; muhamadnurkhozin96@gmail.com[2]; peiburhan@gmail.com[3]; shindyekaf30@gmail.com[4]; zjahravianita@chem.its.ac.id[5]; rizkaberliana42@gmail.com[6]; husnul.rohma@gmail.com[7]
*Corresponding Author: peiburhan@gmail.com

Received: March, 2024
Accepted: October, 2024
Published: December, 2025

DOI:https//doi.org/10.22452/mjs.vol44no4.7
Malaysian Journal of Science 44(4): 65-76 (December 2025)

limited (McIntosh et al., 2008; Rice, 1993; Strapoć et al., 2007). Furthermore, the production of mixed CBM (thermogenic and biogenic) require complex exploration and production strategies based on the local geological and hydrological conditions. Thus, successful CBM exploration largely depends on studying the origin of coal seam gas (Dai et al., 2009; Faiz & Hendry, 2008; Flores et al., 2008; Rice, 1993; Scott et al., 1994; Whiticar, 1999).

Biomarker analysis can be carried out to identify the origin of coal seam gas for CBM exploration. Aromatic hydrocarbon biomarkers with naphthalene, phenanthrene and pentacyclic aromatic triterpenoid structural frameworks indicate that the organic matter originate from terrestrial higher plants. Isomers such as 1,2,5-TMN and 1,2,7-TMN can be used as indicators of coal deposition environments (Burhan et al., 2020; Jiang & George, 2019; Wang et al., 2022). The presence of methylphenanthrene biomarkers can be used to determine the type of kerogen on the van Krevelen diagram. The presence of 3-MP, 2-MP, 9-MP and 1-MP isomers potentially determines whether coal is a gas producer (gas-prone) or oil producer (oil-prone). Kerogen types I and II are oil-prone, whereas kerogen type III is gas-prone (El-Sabagh et al., 2018; Zhang & Li, 2018).

The biogenical formation of CBM with the help of bacteria requires a group of methoxylated aromatic compounds (MACs) or compounds that have methoxy groups to carry out methanogenesis and produce methane gas. Methanosarcinales bacteria convert MACs into methane gas in coal seams. These MACs are derivatives of lignin found in plant wood tissue and are often buried in humic coal sediments, so these compounds can be considered biogenic markers of CBM (Mayumi et al., 2016). In this article, geochemical characterization of the coal samples extracted from the Muara Enim formation is conducted by aromatic biomarker analysis and discusses the implications of the biomarker analysis to determine the origin of organic matter, depositional environment and coal maturity for CBM exploration and production.

2. Method

Sample

The coal samples in this study were extracted from the Muara Enim mine in Rambutan Field, South Sumatra Basin, which were formed in the Cretaceous-Early Tertiary period. The samples taken at a depth of 503.7 m with a layer thickness of 10.67 m were included in the sub-bituminous rank.

Method

A total of 10 g of finely ground coal sample was extracted in a dichloromethane/methanol solvent (97:3 v/v) for 16 h. The solvent mixture was evaporated and the asphaltene and maltene were separated using an excess n-hexane solvent (Theuerkorn et al., 2008). The maltene extract was fractionated by thin layer chromatography using silica gel GF_{254} in an *n*-hexane solvent to separate aliphatic and aromatic hydrocarbon fractions. Furthermore, the aromatic hydrocarbon fraction was analyzed for its components by Gas Chromatography-Mass Spectrometry (GC-MS) using Agilent 122-5561 with an HP-5MS column type (60 µm x 250 µm x 0.33 µm). The carrier gas was helium, the flow rate was set to 1 mL/min and the mass spectrometer was conditioned at an energy of 70 eV. The operating temperature was initiated at 70 ℃ and kept isothermal for 1 minute and then increased to 180 °C at a rate of 10 °C/min. The temperature was increased again to 315 °C at a rate of 4 °C/min and kept isothermal for 30 min. The mass spectrometer was operated in full-scan mode. The biomarker structure was identified based on specific m/z fragmentograms, retention time patterns and by comparing the mass spectrum with reference data published by previous researchers.

3. Results and Discussion

Coal Classification

The analyzed coal sample had a calorific value of 5669 cal/gram, which is equivalent to the subbituminous coal rank (Sharma et al., 2019). This subbituminous coal ranking is in accordance with the results of the proximate analysis carried out by (Sosrowidjojo, 2013). The results include, among others, a low vitrinite reflectance (Ro = 0.31–0.49%) which indicate subbituminous rank, high moisture content (21%), low ash content (5.6 – 19.8%), volatile matter of the seams in the range of 29.3–45.8%, fixed carbon content less than 80% weight (daf) and a maximum fixed carbon of 46.54%.

Identification of Aromatic Hydrocarbon Fraction Biomarkers

The biomarker structure of the aromatic hydrocarbon fraction was identified based on specific m/z fragmentograms, mass spectra and comparing the results with previous publications (Buckley et al., 2021; Burhan et al., 2019; Gan et al., 2023; Lima et al., 2023; Synnott et al., 2021; Zheng et al., 2023). The biomarkers identified were naphthalene, phenanthrene and aromatic pentacyclic triterpenoid compounds (Figure 1 and Table 1).

DOI:https//doi.org/10.22452/mjs.vol44no4.7
Malaysian Journal of Science 44(4): 65-76 (December 2025)

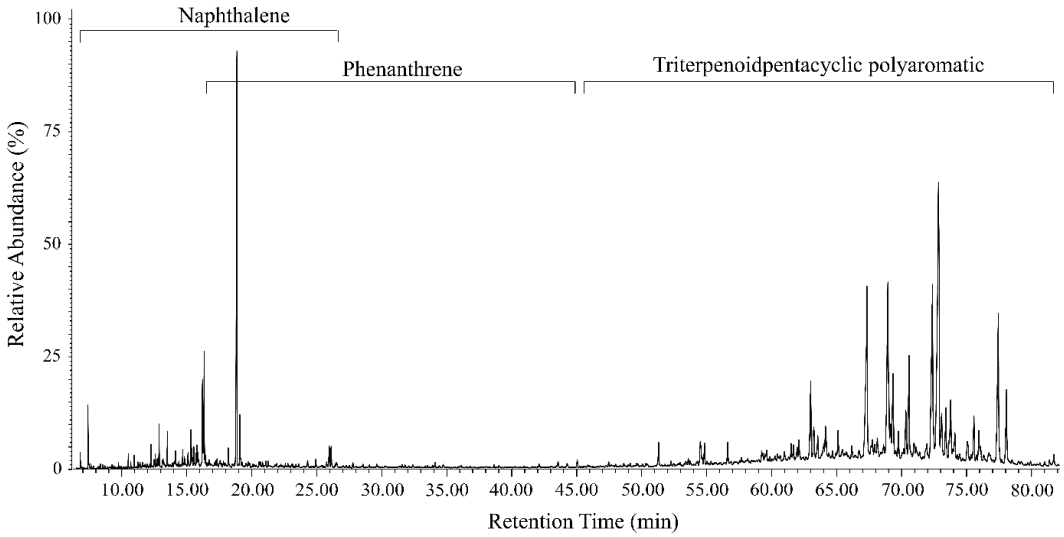

Figure 1. Total ion chromatogram (TIC) of aromatic hydrocarbon compounds

Table 1. Abundance of naphthalene, phenanthrene and pentacyclic polyaromatic triterpenoid compounds

Naphthalene			Phenanthrene			Polyaromatic pentacyclic triterpenoid		
Compounds	*m/z*	% abundance	Compounds	*m/z*	% abundance	Compounds	*m/z*	% abundance
2-MN	142	33.85	3-MP	192	10.63	C_{27} triaromatic-8,14-secotriterpenoid	169	100
1-MN	142	66.15	2-MP	192	38.56	C_{28} triaromatic-8,14-secotriterpenoid	183	100
(2+1)-EN	156	1.33	9-MP	192	23.53	2,9-dimethylpicene	306	100
(2,6+2,7)-DMN	156	10.09	1-MP	192	27.29	1,2,9-trimethylpicene	320	100
(1,3+1,7)-DMN	156	12.58	2,6-DMP	206	3.42	2,2,9-trimethyl-1,2,3,4-tetrahydropicene	324	63.8
1,6-DMN	156	65.52	(1,3+2,10+3,9+3,10)-DMP	206	8.7	1,2,9-trimethyl-1,2,3,4-tetrahydropicene	324	36.2
(1.4+2.3+1.5)-DMN	156	6.5	(1,6+2,9)-DMP	206	37.02	8,14-triaromatic secolupane	145	76.36
1,2-DMN	156	3.99	1,7-DMP	206	29.35	8,14-triaromatic secooleanane	145	23.64

DOI:https//doi.org/10.22452/mjs.vol44no4.7
Malaysian Journal of Science 44(4): 65-76 (December 2025)

Naphthalene			Phenanthrene			Polyaromatic pentacyclic triterpenoid		
Compounds	*m/z*	% abundance	Compounds	*m/z*	% abundance	Compounds	*m/z*	% abundance
1,3,7-TMN	170	2.36	2,3-DMP	206	5.11	1,2,4a,9-tetramethyl-1,2,3,4,4a,5,6,14b-octahydropicene	257	89.02
1,3,6-TMN	170	13.91	(1,9+1,4)-DMP	206	10.48	2,7-dimethyl-1,2-(isopropylpenteno)-1,2,3,4-tetrahydrochrysene	257	10.98
(1,4,6+1,3,5)-TMN	170	7.16	1,8-DMP	206	5.93			
2,3,6-TMN	170	7.08	(1,3,6+1,3,10+2,6,10)-TMP	220	8.82			
1,2,7-TMN	170	23.08	(1,3,7+2,6,9+2,7,9)-TMP	220	15.96			
(1,6,7+1,2,6)-TMN	170	6.38	(1,3,9+2,3,6)-TMP	220	10.46			
1,2,4-TMN	170	28.17	(1,6,9+1,7,9+2,7,3)-TMP	220	14.6			
1,2,5-TMN	170	11.85	1,3,8-TMP	220	12.28			
			2,3,10-TMP	220	8.51			
			1,6,7-TMP	220	9.98			
			1,2,8-TMP	220	19.39			

MN = Methyl Naphthalene MP = Methyl Phenanthrene

EN = Ethyl Naphthalene DMP = Dimethyl Naphthalene

DMN = Dimethyl Naphthalene TMP = Trimethyl Naphthalene

TMN = Trimethyl Naphthalene

DOI:https//doi.org/10.22452/mjs.vol44no4.7
Malaysian Journal of Science 44(4): 65-76 (December 2025)

The presence of alkyl naphthalene in the coal samples is produced by the precursor β-amyrin, which comes from higher Angiosperm plants (Ding et al., 2022; Li et al., 2022). The higher abundance of 1-MN compared to 2-MN is shown in Figure 2 and Table 1. Structurally, the stability of α-substituted 1-MN is lower than that of β-substituted 2-MN. Therefore, the low maturity of the analyzed samples is indicated by the higher abundance of 1-MN compared to 2-MN (Abdullah et al., 2021; Burhan et al., 2019, 2020; Killops & Killops, 2005; Zetra et al., 2016). However, to determine the organic geochemical characteristics, such as maturity, source of organic compounds and depositional environment, it is necessary to conduct other biomarker analysis on the samples.

Dimethylnaphthalene (DMN) compounds can be used to indicate coal maturity based on differences in isomer intensity. The abundance of 1,6-DMN compounds was higher than that of other DMNs, namely 1,2-DMN and 2,6+2,7-DMN (Figure 2). The thermal maturity of the coal samples can be determined from the abundance value of the identified isomers. The high intensity of the 1,6-DMN peak, which is a less stable isomer compared to 2,6+2,7-DMN and 1,2-DMN, indicates immature coal. Therefore, the dominance of 1,6-DMN compounds over 1,2-DMN and 2,6+2,7-DMN in the samples indicates that the coal samples are immature (Fang et al., 2019; He et al., 2019; Killops & Killops, 2005; Wang et al., 2022; Zetra et al., 2016).

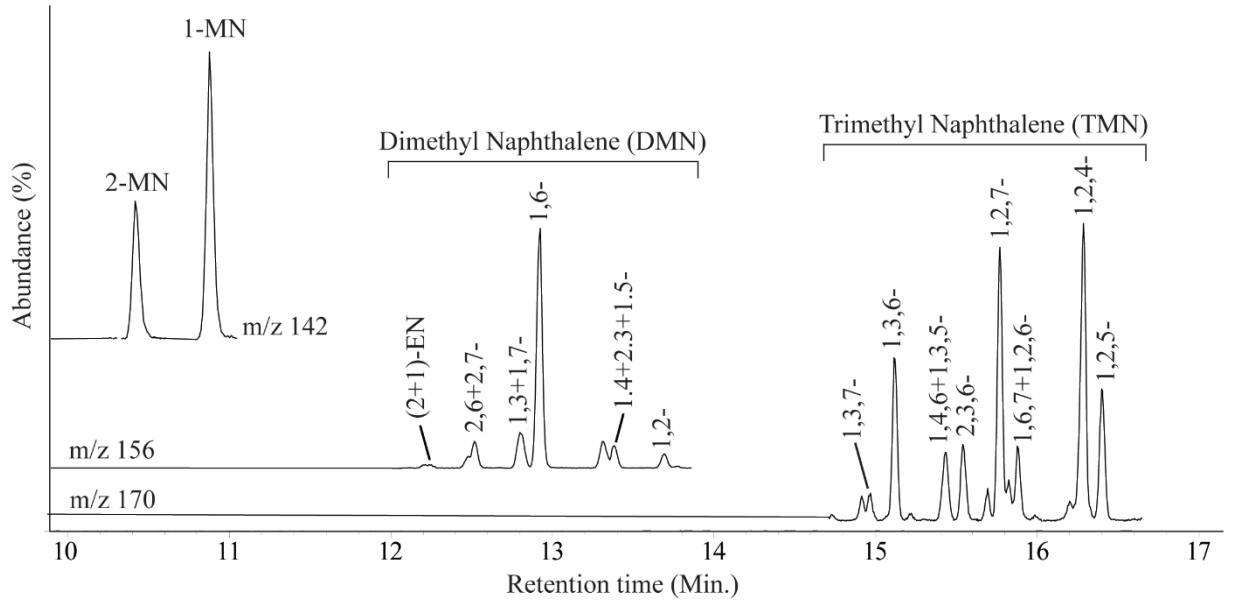

Figure 2. The presence of naphthalene-derived compounds

Another alkyl naphthalene compound in the coal samples that was analyzed was trimethylnaphthalene (TMN). In Figure 2 and Table 1, it can be seen that the isomers 1,2,4-TMN and 1,2,7-TMN have higher abundance values than the other isomers. The higher abundance of less stable isomers indicates the low maturity of the sediment samples (Aboglila et al., 2019; Li et al., 2022). Compounds 1,2,7-TMN and 1,2,4-TMN are less stable isomers compared to 1,2,5-TMN. Therefore, the higher abundance of compounds 1,2,4-TMN and 1,2,7-TMN compared to 1,2,5-TMN indicates immature samples. The presence of the isomers 1,2,5-TMN and 1,2,7-TMN in the analyzed CBM samples also indicates an oxic depositional environment, which were produced through the degradation of β-amyrin compounds as precursors (Burhan et al., 2019). In addition, the formation of 1,2,5,6-TeMN and 1,2,5-TMN compounds in the coal samples indicates the presence of bacterial input via bacteriohopanetetrol as a precursor (Ogungbesan & Adedosu, 2020; Qiao et al., 2021; Rontani et al., 2017).

The cadalene and isocadalene compounds identified based on the m/z 183 fragmentogram are naphthalene derivatives formed through the depolymerization of polycadinene derived from higher plant resins (Zakrzewski & Kosakowski, 2021). These two isomers have the potential to be used as indicators of coal maturity because isocadalene compounds originate from the isomerization of cadalene through thermal enhancement. The deeper the coal deposition environment, the higher the abundance of isocadalene compounds. Therefore, the lower abundance of isocadalene compared to cadalene indicates that the coal samples are immature (Li et al., 2022).

DOI:https//doi.org/10.22452/mjs.vol44no4.7
Malaysian Journal of Science 44(4): 65-76 (December 2025)

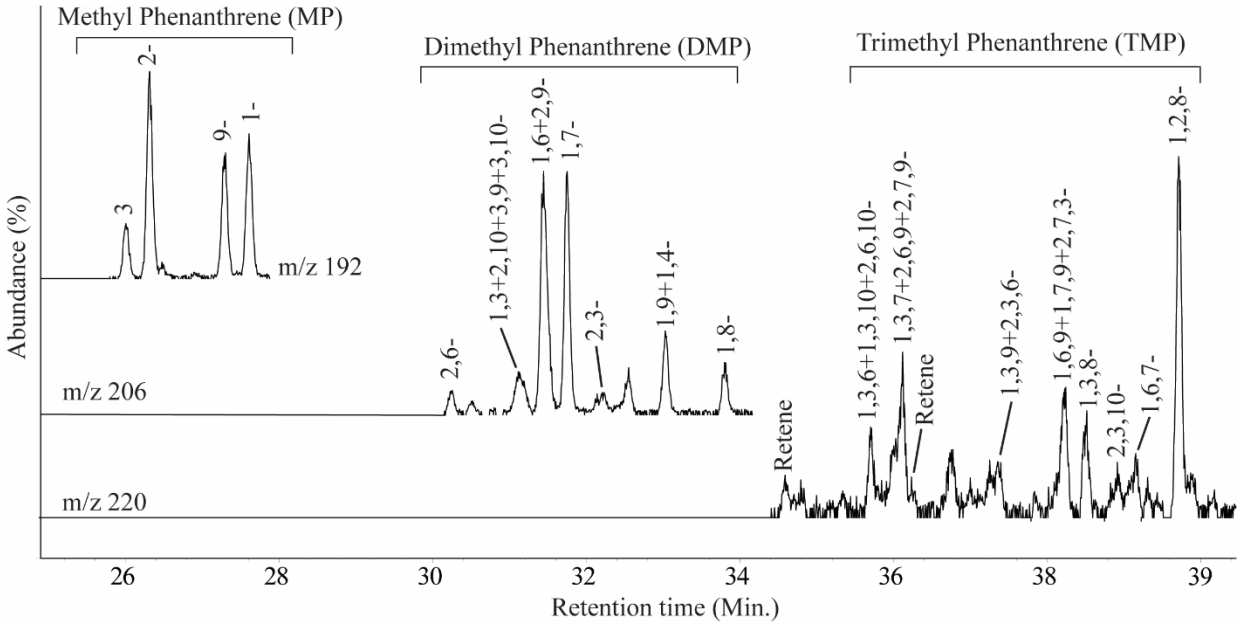

Figure 3. The presence of phenanthrene-derived compounds

The distribution of methylphenanthrene (MP) is shown in Figure 3 and Table 1, with the higher peak of 2-MP indicating a higher abundance. Furthermore, 9-MP and 1-MP showed similar abundance values, with 1-MP having a slightly higher abundance value. The low abundance of 3-MP, which is relatively more stable than 1-MP and 9-MP, indicates the low maturity of the analyzed samples. However, the high abundance of 2-MP, which is a more stable isomer compared to 1-MP and 9-MP, also indicates high maturity (Ayu et al., 2021). To further analyze the maturity of the coal samples, the methylphenanthrene index (MPI) value was used as an indicator of maturity (Sharma et al., 2022; Zheng et al., 2023). The MPI index is a quantitative maturity indicator calculated from the abundance of MP isomers in organic sediments. An MPI value < 0.8 indicate sediments with low maturity, an MPI value in the range of 0.8–1.0 indicate medium maturity, while an MPI value > 1.0 indicate mature sediments (Abdullah et al., 2021; Akinlua et al., 2023; He et al., 2019). The results show an MPI of 0.99, indicating medium-maturity coal.

The presence of MP biomarkers can be used to determine the type of kerogen on the van Krevelen diagram. The presence of 3-MP, 2-MP, 9-MP and 1-MP isomers can potentially determine whether coal, as a source rock, tends to produce gas (gas-prone) or oil (oil-prone). Type I and type II kerogens are oil-prone, whereas type III kerogen are gas-prone. The abundance of 1-MP is related to type III kerogen, the abundance of 9-MP is associated with type II and type III kerogens, while 2-MP and 3-MP are related to type II and type III kerogens (El-Sabagh et al., 2018; Zhang & Li, 2018). The identification of 2-MP and 1-MP biomarkers with relatively high abundance indicates that the analyzed coal samples tend to produce both oil and gas because these MP biomarkers are associated with type II and type III kerogens.

This type II and III kerogen classification is supported by the high vitrinite content in the Muara Enim formation located in the Rambutan Field in the South Sumatra basin (Sosrowidjojo & Sagha, 2009; Zajuli et al., 2017). This high vitrinite content is related to type III kerogen, which is more susceptible to gas than oil. The tendency toward gas- and oil-prone coal in the Muara Enim formation has also been reported by several previous researchers (Sosrowidjojo & Sagha, 2009; Zajuli et al., 2017). In addition to Angiosperm plants as the source of organic matter in the analyzed Muara Enim coal samples, there was also a small amount of organic matter originating from Gymnosperm plants which was identified by the presence of 1-MP and 1,7-DMP biomarkers (Bechtel et al., 2020; Jiang & George, 2019).

Based on the m/z 206 fragmentogram (Figure 3), the distribution of dimethylphenanthrene (DMP) compounds exhibited the highest abundance in the α-isomers such as (1,6+2,9)-DMP and 1,7-DMP. The α-isomer has low stability. Therefore, its high abundance indicates low maturity of the samples (Lima et al., 2023; Zheng et al., 2023). Coal with αβ-substituted DMPs such as 2,9-DMP and 1,9-DMP indicate type II kerogen, which tends to produce oil (oil-prone). Therefore, the presence of 2,9-DMP and 1,9-DMP in the analyzed coal samples indicates that the CBM coal samples possess type II kerogen properties (oil-prone). However, proximate analysis and gas composition in the samples showed high vitrinite and high methane gas content (96.55%), indicating the potential for the coal samples to also produce gas (Sosrowidjojo & Sagha, 2009; Zajuli et al., 2017). In addition, the abundance of 1,6-DMP and 1,7-DMP in the analyzed samples also indicates that the coal was deposited in a terrestrial environment (Lima et al., 2023; Zheng et al., 2023).

The distribution of trimethylphenanthrene (TMP) isomers identified based on the m/z 220 fragmentogram shows the low maturity of the analyzed coal samples. This is indicated by the low intensity of the 2,3,6-TMP peak, which is a more stable isomer than the other isomers, as shown in Figure 3 and Table 1. In addition to being an indicator of maturity, the origin of organic matter in sediment samples can be determined by the presence of TMP isomers. The isomer with the highest abundance, namely

DOI:https//doi.org/10.22452/mjs.vol44no4.7
Malaysian Journal of Science 44(4): 65-76 (December 2025)

1,2,8-TMP, is produced by the precursor β-amyrin, which is abundant in higher terrestrial plants. Therefore, the abundance 1,2,8-TMP is an indicator of the terrestrial environment (Jiang & George, 2019; Ogungbesan & Adedosu, 2020).

A low abundance of another biomarker, namely retene, was also exhibited in the analyzed coal samples using the m/z 218 fragmentogram. Retene can be used as an indicator of organic matter originating from Gymnosperm plants, because retene is produced from abietic acid, a major constituent of coniferous plants which are a group of Gymnosperms (Ghosh et al., 2022; Jurek & Kowalski, 2022; Simoneit et al., 2020). Therefore, the identification of retene compounds in low abundance indicates that the organic matter in the coal samples did not only originate from Angiosperm plants but a small amount of organic matter in the coal samples also originated from Gymnosperm plants.

The presence of C_{27} triaromatic-8,14-secotriterpenoid and C_{28} triaromatic-8,14-secotriterpenoid compounds were identified using the m/z 169 and m/z 183 fragmentograms, respectively (Figure 4). The presence of these biomarkers indicates terrestrial source of organic compound because these biomarkers are produced from β-amyrin, a typical precursor of Angiosperm plants (Fadhliah et al., 2020; Wang et al., 2022). Therefore, the C_{27} triaromatic-8,14-secotriterpenoid and C_{28} triaromatic-8,14-secotriterpenoid compounds produced through triterpenoid aromatization during the diagenesis stage in the Miocene era are related to coals that are immature (Fadhliah et al., 2020; Wang et al., 2022).

Other biomarkers, namely 3,3,7-trimethyl-1,2,3,4-tetrahydrochrysene (m/z 274 fragmentogram), 2,2,9-trimethyl-1,2,3,4-tetrahydrochrysene (m/z 257 fragmentogram), 2,2,9-trimethyl-1,2,3,4-tetrahydropicene (m/z 324 fragmentogram) and 1,2,9-trimethyl-1,2,3,4-tetrahydropicene (m/z 324 fragmentogram), were exhibited to be highly abundant. All of these biomarkers indicates organic matter originating from Angiosperm plants, further indicating the extent of Angiosperm vegetation during the Miocene period (Burhan et al., 2019; Jiang & George, 2019). Furthermore, compounds 2,9-dimethylpicenes and 1,2,9-trimethylpicenes were identified based on the m/z 306 fragmentogram and m/z 306 fragmentogram, respectively. Compound 2,9-dimethylpicenes was exhibited to be more abundant than 1,2,9-trimethylpicenes (Table 1). The compound 1,2,9-trimethylpicenes is derived from α-amyrin, while 2,9-dimethylpicenes is derived from the full aromatization of β-amyrin and are isomers of each other (Jiang & George, 2019; Killops & Killops, 2005). These compounds may also be produced by the microbial aromatization of triterpenoid during diagenesis. This indicates that the dehydrogenation reaction of triterpenoid to produce polyaromatic hydrocarbon compounds does not require a long time and high temperature (Ding et al., 2022; Körmös et al., 2021). Therefore, considering that the Muara Enim coal samples are immature, the identified polyaromatic pentacyclic triterpenoid compounds are suspected to be an indication of Angiosperms.

The presence of triaromatic compounds that underwent ring opening and monoaromatic pentacyclic triterpenoids observed in the partial m/z 145 fragmentogram indicate the presence of 8,14-triaromatic secolupane and 8,14-triaromatic secooleanane compounds in the samples (Fadhliah et al., 2020; Wang et al., 2022). The compounds found in the coal samples that were formed in the Miocene era are thought to have formed due to changes in the hopanoid framework by bacteria, followed by aromatization reactions that occurred during the diagenesis stage. Therefore, the presence of these compounds is an indicator of immature samples (Abdullah et al., 2021).

DOI:https//doi.org/10.22452/mjs.vol44no4.7
Malaysian Journal of Science 44(4): 65-76 (December 2025)

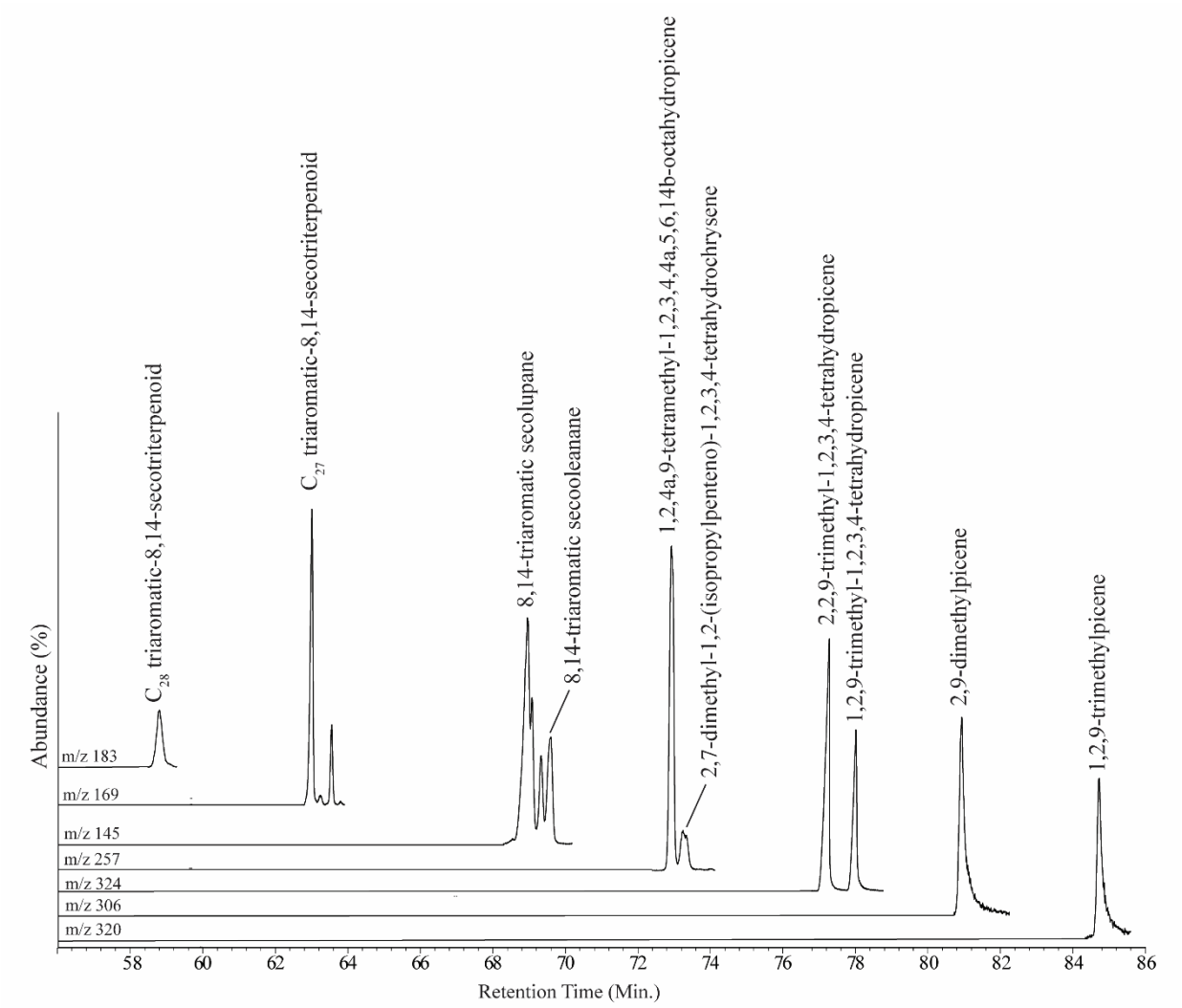

Figure 4. The presence of Polyaromatic pentacyclic triterpenoid-derived compounds

Biomarkers that are indicators of Angiosperm plants, namely the molecule 1,2,4a,9-tetramethyl-1,2,3,4,4a,5,6, 14b-octahydropicene and the compound 2,7-dimethyl-1,2-(isopropylpenteno)-1,2,3,4-tetrahydrochrysene with a triaromatic ursane framework, were observed in the m/z 257 fragmentogram (Burhan et al., 2019; Jiang & George, 2019; Zetra et al., 2016). The high abundance of the compound 2,7-dimethyl-1,2-(isopropylpenteno)-1,2,3,4-tetrahydrochrysene is an indicator of coal that has not yet been produced (Burhan et al., 2019). Furthermore, due to the analyzed coal samples being immature and associated with type II and type III kerogens, the coal samples possess the potential to produce gas (gas-prone) and oil (oil-prone). However, the relatively low abundance value of 2,7-dimethyl-1,2-(isopropylpenteno)-1,2,3,4-tetrahydrochrysene compared to 1,2,4a,9-tetramethyl-1,2,3,4,4a ,5,6,14b-octahydropicene indicates that coal within the Muara Enim formation has a higher potential to produce gas than oil (Burhan et al., 2019).

4. Conclusion

The geochemical implications of the results of biomarker analysis on the Muara Enim coal samples can be used to determine the origin of organic matter, depositional environment and coal maturity. The identification of naphthalene, phenanthrene and pentacyclic aromatic triterpenoid in high abundance indicates the that main origin of organic matter is Angiosperm plants. However, the presence of retene in low abundance shows that a small amount of organic matter in the samples originated from Gymnosperm plants. The dominance of 1-MN isomers compared to 2-MN, the higher abundance value of 1,6-DMN compared to 2,6+2,7-DMN, the higher abundance values of 1,2,4-TMN and 1,2,7-TMN compounds compared to 1,2,5-TMN and the dominance of cadalene compared to isocadalene indicate the low maturity of the coal samples. The MPI value of 0.99 which was calculated from the abundance of MP isomers in organic sediments indicates that the coal samples possess a moderate maturity level. The presence of MP biomarkers was used to determine the type of kerogen based on the van Krevelen diagram. The results show that the MP biomarkers exhibited in the coal samples are associated with type

DOI:https//doi.org/10.22452/mjs.vol44no4.7
Malaysian Journal of Science 44(4): 65-76 (December 2025)

II and type III kerogens, indicating that the coal samples tend to produce oil (oil-prone) and gas (gas-prone). However, the high content of vitrinite and methane gas of the coal samples is related to type III kerogen, indicating the samples are more likely to produce gas (gas-prone) than oil (oil-prone). This is further supported by the low abundance of the compound 2,7-dimethyl-1,2-(isopropylpenteno)-1,2,3,4-tetrahydrochrysene compared to 1,2,4a,9-tetramethyl-1,2,3,4,4a,5,6,14b-octahydropicene in the samples which indicates that the Muara Enim coal samples possess more potential to produce gas than oil. The presence of biomarkers, namely 1,2,8-TMP, C_{27} triaromatic-secotriterpenoid, C_{28} triaromatic-8,14-secotriterpenoid, indicate a terrestrial depositional environment and humic coal. Finally, Angiosperm plants as the main origin of the organic matter in the samples are also indicated by the presence of 1,2,4a,9-tetramethyl-1,2,3,4,4a,5,6, 14b-octahydropicene and 2,7-dimethyl-1,2-(isopropylpenteno)-1,2,3,4-tetrahydrochrysene compounds with a triaromatic ursane framework.

5. Acknowledgement

We would like to acknowledge DRPM ITS for providing the research funds and facilities which made the completion of this publication writing possible. We would also like to thank the students that are members of the molecular geochemistry group of the Chemistry Department of FSAD-ITS that helped in carrying out this research and ensured that this research was completed properly.

6. References

Abdullah, E. S., Ebiad, M. A., Rashad, A. M., El Nady, M. M., & El-Sabbagh, S. M. (2021). Thermal maturity assessment of some Egyptian crude oils as implication from naphthalene, phenanthrene and alkyl substituents. *Egyptian Journal of Petroleum*, *30*(1), 17–24. https://doi.org/10.1016/j.ejpe.2020.12.004

Aboglila, S., Abdulgader, A., Albaghdady, A., Hlal, O., & Farifr, E. (2019). Biomarker Ratios and Stablecarbon Isotopes to Describe Crude Oils Characteristics in the Murzuq Basin (Libya). *Advances in Research*, *December*, 1–12. https://doi.org/10.9734/air/2019/v18i330094

Akinlua, A., Dada, O. R., Usman, F. O., & Adekola, S. A. (2023). Source rock geochemistry of central and northwestern Niger Delta: Inference from aromatic hydrocarbons content. *Energy Geoscience*, *4*(3), 100141. https://doi.org/10.1016/j.engeos.2022.100141

Amijaya, H., Schwarzbauer, J., & Littke, R. (2006). Organic geochemistry of the Lower Suban coal seam, South Sumatra Basin, Indonesia: Palaeoecological and thermal metamorphism implications. *Organic Geochemistry*, *37*(3), 261–279. https://doi.org/10.1016/j.orggeochem.2005.10.012

Ayu, M. W. P., Burhan, P., & Zetra, Y. (2021). Analisis Biomarka Minyak Mentah Sumur Tua Blok Cepu, Formasi Wonocolo, Jawa Timur. *Jurnal Sains Dan Seni ITS*, *9*(2), 1–6. https://doi.org/10.12962/j23373520.v9i2.56936

Bechtel, A., Chekryzhov, I. Y., Pavlyutkin, B. I., Nechaev, V. P., Dai, S., Vysotskiy, S. V., Velivetskaya, T. A., Tarasenko, I. A., & Guo, W. (2020). Composition of lipids from coal deposits of the Far East: Relations to vegetation and climate change during the Cenozoic. *Palaeogeography, Palaeoclimatology, Palaeoecology*, *538*(April 2019), 109479. https://doi.org/10.1016/j.palaeo.2019.109479

Buckley, S., Power, R. C., Andreadaki-Vlazaki, M., Akar, M., Becher, J., Belser, M., Cafisso, S., Eisenmann, S., Fletcher, J., Francken, M., Hallager, B., Harvati, K., Ingman, T., Kataki, E., Maran, J., Martin, M. A. S., McGeorge, P. J. P., Milevski, I., Papadimitriou, A., … Stockhammer, P. W. (2021). Archaeometric evidence for the earliest exploitation of lignite from the bronze age Eastern Mediterranean. *Scientific Reports*, *11*(1), 1–11. https://doi.org/10.1038/s41598-021-03544-w

Burhan, R. Y. P., Chairacita, A. M., Zetra, Y., & Mutiara, E. (2019). Biomarking Study of Aromatic Hydrocarbon Fraction Crude Oil Tarakan, North Kalimantan. *Jurnal Teknik ITS*, *8*(2), 4–10. https://doi.org/10.12962/j23373539.v8i2.49743

Burhan, R. Y. P., Zetra, Y., & Amini, Y. A. (2020). Paleoenvironmental And Maturity Indicator Of Cepu Block Oil, Wonocolo Formation, East Java Indonesia. *Jurnal Teknologi*, *5*, 173–182.

Dai, J., Ni, Y., Zou, C., Tao, S., Hu, G., Hu, A., Yang, C., & Tao, X. (2009). Stable carbon isotopes of alkane gases from the Xujiahe coal measures and implication for gas-source correlation in the Sichuan Basin, SW China. *Organic Geochemistry*, *40*(5), 638–646. https://doi.org/10.1016/j.orggeochem.2009.01.012

Darman, H. (2000). An outline of the geology of Indonesia. *Lecture Notes in Earth Sciences*, *116*(August), 1–31. https://doi.org/10.1007/978-3-540-77076-3_1

Ding, W., Hou, D., Gan, J., Zhang, Z., & George, S. C. (2022). Aromatic hydrocarbon signatures of the late Miocene-early Pliocene in the Yinggehai Basin, South China Sea: Implications for climate variations. *Marine and Petroleum Geology*, *142*(March), 105733. https://doi.org/10.1016/j.marpetgeo.2022.105733

El-Sabagh, S. M., El-Naggar, A. Y., El Nady, M. M., Ebiad, M. A., Rashad, A. M., & Abdullah, E. S. (2018). Distribution of triterpanes and steranes biomarkers as indication of organic matters input and depositional environments of crude oils of oilfields in Gulf of Suez, Egypt. *Egyptian Journal of Petroleum*, *27*(4), 969–977. https://doi.org/10.1016/j.ejpe.2018.02.005

DOI:https//doi.org/10.22452/mjs.vol44no4.7
Malaysian Journal of Science 44(4): 65-76 (December 2025)

ESDM. (2020). Handbook of Energy & Economic Statistics of Indonesia. *Ministry of Energy and Mineral Resources Republic of Indonesia*. https://www.esdm.go.id/en/publication/handbook-of-energy-economic-statistics-of-indonesia-heesi

Fadhliah, A., Zetra, Y., Wahyudi, A., & Burhan, R. Y. P. (2020). Biomarka sebagai Indikator Sumber Asal Usul Senyawa Organik Minyak Mentah Blok Cepu, Formasi Wonocolo, Bojonegoro, Jawa Timur. *Jurnal Sains Dan Seni ITS*, *9*(2), 37–42. https://doi.org/10.12962/j23373520.v9i2.58293

Faiz, M., & Hendry, P. (2008). Microbial Activity in Australian CBM Reservoirs. **Adapted from Oral Presentation at AAPG Annual Convention, San Antonio, TX, April 20-23, 2008*, *80033*, 32.

Fang, R., Littke, R., Zieger, L., Baniasad, A., Li, M., & Schwarzbauer, J. (2019). Changes of composition and content of tricyclic terpane, hopane, sterane, and aromatic biomarkers throughout the oil window: A detailed study on maturity parameters of Lower Toarcian Posidonia Shale of the Hils Syncline, NW Germany. *Organic Geochemistry*, *138*, 103928. https://doi.org/10.1016/j.orggeochem.2019.103928

Flores, R. M., Rice, C. A., Stricker, G. D., Warden, A., & Ellis, M. S. (2008). Methanogenic pathways of coal-bed gas in the Powder River Basin, United States: The geologic factor. *International Journal of Coal Geology*, *76*(1–2), 52–75. https://doi.org/10.1016/j.coal.2008.02.005

Gan, H., Gong, S., Tian, H., Wang, H., Chen, J., Ma, Q., Liu, K., & Lv, Z. (2023). Geochemical characteristics of inclusion oils and charge history in the Fushan Sag, Beibuwan Basin, South China Sea. *Applied Geochemistry*, *150*(February), 105598. https://doi.org/10.1016/j.apgeochem.2023.105598

Gao, L., Schimmelmann, A., Mastalerz, M., Schatzel, S. J., & Su, D. W. H. (2020). The origin of coalbed methane. In *Coal Bed Methane: Theory and Applications* (2nd ed.). Elsevier Inc. https://doi.org/10.1016/B978-0-12-815997-2.00001-9

Ghosh, S., Dutta, S., Bhattacharyya, S., Konar, R., & Priya, T. (2022). Paradigms of biomarker and PAH distributions in lower Gondwana bituminous coal lithotypes. *International Journal of Coal Geology*, *260*(July), 104067. https://doi.org/10.1016/j.coal.2022.104067

He, C., Huang, H., Wang, Q., & Li, Z. (2019). Correlation of Maturity Parameters Derived from Methylphenanthrenes and Methyldibenzothiophenes in the Carboniferous Source Rocks from Qaidam Basin, NW China. *Geofluids*, *2019*. https://doi.org/10.1155/2019/5742902

Huang, Q., Liu, S., Wang, G., Wu, B., & Zhang, Y. (2019). Coalbed methane reservoir stimulation using guar-based fracturing fluid: A review. *Journal of Natural Gas Science and Engineering*, *66*(September 2018), 107–125. https://doi.org/10.1016/j.jngse.2019.03.027

Jiang, L., & George, S. C. (2019). Biomarker signatures of Upper Cretaceous Latrobe Group petroleum source rocks, Gippsland Basin, Australia: Distribution and geological significance of aromatic hydrocarbons. *Organic Geochemistry*, *138*, 103905. https://doi.org/10.1016/j.orggeochem.2019.103905

Jurek, K. J., & Kowalski, A. (2022). Origin of Carpathian ozokerite deposits: determined from biomarkers and aromatic hydrocarbons distributions. *Fuel*, *310*(PB), 122357. https://doi.org/10.1016/j.fuel.2021.122357

Killops, S., & Killops, V. (2005). *Introduction to Organic Geochemistry* (2nd editio). Blackwell Publishing Ltd.

Kim, J. H., Lee, D. H., Yoon, S. H., Jeong, K. S., Choi, B., & Shin, K. H. (2017). Contribution of petroleum-derived organic carbon to sedimentary organic carbon pool in the eastern Yellow Sea (the northwestern Pacific). *Chemosphere*, *168*, 1389–1399. https://doi.org/10.1016/j.chemosphere.2016.11.110

Körmös, S., Sachsenhofer, R. F., Bechtel, A., Radovics, B. G., Milota, K., & Schubert, F. (2021). Source rock potential, crude oil characteristics and oil-to-source rock correlation in a Central Paratethys sub-basin, the Hungarian Palaeogene Basin (Pannonian basin). *Marine and Petroleum Geology*, *127*(January). https://doi.org/10.1016/j.marpetgeo.2021.104955

Li, Z., Huang, H., & George, S. C. (2022). Unusual occurrence of alkylnaphthalene isomers in upper Eocene to Oligocene sediments from the western margin of Tasmania, Australia. *Organic Geochemistry*, *168*(April), 104418. https://doi.org/10.1016/j.orggeochem.2022.104418

Li, Z., Huang, H., Yan, G., Xu, Y., & George, S. C. (2022). Occurrence and origin of perylene in Paleogene sediments from the Tasmanian Gateway, Australia. *Organic Geochemistry*, *168*(November 2021), 104406. https://doi.org/10.1016/j.orggeochem.2022.104406

Lima, B. D., Martins, L. L., Pereira, V. B., Franco, D. M. M., dos Santos, I. R., Santos, J. M., Vaz, B. G., Azevedo, D. A., & da Cruz, G. F. (2023). Weathering impacts on petroleum biomarker, aromatic, and polar compounds in the spilled oil at the northeast coast of Brazil over time. *Marine Pollution Bulletin*, *189*(February). https://doi.org/10.1016/j.marpolbul.2023.114744

DOI:https//doi.org/10.22452/mjs.vol44no4.7
Malaysian Journal of Science 44(4): 65-76 (December 2025)

Martini, A. M., Walter, L. M., & McIntosh, J. C. (2008). Identification of microbial and thermogenic gas components from Upper Devonian black shale cores, Illinois and Michigan basins. *American Association of Petroleum Geologists Bulletin*, *92*(3), 327–339. https://doi.org/10.1306/10180706037

Mayumi, D., Mochimaru, H., Tamaki, H., Yamamoto, K., Yoshioka, H., Suzuki, Y., Kamagata, Y., & Sakata, S. (2016). Methane production from coal by a single methanogen. *Science*, *354*(6309), 222–225. https://doi.org/10.1126/science.aaf8821

McIntosh, J., Martini, A., Petsch, S., Huang, R., & Nüsslein, K. (2008). Biogeochemistry of the Forest City Basin coalbed methane play. *International Journal of Coal Geology*, *76*(1–2), 111–118. https://doi.org/10.1016/j.coal.2008.03.004

Nugroho, H. (2017). Coal as the National Energy Supplier Forward: What are Policies to be Prepared? *Jurnal Perencanaan Pembangunan: The Indonesian Journal of Development Planning*, *1*(1), 1–13. https://doi.org/10.36574/jpp.v1i1.3

Ogungbesan, G. O., & Adedosu, T. A. (2020). Geochemical record for the depositional condition and petroleum potential of the Late Cretaceous Mamu Formation in the western flank of Anambra Basin, Nigeria. *Green Energy and Environment*, *5*(1), 83–96. https://doi.org/10.1016/j.gee.2019.01.008

Qiao, J., Grohmann, S., Baniasad, A., Zhang, C., Jiang, Z., & Littke, R. (2021). High microbial gas potential of Pleistocene lacustrine deposits in the central Qaidam Basin, China: An organic geochemical and petrographic assessment. *International Journal of Coal Geology*, *245*(July), 103818. https://doi.org/10.1016/j.coal.2021.103818

Rice, D. D. (1993). *Composition and Origins of Coalbed Gas* (Vol. 98, Issue 93, pp. 9885–9907). American Association of Petroleum Geologists. https://doi.org/10.1306/St38577C7

Rice, D. D., & Claypool, G. E. (1981). *Generation , Accumulation , and Resource Potential of Biogenic Gas '*.

Rontani, J. F., Galeron, M. A., Amiraux, R., Artigue, L., & Belt, S. T. (2017). Identification of di- and triterpenoid lipid tracers confirms the significant role of autoxidation in the degradation of terrestrial vascular plant material in the Canadian Arctic. *Organic Geochemistry*, *108*, 43–50. https://doi.org/10.1016/j.orggeochem.2017.03.011

Scott, C. D., Woodward, C. A., & Scott, T. C. (1994). Mechanisms and effects of using chemically modified reducing enzymes to enhance the conversion of coal to liquids. *Fuel Processing Technology*, *40*(2–3), 319–329. https://doi.org/10.1016/0378-3820(94)90154-6

Sharma, R., Jha, S. K., Pal, S., & Shrivastava, J. P. (2022). Organic molecules based palaeoenvironmental inferences and U mineralization in Palaeoproterozoic Bijawar basins of Central India. *Applied Geochemistry*, *147*(October), 105489. https://doi.org/10.1016/j.apgeochem.2022.105489

Sharma, S., Saxena, A., & Saxena, N. (2019). *Introduction to Gas Hydrate, In: Unconventional Resources in India: The Way Ahead*. SpringerBriefs in Petroleum Geoscience & Engineering. https://doi.org/10.1007/978-3-030-21414-2

Simoneit, B. R. T., Oros, D. R., Karwowski, Ł., Szendera, Ł., Smolarek-Lach, J., Goryl, M., Bucha, M., Rybicki, M., & Marynowski, L. (2020). Terpenoid biomarkers of ambers from Miocene tropical paleoenvironments in Borneo and of their potential extant plant sources. *International Journal of Coal Geology*, *221*(December 2019), 103430. https://doi.org/10.1016/j.coal.2020.103430

Sosrowidjojo, I. B. (2013). Coal Geochemistry of the Unconventional Muaraenim Coalbed Reservoir , South Sumatera Basin : a Case Study From the Rambutan Field. *Indonesian Mining Journal*, *16*(2), 71–81.

Sosrowidjojo, I. B., & Sagha, A. (2009). *International Journal of Coal Geology Development of the fi rst coal seam gas exploration program in Indonesia : Reservoir properties of the Muaraenim Formation , south Sumatra*. *79*, 145–156. https://doi.org/10.1016/j.coal.2009.07.002

Stanford, C. E. (2013). Coal Resources, Production and Use in Indonesia. In *The Coal Handbook: Towards Cleaner Production* (Vol. 2). Woodhead Publishing Limited. https://doi.org/10.1533/9781782421177.2.200

Strapoć, D., Mastalerz, M., Eble, C., & Schimmelmann, A. (2007). Characterization of the origin of coalbed gases in southeastern Illinois Basin by compound-specific carbon and hydrogen stable isotope ratios. *Organic Geochemistry*, *38*(2), 267–287. https://doi.org/10.1016/j.orggeochem.2006.09.005

Synnott, D. P., Schwark, L., Dewing, K., Percy, E. L., & Pedersen, P. K. (2021). The diagenetic continuum of hopanoid hydrocarbon transformation from early diagenesis into the oil window. *Geochimica et Cosmochimica Acta*, *308*, 136–156. https://doi.org/10.1016/j.gca.2021.06.005

Theuerkorn, K., Horsfield, B., Wilkes, H., di Primio, R., & Lehne, E. (2008). A reproducible and linear method for separating asphaltenes from crude oil. *Organic Geochemistry*, *39*(8), 929–934. https://doi.org/10.1016/j.orggeochem.2008.02.009

DOI:https//doi.org/10.22452/mjs.vol44no4.7
Malaysian Journal of Science 44(4): 65-76 (December 2025)

Wang, Q., Huang, H., He, C., Li, Z., & Zheng, L. (2022). Methylation and demethylation of naphthalene homologs in highly thermal mature sediments. *Organic Geochemistry*, *163*(September 2021), 104343. https://doi.org/10.1016/j.orggeochem.2021.104343

Whiticar, M. J. (1999). *Carbon and hydrogen isotope systematics of bacterial formation and oxidation of methane*.

Yasin, C. M., Yunianto, B., Sugiarti, S., & Hudaya, G. K. (2021). Implementation of Indonesia coal downstream policy in the trend of fossil energy transition. *IOP Conference Series: Earth and Environmental Science*, *882*(1). https://doi.org/10.1088/1755-1315/882/1/012083

Zajuli, M. H. H., Panggabean, H., Hendarmawan, & Syafri, I. (2017). Hubungan Kelompok Maseral Liptinit dan Vitrinit dengan Tipe Kerogen Relationship Between Liptinite and Vitrinite Maceral Groups with Kerogen Type of Hydrocarbon Source Rock on The Shale of Upper Kelesa Formation in Kuburan Panjang, Riau. *Jurnal Geologi Dan Sumberdaya Mineral*, *18*(1), 13–23. http://jgsm.geologi.esdm.go.id

Zakrzewski, A., & Kosakowski, P. (2021). Impact of palaeo-wildfires on higher plant parameter revealed by new biomarker indicator. *Palaeogeography, Palaeoclimatology, Palaeoecology*, *579*(April). https://doi.org/10.1016/j.palaeo.2021.110606

Zetra, Y., Sosrowidjojo, I. B., & Perry Burhan, R. Y. (2016). Aromatic biomarker from brown coal, Sangatta coalfield, East Borneo of middle miocene to late miocene age. *Jurnal Teknologi*, *78*(6), 229–238. https://doi.org/10.11113/jt.v78.8822

Zhang, M., & Li, Z. (2018). Thermal maturity of the Permian Lucaogou Formation organic-rich shale at the northern foot of Bogda Mountains, Junggar Basin (NW China): Effective assessments from organic geochemistry. *Fuel*, *211*(5268), 278–290. https://doi.org/10.1016/j.fuel.2017.09.069

Zheng, T., Zhang, Q., & Deng, E. (2023). Applications of low molecular weight polycyclic aromatic hydrocarbons (PAHs) and diamondoids ratios/indices on the maturity assessment of coal-bearing source rock: Insight from mature to overmature Longtan Shale. *International Journal of Coal Geology*, *269*(November 2022), 104209. https://doi.org/10.1016/j.coal.2023.104209

DOI:https//doi.org/10.22452/mjs.vol44no4.7
Malaysian Journal of Science 44(4): 65-76 (December 2025)

MALAYSIAN JOURNAL OF SCIENCE
MJS
ISSN 1394-3065

Regular Issue

Malaysian Journal of Science 44 (4): 77-91 (December 2025) https://mjs.um.edu.my

Impacts of Soil Environmental Factors on Variability of Soil Organic Carbon and Particle Size Fractions in Obudu Cattle Ranch, Nigeria

S.M. Afu[1a], D.M. Olim[2a]*, F.V. Aberagi[3a], A.I. Akpama[4a], A.I. Afangide[5b], U.I. Uquetan[6c] and A.S. Modey[7a]

Abstract: The knowledge of the influence of environmental factors on soil properties and spatial distribution of soil organic carbon (SOC) and soil particle size fractions is crucial to soil management and sustainable productivity. SOC provides an insight about soil capacity to perform ecosystem services while soil particle size fractions influence several key soil characteristics. This study assessed the impacts of environmental elements on spatial changes in SOC and sand, silt and clay using random forest (RF), regression kriging (RK), cubist regression (CR), multiple linear regression (MLR) and ordinary kriging (OK) models. Sixty (60) composite soil samples were obtained at 0-30 cm depth and distance of 200-500 m apart, and analyzed for physicochemical properties. The digital elevation model (DEM) of the area was acquired at the spatial resolution of 30 m from USGS and processed. The models were evaluated using bias, coefficient of determination (R2), correlation concordance coefficient (CCC), mean square error (MSE) and root mean square error (RMSE). The soil had sandy clay loam, sandy loam and loam texture with strongly acidic pH (pH <5.5) and high OC (2%). Available P and exchangeable cations were all low while cation exchange capacity and base saturation were high. Soil pH> SAVI (soil adjusted vegetation index)> NDVI (normalized difference vegetative index) > rainfall were found to be the top four environmental variables influencing OC prediction while temperature and slope had the least effect. Again, MLR model better predicted OC (R2 of 0.324, CCC of 0.537, MSE of 0.585, RMSE of 0.764), OK better predicted clay (MSE=2.680, RMSE=3.490), CK in sand (MSE = 7.434, RMSE =5.568). Also, MLR, CK and OK proved to have the best capacity in prediction SOC and sand, silt and clay in mountainous soils. The findings could therefore be used by policy makers and planners as tools for decision making on sustainable soil and environmental management and precision agriculture.

Keywords: *SOC, environmental elements, models, soils.*

1. Introduction

Soil organic carbon (SOC) is the equilibrium of plant supply and biologically mediated losses (Arthur *et al*., 2022). Soils are the highest carbon warehouse of the earth carbon cycle and almost thrice the amount of carbon is preserved in soils than in plants and soils contain twice the quantity of carbon that the atmosphere holds (Shiekh *et al*., 2009). Organic carbon content of first 100 cm of soil is estimably 1500 Pg meaning more C than the quantity contained in both atmosphere and vegetation (Lehmann & Kleber, 2015). SOC improves soil nutrient cycling, plant growth and maintenance of soil structure (Wang *et al*., 2016). It is the measure of soil capacity to perform ecosystem services including nutrient supply to crops because SOC performs several roles including soil pH moderation, nutrients supply, soil structure and hydraulic conductivity improvement, and control of microbial activity (Nisha *et al*., 2007; Hussain *et al*., 2019). Critical evaluation of the effects of elements of environment on SOC is necessary in order to identify areas with varying soil characteristics and to assess their performance under a given land management practice and potential ease of degradation specifically for sustainable crop cultivation and environmental management. This is because SOC performs additional ecosystem services such weather moderation, provision of raw materials and food to man, nutrient release, runoff and erosion mitigation (Veronesi & Schillaci, 2019; Mayer *et al*., 2019). Concise and correct mapping of C storage in mountainous soils provides information about the relationship between biogeochemistry cycle and global climatic condition (Bangroo *et al*., 2017) and since SOC play crucial roles soil functioning (Lal *et al*., 2018)

The area of the study, Obudu Cattle ranch, located in hills of Obanliku in Cross River, is well known because of its peculiar land form which is characterized by high mountains, abyss, canyons and cold weather condition. The Obudu Cattle ranch has an elevation of over 1650 m above sea level (asl) and, in Nigeria it is next to Chappal Waddi mountain of Taraba State in height with an elevation of about 2400 m asl. The Cattle ranch has characteristically different climatic conditions; cloudy weather, steady snow fall, low temperature and steady rainfall from other parts of Obanliku and the State. This is because mountains soils regulate climatic variables at local level (via evapotranspiration which reduces the amount of heat in the air and is mostly important in urban areas) and on universal scale via the storing of SOC that forestall its release into the outer space as greenhouse

Authors information:
[a]Department of Soil Science, University of Calabar, Calabar, NIGERIA. Email: afu.suny@yahoo.com[1]; olimdenis001@gmail.com[2]; aberagifidelis@gmai.com[3]; akpamaafrekpe@gmai.com[4]; modeyalice2017@gmail.com[7]
[b]Department Soil Science & Technology, Federal University of Technology, Owerri, NIGERIA. Email: afangideakaninyene2000@gmail.com[5]
[c]Department of Environmental Management, University of Calabar, Calabar, NIGERIA. Email: uquetanuquetanibor@gmail.com[6]
*Correspondence: olimdenis001@gmail.com

Received: April, 2024
Accepted: June, 2024
Published: December, 2025

DOI:https//doi.org/10.22452/mjs.vol44no4.8
Malaysian Journal of Science 44(4): 77-91 (December 2025)

gas (Stanchi *et al*., 2021). It is discovered that SOC stock in mountainous soils is often affected by several factors among which are: vegetation diversity, topographic attributes and impacts of climate (Bangroo *et al*., 2017) which in turn influence the soil physicochemical and biological characteristics essentially in the first soil horizon (Fu *et al.,* 2020; Zhang *et al.*, 2021). Therefore, having a fair knowledge on the effect of environmental variables on how SOC changes with distance in mountainous soil is crucial in decision making for effective land management option particularly for mountainous soils. Accurate mapping of SOC in mountainous soils is therefore crucial in solving local environmental problems, aptly planning best land management alternatives and advocating/enhancing land use practices without damaging effects (Tang *et al*., 2015). It is suggested that among the best processes to efficiently manage agricultural operations and to plan for life long growth is acquisition of accurate understanding on spatial heterogeneity of soil physicochemical characteristics (AbdelRahman *et al.,* 2018) and this can only be perfectly achieved using geospatial technologies or spatial interpolation. Spatial interpolation has been described as a way of estimating the exact values of variable or quantification of substance in an area not sampled (Kalivas *et al.*, 2002), that basically provides valuable information for precision agriculture, planning of soil fertility management and environmental studies (De Menezes *et al*., 2016; Brevik *et al.*, 2015). The emphasis here is on precision agriculture, therefore, understanding space heterogeneity and dynamism of soil characteristics and SOC and particle fractions in particular as this could necessary to provide information for government policy formulation to guide farmers on proper and sustainable utilization and management of soils with minimal inputs.

Variation in environment, soil type, vegetative cover and land use are major causes of spatial variations of SOC in mountainous environment (Hoffmann *et al*., 2014). The space changes in TOC are determined by topographic features and soil texture at the plot scale, especially where it is affected by texture of the soil at the landscape level (Zhu *et al*., 2020). Also, Feng *et al*. (2021) opined that elevated temperature and wrong agricultural operation reduced SOC buildup. Therefore, apart from human influences through land preparation for crop production, SOC is controlled by myriads of environmental variables including lay of the land, altitude, climate and soil characteristics such as soil reaction and arrangement of soil separates. SOC levels appeared to be influenced by weather indices according to a study by Zhang *et al*. (2022). It is also affected by altitude and vegetation (Massaccesi *et al*., 2020; Xu *et al*., 2014) that control nutrient cycling and release (Zhang *et al*., 2014) and elevation has been reported as an alternative for change in temperature used to evaluate the impacts of temperature on SOC level and dynamics (Massacesi *et al*., 2020). Nature of land surface, climate and other environmental elements have been confirmed as factors affecting soil characteristics (Bamutaze *et al*., 2021). Again, Bangroo *et al*. (2017) in their study discovered that SOC stock was decreasing with increasing elevation and concluded that it has an unfavorable influence on SOC stability. The authors suggested that altitude effect should be included in SOC stock assessment equations. Although studies have been conducted on the impacts of environmental factors on SOC stock, little has been done on both SOC and particle size in mountainous soils especially in Nigeria. Most studies in Nigeria on mountainous soils are merely on soil physicochemical properties (Akpanidiok *et al*., 2014; Essoka *et al*., 2010); they have been no detailed studies on spatial distribution or mapping of SOC and soil particle size fractions on mountainous soils.

Considering the importance of SOC and soil separates in management of soil fertility and the need to overcome the challenge of meeting up with the increasing world food demand resulting from rapidly growing population, it is imperative to double effort in evolving strategies that engender sustainable crop production. One of such strategies is the acquisition of proper knowledge of the effect of soil environmental indices on distribution of soil SOC and particle size fractions spatially as yardstick for proper land use and management. These challenges have led to mounting of pressure on mountainous soils which were initially underused or used for forest reserve, watershed and wildlife conservation as a result of stress involved in climbing high mountains for the purpose of crop cultivation. According to FAO (2019), as of the year 2017, only fifteen percent of global population were living and cultivating crops on and around mountains. Consequently, intensive studies on mountainous soils are therefore needed. This study is therefore anchored on the evaluation of the impacts of environmental elements on SOC and particles size fractions and to predict and assess spatial heterogeneity of SOC and particle size fractions of mountainous soils using geostatistics. However, at the global level some studies have been done that focused on land use effect on organic carbon storage (Li *et al*., 2019; Hussain *et al*.,2019; Bamutaze *et al*., 2021; Ota *et al*., 2024) and a few on the influence of environmental factors on soil organic carbon levels (Feng *et al*., 2021) in mountainous soils (Bangroo *et al*., 2017). Mousavi *et al*. (2022), De Menezes *et al*. (2016) and Kalivas *et al*. (2002) have shown that geostatistics can be used to map soil properties, but only Isong *et al*. (2022), Komolafe *et al*. (2021) and Peter-Jerome *et al*. (2022) worked on such concept at the national level in Nigeria. Nevertheless, these studies were not on understudied mountainous soils and also did not consider the effect of environmental factors such as rainfall, temperature, slope, pH, elevation etc on spatial distribution of SOC and particle size. Accurate evaluation of the impact of environmental factors on prediction of SOC and particle size in mountainous soils is therefore needed to guide on soil use and management since SOC and particle are key determinants soil fertility and productivity.

DOI:https//doi.org/10.22452/mjs.vol44no4.8
Malaysian Journal of Science 44(4): 77-91 (December 2025)

2. Materials and Methods

The Study Area, Soil Sample Collection and Laboratory Analysis

This study was done in Obudu Cattle Ranch, Obanliku, Cross River State, located at latitudes 6° 21′ N – 6° 24′ N and longitudes 9° 22′ E – 9° 25′ E (Fig. 1) in the tropical rain forest belt of Nigeria with moist tropical humid climate, diverse land use cover types and has an altitude varying from 689 m to 1654 m above sea level, rainfall range of above 2000 mm/annum and temperature of 15 to 31.80 ^{0}C. Geologically, the area is underlain by basement complex rocks. Major crops cultivated in the area include cassava, cocoa, maize, yam, okra, groundnut and cocoyam. Sixty georeferenced composite soil samples were obtained randomly at 0-30 cm depth from the study area at the distance of 200 m - 500 m apart using soil auger and transported to the laboratory, processed using standard procedures and analyzed for physicochemical properties. Particle size analysis was done using Bouyocous hydrometer method (Gee and Or 2002).

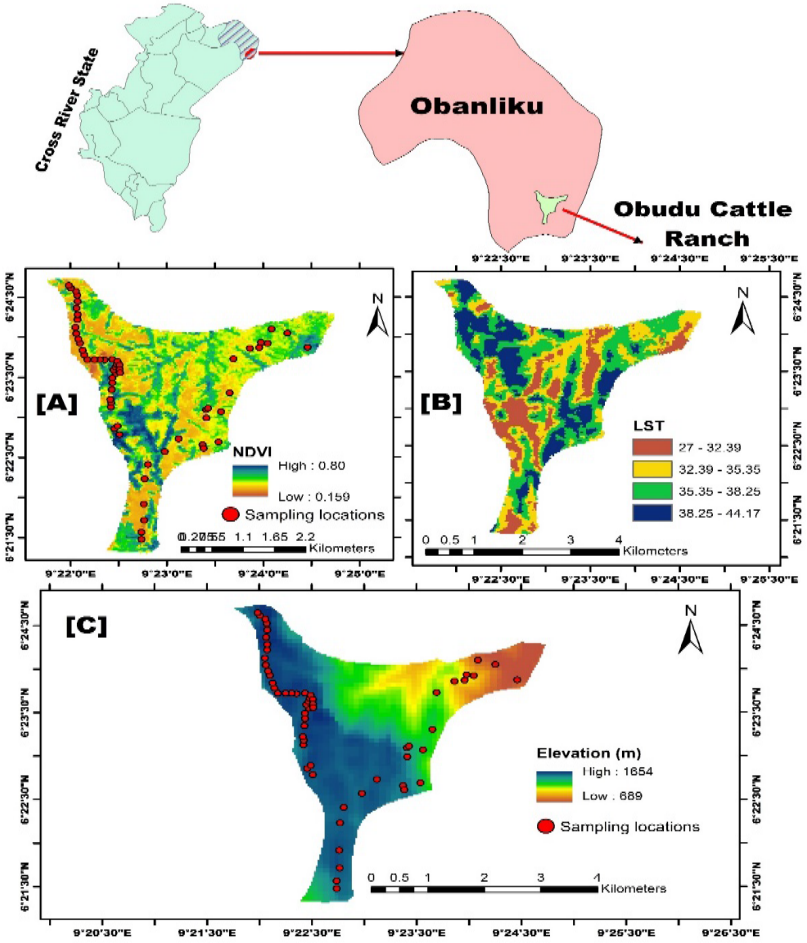

Figure 1. Map of Cross River State showing location of the study area [A] Normalized difference vegetation index (NDVI), [B] Land surface temperature (LST) and [C] Elevation

pH was obtained potentiometrically in soil and water suspension (1:2.5) as reported by Udo *et al*. (2009) while organic carbon was determined by Walkley-Black wet oxidation method using acid dichromate($K_2Cr_20_7$) method (Nelson and Sommers 1996). Total nitrogen was analyzed with modified micro-kjeldhal method (Udo *et al*., 2009) while available phosphorus was obtained using Bray P-1 method outlined by Kuo (1996). Exchangeable cations were also determined using the extract obtained after leaching samples with one normal neutral ammonium acetate (1 *N*, NH_4OAC, pH 7.0) solution. Again, calcium and magnesium were analyzed using the EDTA titration method while potassium and sodium were estimated by Flame photometer. Furthermore, aluminum and hydrogen were determined by titration using 0.1*N* Na0H solution presented by Udo *et al.* (2009). CEC was gotten using the method proposed by Udo *et al*. (2009). And finally, ECEC and base saturation were obtained by computation method.

Environmental Covariates

Environmental covariates used to derive environmental data were digital elevation model (DEM) and Sentinel-2. Elevation, slope and aspect were gotten from DEM obtained at the space resolution of 30 m from ASTER data (https://earthexplorer.usgs.gov) and were processed with the aid

DOI:https//doi.org/10.22452/mjs.vol44no4.8
Malaysian Journal of Science 44(4): 77-91 (December 2025)

of SAGA-GIS software terrain analysis toolbox. The European Space Agency's Copernicus Open Access was used to acquire Cloud-free Sentinel-2 imageries, processed using Google Earth Engine (GEE) to estimate land surface temperature (LST), normalized difference moisture index (NDMI), normalized difference vegetation index (NDVI), soil adjusted vegetation index (SAVI) and cannel network base level. Soil pH and clay were obtained through interpolation techniques using the interpolated soil database at a resolution of 30 m. Climatic parameters including mean rainfall, minimum temperature, maximum temperature and mean temperature covering the study area were gotten from WorldClim database version 2 (Fick *et al.,* 2017) and processed using ArcGIS software. All the maps used in this study were geo-referenced to the Universal Transverse Mercator (UTM) Zone 32 N coordinate system. The area of interest (AOI) for the soil and environmental data were demarcated using polygon feature of the study areas with aid of ArcGIS 10.8 software (ESRI, Redlands, USA) environment.

The covariates used in this study were selected using recursive feature elimination (RFE) and variance inflation factor (VIF). RFE was employed for feature selection to identify the optimal subset of variables that contribute significantly to OC prediction. The RFE algorithm was then executed to determine the most influential variables according to the root mean square error (RMSE). The resulting subsets were visualized using plots, thus allowing the researchers to assess the performance of different subset sizes. The covariates were further screened via variance inflation factor (VIF) which was implemented through multiple linear regression.

Statistical Analysis

Data distributions done using classical statistics are minimum, maximum, mean, standard deviation, coefficient of variability, skewness and kurtosis. The statistical analyses for preprocessing environmental variables were done using SAGA-GIS software terrain analysis toolbox. Again, geostatistics and machine learning modeling and prediction were carried out using R and Rstudio software. ArcGIS 10.8 was used for preparing maps. The descriptive statistical analysis was computed in SPSS v25. The flowchart of the steps followed in prediction of soil properties (OC, sand, silt and clay) is presented in Figure 2.

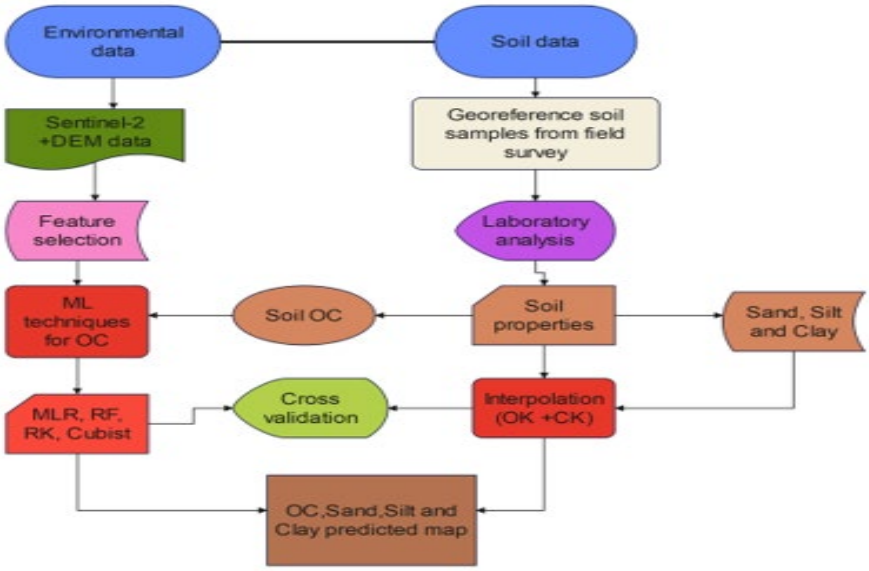

Figure 2. Flowchart illustrating the steps for soil organic carbon and particle size fractions prediction

Geostatistical Interpolation Methods

The geostatistical techniques used in this study were ordinary kriging (OK) and cokriging (CK). OK is broadly used geostatistical method that creates an optimal estimated surface using semi variogram based on regionalized variables. According to Grunwald *et al*. (2008), the OK makes use of an assessed average of a given soil characteristics in a location known to forecast the value of location not sampled (see Eqn. 1). CK is an aspect or continuation of the kriging procedure which combines the information determined by a secondary index in relation to the primary quantity that is being forecasted.

$$Z'(x_0) = \sum_{i=1}^{n} \lambda_i . Z(x_i) \quad (1)$$

where: Z'(x_0) is the estimated/forecasted value for point x_0, Z(xi) is the value known, and λi stands for kriging weight for the Z(xi) values. It obtained using a semi-variance function of the variables with criterion that the predicted value is not biased and optimal (Eqn. 2).

$$\gamma(h) = \frac{1}{2N(h)} \sum_{i=1}^{n} [Z(X_i) - Z(X_i + h)]^2 \quad (2)$$

where γ(h) is the semivariance, h the lag distance, Z stands for soil property, N(h) the number of pairs of areas disconnected by a lag distance h, Z(xi), and Z(X_i+h) are values of Z at positions xi and xi + h according to Wang *et al.* (2013).Exponential, linear,

DOI:https//doi.org/10.22452/mjs.vol44no4.8
Malaysian Journal of Science 44(4): 77-91 (December 2025)

spherical and Gaussian semi variograms models were employed to describe the semi variograms or cross-semi variograms and the most suitable models chosen with the lowest RMSE, MSE and ME between estimated variances and the determined values of soil characteristic. The nugget/sill ratio were employed as a condition to classify how soil characteristics depend of spatial features. Ratio < 25% depicts that property has high dependence on spatial features; varying from 25 to 75% connotes that property has high dependence on spatial features while > 75% depicts the property spatial dependence is feeble (Cambardella *et al.,* 1994).

Machine Learning Algorithms

Four most effective machine learning algorithms for handling small datasets were used in this study to map organic carbon and soil particle size fractions, namely multiple linear regression (MLR), random forest (RF) model, cubist regression (CR) and regression kriging (RK). In MLR, SOC was forecasted as straight line combination of soil-environmental factors. Therefore, the soil characteristic of interest is estimated using;

$$\hat{y}_{(i)} = \hat{\beta}_0 + \sum_{k=1}^{k} \hat{\beta}_k X_{k(i)} \quad (3)$$

Where, ŷ(i) is the estimated soil characteristic at point i, $\hat{\beta}_0$ the predicted intercept, $\hat{\beta}_k$ the predicted regression coefficient for predictor k and $X_k(i)$ the value for the k^{th} predictor at a given point i.

According to Freeman *et al.* (2015) and Fox *et al.* (2019), RF modeling is a commonly used method for regression and grouping with intricate or difficult data sets. Contrary to MLR, RF is an algorithm method that does no *a priori* suppositions concerning the interaction among the predictor quantities and the response. RF has a capacity for better prediction achievement when the data have much number of predictor quantities and there seem to be difficult non-linear and interactive impacts in the association between the predictor quantities and response property (Biau, 2012; John *et al.,* 2020). Nevertheless, RF is not sensitive to the option of tuning parameters and the defaults provided by the RF program perform efficiently for almost all data sets (Freeman *et al.,* 2015). Quinlan (1992) developed cubist regression (CR) model as an extension of the M5 tree model which has same approach as RF. The model design according to Kuhn (2013) is made of parts or piecewise function which acts like choice making tree, join together with MLR models. These trees are diminished or lowered to a set of guidelines that are removed via trimming or joined for ease of usage. This model was put in practice using R with tuning of two hyper-variables which are likely variables having the highest influence on the overall action or achievement of CR model. Also, RK is an extension of MLR. It is a spatial soil mapping method that adds a regression of dependent variables on predictor quantities with kriging of the prediction residuals. RK prediction of $Y(\boldsymbol{S}_0)$, at site not visited $\boldsymbol{S}_0$, is presented thus:

$$Z^*(x_0) = \hat{m}(x_0) + \hat{e}(x_0) = \sum_{k=0}^{P} \hat{\beta}_k * q_k(x_0) + \sum_{i=1}^{n} \lambda_i * e(x_i) \quad (4)$$

where $\hat{m}(x_0)$ is the fitted deterministic part, $\hat{e}(x_0)$ is the interpolated residual, $\hat{\beta}_k$ are the estimated deterministic model coefficients, λ_i are the kriging weights determined by the spatial dependence structure of the residual and e(xi) is the residual at position xi.

Evaluation of Model Performance

Evaluation of the performance or achievement of any model gives valuable ideas into the prediction capacities of various machine learning models for soil characteristics (Barrena-Gonzalez *et al*., 2023). Each model was t improved with 70 % of the dataset which makes up 42 sampling spots) and the authentication or confirmation set which was evaluated using the remaining 30% of the dataset (18 sampling spots). In order to evaluate capabilities of models in mapping organic carbon, the cross-authentication or validation was run on different models. RF, Cubist, MLR, OK and CK were assessed with the aid of bias, coefficient of determination (R^2) and root mean square error (RMSE), mean square error (MSE) and Lin's concordance correlation coefficient (CCC) (see Eqns. 5,6,7,8 & 9)

$$\text{Bias} = \frac{1}{n}\sum_{i=1}^{n}(Z_{oi} - Z_{pi}) \quad (5)$$

$$R^2 = 1 - \frac{\sum_i^n (Z_{oi} - Z_{pi})^2}{\sum_i^n (Z_{oi} - \bar{Z}_{pi})^2} \quad (6)$$

$$\text{RMSE} = \sqrt{\frac{1}{n}\sum_{i=1}^{n}(Z_{pi} - Z_{oi})^2} \quad (7)$$

$$\text{MSE} = \frac{1}{n}\sum_{i=1}^{n}(Z_{pi} - Z_{oi})^2 \quad (8)$$

$$CCC = \frac{2r\sigma_o\sigma_p}{\sigma_o^2 + \sigma_p^2 + (\bar{Z}_p - \bar{Z}_o)} \quad (9)$$

where, Zpi= predicted values, Zoi= observed values, n =observations size for the i-th term observation, $\bar{Z}_i$ = average of the measured variable, σ_o^2 and σ_p^2 are the variances of the estimated and measured values; and r is the coefficient of correlation between the estimated and measured values. Nevertheless, best model estimation is meant to have low bias, MSE, RMSE, CCC and R^2 value close to 1.

DOI:https//doi.org/10.22452/mjs.vol44no4.8
Malaysian Journal of Science 44(4): 77-91 (December 2025)

3. Results and discussion

Properties of The Studied Soil

The results of soil samples used for prediction are given in Table 1. The textural classes of the soil were sandy loam, loam and sandy clay loam indicating higher content of clay. Sand, silt and clay had means of 58.9 %, 26.6 % and 25.9 % respectively. Higher clay values have been reported to improve water and nutrient retention capacity of soils according to Barrena-Gonzalez et al. (2023). The particle size fractions of soil play vital function in determining the structure and infiltration rate of soil. The values of soil reaction(pH) in the area ranged from 5-6.6 with a mean value of 5.4 implying strongly acidic condition. This strong acidity may be responsible for higher content organic carbon in the soil since acidic condition enhances organic matter accumulation in soil. Organic carbon varied from 0.26 % to 4.47 % with a mean of 2.53 % in the soil. These values are very high following the critical limit of Landon (2014). Further result as presented in Table 1 show that TN varied from 0.01 % to 0.38 % with an average value of 0.27 % while available P varied from 2.0 mg/kg to 27 mg/kg averaging 4.3 mg/kg and was rated low following the rating of Landon (2014). The low total nitrogen and available phosphorous in the soil may be due to loss of these nutrients through surface runoff which is common in the area as a result of steep slope which is typical characteristic of mountainous terrain. The mean exchangeable cations; Ca (1.98 cmol/kg), Mg (0.78 cmol/kg), K (0.094 cmol/kg), Na (0.074 cmol/kg) and exchangeable acidity, H+ (0.58 cmol/kg) and Al3+ (0.39 cmol/kg) obtained in the mountainous soil were found to be all low.

Table 1. Summary Statistics for Spatial Soil Properties

	PH	OC	TN	Av.P	Ca	Mg	K	Na	Al	H	ECEC	BS	CEC	CLAY	SILT	SAND
		%	%	mg/kg	→			cmol/kg	←			%	cmol/kg	%	%	%
Minimum	5	0.26	0.01	2	0.8	0.2	0.07	0.05	0	0.08	2.3	68	15	6.8	16	49.2
Maximum	6.6	4.47	0.38	27	7.6	2.8	0.13	0.11	1.12	1.16	10.68	96	44	26.8	37	73.2
Arithmetic Mean	5.443	2.526	0.217	4.3	1.989	0.777	0.094	0.074	0.397	0.584	3.926	70.713	25.9	14.5	26.6	58.9
SD	0.438	0.96	0.083	3.309	1.302	0.593	0.011	0.012	0.313	0.165	1.635	14.374	6.701	3.567	5.353	6.471
CV (%)	8	38	38.1	77	65.5	76.3	11.8	16.1	78.9	28.3	41.6	20.3	25.9	24.6	20.1	11
Skewness	1.329	-0.155	-0.252	5.725	2.812	1.88	0.765	0.621	0.12	0.586	2.476	-1.196	0.66	0.623	0.101	0.492
Kurtosis	0.399	-0.441	-0.261	38.586	8.157	3.217	1.329	0.341	-1.004	2.429	6.638	5.328	-0.026	1.532	-0.703	-0.512

CV = Coefficient of Variation, SD = Standard Deviation, OC=organic carbon, TN= total nitrogen, Av.P=available P, BS=base saturation.

DOI:https//doi.org/10.22452/mjs.vol44no4.8
Malaysian Journal of Science 44(4): 77-91 (December 2025)

The effective cation exchange capacity (ECEC) ranged from 2.3 cmol/kg to 10.68 cmol/kg with an average of 3.93 cmol/kg. ECEC of soil of the site was low following the rating of Landon (2014), while base saturation was high (> 68 %). The CEC obtained from the laboratory results ranged from 15 cmol/kg – 44 cmol/kg averaging 25.9 cmol/kg and was high following critical limit of Landon (2014). The results of physicochemical properties in this study are contrary to observation reported in a similar parent material by Afu *et al*. (2022)

Selected Covariate for Modelling

The results of RFE and Optimal number, VIF and relative importance of covariates are shown in Figure 3. In building of machine learning model, it is highly recommended to employ a feature selection process that aims to minimize the number of predictors and select the most relevant ones. As shown in Figure 3, the optimal number of covariates obtained via RFE was 8, reflecting the variables associated with the lowest RMSE. When the soil properties used for RFE analysis were further subjected to regression analysis, the result obtained showed the respective values of covariates with VIF < 10 (Table 2) to include clay (1.4), minimum temperature (6.19), pH (1.6), slope (1.43), aspect (1.44), NDVI (8.67), mean rainfall (6.76) and SAVI (7.04). RF, cubist and MLR were used to quantify the effect of predictors on the SOC (see Figures 4 to 6). Soil pH was ranked first, with a relative importance of about 100 % in all models used except MLR as variable for predicting soil organic carbon. The result showed that pH, SAVI, NDVI and rainfall were among the top 4 variables influencing SOC prediction in the mountainous areas. NDVI was also found to be the most essential factor that influenced variation of SOC in a study carried out by Falahatkar *et al.* (2016). In a related study Zhang *et al*. (2019) reported that time series properties of NDVI were conducive for predicting soil organic carbon.

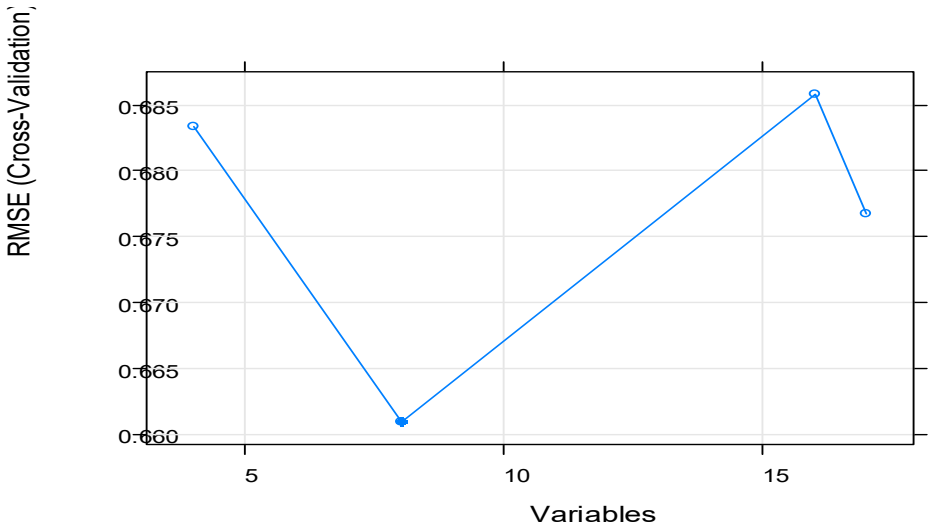

Figure 3. The RMSE values for different numbers of variables as determined by recursive feature elimination (RFE)

DOI:https//doi.org/10.22452/mjs.vol44no4.8
Malaysian Journal of Science 44(4): 77-91 (December 2025)

Table 2. Result of Multiple Regression

Variables	Coefficients	Std. Error	t value	Pr(>|t|)	VIF
Constant	-80.26	49.58	-1.62	0.12	
Clay	-0.04	0.04	-0.98	0.33	1.41
Min temp	0.80	0.61	1.31	0.20	6.19
CNBL	0.03	0.04	0.71	0.48	41.67
pH	-1.08	0.41	-2.62	0.01	1.60
Slope	-0.01	0.01	-0.89	0.38	1.43
Elevation	0.0001	0.00	-0.58	0.56	43.24
Aspect	0.0001	0.00	0.11	0.91	1.44
NDVI	7.99	3.44	2.32	0.03	8.67
SAVI	-9.15	7.49	-1.22	0.23	7.04
NDMI	-5.95	5.64	-1.06	0.30	12.78
Mean rainfall	0.03	0.03	0.83	0.42	6.76
R^2	0.48				
Adjusted R^2	0.29				
F(11,30)	2.15, p = 0.02				

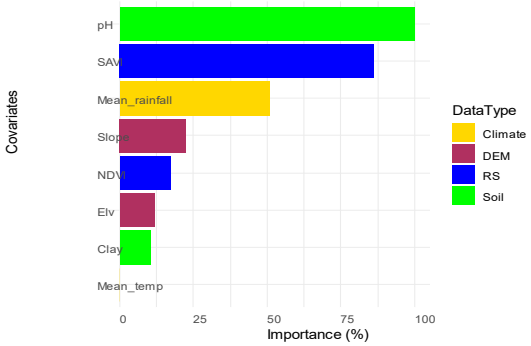

Figure 4. Effect of variables in predicting OC via RF

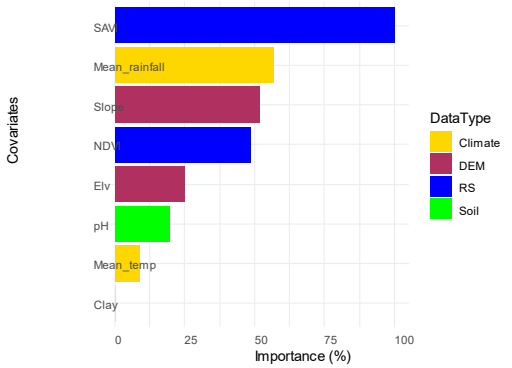

Figure 5. Effect of variables in predicting OC via cubist regression

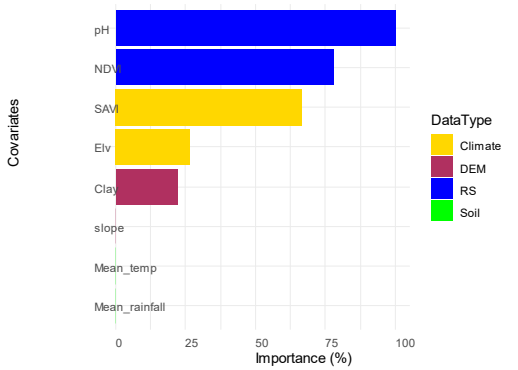

Figure 6. Effect of variables in predicting OC via MLR

DOI:https//doi.org/10.22452/mjs.vol44no4.8
Malaysian Journal of Science 44(4): 77-91 (December 2025)

Spatial Dependency of Measured Soil Organic Carbon and Particle Size

The results presented in Table 3 show the parameters of measured OC model through semi variogram (Figure 7). Soil OC was best modelled by spherical model. In a similar study, John *et al.* (2019) concluded that pH and SOC are perfectly modelled with spherical models. The SOC had a Nugget/Sill ratio of 18.92. The SOC model estimated through OK had strong degree of spatial dependence (Nugget/Sill ratio < 25 %) as shown in Table 3. A lower Nugget/Sill ratio for SOC suggests that parameters such as elements of weather, parent material of soil, terrain, soil characteristics and other natural influences are the determinants of spatial variation of SOC in the study site. As presented in Table 3, the range value of 1669.74 m was obtained for SOC. Therefore, in distance wider than this obtained range of values in present research spatial reliance is found to be nonexistent for SOC.

The geostatistical analysis results (Table 4) for OK and CK show that semivariograms of sand and clay were fitted well by Gaussian model while that of silt was fitted by spherical model. The cross-semivariogram of particle fraction or soil separates were seen to be all suited well by a Gaussian model. The nugget/sill ratios of OK semi variogram of sand, silt and clay were 0.098 %, 0.17 % and 1.92 % while the nugget/sill ratios of the CK cross-semi variogram of sand, silt and clay were 56.25 %, 54.23 % and 55.24 % correspondingly. The range of values of the semivariogram of OK were 65, 100 and 80 m for sand, silt and clay accordingly while that of CK were all 65m for the three soil fractions. The described properties are well shown or observed using the semivariogram plots of the soil particle size fraction as presented in Figure 8 below.

Table 3. Semi Variogram Parameters of Measure SOC

Variable	Model	Nugget (C_0)	Partial Sill(C_1)	Sill (C_0+C_1)	Range (m)	Nugget/Sill	Spatial class
OC (%)	Spherical	0.211	0.904	1.115	1669.74	18.92	Strong

Table 4. Semivariogram Parameters of Particle Size Fractions

	Model	Nugget (C_0)	Partial Sill (C_1)	Sill (C_0+C_1)	Range (m)	Nugget /Sill (%)	Spatial Class
Semivariograms							
Sand	Gaussian	0.056	56.49	57.05	65	0.098	Strong
Silt	Spherical	0.050	28.43	28.48	100	0.17	Strong
Clay	Gaussian	0.25	12.77	13.02	80.97	1.92	Strong
Cross-semivariograms							
Sand	Gaussian	235.70	183.29	418.99	65	56.25	Moderate
Silt	Gaussian	217.23	183.29	400.52	65	54.23	Moderate
Clay	Gaussian	-224.04	181.47	-405.51	65	55.24	Moderate

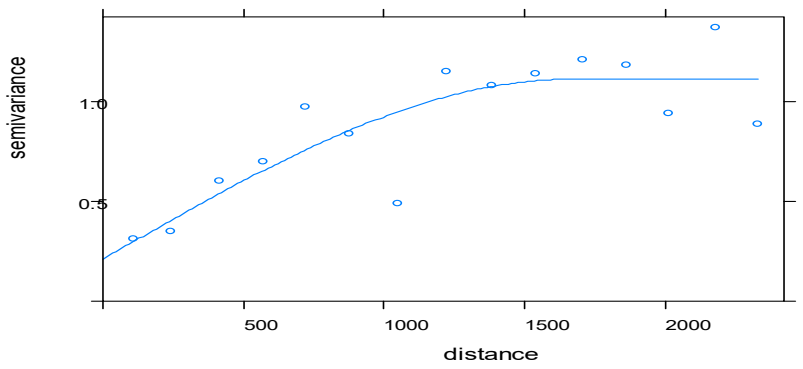

Figure 7. Semi variogram model for measured soil OC

DOI:https//doi.org/10.22452/mjs.vol44no4.8
Malaysian Journal of Science 44(4): 77-91 (December 2025)

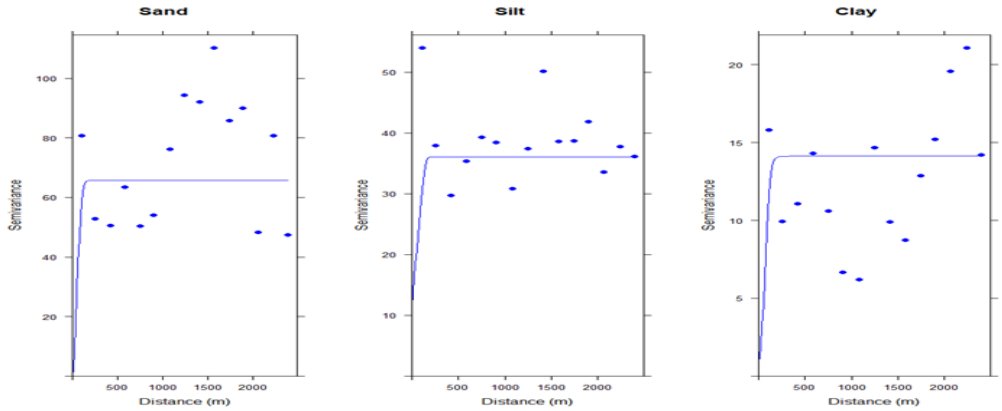

Figure 8. Semivariograms of soil sand, silt and clay content

Mapping of SOC and Particle Size Fractions

The spatial maps of soil OC estimated by RF, cubist, RK, OK and MLR are in Figure 9 and their statistics are shown in Table 5. The mean prediction of OC for the entire study area were 2.25% (Cubist), 2.32% (RF), 2.24%(RK), 2.52% (OK) and 2.40% (MLR). The predictions from all models reported in this study were contained within the observed or laboratory determined OC range, except that obtained from MLR model. This discovery corroborates the finding of Silva *et al*., (2017) who obtained better modelling and validation results for soil properties with RF than MLR. The highest determined OC in the study area was 4.47 and the maximum estimated using RF, OK, RK, Cubist and MLR were 3.78 %, 2.92%, 4.93%, 4.89%, and 6.37%, respectively (see Table 5) which were dominant in the Southwestern side of the research location in all the models investigated. The least laboratory determined OC was 0.26 and the least estimated OC by RF, OK, RK, Cubist and MLR were 1.41%, 1.13%, 0.67%, 0.70% and 0.27 respectively (see Table 5) which were dominant in the Northeastern side of the research location across all the models investigated. These results corroborate the results of research carried out by John *et al.* (2020) and Falahatkar *et al.* (2016), and are further confirmed by report of Mosleh *et al.* (2016) who had carried out related research in Iran. Also, Solly *et al.* (2020) reported results in Switzerland on how SOC can be built up using CEC including other factors in line which is line with this current study.

The spatial variability of soil separates or particle size fraction predicted by OK and CK are illustrated in Figure 10 and Table 6. The mean predicted sand content for both OK and CK were nearly the same and only slightly lower (about 0.49 %) than the laboratory determined sand content. Similarly, the mean predicted silt content for both OK and CK were 26.65 % and 26.64 % respectively which were nearly the same, and only slightly higher (about 0.04 %) than the laboratory determined silt content. Further result showed that the mean predicted clay content for both OK and CK were 14.42 % and 14.96 % respectively which were nearly the same with the clay content (14.5 %) obtained from the laboratory. However, from the results it was also observed that OK model under estimated low sand contents and over-estimated low values of silt and clay whereas, CK model under-estimated low clay values and over-estimated low sand and silt contents. For higher particle size fractions in the study area, CK model under-estimated sand and silt contents and overestimated clay. In both OK and CK predicted map (Fig. 10), sand contents greater than 55 % were found to be dominant in the studied soil. However, for silt predicted maps, it was observed that silt contents greater than 25 % predominated the study area with CK modelled silt map while with OK modelled map, silt content between 22-27% dominated the study area. Meanwhile in clay predicted map, both OK and CK modelled maps, clay contents that were between 14 -20 % were prevalent in the study area. Similar observation was made by John *et al.* (2020) in their study in southern part of Nigeria where they observed that high predicted SOC values occurred in centre, northeastern, easter and northwestern parts of the study.

Table 5. Descriptive Statistics of Predicted Soil OC in this Study

	Min (%)	Max (%)	Mean (%)
Laboratory determined OC	**0.26**	**4.47**	**2.53**
RF predicted OC	1.41	3.78	2.32
OK predicted OC	1.13	2.92	2.52
RK predicted OC	0.67	4.93	2.24
Cubist predicted OC	0.70	4.89	2.25
MLR predicted OC	0.27	6.37	2.40

DOI:https//doi.org/10.22452/mjs.vol44no4.8
Malaysian Journal of Science 44(4): 77-91 (December 2025)

Table 6: Descriptive Statistics of Predicted Soil Particle Fractions in this Study

	Min (%)	Max (%)	Mean (%)
Laboratory determined sand	**49.2**	**73.2**	**58.90**
OK	32.34	72.80	58.41
CK	48.23	63.01	58.40
Laboratory determined silt	**16.0**	**37.0**	**26.60**
OK	17.01	35.77	26.65
CK	18.47	30.35	26.64
Laboratory determined clay	**6.8**	**26.8**	**14.50**
OK	8.22	23.34	14.42
CK	6.64	33.30	14.96

OK = ordinary kriging predicted, CK = Cokriging predicted

Evaluation of The Competence Of Machine Learning Algorithms in Mapping SOC

The average values MSE, RMSE, R^2 and CCC for SOC estimation depict that the models had variations in their capabilities to map or predict SOC at sites not sampled in the research site (Table 7). This is assumed to be as a result of variations in the mathematical program of each machine model and the differences in covariates that were used in fitting. Values of SOC estimated using RF, OK, RK, cubist and MLR were also subjected to comparison and disparities discovered among the models. It was discovered that MLR had the highest R^2 (0.324) indicating very high precision while regression kriging (RK) had the least R^2 of 0.059 and CCC of 0.202. The results further showed that MLR had the largest CCC (0.537) signifying good concordance with the 45^o line, as well as the lowest root mean square error (RMSE = 0.764) and mean square error (MSE = 0.585) signifying high accuracy, compared to other models which indicated extreme cases of over- or underestimation (see Figures 11 to 15). In a related study Farooq *et al*. (2022) found that SOC was best estimated by RF (RMSE 8.21 and R^2 0.9) than OK (RMSE 15.60 and R^2 0.53) and RK (RMSE 17.73 and R^2 0.29)

The MLR model predicted OC was better than other models as seen in the regression lines of observed verses forecasted which are nearer to the 1:1 line compared with what is obtainable by other models under consideration.

Table 7. Performance of Machine Learning Algorithms in Estimating SOC

	R^2	CCC	MSE	RMSE	Bias
RF	0.167	0.319	0.596	0.771	**-0.082**
MLR	**0.324**	**0.537**	**0.585**	**0.764**	-0.031
Cubist	0.085	0.233	0.783	0.885	-0.266
RK	0.059	0.202	0.855	0.925	-0.261
OK	0.202	0.401	0.610	0.781	-0.068

DOI:https//doi.org/10.22452/mjs.vol44no4.8
Malaysian Journal of Science 44(4): 77-91 (December 2025)

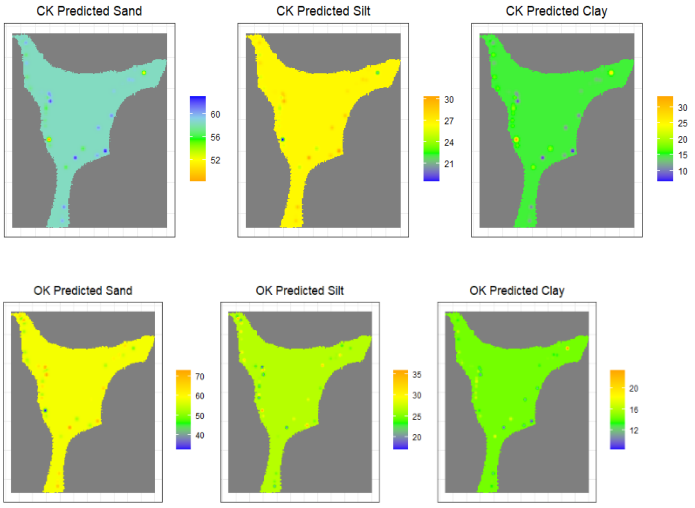

Figure 10. Spatial distribution of particle size fraction using OK & CK

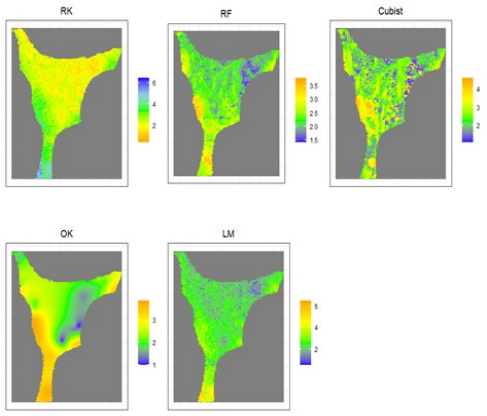

Figure 9. Spatial distribution of SOC using RF, Cubist, MLR, RK & OK

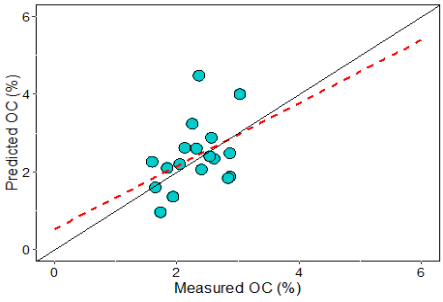

Figure 11. Measured and estimated values of SOC using RF

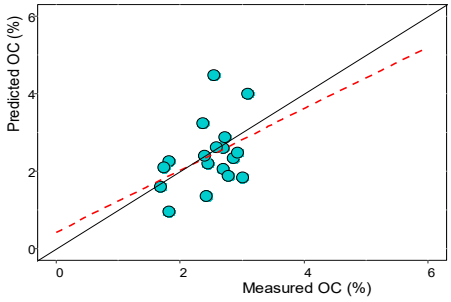

Figure 12. Measured and estimated values of SOC using MLR

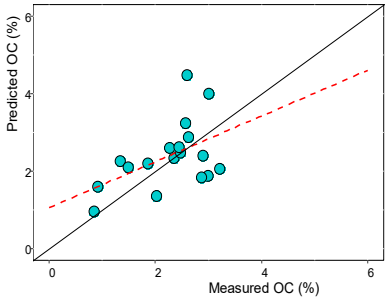

Figure 13. Measured and estimated values of SOC using cubist regression model

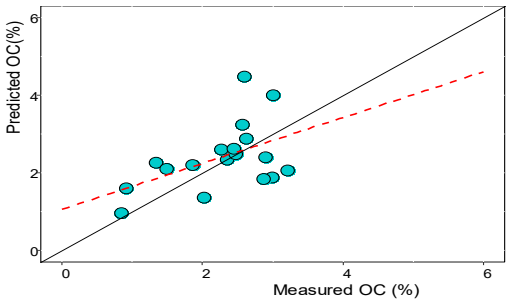

Figure 14. Measured and estimated values of SOC using RK

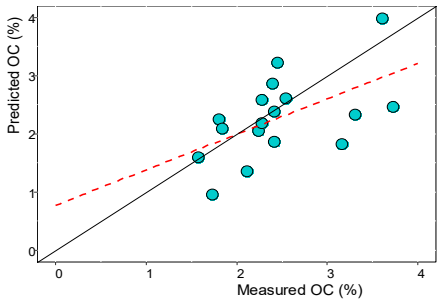

Figure 15. Measured and estimated values of SOC using OK

Evaluation of the Competence of OK And CK Models in Mapping Particle Size Fractions

The cross-validation results of OK and CK are in Table 8. Prediction values of particle size fractions using OK and CK were compared and it was realized that the models have different competence or performing characteristics. Particularly for sand prediction, CK model performed better than OK as shown by lower RMSE (7.434) and MSE (5.568), while for silt and clay contents, OK model performed better than CK model with lower MSE and bias values. Contrary to this study, Barrena-Gonzalez *et al*. (2023) stated that sand content presented more difficulty for prediction in all models- cubist and random forest and stated that the challenges of predicting sand may be determined by rather difficult pattern more than spatial patterns.

DOI:https//doi.org/10.22452/mjs.vol44no4.8
Malaysian Journal of Science 44(4): 77-91 (December 2025)

Table 8. Performance of OK and CK in Estimating Soil Particle Size Fractions

PSF	Model	MSE	RMSE	Bias
Sand	OK	5.702	7.609	**0.071**
	CK	**5.568**	**7.434**	0.082
Silt	OK	**4.229**	5.297	**0.064**
	CK	4.262	**5.278**	0.083
Clay	OK	**2.680**	**3.490**	0.015
	CK	2.967	3.726	**-0.880**

OK = ordinary kriging predicted, CK = Cokriging predicted; PSF= particle size fraction

Summary and Recommendation

This research was conducted to assess the effects soil of environmental elements on spatial distribution of SOC and soil particle size fractions in mountainous area of Obudu cattle ranch using machine learning models. The soil had sandy loam, loam and sandy clay loam texture with acidic pH. Available P, exchangeable cations and exchangeable acidity as and ECEC were high while CEC and base saturation were high. The SOC estimated through OK had strong degree of spatial dependence. The maximum predicted SOC was dominant in the southwestern side of the research site in all the models investigated while minimum predicted SOC was within the northeastern side of the research site in all the models investigated. The MLR model better predicted SOC than other models since it had the highest R^2 (0.324) and CCC (0.537) as well as the lowest RMSE (0.764) and MSE (0.585) signifying high accuracy compared to other models. The mean predicted sand content for both OK and CK were nearly the same, silt was slightly lower than the laboratory determined values while predicted clay were nearly the same with the laboratory determined clay content. In sand prediction, CK model performed better than OK while for silt and clay contents, OK model performed better than CK model. Therefore, the study validates that MLR, CK and OK can be used for assessment of spatial change in SOC and soil particle size fractions in mountainous areas and could also be employed by policy makers and planners as decision support tools for sustainable soil and environmental management and precision agriculture.

5. References

AbdelRahman, M.A., Shalaby, A., Aboelsoud, M. H. & Moghanm, F. S. (2018). Spatial model based for determining actual land degradation status in Kafr El-Sheikh governorate, north Nile Delta. *Modeling Earth Systems and Environment.* 4(1), 359-372.

Adhikari K., Owens P.R., Libohova Z., Miller D.M., Wills S.A. & Nemecek J. (2019) Assessing soil organic carbon stock of Wisconsin, USA and its fate under future land use and climate change. *Science of the Total Environment*. 667: 833-845.

Afu, S.M., Adie, P.I., Olim,D.M., Isong, A.I., Akpama, A.I. & Aaron, M.E.(2022) Properties of soils of different lithology in the humid tropics of southeastern Nigeria. *Global Journal of Agricultural Sciences*. 21, 93-103

Bamutaze, Y., Meadows, M.E., Mwanjalolo, M. & Musinguzi, P. (2021) Effect of land use systems and topographical attributes on the condition of surface soil physicochemical properties in a highland catchment of the Lake Victoria Basin, Uganda. *Catena*. 203. 105343.

Bangroo, S.A., Najar, G.R. & Rasool, A. (2017). Effect of altitude and aspect on soil organic carbon and nitrogen stocks in the Himalayan Mawer Forest Range. *Catena*. 158. 63-68.

Barrena-Gonzalez, J., Gabourel-Landaverde, V.A., Mora, J., Contador, J.F.L. & Fernandez, M.P. (2023) Exploring soil property spatial patterns in a small grazed catchment using machine learning. *Earth Science Information*. 16:3811-3838.

Cambardella, C., Moonan, T.B., Nocak, J.M., Patkin, T.B., Katlem, D.L., Turvo, R.F., & Konopa, A.T. (1994) Field scale variability of soil properties in central Iowa soil. *Soil Science Society of America Journal*, 47, 15011511.

Cotrufo, M.F., Ranalli, M.G., Haddix, M.L., Six J. & Lugato M. (2019) Soil carbon storage informed by particulate and mineral-associated organic matter. *Nat. Geosci*. 12: 989–994. https://doi.org/10.1038/s41561-019-0484-6

De Menezes, M. D., Silva, S. H. G., de Mello, C. R., Owens, P. R. & Curi, N. (2016) Spatial prediction of soil properties in two contrasting physiographic regions in Brazil. *Scientia Agricola* 73 (3) 274 – 284.

Essoka, A., Ibanga, I. & Amalu, U. C. (2010) Physical Properties of the Mountain Soils of Cross River State, Nigeria. Nigerian Journal of Soil Science. 19(2)

Falahatkar, S., Hosseini M. S., Ayoubi, S. & Mahiny, A. S. (2016) Predicting soil organic carbon density using auxiliary environmental variables in northern Iran. *Arch. Agron. Soil Sci.,* 62, 375-393.

Farooq, I., Bangroo, S.A., Owais, B., Shah, T.I., Mlik, A.A., Igbal, A.M., Mahdi, S.S., Wani, O.A, Nazir, N. & Biswas, A. (2022) Comparing random forest and kriging models for soil organic mapping in the Himalayan Region of KASHMIR. *Land*.11(12).

Feng, Z., Wang, L., Peng, Q., Li, J. & Liang, T. (2021) Effect of environmental factors on soil properties under different land use types in a typical basin of the North China Plain. *Journal of Cleaner Production*. 344. 131084.

Fick, S. E. & Hijmans, R. J. (2017) WorldClim 2: new 1km spatial resolution climate surfaces for global land areas. International Journal of Climatology 37 (12): 4302-4315.

DOI:https//doi.org/10.22452/mjs.vol44no4.8
Malaysian Journal of Science 44(4): 77-91 (December 2025)

Fox, E. W., Ver Hoef, J. M. & Olsen, A. R. (2020) Comparing spatial regression to random forests for large environmental data sets. *PLoSONE* 15(3): e0229509.https://doi.org/10.1371/journal.pone.0229509.

Freeman, E. A, Moisen, G. G, Coulston, J. W. & Wilson, B. T. (2015) Random forests and stochastic gradient boosting for predicting tree canopy cover: comparing tuning processes and model performance. *Canadian Journal of Forest Research*, 45,1–17.

Fu, D., Wu, X., Duan, C., Chadwick, D. R. & Jones, D. L. (2020). Response of soil phosphorus fractions and fluxes to different vegetation restoration types in a subtropical mountain ecosystem. *Catena 193, 104663. doi: 10.1016/j.catena.*2020.104663.

Gee, W. G. & Or. D. (2002) Particle-Size Analysis. 255–293. In: Dane, J. and Topp, G.C. (eds.). Methods of Soil Analysis. Book Series: 5. Part 4. Soil Science Society of America. USA.

Hussain, H.,Sharma, V., Arya, V.M., Sharma, K.R. Ch. & Rao, C.S. (2019).Total organic and inorganic carbon in soils under different land use/land cover systems in the foothill Himalayas. *Catena*. 182. 104104.

Isong, A. I., John, K., Okon, P. B., Ogban, P. I. & Afu, S. M. (2022) Soil quality estimation using environmental covariates and predictive models: An example from tropical soils of Nigeria. *Biological processes* 11: 66, 1-22.

John, K., Afu, S. M., Isong, I. A., Aki, E. E., Kebonye, N. M., Ayito, E. O., Chapman, P. A., Eyong, M. O. & Penizek, V. (2021) Mapping soil properties with soil-environmental covariates using geostatistics and multivariate statistic. *International journal of environmental science and technology*. https://doi.org/10.1007/s13762-020-03089.

John, K., Isong, I. A., Kebonye, M. N., Ayito, E. O., Agyeman, P. C. & Afu, S. M. (2020) Using machine learning algorithms to estimate soil organic carbon variability with environmental variables and soil nutrient indicators in an alluvial soil. *Land,* 9, 487; doi:10.3390/land9120487.

John, K., Solomon, O. L., Okon, E. A., Kebonye, N. M.; Ogeh, J. S. & Penížek, V. (2019) Predictive Mapping of Soil Properties for Precision Agriculture Using Geographic Information System (GIS) Based Geostatistics Models. *Modern Applied Science***,** 13, 10, 60-77. doi:10.5539/mas. v13n10p60.

Kalivas, D. P., Triantakonstantis, D. P. & Kollias, V. J. (2002) Spatial prediction of two soil properties using toposequence information. *Global Nest; the International Journal* 4 (1), 41-49.

Komolafe, A. A., Olorunfemi, I. E., Oloruntoba, C. & Akinluyi, F. O. (2021). Spatial prediction of soil nutrients from soil, topography and environment attribute sin Northern part of Ekiti state, Nigeria. *Remote Sensing Applications: Society and Environment 21.*

Kuo, S. (1996) Phosphorus. In:Sparks, D.L., Ed., methods of soil analysis: Part 3, SSSA book series No 5, SSSA and ASA, Madison, 869-919.

Lal, R., Kimble, J.M., Levines, E. & Whiteman C. (1995). World soil and greenhouse effect. Special Publication Number Madison, WI, 57: 51–65.

Lal, R., Smith,P., Jungkunst, H.F., Mitsch, W.J., Lehmann, J., Ramachandran, P.K., McBratney, A.B. De Moraes Sá, J.C., Schneider, J., Zinn, Y.L., Skorupa, A.L.A., Zhang, H.L. Minasny, B., Srinivasrao, C. & Ravindranath, N.H. (2018). The carbon sequestration potential of terrestrial ecosystems. *J. Soil Water Conserv*., 73 145A-152A, 10.2489/jswc.73.6.145A

Landon, J. R. (2014) Booker Tropical Soil Manual. A handbook for soil survey and agricultural land evaluation in the tropics and sub tropics. John Wiley and Sons, New York. P 474.

Li,M., Han,X., Du, S. and Li, L.(2019). Profile stock of soil organic carbon and distribution in croplands of Northeast China. Catena. 174. 285-292.

Massaccesi, L.,De Feudis, M., Leccese, A. & Agnelli, A.(2020) Altitude and Vegetation Affect Soil Organic Carbon, Basal Respiration and Microbial Biomass in Apennine Forest Soils. Forests. 11(6), 710; https://doi.org/10.3390/f11060710

Mayer, S., Kühnel, A., Burmeister, J., Kögel-Knabner, I. & Wiesmeier, M. (2019) Controlling factors of organic carbon stocks in agricultural topsoils and subsoils of Bavaria. *Soil Till. Res*., 192, 22–32, https://doi.org/10.1016/j.still.2019.04.021.

Mishra, G., Sulieman, M.M., Kaya, F., Francaviglia, R., Keshavarzi, A., Bakhshandeh, E., Loum, M., Jangir, A., Ahmed, I. & Elmobarak, A. (2022) Machine Learning for Cation Exchange Capacity Prediction in Different Land Uses. *Catena,* 216, 106404.

Mosleh, Z., Salehi, M. H., Jafari, A., Borujeni, I. E. & Mehnatkesh, A. (2016). The effectiveness of digital soil mapping to predict soil properties over low-relief areas. *Environmental monitoring and assessment*, 188(3):1-13.

Mousavi, A., Karimi, A. & Maleki, S. (2022). Digital mapping of selected soil properties using machine learning and geostatistical techniques in Mashhad plain, northeastern Iran. *Research square* 1-34.

Nelson, D. W. & Sommers, L. E. (1996) Total carbon, organic carbon and organic matter. In D.L. Sparks (Eds.). Methods of soil analysis. Part 3. Chemical methods. SSSA Book Ser. 5. SSSA, Madison, WI. 961-1010.

DOI:https//doi.org/10.22452/mjs.vol44no4.8
Malaysian Journal of Science 44(4): 77-91 (December 2025)

Nisha, R., Kaushik A. & Kaushik C.P. (2007) Effect of indigenous cyanobacterial application on structural stability and productivity of an organically poor semi-arid soil. *Geoderma*, 138: 49–56.

Ota, H.O., Mohan, K.C., Udume, B.U., Olim, D.M. & Okolo, C.C. (2024), Assessment of land use management and its effect on soil quality and carbon stock in Ebonyi State, Southeast Nigeria. Journal of environmental Management, 358. 120889.

Peter-Jerome, H., Adewopo, J. B., Kamara, A. Y., Aliyu, K. T. & Dawaki, M. U. (2022). Assessing the spatial variability of soil properties to delineate nutrient management zones in small holder maize-based system of Nigeria. *Applied and Environmental Soil Science*. 2022. 1-14

Quinlan, J. R. (1992) Learning with continuous classes. In Proceedings of the 5th Australian Joint Conference on Artificial Intelligence, Tasmania, Australia, 16–18 November 1992; 343–348.

Sheikh,M.A., Kumar,M. and & Bussmann, R.W.(2009) Altitudinal variation in soil organic carbon stock in coniferous subtropical and broadleaf temperate forests in Garhwal Himalaya. *Carbon Balance Manag*. 4, 6.

Silva, S.H.G., Teixeira, A.F.D., de Menezes, M.D., Guilherme, L.R.G., Moreira, F.M. & Curi, N. (2017) Multiple linear regression and random forest to predict and map soil properties using data from portable X-ray fluorescence spectrometer (Pxrf). *Ciencia e Agrotecnologia*, 41(16):648-661.

Stanchi, S., D'Amico, M.E., Pintaldi, E., Colombo,N., Romeo,R. & Freppaz, M.(2021) Mountain soils. In book: Recarbonizing global soils – A technical manual of recommended management practices. 2 – hot spots and bright spots of soil organic carbon 116-138.

Solly, E. F., Weber, V., Zimmermann, S., Walthert, L., Hagedorn, F. & Schmidt, M. W. I. A. (2020) Critical Evaluation of the Relationship between the Effective Cation Exchange Capacity and Soil Organic Carbon Content in Swiss Forest Soils. *Frontiers in Forests and Global Change*,3, 98. doi:10.3389/ffgc.2020.00098.

Tang, Q., Xu, Y., Benett, S.J. & Li, Y. (2015) Assessment of soil erosion using RUSSLE and GIS: a case study of the Yangou watershed in the Loess Plateau, China. Environmental Earth Science. 73:1715-1724.

Tsozué, D., Noubissie, N. M. M., Mamdem, E. L. T., Basga, S. D., & Oyono, D. L. B. (2021). Effects of environmental factors and soil properties on soil organic carbon stock in a natural dry tropical area of Cameroon, SOIL, 7, 677–691, https://doi.org/10.5194/soil-7-677-2021.

Tsozué, D., Nghonda, J. P., Tematio, P. & Basga, S. D. (2019) Changes in soil properties and soil organic carbon stocks along an elevation gradient at Mount Bambouto, Central Africa. Catena 175, 251–262. doi: 10.1016/j.catena.2018.12.028.

Udo, E J., T.O. Ibia, J.O. Ogunwale, A.O. Ano & I. Esu (2009) *Manual of Soil, Plant and Water Analysis*. Sibon Books Ltd. Lagos.

Veronesi, F. & Schillaci, C. (2019) Comparison between geostatistical and machine learning models as predictors of topsoil organic carbon with a focus on local uncertainty estimation. *Ecological Indicators*. 101. 1032-1044.

Wang, J. (2022) Influence of environmental factors on soil organic carbon in different soil layers for Chinese Mollisols under intensive maize cropping. *Science of The Total Environment*. 835. 155443.

Wang, T., Kang, F., Cheng, X., Han,H. & Ji, W. 2016). Soil organic carbon and total nitrogen stocks under different land uses in a hilly ecological restoration area of North China. *Soil and Tillage Research*. 163. 176-184.

Wang, Y., Shao, M., Liu, Z. & Horton, R. (2013) Regional-scale variation and distribution patterns of soil saturated hydraulic conductivities in surface and subsurface layers in the loessial soils of China. *Journal of Hydrology,* 487, 13–23.

Xu, M., Li, X., Cai, X., Gai, J., Li, X., Christie, P. & Zhang, J. (2014) Soil microbial community structure and activity along a montane elevational gradient on the Tibetan Plateau. *Eur. J. Soil Biol*. 2014, 64, 6–14.

Zhang, W., Munkholm, L.J., An, T., Liu, X., Zhang, B., Xu, Y., Ge, Z., Zhang, Y., Zhang, J.,Li,S. & Zhang, Y., Ai, J., Sun, Q., Li, Z., Hou, L. & Song, L. (2021) Soil organic carbon and total nitrogen stocks as affected by vegetation types and altitude across the mountainous regions in the Yunnan Province, south-western China. Catena 196, 104872. doi: 10.1016/j.*catena*.2020.104872.

Zhang,Y., Guo.,L.,Chen, Y., Shi,T., Luo, M.,Ju, Q., Zhang, H. & Wang, S.(2019) Predicting soil organic carbon based on landsat 8 monthly NDVI Data for Jianghan plain in Hubei Province, China. *Remote Sens*. 11(14), 168.

Zhang, G.N., Chen, Z.H.; Zhang, A.M., Chen, L.J. & Wu, Z.J. (2014) Influence of climate warming and nitrogen deposition on soil phosphorus composition and phosphorus availability in a temperate grassland, China. *J. Arid Land*. 6, 156–163.

Zhu, Q., Liao, K., Lai, X. & Lv, L. (2020) Scale-dependent effects of environmental factors on soil organic carbon, soil nutrients and stoichiometry under two contrasting land-use types. *Soil Use and Management*.

DOI:https//doi.org/10.22452/mjs.vol44no4.8
Malaysian Journal of Science 44(4): 77-91 (December 2025)

MALAYSIAN JOURNAL OF SCIENCE
MJS
ISSN 1394-3065

Regular Issue

Malaysian Journal of Science 44 (4): 92-101 (December 2025) https://mjs.um.edu.my

New Developments in Ostrowski's Type Inequalities by Using 13-Step Quadratic Kernel

Muhammad Muawwaz[1a], Muhammad Maaz[2a]*, Ather Qayyum[3ab]*, Siti Suzlin Supadi[4b], Usman Ali[5a] and Muhammad Danial Faiz[6a]

Abstract: The Ostrowski inequality has recently been widely recognized as a powerful mathematical tool for modeling and analysing many physical and real-world events. This inequality has been applied across diverse mathematical fields, including complex analysis, numerical analysis, functional analysis, and stochastic analysis. The purpose of this paper is to develop Ostrowski's type integral inequalities by using a special type of 13-steps quadratic kernel. The incorporation of this new kernel gives some new error bounds for various quadrature rules. Applications for cumulative distributive functions are also discussed.

Keywords: *Ostrowski inequalities, numerical integration, quadratic kernel, cumulative distributive functions.*

1. Introduction

Integral inequalities play a crucial role in various mathematical applications. These inequalities have gained significant prominence in recent years, evolving into a distinct field of study within mathematics. This evolution has led to significant advancements and deeper insights, enhencing our understanding and application of integral inequalities in complex mathematical and real-world problems. Notably, Ostrowski [1] discovered the integral inequality now known as the "Ostrowski inequality" in 1938. Inequalities and their applications have been extensively discussed in various research publications and articles (for example, [2-6]). The primary objective of our research is to develop generalized results using a novel approach "a 13-step quadratic kernel" that extends previously published findings in [7-12]. Recent work by various authors (e.g., [13-17]) has further utilized these developments to establish numerous valuable and noteworthy inequalities. Furthermore, we explore different results by utilizing the Diaz-Metcalf inequality, Cauchy inequality, and Grüss inequality. Finally, these inequalities are applied to the cumulative distribution function.

2. Main Findings

Before presenting our main results, we must first establish the following lemma.

Lemma: Let $Y:[\mathcal{r},\check{s}]\to\mathbb{R}$ be such that Y' is absolutely continuous on $[\mathcal{r},\check{s}]$. Define the kernel $P(t,\check{u})$ as

$$P(t,\check{u})=\begin{cases}\frac{1}{2}(\check{u}-\mathcal{r})^2 & ; \quad \check{u}\in\left(\mathcal{r},\frac{31\mathcal{r}+t}{32}\right]\\ \frac{1}{2}\left(\check{u}-\frac{63\mathcal{r}+\check{s}}{64}\right)^2 & ; \quad \check{u}\in\left(\frac{31\mathcal{r}+t}{32},\frac{15\mathcal{r}+t}{16}\right]\\ \frac{1}{2}\left(\check{u}-\frac{31\mathcal{r}+\check{s}}{32}\right)^2 & ; \quad \check{u}\in\left(\frac{15\mathcal{r}+t}{16},\frac{7\mathcal{r}+t}{8}\right]\\ \frac{1}{2}\left(\check{u}-\frac{15\mathcal{r}+\check{s}}{16}\right)^2 & ; \quad \check{u}\in\left(\frac{7\mathcal{r}+t}{8},\frac{3\mathcal{r}+t}{4}\right]\\ \frac{1}{2}\left(\check{u}-\frac{7\mathcal{r}+\check{s}}{8}\right)^2 & ; \quad \check{u}\in\left(\frac{3\mathcal{r}+t}{4},\frac{\mathcal{r}+t}{2}\right]\\ \frac{1}{2}\left(\check{u}-\frac{3\mathcal{r}+\check{s}}{4}\right)^2 & ; \quad \check{u}\in\left(\frac{\mathcal{r}+t}{2},t\right]\\ \frac{1}{2}\left(\check{u}-\frac{\mathcal{r}+\check{s}}{2}\right)^2 & ; \quad \check{u}\in(t,\mathcal{r}+\check{s}-t]\\ \frac{1}{2}\left(\check{u}-\frac{\mathcal{r}+3\check{s}}{4}\right)^2 & ; \quad \check{u}\in\left(\mathcal{r}+\check{s}-t,\frac{\mathcal{r}+2\check{s}-t}{2}\right]\\ \frac{1}{2}\left(\check{u}-\frac{\mathcal{r}+7\check{s}}{8}\right)^2 & ; \quad \check{u}\in\left(\frac{\mathcal{r}+2\check{s}-t}{2},\frac{\mathcal{r}+4\check{s}-t}{4}\right]\\ \frac{1}{2}\left(\check{u}-\frac{\mathcal{r}+15\check{s}}{16}\right)^2 & ; \quad \check{u}\in\left(\frac{\mathcal{r}+4\check{s}-t}{4},\frac{\mathcal{r}+8\check{s}-t}{8}\right]\\ \frac{1}{2}\left(\check{u}-\frac{\mathcal{r}+31\check{s}}{32}\right)^2 & ; \quad \check{u}\in\left(\frac{\mathcal{r}+8\check{s}-t}{8},\frac{\mathcal{r}+16\check{s}-t}{16}\right]\\ \frac{1}{2}\left(\check{u}-\frac{\mathcal{r}+63\check{s}}{64}\right)^2 & ; \quad \check{u}\in\left(\frac{\mathcal{r}+16\check{s}-t}{16},\frac{\mathcal{r}+32\check{s}-t}{32}\right]\\ \frac{1}{2}(\check{u}-\check{s})^2 & ; \quad \check{u}\in\left(\frac{\mathcal{r}+32\check{s}-t}{32},\check{s}\right],\end{cases} \tag{2.1}$$

$$\forall t\in\left[\mathcal{r},\frac{\mathcal{r}-\check{s}}{2}\right].$$

Authors information:
[a]Department of Mathematics, University of Southern Punjab, Multan, PAKISTAN. E-mail: muawwaz123@gmail.com[1]; muhammadmaaz4991@gmail.com[2]; dratherqayyum@um.edu.my[3]; ua3260040@gmail.com[5]; muhammaddanial119347@gmail.com[6]
[a]Institute of Mathematical Sciences, Universti Malaya, MALAYSIA. E-mail: dratherqayyum@um.edu.my[3]; suzlin@um.edu.my[4]
*Corresponding Author: muhammadmaaz4991@gmail.com

Received: February, 2024
Accepted: August, 2024
Published: December, 2025

DOI:https//doi.org/10.22452/mjs.vol44no4.9
Malaysian Journal of Science 44(4): 92-101 (December 2025)

Proof:

Integrating by parts, we have the following identity

$$\begin{aligned}
&\int_{r}^{š} P(t,ŭ)\,Y''(ŭ)dŭ \\
&= \int_{r}^{š} Y(ŭ)dŭ - \frac{š-r}{4}\Big[Y(t)+Y(r+š-t)+\frac{1}{2}\Big\{Y\Big(\frac{r+t}{2}\Big)+Y\Big(\frac{r+2š-t}{2}\Big)\Big\} \\
&+\frac{1}{4}\Big\{Y\Big(\frac{3r+t}{4}\Big)+Y\Big(\frac{r+4š-t}{4}\Big)\Big\}+\frac{1}{8}\Big\{Y\Big(\frac{7r+t}{8}\Big)+Y\Big(\frac{r+8š-t}{8}\Big)\Big\} \\
&+\frac{1}{16}\Big\{Y\Big(\frac{15r+t}{16}\Big)+Y\Big(\frac{r+16š-t}{16}\Big)+Y\Big(\frac{31r+t}{32}\Big)+Y\Big(\frac{r+32š-t}{32}\Big)\Big\} \\
&+\Big(t-\frac{5r+3š}{8}\Big)\Big\{2\{Y(r+š-t)-Y(t)\}+\frac{1}{2}\Big\{Y\Big(\frac{r+2š-t}{2}\Big) \\
&-Y\Big(\frac{r+t}{2}\Big)\Big\}+\frac{1}{8}\Big\{Y\Big(\frac{r+4š-t}{4}\Big)-Y\Big(\frac{3r+t}{4}\Big)\Big\}+\frac{1}{32}\Big\{Y\Big(\frac{r+8š-t}{8}\Big) \\
&-Y\Big(\frac{7r+t}{8}\Big)\Big\}+\frac{1}{128}\Big\{Y\Big(\frac{r+16š-t}{16}\Big)-Y\Big(\frac{15r+t}{16}\Big)\Big\}\Big\} \\
&+\tfrac{1}{512}\Big(t-\tfrac{3r+š}{4}\Big)\Big\{Y\Big(\tfrac{r+32š-t}{32}\Big)-Y\Big(\tfrac{31r+t}{32}\Big)\Big\}\Big]. \qquad (2.2)
\end{aligned}$$

.

Now, we are going to use following three different conditions on $Y''and\ Y'''$ to present our results.

***Case* 1**: *For* $Y'' \in L^1[r,š]$

***Theorem* 1**. Let $Y:[r,š]\to\mathbb{R}$ be differentiable on $(r,š)$, $Y'$is absolutely continuous on $[r,š]and\ \gamma \le Y''(ŭ) \le \Gamma,\ \forall\ ŭ \in [r,š]$. Then $\forall\ t \in \Big[r,\Big(\frac{(r+š)}{2}\Big)\Big]$, we get

$$\begin{aligned}
&\Big|\frac{1}{4}\Big[Y(t)+Y(r+š-t)+\frac{1}{2}\Big\{Y\Big(\frac{r+t}{2}\Big)+Y\Big(\frac{r+2š-t}{2}\Big)\Big\}+\Big\{\frac{1}{4}Y\Big(\frac{3r+t}{4}\Big) \\
&+Y\Big(\frac{r+r-t}{4}\Big)\Big\}+\frac{1}{8}\Big\{Y\Big(\frac{7r+t}{8}\Big)+Y\Big(\frac{r+8š-t}{8}\Big)\Big\}+\frac{1}{16}\Big\{Y\Big(\frac{15r+t}{16}\Big) \\
&+Y\Big(\frac{r+16š-t}{16}\Big)+Y\Big(\frac{31r+t}{32}\Big)+Y\Big(\frac{r+32š-t}{32}\Big)\Big\}+\Big(t-\frac{5r+3š}{8}\Big)\{\{2Y(r+š-t) \\
&-Y(t)\}+\frac{1}{2}\Big\{Y\Big(\frac{r+2š-t}{2}\Big)-Y\Big(\frac{r+t}{2}\Big)\Big\}+\frac{1}{8}\Big\{Y\Big(\frac{r+4š-t}{4}\Big)-Y\Big(\frac{3r+t}{4}\Big)\Big\} \\
&+\frac{1}{32}\Big\{Y\Big(\frac{r+8š-t}{8}\Big)-Y\Big(\frac{7r+t}{8}\Big)\Big\}+\frac{1}{128}\Big\{Y\Big(\frac{r+16š-t}{16}\Big)-Y\Big(\frac{15r+t}{16}\Big)\Big\}\Big\} \\
&+\frac{1}{512}\Big(t-\frac{3r+š}{4}\Big)\Big\{Y\Big(\frac{r-32š-t}{32}\Big)-Y\Big(\frac{31r+t}{32}\Big)\Big\}\Big]+\frac{Y(š)-Y(r)}{(š-r)^2} \\
&\times\Big\{\frac{1}{98304}(t-r)^3+\frac{4681}{12288}\Big(t-\frac{3r+š}{4}\Big)^3-\frac{12483}{32768}\Big(t-\frac{r+š}{2}\Big)^3\Big\}-\frac{1}{š-r}\int_{r}^{š}Y(ŭ)dŭ\Big| \\
&\le v(t)(š-r)(S-\gamma) \qquad (2.3)
\end{aligned}$$

and

$$\begin{aligned}
&\Big|\frac{1}{4}\Big[Y(t)+Y(r+š-t)+\frac{1}{2}\Big\{Y\Big(\frac{r+t}{2}\Big)+Y\Big(\frac{r+2š-t}{2}\Big)\Big\}+\Big\{\frac{1}{4}Y\Big(\frac{3r+t}{4}\Big) \\
&+Y\Big(\frac{r+r-t}{4}\Big)\Big\}+\frac{1}{8}\Big\{Y\Big(\frac{7r+t}{8}\Big)+Y\Big(\frac{r+8š-t}{8}\Big)\Big\}+\frac{1}{16}\Big\{Y\Big(\frac{15r+t}{16}\Big) \\
&+Y\Big(\frac{r+16š-t}{16}\Big)+Y\Big(\frac{31r+t}{32}\Big)+Y\Big(\frac{r+32š-t}{32}\Big)\Big\}+\Big(t-\frac{5r+3š}{8}\Big)\{\{2Y(r+š-t) \\
&-Y(t)\}+\frac{1}{2}\Big\{Y\Big(\frac{r+2š-t}{2}\Big)-Y\Big(\frac{r+t}{2}\Big)\Big\}+\frac{1}{8}\Big\{Y\Big(\frac{r+4š-t}{4}\Big)-Y\Big(\frac{3r+t}{4}\Big)\Big\} \\
&+\frac{1}{32}\Big\{Y\Big(\frac{r+8š-t}{8}\Big)-Y\Big(\frac{7r+t}{8}\Big)\Big\}+\frac{1}{128}\Big\{Y\Big(\frac{r+16š-t}{16}\Big)-Y\Big(\frac{15r+t}{16}\Big)\Big\}\Big\} \\
&+\frac{1}{512}\Big(t-\frac{3r+š}{4}\Big)\Big\{Y\Big(\frac{r-32š-t}{32}\Big)-Y\Big(\frac{31r+t}{32}\Big)\Big\}\Big]+\frac{Y(š)-Y(r)}{(š-r)^2} \\
&\times\Big\{\frac{1}{98304}(t-r)^3+\frac{4681}{12288}\Big(t-\frac{3r+š}{4}\Big)^3-\frac{12483}{32768}\Big(t-\frac{r+š}{2}\Big)^3\Big\}-\frac{1}{š-r}\int_{r}^{š}Y(ŭ)dŭ\Big| \\
&\le v(t)(š-r)(\Gamma-S), \qquad (2.4)
\end{aligned}$$

where

DOI:https//doi.org/10.22452/mjs.vol44no4.9
Malaysian Journal of Science 44(4): 92-101 (December 2025)

$$S = \frac{Y(š) - Y(r)}{š - r}$$

and

$$v(t) = max\left\{\left|\frac{1}{2048}(t-r)^2 - \frac{\propto(t)}{š-r}\right|, \left|\frac{1}{512}\left(t - \frac{3r+š}{4}\right)^2 - \frac{\propto(t)}{š-r}\right|, \left|\frac{1}{128}\left(t - \frac{3r+š}{4}\right)^2 - \frac{\propto(t)}{š-r}\right|, \left|\frac{1}{32}\left(t - \frac{3r+š}{4}\right)^2 - \frac{\propto(t)}{š-r}\right|, \left|\frac{1}{8}\left(t - \frac{3r+š}{4}\right)^2 - \frac{\propto(t)}{š-r}\right|, \left|\frac{1}{2}\left(t - \frac{3r+š}{4}\right)^2 - \frac{\propto(t)}{š-r}\right|, \left|\frac{1}{2}\left(t - \frac{r+š}{2}\right)^2 - \frac{\propto(t)}{š-r}\right|, \left|\frac{1}{8}\left(t - \frac{r+š}{2}\right)^2 - \frac{\propto(t)}{š-r}\right|, \left|\frac{1}{32}\left(t - \frac{r+š}{2}\right)^2 - \frac{\propto(t)}{š-r}\right|, \left|\frac{1}{128}\left(t - \frac{r+š}{2}\right)^2 - \frac{\propto(t)}{š-r}\right|, \left|\frac{1}{512}\left(t - \frac{r+š}{2}\right)^2 - \frac{\propto(t)}{š-r}\right|, \left|\frac{1}{2048}\left(t - \frac{r+š}{2}\right)^2 - \frac{\propto(t)}{š-r}\right|, \left|\frac{\propto(t)}{š-r}\right|\right\}.$$

Proof:

We know that

$$\frac{1}{š-r}\int_r^š Y''(ŭ)dŭ - \frac{Y\prime(š)-Y\prime(r)}{š-r} \tag{2.5}$$

and

$$\frac{1}{š-r}\int_r^š P(t,ŭ)dŭ = \frac{1}{š-r}\left[\frac{1}{98304}(t-r)^3 + \frac{4681}{12288}\left(t - \frac{3r+š}{4}\right)^3 - \frac{12483}{32768}\left(t - \frac{r+š}{2}\right)^3\right], \tag{2.6}$$

which implies that

$$\begin{aligned}
&\frac{1}{š-r}\int_r^š P(t,ŭ)Y''(ŭ)dŭ - \frac{1}{(š-r)^2}\int_r^š P(t,ŭ)\int_r^š Y''(ŭ)dŭ \\
&= \frac{1}{š-r}\int_r^š Y''(ŭ)dŭ - \frac{1}{4}\left[Y(t) + Y(r+š-t) + \frac{1}{2}\left\{Y\left(\frac{r+t}{2}\right) + Y\left(\frac{r+2š-t}{2}\right)\right\}\right. \\
&\quad + \frac{1}{4}\left\{Y\left(\frac{3r+t}{4}\right) + Y\left(\frac{r+4š-t}{4}\right)\right\} + \frac{1}{8}\left\{Y\left(\frac{7r+t}{8}\right) + Y\left(\frac{r+8š-t}{8}\right)\right\} \\
&\quad + \frac{1}{16}\left\{Y\left(\frac{15r+t}{16}\right) + Y\left(\frac{r+16š-t}{16}\right) + Y\left(\frac{31r+t}{32}\right) + Y\left(\frac{r+32š-t}{32}\right)\right\} \\
&\quad + \left(t - \frac{5t+3š}{8}\right)\left\{2\{Y'(r+š-t) - Y'(t)\} + \frac{1}{2}\left\{+Y'\left(\frac{r+2š-t}{2}\right)\right.\right. \\
&\quad \left.\left. - Y'\left(\frac{r+t}{2}\right)\right\} + \frac{1}{8}\left\{Y'\left(\frac{r+4š-t}{4}\right) - Y'\left(\frac{3r+t}{4}\right)\right\} + \frac{1}{32}\left\{Y'\left(\frac{r+8š-t}{8}\right)\right. \\
&\quad \left.\left.\left. - Y'\left(\frac{7r+t}{8}\right)\right\} + \frac{1}{128}\left\{Y'\left(\frac{r+16š-t}{16}\right) - Y'\left(\frac{15r+t}{16}\right)\right\}\right\} \\
&\quad + \frac{1}{512}\left(t - \frac{3r+š}{4}\right)\left\{Y'\left(\frac{r+32š-t}{32}\right) - Y'\left(\frac{31r+t}{32}\right)\right\}\Bigg] \\
&\frac{Y\prime(š)-Y\prime(r)}{(š-r)^2}\left\{\frac{1}{98304}(t-r)^3 + \frac{4681}{12288}\left(t - \frac{3r+š}{4}\right)^3 - \frac{12483}{32768}\left(t - \frac{r+š}{2}\right)^3\right\}.
\end{aligned} \tag{2.7}$$

We suppose that

$$R_n(t) = \frac{1}{š-r}\int_r^š P(t,ŭ)Y''(ŭ)dŭ - \frac{1}{(š-r)^2}\int_r^š P(t,ŭ)\int_r^š Y''(ŭ)dŭ. \tag{2.8}$$

If $C \in R$ is an arbitrary constant, then we have

$$R_n(t) = \frac{1}{š-r}\int_r^š (Y''(ŭ) - c)\left[P(t,ŭ) - \frac{1}{š-r}\int_r^š P(t,š)dš\right]dŭ. \tag{2.9}$$

Furthermore, we have

$$\begin{aligned}
&R_n(t) \\
&\leq \frac{1}{š-r}max_{ŭ\in[r,š]}\int_r^š (Y''(ŭ) - c)\left|P(t,ŭ) - \frac{1}{š-r}\int_r^š P(t,š)dš\right|\int_r^š |Y''(ŭ) - c|\,dŭ.
\end{aligned} \tag{2.10}$$

Now

$$\begin{aligned}
&max\left|P(t,ŭ) - \frac{1}{š-r}\int_r^š P(t,š)\,dš\right| \\
&= max\left\{\left|\frac{1}{2048}(t-r)^2 - \frac{\propto(t)}{š-r}\right|, \left|\frac{1}{512}\left(t - \frac{3r+š}{4}\right)^2 - \frac{\propto(t)}{š-r}\right|, \left|\frac{1}{128}\left(t - \frac{3r+š}{4}\right)^2 - \frac{\propto(t)}{š-r}\right|, \left|\frac{1}{32}\left(t - \frac{3r+š}{4}\right)^2 - \frac{\propto(t)}{š-r}\right|, \left|\frac{1}{8}\left(t - \frac{3r+š}{4}\right)^2 - \frac{\propto(t)}{š-r}\right|,\right.
\end{aligned}$$

DOI:https//doi.org/10.22452/mjs.vol44no4.9
Malaysian Journal of Science 44(4): 92-101 (December 2025)

$$\left|\frac{1}{2}\left(t-\frac{3r+\check{s}}{4}\right)^2-\frac{\propto(t)}{\check{s}-r}\right|,\left|\frac{1}{2}\left(t-\frac{r+\check{s}}{2}\right)^2-\frac{\propto(t)}{\check{s}-r}\right|,\left|\frac{1}{8}\left(t-\frac{r+\check{s}}{2}\right)^2-\frac{\propto(t)}{\check{s}-r}\right|,$$
$$\left|\frac{1}{32}\left(t-\frac{r+\check{s}}{2}\right)^2-\frac{\propto(t)}{\check{s}-r}\right|,\left|\frac{1}{128}\left(t-\frac{r+\check{s}}{2}\right)^2-\frac{\propto(t)}{\check{s}-r}\right|,\left|\frac{1}{512}\left(t-\frac{r+\check{s}}{2}\right)^2-\frac{\propto(t)}{\check{s}-r}\right|,$$
$$\left|\frac{1}{2048}\left(t-\frac{r+\check{s}}{2}\right)^2-\frac{\propto(t)}{\check{s}-r}\right|,\left|\frac{\propto(t)}{\check{s}-r}\right|\Big\}. \tag{2.11}$$

Where

$$\propto(t)=\frac{1}{98304}(t-r)^3+\frac{4681}{12288}\left(t-\frac{3r+\check{s}}{4}\right)^3-\frac{12483}{32768}\left(t-\frac{r+\check{s}}{2}\right)^3.$$

We suppose that

$$v(t)=max\Big\{\left|\frac{1}{2048}(t-r)^2-\frac{\propto(t)}{\check{s}-r}\right|,\left|\frac{1}{512}\left(t-\frac{3r+\check{s}}{4}\right)^2-\frac{\propto(t)}{\check{s}-r}\right|,$$
$$\left|\frac{1}{128}\left(t-\frac{3r+\check{s}}{4}\right)^2-\frac{\propto(t)}{\check{s}-r}\right|,\left|\frac{1}{32}\left(t-\frac{3r+\check{s}}{4}\right)^2-\frac{\propto(t)}{\check{s}-r}\right|,\left|\frac{1}{8}\left(t-\frac{3r+\check{s}}{4}\right)^2-\frac{\propto(t)}{\check{s}-r}\right|,$$
$$\left|\frac{1}{2}\left(t-\frac{3r+\check{s}}{4}\right)^2-\frac{\propto(t)}{\check{s}-r}\right|,\left|\frac{1}{2}\left(t-\frac{r+\check{s}}{2}\right)^2-\frac{\propto(t)}{\check{s}-r}\right|,\left|\frac{1}{8}\left(t-\frac{r+\check{s}}{2}\right)^2-\frac{\propto(t)}{\check{s}-r}\right|,$$
$$\left|\frac{1}{32}\left(t-\frac{r+\check{s}}{2}\right)^2-\frac{\propto(t)}{\check{s}-r}\right|,\left|\frac{1}{128}\left(t-\frac{r+\check{s}}{2}\right)^2-\frac{\propto(t)}{\check{s}-r}\right|,\left|\frac{1}{512}\left(t-\frac{r+\check{s}}{2}\right)^2-\frac{\propto(t)}{\check{s}-r}\right|,$$
$$\left|\frac{1}{2048}\left(t-\frac{r+\check{s}}{2}\right)^2-\frac{\propto(t)}{\check{s}-r}\right|,\left|\frac{\propto(t)}{\check{s}-r}\right|\Big\}. \tag{2.12}$$

We also have

$$\int_r^{\check{s}}|Y''(\check{u})-\gamma|d\check{u}=(S-\gamma)(\check{s}-r), \tag{2.13}$$
$$\int_r^{\check{s}}|Y''(\check{u})-\Gamma|d\check{u}=(\Gamma-S)(\check{s}-r). \tag{2.14}$$

So, we attain (2.3) and (2.4) by using (2.5)-(2.14) and taking $C=\gamma$ and $C=\Gamma$ in (2.10) respectively.

***Corollary* 1**. By replacing $t=\frac{r+\check{s}}{2}$ (2.3) and (2.4), then

$$\left|\frac{1}{4}Y\left(\frac{r+\check{s}}{2}\right)+\frac{1}{8}\left\{Y\left(\frac{3r+\check{s}}{4}\right)+Y\left(\frac{r+3\check{s}}{4}\right)\right\}+\frac{1}{16}\left\{Y\left(\frac{7r+\check{s}}{8}\right)+Y\left(\frac{r+7\check{s}}{8}\right)\right\}$$
$$\frac{1}{32}\left\{Y\left(\frac{15r+\check{s}}{16}\right)+Y\left(\frac{r+15\check{s}}{16}\right)\right\}+\frac{1}{64}\left\{Y\left(\frac{31r+\check{s}}{32}\right)+Y\left(\frac{r+31\check{s}}{32}\right)+Y\left(\frac{63r+\check{s}}{64}\right)\right.$$
$$\left.+Y\left(\frac{r+63\check{s}}{64}\right)\right\}+(\check{s}-r)\left\{\frac{1}{64}\left\{Y'\left(\frac{r+3\check{s}}{4}\right)-Y'\left(\frac{3r+\check{s}}{4}\right)\right\}+\frac{1}{256}\left\{Y'\left(\frac{r+7\check{s}}{8}\right)\right.\right.$$
$$\left.-Y'\left(\frac{7r+\check{s}}{8}\right)\right\}+\frac{1}{1024}\left\{Y'\left(\frac{r+15\check{s}}{16}\right)-Y'\left(\frac{15r+\check{s}}{16}\right)\right\}+\frac{1}{4096}\left\{Y'\left(\frac{r+31\check{s}}{32}\right)\right.$$
$$\left.\left.-Y'\left(\frac{31r+\check{s}}{32}\right)\right\}+\frac{1}{8192}\left\{Y'\left(\frac{r+63\check{s}}{64}\right)-Y'\left(\frac{63r+\check{s}}{64}\right)\right\}\right\}$$
$$+\frac{2341}{393216}(\check{s}-r)\{Y'(\check{s})-Y'(r)\}-\frac{1}{\check{s}-r}\int_r^{\check{s}}Y(\check{u})d\check{u}$$
$$\leq v\left(\frac{r+\check{s}}{2}\right)(S-\gamma)(\check{s}-r).$$

And

$$\left|\frac{1}{4}Y\left(\frac{r+\check{s}}{2}\right)+\frac{1}{8}\left\{Y\left(\frac{3r+\check{s}}{4}\right)+Y\left(\frac{r+3\check{s}}{4}\right)\right\}+\frac{1}{16}\left\{Y\left(\frac{7r+\check{s}}{8}\right)+Y\left(\frac{r+7\check{s}}{8}\right)\right\}$$
$$\frac{1}{32}\left\{Y\left(\frac{15r+\check{s}}{16}\right)+Y\left(\frac{r+15\check{s}}{16}\right)\right\}+\frac{1}{64}\left\{Y\left(\frac{31r+\check{s}}{32}\right)+Y\left(\frac{r+31\check{s}}{32}\right)+Y\left(\frac{63r+\check{s}}{64}\right)\right.$$
$$\left.+Y\left(\frac{r+63\check{s}}{64}\right)\right\}+(\check{s}-r)\left\{\frac{1}{64}\left\{Y'\left(\frac{r+3\check{s}}{4}\right)-Y'\left(\frac{3r+\check{s}}{4}\right)\right\}+\frac{1}{256}\left\{Y'\left(\frac{r+7\check{s}}{8}\right)\right.\right.$$
$$\left.-Y'\left(\frac{7r+\check{s}}{8}\right)\right\}+\frac{1}{1024}\left\{Y'\left(\frac{r+15\check{s}}{16}\right)-Y'\left(\frac{15r+\check{s}}{16}\right)\right\}+\frac{1}{4096}\left\{Y'\left(\frac{r+31\check{s}}{32}\right)\right.$$
$$\left.\left.-Y'\left(\frac{31r+\check{s}}{32}\right)\right\}+\frac{1}{8192}\left\{Y'\left(\frac{r+63\check{s}}{64}\right)-Y'\left(\frac{63r+\check{s}}{64}\right)\right\}\right\}$$
$$+\frac{2341}{393216}(\check{s}-r)\{Y'(\check{s})-Y'(r)\}-\frac{1}{\check{s}-r}\int_r^{\check{s}}Y(\check{u})d\check{u}$$

DOI:https//doi.org/10.22452/mjs.vol44no4.9
Malaysian Journal of Science 44(4): 92-101 (December 2025)

$$\leq v\left(\frac{r+\check{s}}{2}\right)(\Gamma - S)(\check{s}-r).$$

Case 2: *For* $Y''' \in L^2[r,\check{s}]$

Theorem 2. *Let* $Y\colon [r,\check{s}] \to \mathbb{R}$ be three times differentiable function *on* $(r,\check{s})$. *If* $Y''' \in L^2[r,\check{s}]$, then for all $t \in \left[r, \frac{r+\check{s}}{2}\right]$, we have

$$\left|\frac{1}{4}\left[Y(t)+Y(r+\check{s}-t)+\frac{1}{2}\left\{Y\left(\frac{r+t}{2}\right)+Y\left(\frac{r+2\check{s}-t}{2}\right)\right\}+\frac{1}{4}\left\{Y\left(\frac{3r+t}{4}\right)\right.\right.$$
$$+Y\left(\frac{r+4\check{s}-t}{4}\right)\Big\}+\frac{1}{8}\left\{Y\left(\frac{7r+t}{8}\right)+Y\left(\frac{r+8\check{s}-t}{8}\right)\right\}+\frac{1}{16}\left\{Y\left(\frac{15r+t}{16}\right)\right.$$
$$+Y\left(\frac{r+16\check{s}-t}{16}\right)+Y\left(\frac{31r+t}{32}\right)+Y\left(\frac{r+32\check{s}-t}{32}\right)\Big\}+\left(t-\frac{5r+3\check{s}}{8}\right)$$
$$\times\left\{2\{Y'(r+\check{s}-t)-Y'(t)\}+\frac{1}{2}\left\{Y'\left(\frac{r+2\check{s}-t}{2}\right)-Y'\left(\frac{r+t}{2}\right)\right\}\right.$$
$$+\frac{1}{8}\left\{Y'\left(\frac{r+4\check{s}-t}{4}\right)-Y'\left(\frac{3r+t}{4}\right)\right\}+\frac{1}{32}\left\{Y'\left(\frac{r+8\check{s}-t}{8}\right)-Y'\left(\frac{7r+t}{8}\right)\right\}$$
$$\left.+\frac{1}{128}\left\{Y'\left(\frac{r+16\check{s}-t}{16}\right)-Y'\left(\frac{15r+t}{16}\right)\right\}\right\}+\frac{1}{512}\left(t-\frac{3r+\check{s}}{4}\right)$$
$$\times\left\{Y'\left(\frac{r+32\check{s}-t}{32}\right)-Y'\left(\frac{31r+t}{32}\right)\right\}\Big]+\frac{Y'(\check{s})-Y'(r)}{(\check{s}-r)^2}\left\{\frac{1}{98304}(t-r)^3\right.$$
$$\left.+\frac{4681}{12288}\left(t-\frac{3r+\check{s}}{4}\right)^3-\frac{12483}{32768}\left(t-\frac{r+\check{s}}{2}\right)^3\right\}-\frac{1}{\check{s}-r}\int_r^{\check{s}}Y(\check{u})d\check{u}\Bigg|$$
$$\leq\frac{1}{\pi}\|Y'''\|_2\left[\frac{1}{167772160}(t-r)^5+\frac{1082401}{5242880}\left(t-\frac{3r+\check{s}}{4}\right)^5\right.$$
$$-\frac{34636833}{167772160}\left(t-\frac{r+\check{s}}{2}\right)^5$$
$$\left.-\frac{1}{\check{s}-r}\left\{\frac{1}{98304}(t-r)^3+\frac{4681}{12288}\left(t-\frac{3r+\check{s}}{4}\right)^3-\frac{12483}{32768}\left(t-\frac{r+\check{s}}{2}\right)^3\right\}^2\right]^{\frac{1}{2}}. \tag{2.15}$$

Proof: *Let* $R_n(t)$ *is defined as in* (2.8)

$R_n(t)$

$$=\frac{1}{\check{s}-r}\int_r^{\check{s}}P(t,\check{u})Y''(\check{u})d\check{u}-\frac{1}{(\check{s}-r)^2}\int_r^{\check{s}}P(t,\check{u})\int_r^{\check{s}}Y''(\check{u})d\check{u}.$$

If we take $C = Y''\left(\frac{r+\check{s}}{2}\right)$ in (2.9) and by applying the Cauchy inequality, then

$$|R_n(t)| \leq \frac{1}{\check{s}-r}\int_r^{\check{s}}\left|Y''(\check{u})-Y''\left(\frac{r+\check{s}}{2}\right)\right|\left|P(t,\check{u})-\frac{1}{\check{s}-r}\int_r^{\check{s}}P(t,\check{s})d\check{s}\right|d\check{u}$$
$$\leq\frac{1}{\check{s}-r}\left[\int_r^{\check{s}}\left(Y''(\check{u})-Y''\left(\frac{r+\check{s}}{2}\right)\right)^2d\check{u}\right]^{\frac{1}{2}}\left[\int_r^{\check{s}}\left(P(t,\check{u})-\frac{1}{\check{s}-r}\int_r^{\check{s}}P(t,\check{s})\,d\check{s}\right)^2d\check{u}\right]^{\frac{1}{2}}.$$

We apply the Diaz-Metcalf inequality to get

$$\int_r^{\check{s}}\left(Y''(\check{u})-Y''\left(\frac{r+\check{s}}{2}\right)\right)^2d\check{u}\leq\frac{(\check{s}-r)^2}{\pi^2}\|Y'''\|_2^2.$$

So

$$\int_r^{\check{s}}\left(P(t,\check{u})-\frac{1}{\check{s}-r}\int_r^{\check{s}}P(t,\check{s})\,d\check{s}\right)^2d\check{u}$$
$$=\frac{1}{167772160}(t-r)^5+\frac{1082401}{5242880}\left(t-\frac{3r+\check{s}}{4}\right)^5-\frac{34636833}{167772160}\left(t-\frac{r+\check{s}}{2}\right)^5$$
$$-\frac{1}{\check{s}-r}\left\{\frac{1}{98304}(t-r)^3+\frac{4681}{12288}\left(t-\frac{3r+\check{s}}{4}\right)^3-\frac{12483}{32768}\left(t-\frac{r+\check{s}}{2}\right)^3\right\}^2. \tag{2.16}$$

By using (2.7) in above inequalities, we get (2.15).

Corollary 2. By replacing $t=\frac{r+\check{s}}{2}$ in (2.15), we get

$$\left|\frac{1}{4}Y\left(\frac{r+\check{s}}{2}\right)+\frac{1}{8}\left\{Y\left(\frac{3r+\check{s}}{4}\right)+Y\left(\frac{r+3\check{s}}{4}\right)\right\}+\frac{1}{16}\left\{Y\left(\frac{7r+\check{s}}{8}\right)+Y\left(\frac{r+7\check{s}}{8}\right)\right\}\right.$$
$$\frac{1}{32}\left\{Y\left(\frac{15r+\check{s}}{16}\right)+Y\left(\frac{r+15\check{s}}{16}\right)\right\}+\frac{1}{64}\left\{Y\left(\frac{31r+\check{s}}{32}\right)+Y\left(\frac{r+31\check{s}}{32}\right)+Y\left(\frac{63r+\check{s}}{64}\right)\right.$$
$$\left.+Y\left(\frac{r+63\check{s}}{64}\right)\right\}+(\check{s}-r)\left\{\frac{1}{64}\left\{Y'\left(\frac{r+3\check{s}}{4}\right)-Y'\left(\frac{3r+\check{s}}{4}\right)\right\}+\frac{1}{256}\left\{Y'\left(\frac{r+7\check{s}}{8}\right)\right.\right.$$

DOI:https//doi.org/10.22452/mjs.vol44no4.9
Malaysian Journal of Science 44(4): 92-101 (December 2025)

$$-Y'\left(\frac{7r+\check{s}}{8}\right)\Big\}+\frac{1}{1024}\Big\{Y'\left(\frac{r+15\check{s}}{16}\right)-Y'\left(\frac{15r+\check{s}}{16}\right)\Big\}+\frac{1}{4096}\Big\{Y'\left(\frac{r+31\check{s}}{32}\right)$$
$$-Y'\left(\frac{31r+\check{s}}{32}\right)\Big\}+\frac{1}{8192}\Big\{Y'\left(\frac{r+63\check{s}}{64}\right)-Y'\left(\frac{63r+\check{s}}{64}\right)\Big\}\Big\}$$
$$+\frac{2341}{393216}(\check{s}-r)\{Y'(\check{s})-Y'(r)\}-\frac{1}{\check{s}-r}\int_r^{\check{s}}Y(\check{u})d\check{u}$$
$$\leq\frac{1}{\pi}\|Y'''\|_2(\check{s}-r)^{\frac{5}{2}}\frac{1}{196608}\sqrt{\frac{2337080251}{10}}.$$

***Case* 3**: *For* $Y''\in L^2[r,\check{s}]$

***Theorem* 3**. *Let* $Y:[r,\check{s}]\to\mathbb{R}$ be an absolutely continuous function on $(r,\check{s})$, with $Y'''\in L^2[r,\check{s}]$. Then

$$\left|\frac{1}{4}\Big[Y(t)+Y(r+\check{s}-t)+\frac{1}{2}\Big\{Y\left(\frac{r+t}{2}\right)+Y\left(\frac{r+2\check{s}-t}{2}\right)\Big\}+\frac{1}{4}\Big\{Y\left(\frac{3r+t}{4}\right)\right.$$
$$+Y\left(\frac{r+4\check{s}-t}{4}\right)\Big\}+\frac{1}{8}\Big\{Y\left(\frac{7r+t}{8}\right)+Y\left(\frac{r+8\check{s}-t}{8}\right)\Big\}+\frac{1}{16}\Big\{Y\left(\frac{15r+t}{16}\right)$$
$$+Y\left(\frac{r+16\check{s}-t}{16}\right)+Y\left(\frac{31r+t}{32}\right)+Y\left(\frac{r+32\check{s}-t}{32}\right)\Big\}+\left(t-\frac{5r+3\check{s}}{8}\right)$$
$$\times\Big\{2\{Y'(r+\check{s}-t)-Y'(t)\}+\frac{1}{2}\Big\{Y'\left(\frac{r+2\check{s}-t}{2}\right)-Y'\left(\frac{r+t}{2}\right)\Big\}$$
$$+\frac{1}{8}\Big\{Y'\left(\frac{r+4\check{s}-t}{4}\right)-Y'\left(\frac{3r+t}{4}\right)\Big\}+\frac{1}{32}\Big\{Y'\left(\frac{r+8\check{s}-t}{8}\right)-Y'\left(\frac{7r+t}{8}\right)\Big\}$$
$$+\frac{1}{128}\Big\{Y'\left(\frac{r+16\check{s}-t}{16}\right)-Y'\left(\frac{15r+t}{16}\right)\Big\}\Big\}+\frac{1}{512}\left(t-\frac{3r+\check{s}}{4}\right)$$
$$\times\Big\{Y'\left(\frac{r+32\check{s}-t}{32}\right)-Y'\left(\frac{31r+t}{32}\right)\Big\}\Big]+\frac{Y'(\check{s})-Y'(r)}{(\check{s}-r)^2}\Big\{\frac{1}{98304}(t-r)^3$$
$$\left.+\frac{4681}{12288}\left(t-\frac{3r+\check{s}}{4}\right)^3-\frac{12483}{32768}\left(t-\frac{r+\check{s}}{2}\right)^3\Big\}-\frac{1}{\check{s}-r}\int_r^{\check{s}}Y(\check{u})d\check{u}\right|$$
$$\leq\frac{\sqrt{\sigma(Y'')}}{\check{s}-r}\Big[\frac{1}{167772160}(t-r)^5+\frac{1082401}{5242880}\left(t-\frac{3r+\check{s}}{4}\right)^5-\frac{34636833}{167772160}\left(t-\frac{r+\check{s}}{2}\right)^5$$
$$-\frac{1}{\check{s}-r}\Big\{\frac{1}{98304}(t-r)^3+\frac{4681}{12288}\left(t-\frac{3r+\check{s}}{4}\right)^3-\frac{12483}{32768}\left(t-\frac{r+\check{s}}{2}\right)^3\Big\}^2\Big]^{\frac{1}{2}},\qquad(2.17)$$

$\forall\, t\in\left[r,\frac{r+\check{s}}{2}\right]$,

where

$$\sigma(Y'')=\|Y''\|_2-\frac{\left(Y'^{(\check{s})}-Y'^{(r)}\right)^2}{\check{s}-r}=\|Y''\|_2^2-\check{s}^2(\check{s}-r)$$

and S is defined in $Theorem$ 1.

Proof: *Let* $R_n(t)$ be defined as in (2.8). If we take $C=\frac{1}{\check{s}-r}\int_r^{\check{s}}Y''(\check{s})\,d\check{s}$ in (2.9) and by applying the Cauchy inequality and (2.16), then

$$|R_n(t)|\leq\frac{1}{\check{s}-r}\int_r^{\check{s}}\left|Y''(\check{u})-\frac{1}{\check{s}-r}\int_r^{\check{s}}Y''(\check{s})d\check{s}\right|\left|P(t,\check{u})-\frac{1}{\check{s}-r}\int_r^{\check{s}}P(t,\check{s})d\check{s}\right|d\check{u}$$
$$\leq\frac{1}{\check{s}-r}\left[\int_r^{\check{s}}\left(Y''(\check{u})-\frac{1}{\check{s}-r}\int_r^{\check{s}}Y''(\check{s})d\check{s}\right)^2d\check{u}\right]^{\frac{1}{2}}\left[\int_r^{\check{s}}\left(P(t,\check{u})-\frac{1}{\check{s}-r}\int_r^{\check{s}}P(t,\check{s})\,d\check{s}\right)^2d\check{u}\right]^{\frac{1}{2}}$$
$$=\frac{\sqrt{\sigma(Y'')}}{\check{s}-r}\Big[\frac{1}{167772160}(t-r)^5+\frac{1082401}{5242880}\left(t-\frac{3r+\check{s}}{4}\right)^5-\frac{34636833}{167772160}\left(t-\frac{r+\check{s}}{2}\right)^5$$
$$-\frac{1}{\check{s}-r}\Big\{\frac{1}{98304}(t-r)^3+\frac{4681}{12288}\left(t-\frac{3r+\check{s}}{4}\right)^3-\frac{12483}{32768}\left(t-\frac{r+\check{s}}{2}\right)^3\Big\}^2\Big]^{\frac{1}{2}}.$$

By using above equations, we get (2.17).

***Corollary* 3**. By replacing $t=\frac{r+\check{s}}{2}$ in (2.17), we get

$$\left|\frac{1}{4}Y\left(\frac{r+\check{s}}{2}\right)+\frac{1}{8}\Big\{Y\left(\frac{3r+\check{s}}{4}\right)+Y\left(\frac{r+3\check{s}}{4}\right)\Big\}+\frac{1}{16}\Big\{Y\left(\frac{7r+\check{s}}{8}\right)+Y\left(\frac{r+7\check{s}}{8}\right)\Big\}\right.$$
$$\frac{1}{32}\Big\{Y\left(\frac{15r+\check{s}}{16}\right)+Y\left(\frac{r+15\check{s}}{16}\right)\Big\}+\frac{1}{64}\Big\{Y\left(\frac{31r+\check{s}}{32}\right)+Y\left(\frac{r+31\check{s}}{32}\right)+Y\left(\frac{63r+\check{s}}{64}\right)$$
$$\left.+Y\left(\frac{r+63\check{s}}{64}\right)\Big\}+(\check{s}-r)\Big\{\frac{1}{64}\Big\{Y'\left(\frac{r+3\check{s}}{4}\right)-Y'\left(\frac{3r+\check{s}}{4}\right)\Big\}+\frac{1}{256}\Big\{Y'\left(\frac{r+7\check{s}}{8}\right)\right.$$

DOI:https//doi.org/10.22452/mjs.vol44no4.9
Malaysian Journal of Science 44(4): 92-101 (December 2025)

$$-Y'\left(\frac{7r+\check{s}}{8}\right)\Big\}+\frac{1}{1024}\Big\{Y'\left(\frac{r+15\check{s}}{16}\right)-Y'\left(\frac{15r+\check{s}}{16}\right)\Big\}+\frac{1}{4096}\Big\{Y'\left(\frac{r+31\check{s}}{32}\right)$$
$$-Y'\left(\frac{31r+\check{s}}{32}\right)\Big\}+\frac{1}{8192}\Big\{Y'\left(\frac{r+63\check{s}}{64}\right)-Y'\left(\frac{63r+\check{s}}{64}\right)\Big\}\Big\}$$
$$+\frac{2341}{393216}(\check{s}-r)\{Y'(\check{s})-Y'(r)\}-\frac{1}{\check{s}-r}\int_r^{\check{s}}Y(\check{u})d\check{u}$$
$$\leq\sqrt{\sigma(Y'')}(\check{s}-r)^{\frac{5}{2}}\frac{1}{196608}\sqrt{\frac{2337080251}{10}}.$$

3. An Applications to Cumulative Distributive Function

Let X be a random variable taking values in the finite interval $[r,\check{s}]$ with the probability density function $Y:[r,\check{s}]\to[0,1]$ and cumulative distributive function

$$F(t)=Pr(T\leq t)=\int_r^t Y(\check{u})d\check{u},$$
$$F(\check{s})=Pr(T\leq\check{s})=\int_r^{\check{s}}Y(e)de=1.$$

***Theorem* 4**. With the assumptions of $Theorem$ 1, we have the following inequality which holds

$$\left|\frac{\check{s}-E(T)}{\check{s}-r}-\frac{1}{4}\Big[F(t)+F(r+\check{s}-t)+\frac{1}{2}\Big\{F\left(\frac{r+t}{2}\right)+F\left(\frac{r+2\check{s}-t}{2}\right)\Big\}+\frac{1}{4}\Big\{F\left(\frac{3r+t}{4}\right)\right.$$
$$+F\left(\frac{r+4\check{s}-t}{4}\right)\Big\}+\frac{1}{8}\Big\{F\left(\frac{7r+t}{8}\right)+F\left(\frac{r+8\check{s}-t}{8}\right)\Big\}+\frac{1}{16}\Big\{F\left(\frac{15r+t}{16}\right)$$
$$\left.+F\left(\frac{r+16\check{s}-t}{16}\right)+F\left(\frac{31r+t}{32}\right)+F\left(\frac{r+32\check{s}-t}{32}\right)\Big\}+\left(t-\frac{5r+3\check{s}}{8}\right)\{2\{F'(r+\check{s}-t)\right.$$
$$-F'(t)\}+\frac{1}{2}\Big\{F'\left(\frac{r+2\check{s}-t}{2}\right)-F'\left(\frac{r+t}{2}\right)\Big\}+\frac{1}{8}\Big\{F'\left(\frac{r+4\check{s}-t}{4}\right)-F'\left(\frac{3r+t}{4}\right)\Big\}$$
$$+\frac{1}{32}\Big\{F'\left(\frac{r+8\check{s}-t}{8}\right)-F'\left(\frac{7r+t}{8}\right)\Big\}+\frac{1}{128}\Big\{F'\left(\frac{r+16\check{s}-t}{16}\right)-F'\left(\frac{15r+t}{16}\right)\Big\}\Big\}$$
$$+\frac{1}{512}\left(t-\frac{3r+\check{s}}{4}\right)\Big\{F'\left(\frac{r+32\check{s}-t}{32}\right)-F'\left(\frac{31r+t}{32}\right)\Big\}\Big]-\frac{F'(\check{s})-F'(r)}{(\check{s}-r)^2}$$
$$\times\frac{1}{98304}(t-r)^3+\frac{4681}{12288}\left(t-\frac{3r+\check{s}}{4}\right)^3-\frac{12483}{32768}\left(t-\frac{r+\check{s}}{2}\right)^3\Bigg|$$
$$\leq v(t)(\check{s}-r)(S-\gamma)\qquad(3.1)$$

and

$$\left|\frac{\check{s}-E(T)}{\check{s}-r}-\frac{1}{4}\Big[F(t)+F(r+\check{s}-t)+\frac{1}{2}\Big\{F\left(\frac{r+t}{2}\right)+F\left(\frac{r+2\check{s}-t}{2}\right)\Big\}+\frac{1}{4}\Big\{F\left(\frac{3r+t}{4}\right)\right.$$
$$+F\left(\frac{r+4\check{s}-t}{4}\right)\Big\}+\frac{1}{8}\Big\{F\left(\frac{7r+t}{8}\right)+F\left(\frac{r+8\check{s}-t}{8}\right)\Big\}+\frac{1}{16}\Big\{F\left(\frac{15r+t}{16}\right)$$
$$\left.+F\left(\frac{r+16\check{s}-t}{16}\right)+F\left(\frac{31r+t}{32}\right)+F\left(\frac{r+32\check{s}-t}{32}\right)\Big\}+\left(t-\frac{5r+3\check{s}}{8}\right)\{2\{F'(r+\check{s}-t)\right.$$
$$-F'(t)\}+\frac{1}{2}\Big\{F'\left(\frac{r+2\check{s}-t}{2}\right)-F'\left(\frac{r+t}{2}\right)\Big\}+\frac{1}{8}\Big\{F'\left(\frac{r+4\check{s}-t}{4}\right)-F'\left(\frac{3r+t}{4}\right)\Big\}$$
$$+\frac{1}{32}\Big\{F'\left(\frac{r+8\check{s}-t}{8}\right)-F'\left(\frac{7r+t}{8}\right)\Big\}+\frac{1}{128}\Big\{F'\left(\frac{r+16\check{s}-t}{16}\right)-F'\left(\frac{15r+t}{16}\right)\Big\}\Big\}$$
$$+\frac{1}{512}\left(t-\frac{3r+\check{s}}{4}\right)\Big\{F'\left(\frac{r+32\check{s}-t}{32}\right)-F'\left(\frac{31r+t}{32}\right)\Big\}\Big]-\frac{F'(\check{s})-F'(r)}{(\check{s}-r)^2}$$
$$\times\left\{\frac{1}{98304}(t-r)^3+\frac{4681}{12288}\left(t-\frac{3r+\check{s}}{4}\right)^3-\frac{12483}{32768}\left(t-\frac{r+\check{s}}{2}\right)^3\right\}\Bigg|$$
$$\leq v(t)(\check{s}-r)(\Gamma-S).\qquad(3.2)$$

$\forall\, t\in\left[r,\frac{r+\check{s}}{2}\right]$, where $E(T)$ is the expectation of T.

Proof: By (2.3) and (2.4) on choosing $Y=F$ and using the fact

$$E(T)=\int_r^t\check{u}dF(U)=t-\int_r^t F(\check{u})d\check{u},$$

we obtain $(3.1)\ and\ (3.2)$.

***Corollary* 4**. By replacing $t=\frac{r+\check{s}}{2}$ in$(3.1)\ and\ (3.2)$, then

DOI:https//doi.org/10.22452/mjs.vol44no4.9
Malaysian Journal of Science 44(4): 92-101 (December 2025)

$$\left|\frac{\check{s}-E(T)}{\check{s}-r}-\left[\frac{1}{2}F\left(\frac{r+\check{s}}{2}\right)+\frac{1}{8}\left\{F\left(\frac{3r+\check{s}}{4}\right)+F\left(\frac{r+3\check{s}}{4}\right)\right\}+\frac{1}{16}\left\{F\left(\frac{7r+\check{s}}{8}\right)\right.\right.$$
$$\left.+F\left(\frac{r+7\check{s}}{8}\right)\right\}+\frac{1}{32}\left\{F\left(\frac{15r+\check{s}}{16}\right)+F\left(\frac{r+15\check{s}}{16}\right)\right\}+\frac{1}{64}\left\{F\left(\frac{31r+\check{s}}{32}\right)+F\left(\frac{r+31\check{s}}{32}\right)\right.$$
$$\left.+F\left(\frac{63r+\check{s}}{64}\right)+F\left(\frac{r+63\check{s}}{64}\right)\right\}+(\check{s}-r)\left\{\frac{1}{64}\left\{F'\left(\frac{r+3\check{s}}{4}\right)-F'\left(\frac{3r+\check{s}}{4}\right)\right\}\right.$$
$$+\frac{1}{256}\left\{F'\left(\frac{r+7\check{s}}{8}\right)-F'\left(\frac{7r+\check{s}}{8}\right)\right\}+\frac{1}{1024}\left\{F'\left(\frac{r+15\check{s}}{16}\right)-F'\left(\frac{15r+\check{s}}{16}\right)\right\}$$
$$\left.+\frac{1}{4096}\left\{F'\left(\frac{r+31\check{s}}{32}\right)-F'\left(\frac{31r+\check{s}}{32}\right)\right\}+\frac{1}{8192}\left\{F'\left(\frac{r+63\check{s}}{64}\right)-F'\left(\frac{63r+\check{s}}{64}\right)\right\}\right]$$
$$\left.-\frac{2341}{393216}(\check{s}-r)\{F'(\check{s})-F'(r)\}\right|$$
$$\leq v(t)(\check{s}-r)(S-\gamma)$$

and

$$\left|\frac{\check{s}-E(T)}{\check{s}-r}-\left[\frac{1}{2}F\left(\frac{r+\check{s}}{2}\right)+\frac{1}{8}\left\{F\left(\frac{3r+\check{s}}{4}\right)+F\left(\frac{r+3\check{s}}{4}\right)\right\}+\frac{1}{16}\left\{F\left(\frac{7r+\check{s}}{8}\right)\right.\right.$$
$$\left.+F\left(\frac{r+7\check{s}}{8}\right)\right\}+\frac{1}{32}\left\{F\left(\frac{15r+\check{s}}{16}\right)+F\left(\frac{r+15\check{s}}{16}\right)\right\}+\frac{1}{64}\left\{F\left(\frac{31r+\check{s}}{32}\right)+F\left(\frac{r+31\check{s}}{32}\right)\right.$$
$$\left.+F\left(\frac{63r+\check{s}}{64}\right)+F\left(\frac{r+63\check{s}}{64}\right)\right\}+(\check{s}-r)\left\{\frac{1}{64}\left\{F'\left(\frac{r+3\check{s}}{4}\right)-F'\left(\frac{3r+\check{s}}{4}\right)\right\}\right.$$
$$+\frac{1}{256}\left\{F'\left(\frac{r+7\check{s}}{8}\right)-F'\left(\frac{7r+\check{s}}{8}\right)\right\}+\frac{1}{1024}\left\{F'\left(\frac{r+15\check{s}}{16}\right)-F'\left(\frac{15r+\check{s}}{16}\right)\right\}$$
$$\left.+\frac{1}{4096}\left\{F'\left(\frac{r+31\check{s}}{32}\right)-F'\left(\frac{31r+\check{s}}{32}\right)\right\}+\frac{1}{8192}\left\{F'\left(\frac{r+63\check{s}}{64}\right)-F'\left(\frac{63r+\check{s}}{64}\right)\right\}\right]$$
$$\left.-\frac{2341}{393216}(\check{s}-r)\{F'(\check{s})-F'(r)\}\right|$$
$$\leq v\left(\frac{r+\check{s}}{2}\right)(\Gamma-S)(\check{s}-r).$$

***Theorem* 5.** With the assumptions of $Theorem$ 2, we have the following inequality which holds

$$\left|\frac{\check{s}-E(T)}{\check{s}-r}-\frac{1}{4}\left[F(t)+F(r+\check{s}-t)+\frac{1}{2}\left\{F\left(\frac{r+t}{2}\right)+F\left(\frac{r+2\check{s}-t}{2}\right)\right\}+\frac{1}{4}\left\{F\left(\frac{3r+t}{4}\right)\right.\right.$$
$$\left.+F\left(\frac{r+4\check{s}-t}{4}\right)\right\}+\frac{1}{8}\left\{F\left(\frac{7r+t}{8}\right)+F\left(\frac{r+8\check{s}-t}{8}\right)\right\}+\frac{1}{16}\left\{F\left(\frac{15r+t}{16}\right)\right.$$
$$\left.+F\left(\frac{r+16\check{s}-t}{16}\right)+F\left(\frac{31r+t}{32}\right)+F\left(\frac{r+32\check{s}-t}{32}\right)\right\}+\left(t-\frac{5r+3\check{s}}{8}\right)\{2\{F'(r+\check{s}-t)$$
$$-F'(t)\}+\frac{1}{2}\left\{F'\left(\frac{r+2\check{s}-t}{2}\right)-F'\left(\frac{r+t}{2}\right)\right\}+\frac{1}{8}\left\{F'\left(\frac{r+4\check{s}-t}{4}\right)-F'\left(\frac{3r+t}{4}\right)\right\}$$
$$\left.+\frac{1}{32}\left\{F'\left(\frac{r+8\check{s}-t}{8}\right)-F'\left(\frac{7r+t}{8}\right)\right\}+\frac{1}{128}\left\{F'\left(\frac{r+16\check{s}-t}{16}\right)-F'\left(\frac{15r+t}{16}\right)\right\}\right\}$$
$$\left.+\frac{1}{512}\left(t-\frac{3r+\check{s}}{4}\right)\left\{F'\left(\frac{r+32\check{s}-t}{32}\right)-F'\left(\frac{31r+t}{32}\right)\right\}\right]-\frac{F'(\check{s})-F'(r)}{(\check{s}-r)^2}$$
$$\left.\times\frac{1}{98304}(t-r)^3+\frac{4681}{12288}\left(t-\frac{3r+\check{s}}{4}\right)^3-\frac{12483}{32768}\left(t-\frac{r+\check{s}}{2}\right)^3\right|$$
$$\leq\frac{1}{\pi}\|F'''\|_2\left[\frac{1}{167772160}(t-r)^5+\frac{1082401}{5242880}\left(t-\frac{3r+\check{s}}{4}\right)^5-\frac{34636833}{167772160}\left(t-\frac{r+\check{s}}{2}\right)^5\right.$$
$$\left.-\frac{1}{\check{s}-r}\left\{\frac{1}{98304}(t-r)^3+\frac{4681}{12288}\left(t-\frac{3r+\check{s}}{4}\right)^3-\frac{12483}{32768}\left(t-\frac{r+\check{s}}{2}\right)^3\right\}^2\right]^{\frac{1}{2}},\qquad(3.3)$$

$\forall\, t\in\left[r,\frac{r+\check{s}}{2}\right]$, where $E(T)$ is the expectation of T.

Proof: By using (2.15) and the same condition that we use in above theorem, we get the required inequality (3.3).

***Corollary* 5.** By replacing $t=\frac{r+\check{s}}{2}$ in (3.3), then

$$\left|\frac{\check{s}-E(T)}{\check{s}-r}-\left[\frac{1}{2}F\left(\frac{r+\check{s}}{2}\right)+\frac{1}{8}\left\{F\left(\frac{3r+\check{s}}{4}\right)+F\left(\frac{r+3\check{s}}{4}\right)\right\}+\frac{1}{16}\left\{F\left(\frac{7r+\check{s}}{8}\right)\right.\right.$$
$$\left.+F\left(\frac{r+7\check{s}}{8}\right)\right\}+\frac{1}{32}\left\{F\left(\frac{15r+\check{s}}{16}\right)+F\left(\frac{r+15\check{s}}{16}\right)\right\}+\frac{1}{64}\left\{F\left(\frac{31r+\check{s}}{32}\right)+F\left(\frac{r+31\check{s}}{32}\right)\right.$$
$$\left.+F\left(\frac{63r+\check{s}}{64}\right)+F\left(\frac{r+63\check{s}}{64}\right)\right\}+(\check{s}-r)\left\{\frac{1}{64}\left\{F'\left(\frac{r+3\check{s}}{4}\right)-F'\left(\frac{3r+\check{s}}{4}\right)\right\}\right.$$

DOI:https//doi.org/10.22452/mjs.vol44no4.9
Malaysian Journal of Science 44(4): 92-101 (December 2025)

$$+\frac{1}{256}\left\{F'\left(\frac{r+7\check{s}}{8}\right)-F'\left(\frac{7r+\check{s}}{8}\right)\right\}+\frac{1}{1024}\left\{F'\left(\frac{r+15\check{s}}{16}\right)-F'\left(\frac{15r+\check{s}}{16}\right)\right\}$$
$$+\frac{1}{4096}\left\{F'\left(\frac{r+31\check{s}}{32}\right)-F'\left(\frac{31r+\check{s}}{32}\right)\right\}+\frac{1}{8192}\left\{F'\left(\frac{r+63\check{s}}{64}\right)-F'\left(\frac{63r+\check{s}}{64}\right)\right\}\Bigg]$$
$$-\frac{2341}{393216}(\check{s}-r)\{F'(\check{s})-F'(r)\}\Bigg|$$
$$\leq\frac{1}{\pi}\|F'''\|_2(\check{s}-r)^{\frac{5}{2}}\frac{1}{196608}\sqrt{\frac{2337080251}{10}}.$$

***Theorem* 6**. With the assumptions of *Theorem* 3, we have the following inequality which holds

$$\left|\frac{\check{s}-E(T)}{\check{s}-r}-\frac{1}{4}\Bigg[F(t)+F(r+\check{s}-t)+\frac{1}{2}\left\{F\left(\frac{r+t}{2}\right)+F\left(\frac{r+2\check{s}-t}{2}\right)\right\}+\frac{1}{4}\left\{F\left(\frac{3r+t}{4}\right)\right.\right.$$
$$\left.+F\left(\frac{r+4\check{s}-t}{4}\right)\right\}+\frac{1}{8}\left\{F\left(\frac{7r+t}{8}\right)+F\left(\frac{r+8\check{s}-t}{8}\right)\right\}+\frac{1}{16}\left\{F\left(\frac{15r+t}{16}\right)\right.$$
$$\left.+F\left(\frac{r+16\check{s}-t}{16}\right)+F\left(\frac{31r+t}{32}\right)+F\left(\frac{r+32\check{s}-t}{32}\right)\right\}+\left(t-\frac{5r+3\check{s}}{8}\right)\{2\{F'(r+\check{s}-t)$$
$$-F'(t)\}+\frac{1}{2}\left\{F'\left(\frac{r+2\check{s}-t}{2}\right)-F'\left(\frac{r+t}{2}\right)\right\}+\frac{1}{8}\left\{F'\left(\frac{r+4\check{s}-t}{4}\right)-F'\left(\frac{3r+t}{4}\right)\right\}$$
$$\left.+\frac{1}{32}\left\{F'\left(\frac{r+8\check{s}-t}{8}\right)-F'\left(\frac{7r+t}{8}\right)\right\}+\frac{1}{128}\left\{F'\left(\frac{r+16\check{s}-t}{16}\right)-F'\left(\frac{15r+t}{16}\right)\right\}\right\}$$
$$+\frac{1}{512}\left(t-\frac{3r+\check{s}}{4}\right)\left\{F'\left(\frac{r+32\check{s}-t}{32}\right)-F'\left(\frac{31r+t}{32}\right)\right\}\Bigg]-\frac{F'(\check{s})-F'(r)}{(\check{s}-r)^2}$$
$$\times\left\{\frac{1}{98304}(t-r)^3+\frac{4681}{12288}\left(t-\frac{3r+\check{s}}{4}\right)^3-\frac{12483}{32768}\left(t-\frac{r+\check{s}}{2}\right)^3\right\}\Bigg|$$
$$\leq\frac{\sqrt{\sigma(F'')}}{\check{s}-r}\Bigg[\frac{1}{167772160}(t-r)^5+\frac{1082401}{5242880}\left(t-\frac{3r+\check{s}}{4}\right)^5-\frac{34636833}{167772160}\left(t-\frac{r+\check{s}}{2}\right)^5$$
$$-\frac{1}{\check{s}-r}\left\{\frac{1}{98304}(t-r)^3+\frac{4681}{12288}\left(t-\frac{3r+\check{s}}{4}\right)^3-\frac{12483}{32768}\left(t-\frac{r+\check{s}}{2}\right)^3\right\}^2\Bigg]^{\frac{1}{2}}. \tag{3.4}$$

$\forall\, t\in\left[r,\frac{r+\check{s}}{2}\right]$, where $E(T)$ is the expectation of T.

Proof: By using (2.17) and the same condition that we use in above theorem, we get the required inequality (3.4).

***Corollary* 6**. By replacing $t=\frac{r+\check{s}}{2}$ in(3.4), then

$$\left|\frac{\check{s}-E(T)}{\check{s}-r}-\Bigg[\frac{1}{2}F\left(\frac{r+\check{s}}{2}\right)+\frac{1}{8}\left\{F\left(\frac{3r+\check{s}}{4}\right)+F\left(\frac{r+3\check{s}}{4}\right)\right\}+\frac{1}{16}\left\{F\left(\frac{7r+\check{s}}{8}\right)\right.$$
$$\left.+F\left(\frac{r+7\check{s}}{8}\right)\right\}+\frac{1}{32}\left\{F\left(\frac{15r+\check{s}}{16}\right)+F\left(\frac{r+15\check{s}}{16}\right)\right\}+\frac{1}{64}\left\{F\left(\frac{31r+\check{s}}{32}\right)+F\left(\frac{r+31\check{s}}{32}\right)\right.$$
$$\left.+F\left(\frac{63r+\check{s}}{64}\right)+F\left(\frac{r+63\check{s}}{64}\right)\right\}+(\check{s}-r)\left\{\frac{1}{64}\left\{F'\left(\frac{r+3\check{s}}{4}\right)-F'\left(\frac{3r+\check{s}}{4}\right)\right\}\right.$$
$$+\frac{1}{256}\left\{F'\left(\frac{r+7\check{s}}{8}\right)-F'\left(\frac{7r+\check{s}}{8}\right)\right\}+\frac{1}{1024}\left\{F'\left(\frac{r+15\check{s}}{16}\right)-F'\left(\frac{15r+\check{s}}{16}\right)\right\}$$
$$+\frac{1}{4096}\left\{F'\left(\frac{r+31\check{s}}{32}\right)-F'\left(\frac{31r+\check{s}}{32}\right)\right\}+\frac{1}{8192}\left\{F'\left(\frac{r+63\check{s}}{64}\right)-F'\left(\frac{63r+\check{s}}{64}\right)\right\}\Bigg]$$
$$-\frac{2341}{393216}(\check{s}-r)\{F'(\check{s})-F'(r)\}\Bigg|$$
$$\leq\sqrt{\sigma(F'')}(\check{s}-r)^{\frac{3}{2}}\frac{1}{196608}\sqrt{\frac{2337080251}{10}}.$$

DOI:https//doi.org/10.22452/mjs.vol44no4.9
Malaysian Journal of Science 44(4): 92-101 (December 2025)

4. Conclusion

In this paper, we introduced some new results of Ostrowski's type inequalities for various norms by using well known inequalities. We also examined modified results. Notably, we developed a new peano kernel i.e., 13-step quadratic kernel. Lastly, we implemented our outcomes to the domain of cumulative distributive functions. In future, one can extend this work by using n-step kernel for different norms and for the function of bounded variation.

6. References

A. Guessab and G. Schmeisser, Sharp integral inequalities of the Hermite-Hadamard type, Journal of Approximation Theory. (2002) 115(2):260-288.

A. Munir, M. Vivas-Cortez, A. Qayyum, H. Budak, I. Faiz and S. S. Supadi, Some new fractional corrected Euler-Maclaurin type inequalities for function whose second derivatives are s-convex function. Mathematical and Computer Modelling of Dynamical Systems, (2024), 30(1), 543–566.

A. Munir, A. Qayyum, L. Rathour, G. Atta, S. S. Supadi and U. Ali, A study on Milne-type inequalities for a specific fractional integral operator with applications, Korean J. Math. (2024), 32 No. 2, pp. 297–314.

A. Ostrowski. Über die Absolutabweichung einer differentiierbaren Funktion von ihrem Integralmittelwert.Comment.Math.Helv. (1938) 10,226-227.

A. Qayyum, M. Shoaib, I. Faye, On New Weighted Ostrowski Type inequalities Involving Integral Means Over End Intervals and Application, Turkish Journal of Analysis and Number Theory, (2015) Vol.3, No.2, 61-67.

A. Qayyum, M. Shoaib and I. Faye, Some New Generalized Results on Ostrowski Type Integral Inequalities With Application, Journal of computational analysis and applications. (2015) vol.19,No.4.

A. Qayyum, M. Shoaib, S. Erden, On Generalized fractional Ostrowski type inequalities for higher order derivatives, communication in mathematical modeling and applications, (2019) vol.4 (2).

F. Zafar, H. Kalsoom and N. Hussain, Some inequalities of Hermite-Hadamard type for n-times di erentiable (rho,m)-geometrically convex functions, Journal of Nonlinear Science and Applications. (2015) 8 201-217.

H. Budak, M. Z. Sarikaya, A. Qayyum, New Refinements And Applications Of Ostrowski Type Inequalities For Mappings Whose nth Derivatives Are Of Bounded Variation, TWMS J. App. Eng. Math. (2021) Vol.11, No.2.

Junjua, M.-u.-D.; Qayyum,A.; Munir, A.; Budak, H.; Saleem,M.M.; Supadi, S.S. A Study of SomeNew Hermite–Hadamard Inequalitiesvia Specific Convex Functions withApplications. Mathematics 2024, 12,478.

M.M. Jamei and N. Hussain, On orthogonal polynomials and quadrature rules related to the second kind of Beta distribution,Journal of Inequalities and Applications. (2013) 2013:157.

M. Maaz, M. Muawwaz, U. Ali, M. D. Faiz, E. Abdulrehman and A. Qayyum, New Extension in Ostrowski's Type Inequalities by Using 13-Step Linear Kernel, Advances in Analysis and Applied Mathematics, (2024), 1(1), 55–67.

M. Muawwaz, M. Maaz, A. Qayyum, M. Ahmad, M. D. Faiz, and A. Mehboob, Innovative Ostrowski's Type Inequalities Based on Linear Kernel and Applications, Palestine Journal of Mathematics, (2025), 14(1), 802–812.

Muhammad Muawwaz, Muhammad Maaz and Ather Qayyum, Ostrowski's type inequalities by using the modified 2-step linear kernel, Eur. J. Math. Appl. (2024) 4, Article ID 6.

M.W. Alomari, A companion of Ostrowski's inequality with applications. Transylvanian Journal of Mathematics and Mechanics. (2011) 3:9-14.

M.W. Alomari, A companion of ostrowski's inequality for mappings whose rst derivatives are bounded and applications numerical integration, Kragujevac Journal of Mathematics. (2012) 36:77-82.

W. Liu, Y. Zhu and J. Park, Some companions of perturbed Ostrowski-type inequalities based on the quadratic kernel function with three sections and applications, Journal of Inequalities and Applications. (2013):226.

DOI:https//doi.org/10.22452/mjs.vol44no4.9
Malaysian Journal of Science 44(4): 92-101 (December 2025)

MALAYSIAN JOURNAL OF SCIENCE
MJS
ISSN 1394-3065
Regular Issue
Malaysian Journal of Science 44 (3): 102-119 (December 2025)
https://mjs.um.edu.my

Detection and Analysis of MOSH/MOAH Contamination in Edible Vegetable Oils: A Comprehensive Review

Kasturi Indiran[1a], Nur Hidayah Azeman[2b], Nadhratun Naiim Mobarak[3a]* and Ahmad Ashrif A. Bakar[4b]

Abstract: Consuming edible vegetable oil (EVO) is highly beneficial for human health due to its abundant nutrients, yet it might pose a risk if contaminated. Common pollution including mycotoxins, pesticides, heavy metals, and mineral oil are most likely to occur during harvesting, industrial processing, and environmental pathways. Particularly, mineral oil, a type of petrogenic pollutant can be further classified into two subgroups namely mineral oil saturated hydrocarbon (MOSH) and mineral oil aromatic hydrocarbon (MOAH). Exposure to MOSH/MOAH in EVO has a detrimental impact on human health, to the point that both subgroups are considered hazardous. Indeed, MOSH can bioaccumulate in specific organs, and certain MOAH compounds have a strong potential to cause cancer. The European Food Safety Association (EFSA) has established standards for vegetable oil, updated in 2022, which provide a maximum limit of 13 mg MOSH/kg and 0.5 mg MOAH/kg. Additionally, a pragmatic monitoring method is implemented, including identifying and evaluating MOSH/MOAH presence in the specific matrix using analytical techniques that can accurately measure their quantities. Despite the existence of various techniques, the Liquid Chromatography–Gas Chromatography-Flame Ionisation Detector (LC-GC-FID) technique stands out for its adaptability, efficiency, sensitivity, and excellent reproducibility, even in the presence of complicated matrix and analyte. Therefore, this study comprehensively explains the operating principle, sample preparation, column selection, and assessment results. Various advanced techniques including additional instruments; in certain instances, innovative approaches were employed to detect, measure, and distinguish individual MOSH/MOAH structures. Comprehensive analysis of the current literature, focusing on articles published between 2018 and 2024, is conducted to explore the occurrence and implications of MOSH/MOAH contamination in EVO. Additionally, this review delves into the application of the LC-GC-FID method, providing an in-depth evaluation of its efficacy in detecting and quantifying these contaminants within EVO matrices.

Keywords: *MOSH/MOAH, edible vegetable oil, contamination, LC-GC-FID, chromatography.*

1. Introduction

Mineral oil is derived from crude petroleum oil through refining processes, starting with atmospheric pressure distillation. Subsequently, the heaviest residues obtained from former process undergo vacuum distillation. The resulting filtrate, which has a boiling point ranging from 300 to 600°C, undergoes additional processing steps like solvent extraction, hyper treatment, and dewaxing, which are employed (Rawlings & Lombard 2012). At this stage, the resultant is referred to base oil, and further refinement yields mineral oil (MO) as finished goods (IARC 2012; Pirow et al. 2019).

Mineral oil can be defined as a mixture of various molecules with carbon numbers ranging from C1 to C50 (Rawlings & Lombard 2012). It is technically a blend of open or branched paraffinic compounds (saturated), naphthenic (cyclosaturated), and alkylated aromatic hydrocarbons (IARC 2012; Pirow et al. 2019; Weber et al. 2018). Hydrocarbon (HC) mixtures of the mentioned carbon count are relevant because compounds beyond this range pose high volatility and low absorption (Buijtenhuijs & Van de Ven 2019; Pirow et al. 2019).

Mineral oil (MO) can be structurally divided into two main categories: saturated hydrocarbons (MOSH) and aromatic hydrocarbons (MOAH), as illustrated in Figure 1. These terms were introduced by Biederman and his team in 2009 to distinguish mineral oil from pyrogenic polycyclic aromatic compounds (by-products of combustion) and hydrocarbons derived from plants (Pirow et al. 2019). The composition of both MOSH and MOAH can vary depending on the source of origin, which is why they are assigned different Chemical Abstract Service (CAS) numbers, as indicated in (Rawlings & Lombard 2012). Even when subjected to the same refining process, the association categorises them based on their description and characterisation (IARC 2012). Typically, MOSH constitutes the majority, ranging from 65% to 85%, compared to MOAH, which accounts for only about 15% to 35% of the total composition.

Authors information:
[a]Department of Chemical Sciences, Faculty of Science and Technology, Universiti Kebangsaan Malaysia, 43600 UKM Bangi, MALAYSIA. E-mail: p126029@siswa.ukm.edu.my[1]; nadhratunnaiim@ukm.edu.my[3]
[b]Faculty of Enginnering and Build Environment, Universiti Kebangsaan Malaysia, 43600 UKM Bangi, MALAYSIA. E-mail: nhidayah.az@ukm.edu.my[2]; ashrif@ukm.edu.my[4]
*Corresponding Author: nadhratunnaiim@ukm.edu.my

Received: June, 2023
Accepted: June, 2024
Published: December, 2025

DOI:https//doi.org/10.22452/mjs.vol44no4.10
Malaysian Journal of Science 44(2): 102-119 (June 2025)

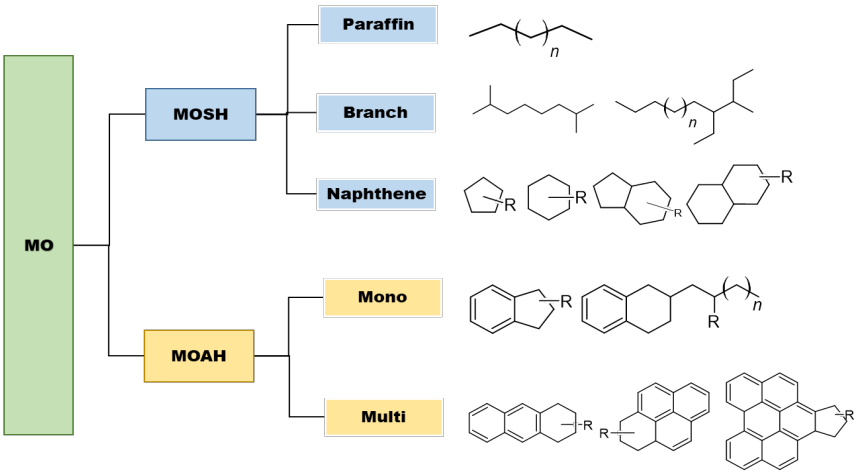

Figure 1. Chemical structures of MOSH and MOAH (Weber et al. 2018)

Mineral Oil Saturated Hydrocarbon (MOSH)

MOSH is named after the characterisation by the chemical arrangement of linear or branched alkylated cycloalkanes such as paraffins or isoparaffins (e.g., n-undecane, bicyclohexyl, cyclohexyl cyclohexane) as well as naphthene (e.g., methylnaphthalene) (Srbinovska et al. 2020). In terms of terminology, MOSH is often referred by various names such as light mineral oil, white mineral oil, white oil, liquid paraffin, liquid petrolatum, mineral oil mist, paraffin oil, paraffinic liquid, petrolatum liquid, petroleum oil (Rawlings & Lombard 2012). This subgroup predominated over total MO, especially between a carbon number of C25- C35 depending on origin, while others were found in smaller fractions or below the limit of quantification (LOQ) (Srbinovska et al. 2020).

Mineral Oil Aromatic Hydrocarbon (MOAH)

MOAH comprises mono and/or polyaromatic hydrocarbons that are alkylated and hydrogenated. Despite the name aromatic, MOAH often has no scent, but in some cases, it is exceptional (Finch, Eilers & Harzke 2006). For instance, MOAH compounds are like perylene and 1,3,5-tri-tert-butylbenzene are fractions that can be separated from MOSH analytically (Jaén et al., 2022; Moret et al., 2016; Nestola, 2022; Rossum et al., 2022). Upon analysis, MOAH may result in a lower concentration, but it appears as a big hump that comprises a mix of aromatic hydrocarbon.

Thus, it is important to focus on petrogenic origin. In that mixture, polycyclic aromatic hydrocarbon (PAH) is usually mistaken for MOAH due to its inclusivity. However, it is a product of pyrolysis, where massive forest fires, volcanoes, and incomplete combustion of many sources are the reasons for its generation (Gharbi et al., 2016; Lachenmeier et al., 2017). Another nonpetrogenic HC, polyolefin oligomeric saturated hydrocarbon (POSH) contaminant found in edible oil where those compounds are in contact with or migrated from polyethylene (PE) or polypropylene (PP) packaging material (Gharbi et al. 2016; Srbinovska et al. 2020).

Properties of MO

Physical properties

MO is typically colourless (transparent), odourless, and tasteless in terms of their physical properties. However, there are exceptions to this general rule due to the complexity of the compounds (Rawlings & Lombard 2012; United States Pharmacopeial Convention 2014). In many cases, odorants are added to MO to provide a scent that warns of their presence for safety purposes or to mask any unpleasant odours (Finch, Eilers & Harzke 2006). This is supported by research indicating that MOSH and MOAH can potentially possess odorous characteristics, which can be detected individually or in a mixture through experiments conducted on mice (Gamble & Smith 2009).

MO exhibits variations in boiling points, which correspond to their specific applications (Finch, Eilers & Harzke 2006). The boiling point range typically falls between 218°C and 643°C. The flash point of MO is measured at 135°C for the closed cup method and 193°C for the open cup (OC) method. However, according to the ASTM D92 method (OC), a flash point of 115°C can also be triggered (United States Pharmacopeial Convention 2014). Generally, paraffinic oil tends to have higher flash and boiling points than naphthenic structures. Viscosity plays a crucial role in determining the molecular geometry, electrical, and thermal properties of the MO (Jin et al. 2014). Regarding kinematic viscosity, MO can exceed 38 mm^2/s while maintaining its characteristic as a viscous liquid (United States Pharmacopeial Convention 2014; Yuliastuti 2010).

It is important to note that viscosity measurements should be accompanied by information about the test conditions, such as temperature, which is closely related to the pour point and influences the applicability of MO in specific uses. When analysing MO, the characterisation of properties like viscosity and the average molecular weight is often prioritised over determining the precise chemical composition, which can vary based on carbon number and structure (Polyakova, van Leeuwen & Peters 2022). Table 1 compares the general physio-chemical properties of EVO and MO, which makes sense for easy contamination.

DOI:https//doi.org/10.22452/mjs.vol44no4.10
Malaysian Journal of Science 44(2): 102-119 (June 2025)

Table 1. A comparison of physio-chemical properties between EVO and MO

Properties	EVO	MO
Origin	Plant	Petroleum (Animal Fossil)
Appearance	Light greenish yellow to red	Colourless
Viscosity	Varies; 33	>38
Density	Varies; 0.9	0.845 – 0.905
Solubility	Insoluble in water; Soluble in organic solvent, as in acetone, hexane and toluene	Insoluble in water & ethanol; Soluble in benzene, ether, carbon disulphide & volatile solvents
Pour point	-3ºC – 15ºC	~ -40ºC
Cloud point	-1ºC – 17.5ºC	< –8ºC
Fire point	323ºC – 378ºC	160ºC
Chemical stability	Oxidizable	Inert
Surface tension	31- 32 mN/m	40-60 mN/m

Additionally, MO has a partition coefficient in n-octanol/water of more than six (United States Pharmacopeial Convention 2014). The solubility of certain gaseous substances in MO has also been studied. According to Müller et al., (2012), nitrogen is highly soluble in MO compared to hydrogen and oxygen, which raises concerns for specific applications. Furthermore, a study by Liao et al., (2011) reported low moisture content in MO even after ageing, suggesting that moisture dissolves slowly in MO rather than absorbed by it.

Chemical Properties

Chemically, MO is mostly able to undergo a hydrogenation process, especially by naphthenic and aromatic compounds, leading to the formation of paraffinic and isoparaffinic HCs, which are widely used in the cosmetic and medical industries (Klaus, Tewksbury & Fenske 1962; Rausch et al. 1981). This chemical transition greatly impacts colour, odour, oxidation stability, and emulsification properties, not only by removing undesirable MOSH/MOAH but also nitrogen- and sulphur-containing compounds (Flinn et al. 1965; Wright n.d.).

Although MO is capable of acting as a strong oxidising agent and readily undergoes reduction under normal conditions, most MO compounds are chemically inert with respect to oxidation (United States Pharmacopeial Convention 2014). However, some compounds, particularly MOAH, tend to oxidise at elevated temperatures with excess oxygen to produce aldehyde, ketone and ester (Martin 2008; Zoccali et al. 2016).

This is like the EVO oxidation process, capable of rancidity over a prolonged period. The same phenomenon applies to the MO oxidation process, where its performance will be subpar due to sludge formation or crystallisation. To avoid this undesirable reaction, an oxidation inhibitor, such as sulphur, should be included in the formulation upon application to prolong the benefits (Kojic et al. 2019). MO has been used in various sectors, notably as a lubricant in machinery due to its high-temperature stability (Tuei 2023).

Thermal Properties

In addition to the properties above, MO also exhibits various thermal properties. The decomposition temperature of MO was initially unavailable, but it was predicted using time-temperature functionality to be around 371°C after 50 hours, as mentioned in Klaus et al., (1962). Later, the onset decomposition temperature was determined to be approximately 291.2°C using thermogravimetric analysis (TGA) by Patel et al., (2018). However, it should be noted that the actual decomposition temperature may vary depending on the specific application. For instance, in a research by Liao et al., (2011), a lower value was recorded for MO in an impregnated insulating pressboard system.

The thermal conductivity of MO, determined through the ASTM D2717 hot wire method, is an essential property for heat transfer under temperature differential conditions. In this test, a constant voltage is applied to a platinum wire, and the change in voltage flow is recorded as a function of the sample's thickness (Jin et al. 2014). The thermal conductivity value of MO has been reported as approximately 1.11 W/mK (Jin 2015). This property plays a crucial role in managing the heat generated by the magnetic circuit and windings in transformers, allowing for extended usability without causing harm to the circuit. Overall, the thermal properties of MO play a significant role in determining its shelf life.

Electrical Properties

As MO is a soup of all hydrocarbons, naphthenic compounds are highly valued for their versatile properties. They are extensively used in electrical appliances like insulating transformers due to their electrical characteristics, cost-effectiveness, and machinery efficiency (Rouabeh et al. 2019). Another essential electrical criterion is the dielectric constant (DC), also known as relative permittivity, which measures a material's ability to store electrical charge or energy relative to a vacuum. As a non-conductive material, MO exhibits a low DC value of approximately 2.22 at 90°C, which depends on its composition (Spohner 2017).

The DC value is influenced by internal factors such as polarity and oxidation tendencies of the oil (Martin 2008; Toudja et al. 2014; Yuliastuti 2010). While a high DC value is undesirable as it can lead to failure under intense electric fields, even a low value is sufficient for energy storage and other withstand capabilities. MO's suitability for transformer oil insulation, particularly in high-voltage electrical units, is attributed to its low DC value and ability

DOI:https//doi.org/10.22452/mjs.vol44no4.10
Malaysian Journal of Science 44(2): 102-119 (June 2025)

to keep the unit cool by preventing heat transfer during its shelf life (Jin et al. 2014).

Another important characteristic is the dissipation factor (DF), which represents the inefficiency of an insulating material and is defined as the tangent of the loss angle between changes in applied voltage and resulting current. A lower dissipation factor indicates better insulation. Tests conducted according to IEC 60247 standards compared the DF of MO with synthetic ester oil under different voltage conditions (Yuliastuti 2010). Generally, a good insulating oil exhibits a low DF, although it may increase with rising temperatures and conductivity (Rouabeh et al. 2019).

Next, breakdown voltage (BDV), the insulation strength, is measured where the electric field generates enough energy to ionise the electrons, and this causes chemical reactions that affect the performance of the dielectric properties. This is supported by Suwarno and Darma, (2008), who mentioned that MOAH is oxidised and forms precipitation in the form of sludge, which eventually reduces the initial BDV value. The BDV of MO recorded in (Yuliastuti 2010) is 38.63 kV, and this value can vary under the influence of methyl ester, moisture content, and temperature, as measured and tabulated in Table 2.

Table 2. Brief comparison on electrical properties (Rouabeh et al. 2019; Spohner 2017)

Characteristics	MO	EVO (Olive oil)	Unit
Viscosity @40°C	9.3	175.5	cSt
Dielectric Constant	2.43 – 2.29	3.43 – 3.02*	-
Dissipation Factor	14e-4	11e-4	Tan δ
Breakdown Voltage	32	46.5	kV
Resistivity@ 40°C	5.7	3.1	TΩ/cm
Humidity	90	200	ppm
Electrical Conductivity @ 40°C	175e-3	322e-3	S/m
Electrical regency	128	175.5	kV/mm

*sunflower oil

MO Application in the Food Industry

The versatile properties of MO make it highly valuable in numerous industrial and consumer applications. However, this review primarily focuses on MOSH/MOAH in EVO, with only brief discussions regarding food applications. In the food industry, food-grade MO is used as additives, glazing agents for candy, sprays for baked goods, and surface-treating agents for fruits and vegetables. Additionally, highly refined and treated MO is employed in the animal feed production (Buijtenhuijs & Van de Ven 2019; Moret et al. 2016). MOSH-derived paraffinic and naphthenic waxes find application in crop protection products, extending the shelf life of agricultural goods. It is also worth noting that MO is commonly used as a lubricant in mechanical components like bearings and gears in food manufacturing machinery. Despite the diverse uses, it is crucial to acknowledge that exposure or ingestion of MO above certain threshold levels can severely impact human well-being and the ecosystem within our food supply chain.

Contamination of MO in EVO

MO exposure in EVO occurs due to intentional or unintentional contamination throughout the production process of the primary raw material, vegetable oil. In 2008, a significant concern arose when sunflower oil exported from Ukraine to European countries contained MO levels exceeding 1000 mg/kg (Ahmad et al. 2019; Nestola 2022). The contamination was suspected of fraud or intentional admixture of base oil used in lubricating oil production rather than migration (Biedermann & Grob 2009).

However, according to Wrona et al., (2013), the typical contamination of MO in food is 10-100 µg/g, with additional amounts contributed by migration from packaging. Migration predominantly occurs through the gas phase and direct contact, with the gas phase being susceptible to MOSH in the range of C16 to C35 and MOAH below C25, while direct contact depends on the origin of contamination and is not limited to saturated structures (Buijtenhuijs & Van de Ven 2019; Moret et al. 2016).

Figure 2 illustrates the general pathways of MOSH/MOAH contamination and migration into food products, including EVO, encompassing environmental sources such as the atmosphere and aquatic ecosystems (EFSA 2012). Air pollution studies conducted by Buijtenhuijs and Van de Ven, (2019), revealed MO concentrations ranging from 0.03 to 5 parts per billion (ppb) in rural areas, particularly near road tunnels, where contamination or deposition is common. This contamination extends to plantation areas, where crops are harvested under the influence of MOSH/MOAH content and proceed to the processing stage. During processing, MO contamination increases due to leakage from machinery, including engine oil, lubricating oil, heating oil, and diesel oil in mills that come into contact with edible oil due to inadequate machinery maintenance or improper Good Manufacturing Practices (GMP) (Jaén et al., 2022).

DOI:https//doi.org/10.22452/mjs.vol44no4.10
Malaysian Journal of Science 44(2): 102-119 (June 2025)

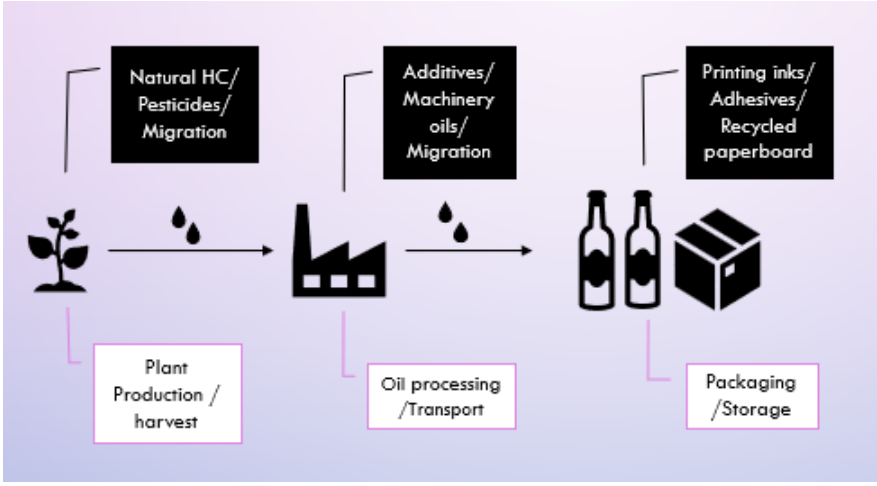

Figure 2. MOSH/MOAH contamination routes (adapted from Oppermann and Leitner, 2017)

Additionally, the use of recycled cardboard for packaging, printed with mineral oil-based inks, has been identified as a source of contamination. The printing inks and certain paper and packaging adhesives contribute to MOSH/MOAH contamination due to their sorption, diffusion properties, and partition coefficients (Fengler & Gruber 2022; Wrona, Pezo & Nerin 2013). According to the lab-scale experiment by Purcaro (n.d.), lighter C-fractions cause migration from jute bags to cocoa beans to occur more frequently due to its high volatility. The cocoa bean's shell functions as a barrier, letting only the lightest portion to get to the nibs. The total migration of pollutants depends critically on contact time. In some cases, migration of MO from adhesives is mistakenly attributed to contamination from the cardboard itself. It was found that one gram of hot glue used in food packaging can contain up to 8.2-118 mg of MOSH and 59 mg of MOAH in dry foods as shown in experiment by Lommatzsch and other fellows, (2016).

Various studies have confirmed the presence of MOSH/MOAH in food samples from 120 different countries, with nearly half of the samples (43%) testing positive for MOAH in 2015 (Jaén et al. 2021). Specifically, researcher Buijtenhuijs and Van de Ven (2019) investigated foods prepared with vegetable oil such as ice cream, desserts, and pasta and they found contamination levels of 0.4 mg/kg for MOSH and 0.028 mg/kg for MOAH in food product with a sample population of children aged 2-6 years. More shockingly, in 2019, the EFSA published an opinion on the presence of MOAH in infant formula, quantitatively assessing contamination levels ranging from 0.5 to 3 mg/kg (Hochegger et al. 2022). While highly refined MO is intentionally used in food products, non-intentional contamination can occur during various stages, including processing, packaging, transport, and storage (García-Cicourel et al. 2020). According to Pirow et al., (2019), the highest value obtained for vegetable oil is about 41-45mg/kg.

The mobility of MO compounds in edible oil depends on volatility, re-condensability, and vapour pressure, which determine the contamination rate or migration (Lorenzini et al. 2010). Precisely, medium-sized MO compounds with molecular mass up to C24 have high volatility, and the velocity depends on temperature, where high temperature can cause rapid migration with a wide range of hydrocarbon (HC) from contaminated packaging into the oil (Fengler & Gruber 2022).

Other factors that affect the rate include storage conditions, the structure of foods (high-fat content), which tend to have high migration, and the physiochemical properties of the barriers (Buijtenhuijs & Van de Ven 2019; Lorenzini et al. 2013). They recommend a temperature range between 20 to 40 °C and a 1 to 12 days storage time, indicating actual migration conditions. A migration test at equivalent conditions was done, whereby 60-80% of MOSH/MOAH compounds up to C24 proved to evaporate and migrate from paperboard into food by using modified polyphenylene oxide (MPPO – Tenax®) (Lorenzini et al. 2010).

Impact of MO towards human

Studies conducted on animals have investigated the effects of MO on tissues and illnesses associated with humans. Reference by Pirow et al., (2019) provides a summary of MOSH/MOAH levels found in animal and human tissues, as well as the observed effects such as increased organ weight, the presence of microgranulomas in mesenteric lymph nodes or liver, and changes in haematological and clinical chemistry parameters. These effects were observed in laboratory rats. In particular, rats' intake of MO in the form of transformer oil under designated conditions raised significant concerns, as it led to various toxicities affecting the skin, blood, liver, kidneys, and small intestines (Otunga et al. 2019).

MOSH can bioaccumulate in tissues, especially at lymph nodes, spleen and liver, leading to serious illness as mentioned above (Hochegger et al. 2021; Ruiz et al. 2021). If lymph nodes malfunction, it will lead to infections, blockage (build-up of body fluid) and cancer. This applies to almost all synthetic HCs like polyolefin oligomeric hydrocarbon (POH) and POSH. Although the human body is gifted with metabolism, only some low and medium-mass oil below C20 can be converted into smaller volatile compounds and excreted (Wrona, Pezo & Nerin 2013). In early 2024, a study found that pig's back fat showed distinct patterns of bioaccumulation, especially for MOSH with higher carbon numbers (n-C24 to n-C36, centered on n-C32) (Albendea et al. 2024).

DOI:https//doi.org/10.22452/mjs.vol44no4.10
Malaysian Journal of Science 44(2): 102-119 (June 2025)

Naphthenic hydrocarbon in the range of C20- C35, also called 'grey cloud' fractions, are likely to be retained and absorbed in the liver due to a lower elimination rate than iso and cycloalkanes, causing the formation of lipogranuloma (Carrillo et al. 2022). However, in late 2022, an assessment on MOSH adversity and relatability of animal and human tissue was discussed, noting that retention of HC of C20-C35, was not the cause of microgranuloma formation in rats (F344) and, therefore, not relevant to human conditions (Isola et al. 2023). Nevertheless, this scope of study is still debatable and requires detailed data for verification.

Meanwhile, certain MOAH compounds is surely recognised as potential carcinogenic and mutagenic substances, as mentioned earlier, where compounds with 3-7 ring PAC are considered so (Hochegger et al. 2022; Pirow et al. 2019; Ruiz et al. 2021; Srbinovska et al. 2020). These compounds are indicative of unrefined or poor process quality. In addition, short alkylated MOAH also contains heteroatoms that can induce cancer cell (Pirow et al. 2019). Not only that, a tumour may develop due to recurrence of dermal irritation at the stage where it cannot mutate or activate the cancer cell (Pirow et al. 2019). This is supported by (Hochegger et al. 2022), whereby selective MOAH compounds are involved in tumour development and DNA alteration via a non-genotoxic mechanism. MOAH exposure is, therefore, creating quite a concern among people, and the consumable product (food and cosmetics) should be free from MOAH or hazardous MOSH compounds.

2. Guideline

An extensive contamination of MO in sunflower oil makes the EU Commission established a limitation of 50 mg/kg for paraffin content in the sunflower oil (Gómez-Coca et al. 2016). Later, EFSA's Panel on Contamination in the Food Chain (CONTAM) issued a scientific opinion on the presence of MO in food based on a few case studies (Fiselier & Grob 2009; Pirow et al. 2019; Ruiz et al. 2021). In addition, preliminary data on the acceptable daily intake (ADI) of medium- and low-viscosity foods MO are published, although these data are from poor analysis (EFSA 2012). Based on this publication, the European Union issued a proposal (EU 2017/84) shortly after in 2017 to monitor MO, focusing on its content in food and food packaging (Andriukaitis 2017).

In the year 2022, the Member States of European countries agreed that MOAH concentration should be followed without regard to fractions in a variety of food products that focus on infant formula and toddler food, irrespective of the MOAH sources, as stated in Table 3 (European Commission 2022). An updated version of the scientific opinion was drafted in 2023 after some thorough toxicity evaluation. As per EFSA and fellow contributors (2023), most of the uncertainty was clarified, including conclusions of the EFSA (2012) opinion that the genotoxicity of MOH is associated with the presence of three or more ring MOAH.

Table 3. Benchmark for MOSH/MOAH in food related product

Food Categories	Limit value (mg/Kg)		References
	MOSH	MOAH	
Dry foods with a low-fat content (≤ 4% fat/oil	-	0.5	(European Commission 2022; Parkinson 2022)
Foods with a higher fat content (> 4% fat/oil, ≤ 50 % fat/oil)	-	1	
Fats/oils and foods with (> 50 % fat/oil)	-	2	
Vegetable oil	13	0.5	(Sabrina & Giorgia 2022)
Dry food: bread, pastry, cakes, biscuits, cereal	6	0.5	(Institute for Publication n.d.)
Confectionary except	9	0.5	
Migration from packaging	0.6	0.5	(Pirow et al. 2019)

In certain food categories, MOSH has no permissible limits for the migration that recognised as non-dangerous, while MOAH should be below 0.5 mg/Kg as the limit of determination (LOD), which cannot be exceeded analytically as stated in Table 3. However, the estimation of human exposure is less accurate, so that still no "tolerable daily intake" (TDI) has been registered by a national legislation (Buijtenhuijs & Van de Ven 2019). Additional toxicity data are needed, especially on bioaccumulation of MOSH and potential effects on human tissues, i.e., inflammation, liver and spleen diseases. Furthermore, the technical specifications for MOAH used as food additives and packaging materials should be updated to avoid composition and content of three or more ring compounds. The issue is difficult due to its complexity, both in terms of the toxicological evaluation (which requires characterizing the toxicity of each molecule and their interactions, such as synergism or antagonism) and the analytical determination (Matheson 2023).

DOI:https//doi.org/10.22452/mjs.vol44no4.10
Malaysian Journal of Science 44(2): 102-119 (June 2025)

3. Analysis

Detection Method

Initially, the gravimetric analysis (IP 346 method) was introduced by the European Petroleum Refiners Association specifically for testing unused lubricating oil to ensure that carcinogens are not detected as well as to maintain the quality of MO (Ruiz et al. 2021). There are three categories of petroleum: lubricating oil, foot oil, and treated distillate (aromatic extracts), the latter of, is considered a carcinogen under certain conditions according to CLP Regulation No. 1272/2008 (Pirow et al. 2019). To determine the presence of those compounds, this method has been utilised as a qualifier for refining efficacy. According to Hochegger et al., (2022), this method also measures and evaluates the weight percentage of PACs in dimethyl sulfoxide (DMSO) extracts of lubricating oil to obtain good quality.

In earlier times, infrared (IR) spectroscopy was used to detect MO through the C-H stretching vibration. Still, this method is the most ineffective as it is non-quantitative and cannot distinguish the source (EFSA 2012). Another test, AMES, is the common method for testing mutagenic propertied compounds using biological assays like bacteria. This method was named after its developer, Bruce N. Ames, Berkeley and is especially used in the pharmaceutical and cosmetic industries where compounds are formulated into (Boogaard et al. 2012). Compounds that fall under mutagenic criteria are usually considered carcinogenic, too. Therefore, this test was modified to detect such complexes using bacteria (Biopharma n.d.; Boogaard et al. 2012; Hochegger et al. 2022).

Next, Hochegger et al. (2022) revealed that manual separation into MOSH and MOAH using silica was followed by HPLC clean separation, during which MOAH was further separated into three-ring and larger (>3 ring) MOAH structures. HPLC is a vital instrument for investigation and quality control measures related to edible oils because of its ability to perform high-resolution separations and detect trace quantities of constituents (Ali & Neha 2024). Then the resultant further conditioned before proceeding with the AMES test. In brief, a 10µl sample was placed in duplicate on 24-well plates and diluted with a combination comprising 5% (v/v) bacteria (Salmonella typhimurium TA98, about 109 CFU/mL) and 4.5% (v/v) phenobarbital/-naphthoflavone-activated rat liver S9, which was incubated for 90 minutes at 37°C with agitation. The mixture was then dispersed into 48 wells with a reversion indicator and incubated for another 2-3 days. When revertant levels were 2-fold higher than the baseline, samples were identified as DNA reactive or carcinogens, as shown in Figure 3.

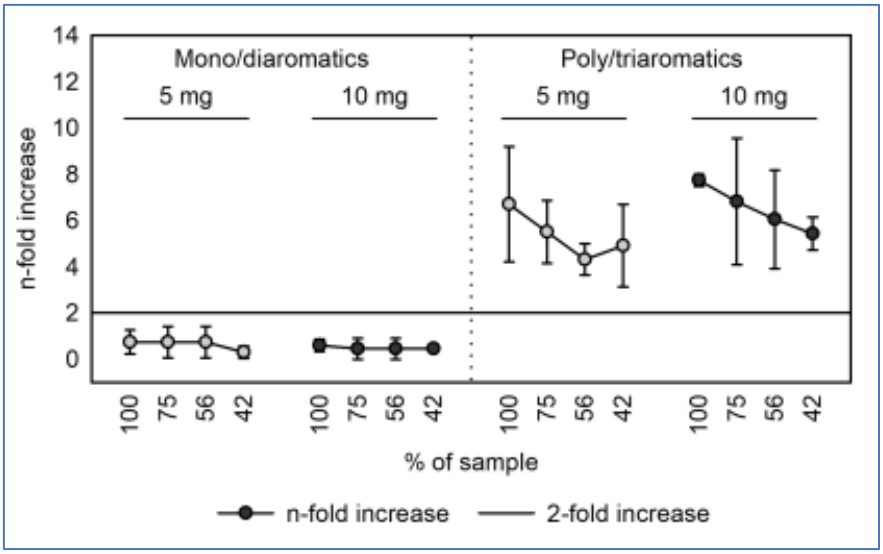

Figure 3. AMES test result for mono-diaromatic and polyaromatic fractionates with 250µl DMSO extraction (Hochegger et al. 2022)

In addition, the mouse skin painting model also serves as an indicator for toxicity assay, as human and mouse skin may develop similar dermatological effects (tumour) when exposed to the carcinogenic MO substance (Carrillo et al. 2019). This study provides the most realistic response to chemical consumption at various parameters such as latency, mechanism including multiplicity and malignancy, etc. (Walaszek, Hanausek & Slaga 2007). Another test using alcoholic potassium hydroxide solution with distilled water, where turbidity indicates concentration after slight mixing, is another traditional method for detecting MO in cooking oil.

Due to the massive contamination of MO in sunflower oil, 2008 IUPAC (1987) and AOCS (1997) were standardised for contamination in oil and fat, measured by densitometry and column chromatography, respectively. But quantification of these methods yields a high limit of detection (LOD), about 500 – 1000mg/kg. The following section will brief on the current analytical approach that enables MO quantification in EVO and other complementary matrices, as well as room for alternative emerging methods.

MO Analysis by LC-GC-FID and its Preface

Initially, the quality of MO was the focus; soon after scientific reports were published, detecting MOSH/MOAH in foods was of

DOI:https//doi.org/10.22452/mjs.vol44no4.10
Malaysian Journal of Science 44(2): 102-119 (June 2025)

keen interest. Thus, an advanced technique, Liquid chromatography (LC) - Gas chromatography (GC), was reborn and is very applicable in MO detection and quantification, particularly in separating MOSH and MOAH individually. High-Performance Liquid Chromatography (HPLC) with capillary Gas Chromatography (GC) technique was introduced by Grob et al. in 1984 for the fractionation of trace components in the mixture. Later, this method was coupled with a flame ionisation detector (FID) for MOSH/MOAH determination in food samples in 2009. Since then, analysis of MOSH/MOAH has been intensively studied (M. Biedermann et al., 2011; M. Biedermann et al., 2009; M. Biedermann & Grob, 2015; Hochegger et al., 2021).

Moreover, method with a chromatographic separation column LC coupled with GC-FID was developed by Gómez-Coca et al.,(2016). Currently, this LC-GC-FID method is the most common technique due to its high sensitivity towards analytes and less solvent usage, which indirectly improvises the quantification (Moret et al. 2016; Purcaro et al. 2013; Wagner & Oellig 2019). In other words, it is considered as the gold standard for MO analysis in the refinery (Weber et al. 2018). Also, it provides high resolution featuring fully automated that enables analysis of a complex sample with less error in terms of contamination and interference (Biedermann, Fiselier & Grob 2009). Due to these features, technical guidance of the European Commission, Joint Research Centre (JRC) used online LC-GC-FID as analytical method for determining MOSH/MOAH in food products and result verification by GC-GC-MS for current EU-wide monitoring (Foodwatch 2021). This LC-GC-FID method uses internal standards or markers to identify MOSH/MOAH fractions, mostly, to control the performance of the entire system.

LC-GC-FID: Principle

First, LC ensures the determination of MOSH/MOAH fraction by distinguishing into paraffin, naphthene and aromatic according to retention or elution time, which correlated to molecular mass that is quantifiable by GC-FID under the same chromatographic conditions as shown in Figure 4 (Buijtenhuijs & Van de Ven 2019). A significant step where LC executes the isolation of analytes (in this case, MOSH and MOAH) from potential interference like lipids, plant HCs (C23-C35) and wax esters in food samples (EFSA 2012). This step is usually done in the normal phase with bare silica and is always up for improvement (García-Cicourel et al. 2019).

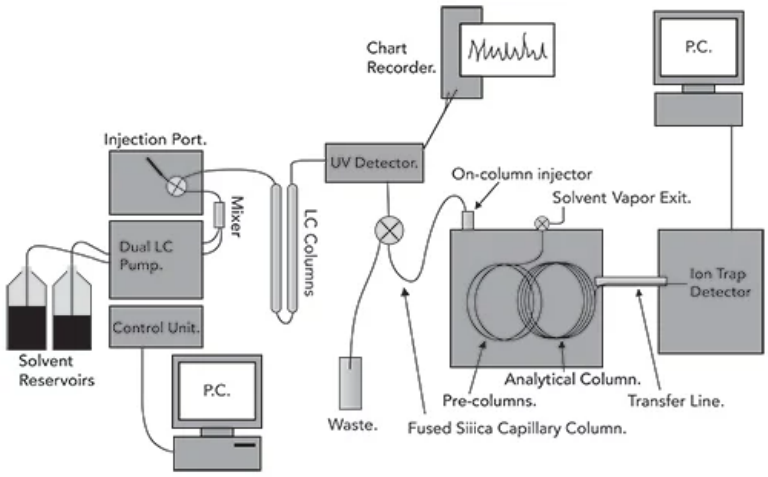

Figure 4. Schematic diagram of LC-GC-FID (Apedo & Snow 2019)

Then, the eluent is transferred to the GC column as described by Biedermann et al., (2009), using the retention gap technique with simultaneous eluent evaporation through the interface on the column. The interface must be carefully designed to handle the transition between these two phases. Techniques such as partially concurrent eluent evaporation (PCEE) are used to optimize this transfer, ensuring that volatile compounds are not lost during the process. The interface also minimizes issues like memory effects, which can occur when residues from previous samples affect the analysis of subsequent samples. This technique was well differentiated by Sdrigotti and team (2021) with fully concurrent eluent evaporation and solvent flooding.

Following to GC stage, the eluent is evaporated as per individual boiling point, and the gas molecules are injected into the stationary phase to determine a unique molecular mass. A nonpolar stationary phase with a short capillary column is commonly used, while the mobile phase uses inert gas like helium or nitrogen (EFSA 2012).

When the vaporised sample reaches FID, it is ionised in the flame by the reaction of hydrogen and oxygen, causing the ions to generate a current that is measured by the electrodes in the detector. This measurement will be displayed as a peak or signal at a certain time of elution in response to unit mass for HC. Therefore, this signal is directly proportional to the amount of targeted compound over a wide array of compounds (Weber et al. 2018). In addition, with this detection method, LOD for MOSH and MOAH is about 0.05mg/kg. But this is not the actual case for the oil sample, where paper by EFSA, (2012) & Fiorini et al., (2010) points out the LOD was recorded as 5 mg/kg with a modified GC-FID technique.

DOI:https//doi.org/10.22452/mjs.vol44no4.10
Malaysian Journal of Science 44(2): 102-119 (June 2025)

Although a FID can readily measure all HCs, it is not selective and has uncertain sensitivity regarding the formation of broad unresolved peaks of MO compounds (EFSA 2012). Alternatively, with the help of chemical markers and internal standards, this detection method can differentiate compounds in the chromatographic profile. This is done by identifying peaks, eliminating potential interference, and measuring quantification based on the total area (Ahmad et al. 2019; Biedermann, Uematsu & Grob 2011; Srbinovska et al. 2020). By having proper sample preparation (highly selective separation and elimination process) in the early stage, only then, target compounds (MOSH/MOAH) detected by this FID (Zoccali et al. 2016).

LC-GC-FID: Sample Preparation

Sample preparation is a critical step before the analytical run because it requires saponification (separation of triglycerides), epoxidation (separation of MOSH) and extraction (removal of olefins and endogenous n-alkanes) to achieve adequate sensitivity of determination (Hochegger et al. 2021; Srbinovska et al. 2020). Saponification was the pioneering step to separate from triglyceride, particularly in high-fat content samples (Hochegger et al. 2021, 2022). According to EFSA (2012), the saponification step is labour-, time-, and solvent-consuming and should therefore be performed meticulously to avoid additional errors in the analysis.

In the case of EVO as a sample matrix, epoxidation helps to separate MOSH from unsaponifiable matter to obtain more polar derivatives of unsaturated compounds that can be retained strongly in the LC (Gómez-Coca et al. 2016; Zoccali et al. 2016). However, conventional epoxidation is unable to detect MOAH as most of them are unaffected, thus need harsh or improved epoxidation to eliminate olefins. As per detailed explanation written in Nestola (2022), where the MOAH fraction can potentially co-elute with biogenic olefins, the researcher focused on the removal of biogenic interferences in palm oil samples through enhanced saponification and epoxidation in an automated online LC-GC-FID method, thus achieved a group of individual MOAH peaks (Albendea et al. 2024).

As per Sdrigotti et al. (2021), loss of 20-35% of MOAH may occur during these purification steps, as well as the removal of the interferences may remain incomplete. In terms of EVO, there are olefins, HCs (plant-based), and other trace compounds as interferences, that shall be removed through epoxidation in the occasion of off-line column chromatography used, the sample extraction stage proceeded (Ruiz et al. 2021). If not properly accounted for, co-migration of other HCs; POSH, native n-alkanes, terpenes and essential oils or sterol esters can cause an overestimation of MOSH/MOAH (Wagner & Oellig 2019). Particularly, natural polyolefins and unsaturated poly-a-olefins are misinterpreted for MOAH humps (Pirow et al. 2019).

In certain cases, hexane extraction is sufficient, like food products. However, complicated samples, such as those involving high-fat and cosmetic products, require an effective sample clean-up process (Weber et al. 2018). Lipid matrices require sophisticated decontamination techniques such as saponification and column chromatography using a silica or cartridge (Purcaro et al. 2013). Thus, choosing the optimal column for the best separation is considered significant.

LC-GC-FID: Separation Column

Since MOSH/MOAH is categorised into nonpolar compounds and is lipophilic, it is highly possible to dissolve well in nonpolar solvents and migrate to the lipids (Wrona, Pezo & Nerin 2013). Therefore, separating targeted chemical compounds from unwanted, may encounter some challenges. Few pre-treatments were carried out to avoid clumps of peaks and improve analyte identification sensitivity. Among that, solid phase extraction (SPE) has been widely used.

Regarding SPE, supercritical fluid chromatography has been utilised as a rapid and easy method to analyse MOSH/MOAH fractions in crude and refined oil, whereby detection is done by FID and UV detectors parallelly. However, this method of analysis is achievable if the oil viscosity ranges below 56 mm^2/s and the molecular weight is less than 450 g/mol. Additionally, extra precautions are taken to reduce matrix interferences to get more precise data (García-Cicourel et al. 2020). Likely, Gómez-Coca et al. (2016) used n-hexane as the mobile phase in a silica column loaded with silver (Ag) to separate HC fractions and interferences brought on by the high-affinity Ag+ ion for double bonds. As a result of limited solubility, bigger aliphatic structured compounds can retain more (García-Cicourel et al. 2020). For nonpolar fractions of EVO that were separated by silica gel-SPE step with n-hexane and detected by GC-MS similarly in Weber et al. (2018).

Additionally, activated silica gel impregnated with 1% silver nitrate ($AgNO_3$) acts as a sorbent in the column pack for offline chromatography. It separates MO from olefin and triglycerides (interference) by retaining them in the column (Ruiz et al. 2021). The elution sequence goes like low molecular weight paraffin to naphthene (MOSH fractions). It is followed by highly alkylated benzene and alkylated polyaromatic through a normal phase column (Weber et al. 2019).

Sulphuric acid-impregnated silica gel (SAISG) column was demonstrated by Wrona et al. (2013) for the extraction of edible oil at where it was capable of providing good quantification, unmistakable MO identification as well as allowing the removal of fatty acids and lipids without the creation of an emulsion. Additionally, Moret et al. (2016) suggested a more effective extraction technique called microwave-aided saponification (MAS), followed by online LC-GC with FID for the MO determination in various food products, particularly those with high fat content. A similar method of MAS was used by Srbinovska et al., (2020) to determine HC, including MOSH/MOAH in packed fish and fish products.

DOI:https//doi.org/10.22452/mjs.vol44no4.10
Malaysian Journal of Science 44(2): 102-119 (June 2025)

LC-GC-FID: Assessment

Basically, there are two: online LC-GC-FID and offline SPE-GC-FID techniques that have been widely used in MOSH/MOAH determination in EVO as a food matrix. Regarding online LC-GC-FID, saponification and extraction are first performed with n-hexane and water. In the former step, a few millilitres of oil samples are provisionally obtained and then fed to the epoxidation process before being injected into the LC-GC-FID system. At this time, the LC separation is performed according to the elution of MOSH at 2-4 minutes and MOAH at 4.1-6.1 minutes, then the sample is transferred to the GC by the retention gap technique or partial simultaneous solvent evaporation (PCSE) through the connector as described in Nestola (2022). At a specific degree of alkylation, various structural isomers of MOAH can have similar volatility characteristics, leading to their elution within a narrow range of carbon atoms (up to 4 atoms) (Biedermann et al. 2022).

Moreover, parameters such as the inlet pressure of the carrier gas, the oven temperature, and the flow rate of the fraction were programmed before the run. Once the fraction exited the GC, data processing continued using FID to quantify each compound recorded in the peak/signal as shown in Figure 5. Cross-checking with GC-MS is recommended for molecular identification, as mentioned in the article by Nestola (2022).

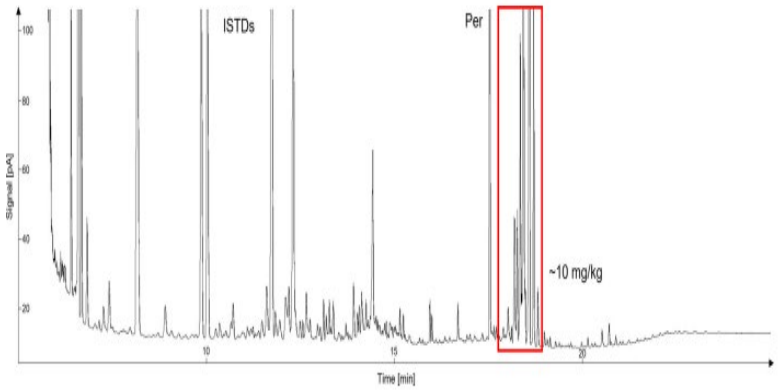

Figure 5. Chromatographic plot on MOAH by LC-GC-FID for EVO after epoxidation (Nestola 2022)

That being said, in the study published by Foodwatch (2021) also mentioned on GC*GC-TOF technology is efficient for results verification and marker assessment. Recently, GC×GC–TOF/MS has become a popular choice of analytical instrument because of its superior ability to separate complex mixtures of volatile compounds by distinguishing even subtle volatiles, offering better peak shape, enhanced purity, and greater accuracy in both qualitative and quantitative analyses. The chromatographic peaks are displayed on a 2D plane, giving each volatile two retention indices with a fixed position. Also, due to its super-fast spectral generation rate (up to 500 spectra per second), GC×GC–TOF/MS can analyze thousands of components in a very short period (Fang et al. 2023).

Back to offline SPE-GC-FID, this method is defined by the manual preparation of the chromatographic column, as the sorbent and activated silica gel column were compacted and followed by dropwise addition of $AgNO_3$ solution, then proceeded to vortex process to make it bubble-free and again to compact the sorbent together with mobile phase, n-hexane. This is the most important step for separating MOSH and MOAH after the epoxidation process, as described in Ruiz et al. (2021). The next step is the extraction, which was improvised to isolate interferences with solvents. In the work of J. C. Carrillo et al. (2019), DMSO was used as a solvent because it efficiently removes PAH and sulphur- and nitrogen-containing heterocycles.

This type of extraction was then developed as a combination with aliphatic solvents such as pentane and water to separate polycyclic compounds from aliphatic HCs and other organics. However, in some cases, a mixture of solvents such as toluene, n-hexane, and dichloromethane was used in a specific ratio to keep the sample from a complete evaporation (Ruiz et al. 2021). The extracted sample is then injected into the GC-FID, which has already been programmed for temperature and gas flow rate. The outcome of this detection of individual targeted compounds can be seen in signal or peak as a display. Especially on the aromatic compounds with high molecular weight, a specified hump is usually seen yet can be interpreted by the help of markers and internal standards (García-Cicourel et al. 2020; Gómez-Coca et al. 2016).

Method Performance

At the end of the plot, the performance of the analysis will be measured in terms of LOD, LOQ, linearity (R^2), and recovery. The detection limit depends on MO distribution in the sample amount that injected into the system but mostly, relies on the context of the oil or fat composition. To improve the detection, a higher capacity system and food origin markers (n-alkanes) are used (EFSA 2012). A complete guidance on sampling, analysis and data reporting was written in the frame of Commission Recommendation (EU) 2017/84 for MO determination (Hoekstra, Bratinova &

DOI:https//doi.org/10.22452/mjs.vol44no4.10
Malaysian Journal of Science 44(2): 102-119 (June 2025)

(Editors) 2019). The chosen method must meet certain performance parameters, including a response factor of 0.8-1.2 for C50 over C20, a target and maximum accepted limit of quantification (LOQ) based on food fat content (ranging from 0.1 to 10 mg/kg), recovery (70-120%), and intermediate-precision (10-20%) (Bauwens, Pantó & Purcaro 2021). As well as with other EVO matrices, Table 4 has a brief summary on analytical method chosen to determine MOSH/MOAH.

In LC-GC-FID, the distribution of molecular weight was associated with the breadth of a hump, which occurred at a certain reaction time owing to molecule elution (Srbinovska et al. 2020). Retention and selectivity in a packed column are strongly dependent on the mobile phase's solubility and the interaction and displacement of analytes from the stationary phase by the mobile phase (García-Cicourel et al. 2020). Continuity to GC and detector create chromatographic profile identification, counter-verified with certified reference material.

Thus, selection of internal verification standard is crucial. For MOSH, cyclohexyl cyclohexane (Cycy) is used as a suitable internal standard for mineral oil analysis due to its absence in significant quantities in mineral oils and packaging. Also, to control standard loss, n-C11 can be added in the same amount as Cycy, as it is more prone to volatilization. If the n-C11 area is smaller than Cycy, it may indicate Cycy loss or co-elution. n-C13, at half the amount of Cycy, is also added to verify chromatographic separation. Meanwhile, For MOAH analysis, 1- and 2-methylnaphthalene serve as internal standards due to their close elution, with equal peak areas confirming the absence of co-elution issues. n-Pentyl benzene is used to monitor volatile losses. While 1,3,5-tri-tert-butyl benzene (TBB) was traditionally a marker for the start of the MOAH fraction, di(2-ethylhexyl) benzene (DEHB) has proven to be more suitable, as it elutes with the first MOAH. Both DEHB and perylene can verify the boundaries of the MOAH fraction (Hoekstra, Bratinova & (Editors) 2019).

Gómez-Coca et al., (2016) established repeatability at the 50 mg/kg level by assessing oil sample containing 51 mg/kg with standard deviation (SD) of 1.9 and a variation coefficient of 4.0%. The LOD was calculated using "blank" refined sunflower oil supplemented with 10 mg/kg MO. While calculating the lowest analyte concentration, 0.5 mg/kg was used as LOD for both MOSH/MOAH as per the JRC limit guideline (Ruiz et al. 2021). Same was revealed by experimenting 152 sample originating from few countries and 12% of the samples tested positive for MOAH, with values ranging from 0.63 mg/kg to 82 mg/kg. Meanwhile, MOSH levels were identified above the LOQ in 92% of the goods, ranging from 0.5 mg/kg to 1152 mg/kg. As per investigation by Albendea et al. (2024), the LC-GC-FID system offers a sensitive method for detecting MO, with LOQ ranging from 0.05 mg/kg for the loin to around 0.2 mg/kg for the back fat and lipid sources.

Spiking technique was used in method validation to determine characteristics such as recovery, accuracy (intra and inter-day), and low relative SD with the highest R2. Furthermore, the validation may be cross-checked using a separate platform that has high relevance; in this instance, the analysis is completed parallelly with the MS detector, allowing quantitative and qualitative assessment of MOSH/MOAH. Further experiment by Purcaro (n.d.) says on reproducibility of <16% as to compare with JRC Guidance, that is 20%, but were chosen as reference and trueness between +10% and -20%. The high uncertainty and low trueness reported for markers may indicate that these single peaks were incorrectly assigned due to additional interferences.

In short, online linked LC-GC combination provides great repeatability, sample throughput, resilience, and sensitivity while minimising sample waste. As a result, it is regarded as the golden option for an analytical procedure that allows for the effective separation and detection of specific molecules. But it has its limitations too, and this is due to not all compounds are amenable to LC-GC analysis. Certain analytes may not volatilize well for the GC step, or they may degrade at high temperatures, making it challenging to analyze thermally unstable or highly polar compounds.

Moreover, FID is a non-selective detector, meaning it can detect compounds based on carbon content, but it does not provide structural information about the compounds (counting aromatic rings or degree of alkylation), unlike detectors such as mass spectrometry (MS) (EFSA, 2019; Matheson, 2023). Molecules which has a similar molecular structure to POH, polyalphaolefin (POA), and lipids are frequently overlooked due to structure similarity (Buijtenhuijs & Van de Ven 2019). This is because uncertainty of interpretation and integration of LC-GC-FID was estimated to be around 20% owing to baseline drift, huge hump, and removal of riding peaks on the top of humps. Additionally, high boiling point substances may coelute with column bleed, creating inaccuracy in quantification (Bauwens, Pantó & Purcaro 2021). To minimize overestimation or underestimation of MOSH/MOAH identification and quantification, the data should be interpreted by a qualified and skilled individual.

Other Methods

The online approach LC-GC is still in demand and works very well quantitatively by FID and structural characterisation by UV detection or mass spectrometry (MS) (García-Cicourel et al. 2020). However, this method requires time, expertise and difficult data interpretation (Wagner & Oellig 2019). According to Ali & Neha (2024), integrating HPLC and LC/MS in conjunction is an effective method for comprehensively analyzing edible oils. Due to its superior ability to separate and quantify specific constituents, HPLC offers information on the nutritional value and qualitative characteristics of oil. While LC/MS ensures the safety of the oil and compliance with regulatory standards, it also extends the examination to trace-level contaminants.

Apart from this, characterisation and quantification of MOSH/MOAH, from complex to single hump, can be performed using two-dimensional gas chromatography (GC-GC)-FID due to its high separation capability. However, GC-GC-MS is prefreable for compound verification because it

DOI:https//doi.org/10.22452/mjs.vol44no4.10
Malaysian Journal of Science 44(2): 102-119 (June 2025)

allows both structural characterisation and determination of the degree of substitution of the aromatic compound (Bratinova et al. 2020; Pirow et al. 2019). In a few cases, GC-GC-FID/MS is used, where GC-GC (polar x apolar medium) allows separation according to volatility and polarity, while FID is used for quantification and MS for structural identification (Hochegger et al. 2021; Purcaro et al. 2013).

Lately in November 2022, Biedermann et al. (2022) has proven that GC×GC which uses two columns with distinct stationary phases and thermal modulation with FID, able to provide higher compound separation and resolution, which improves analysis of complex combinations, MO in main food products. This method was verified with conventional LC-GC-FID, and demonstrates greater sensitivity and the capacity to measure values as low as 0.02 mg/kg in spiked samples with internal standard, indicating the potential to detect lower MOAH concentrations. Also, LC-GC-FID/MS has been recommended as a marker for determination based on reliable detection of the compound and its origin (Hochegger et al. 2021). However, this strategy is currently being debated for maximal selectivity and accuracy. Purcaro et al. (2013) employed large volume (LVI) GC FID following the same Ag-SPE fractionation phase to get quantitative results as the LC-GC procedure.

Furthermore, Hochegger et al. (2021) introduced LC-GC x GC-ToF/MS/FID in 2020, where multi-measurement is done in a single analysis, and the greatest part is the distinguishing of MOAH in percentage without any advanced LC separation. Later in the year 2021, the researchers created specific 2D software that allows for the integration of data from the platform's numerous components, providing that MOSH and MOAH measurement is reliable and precise (Bauwens, Pantó & Purcaro 2021). This approach was also used in Fang et al. (2023) to identify and characterize the volatile organic compounds (VOCs) in samples in order to distinguish consumable products from their original source. The expensive cost of ToF/MS restricts its laboratory applicability, despite the fact that it may effectively capture spectra for precise peak identification and quantification in GC×GC (Cardoso et al. 2023).

Planar solid phase extraction (pSPE) was developed as for paper and cardboard matrices screening method. It was connected with densitometry in UV and fluorescence detector (UV-FLD) for rapid analysis. Despite its high cost, this technique can extract 20 samples in parallel and perform a rapid clean-up and a chemical screening (Wagner & Oellig 2019). Pesticides were separated from tea (consumable matrix) using thin layer chromatography (TLC) with MS (Oellig & Schwack, 2011), and the method was improved by Oellig & Schwack (2014), where high throughput planar SPE (HTpSPE) was used in microliter-flow injection analysis coupled with TOFMS approach for pesticide determination in food.

Out of scope, the Nuclear Magnetic Resonance (NMR) analytical approach was chosen to detect the presence of MOSH/MOAH and even perform quick screening, potentially replacing the MO mist test according to IP346 (Buijtenhuijs & Van de Ven 2019). Few researchers used the NMR approach to measure MO in cosmetic products without significant sample preparation unless additional or defined determination of material, such as zero interferences, was required (Lachenmeier et al., 2017; Weber et al., 2019). This is due to the instrument's ease of use and the lack of a high level of skill or expense. However, EVO has not been used as a sample matrix by NMR. In terms of innovative methodologies, Bunaciu et al. (2022) employed IR spectroscopy (absorbance research) to test paraffinic compound adulteration in edible oil, namely olive and maise oil, using commercial software that is both precise and time efficient.

DOI:https//doi.org/10.22452/mjs.vol44no4.10
Malaysian Journal of Science 44(2): 102-119 (June 2025)

Table 4. Brief on analytical method on MOSH/MOAH determination

Matrix	Analyte	Pre-treatment/SPE	Clean-up Solvent	Analytical Method	LOD/LOQ mg/kg	Reference
Olive Oil	MO	SAISG	hexane	GC-FID	0.07 / 0.21	(Wrona, Pezo & Nerin 2013)
Edible Oil	MOSH/MOAH	Silver nitrated silica gel stationary phase/ epoxidation	-	GC-FID	-	(Ruiz et al. 2021)
Vegetable Oil	MOSH	Deactivated Silver silica gel	-	GC-FID	5 / 15	(Gómez-Coca et al. 2016)
Vegetable oil	MOSH	Offline SPE (1% Ag-activated silica gel)	n-hexane	LVI-GC-FID	-	(Liu et al. 2017)
Sunflower oil	MOAH	-	hexane	HPLC-GC-GC-FID/MS	-	(Biedermann & Grob 2009)
Olive /corn oil	MOSH	-	-	Infrared	-	(Bunaciu, Fleschin & Aboul-enein 2022)
Edible oil / fats	MOSH/MOAH	Automated workflow- saponification and epoxidation	n-hexane	LC-GC-FID	- / 1	(Nestola 2022)
Fats	MO	microwave-assisted saponification (MAS) and epoxidation	n-hexane	online LC-GC-FID	/0.2	(Albendea et al. 2024)
Food Products	MOSH/MOAH	Silver silica solid-phase extraction (SPE) cartridge	n-hexane	LC-GC-FID/MS	/ 1.2	(Purcaro et al. 2013)
Rice, Pasta, Cornflakes	MOSH /MOAH	-	-		0.2 /	(Buijtenhuijs & Van de Ven 2019)
Paper and Cardboard	MOSH /MOAH	Planar SPE	n-hexane	UV/FLD	-	(Wagner & Oellig 2019)

*__Blue__ – non-oil matrix but closely related with analysis part

DOI:https//doi.org/10.22452/mjs.vol44no4.10
Malaysian Journal of Science 44(4): 102-119 (December2025)

4. Conclusion

To put it simply, EVO is prone to MO contamination, which is further classified into MOSH and MOAH, either purposely, because of thermal stability, which improves oil shelf life, or accidentally due to migration from packing or processing via gas phase, depending on the volatility of the compounds. As it has a significant impact on human health, there is an advisory limit of 13mg MOSH/kg and 0.5mg MOAH/kg in the vegetable oil category in 2022; thus, several analytical methods have been carried out; however, the LC-GC-FID technique has been highly adapted in favour of high sensitivity, reproducibility, and the ability to quantify compounds in the absence of a pure sample. To acquire quantification of MOSH and MOAH in edible oil, a specific variant of this approach needs precise sample preparation and separation column type. There is still room for improvement in determining MOSH/MOAH in consumable products, especially in base food.

5. Acknowledgements

This research is financially supported by Malaysian Ministry of Higher Education (MOHE) with the Fundamental Research Grant Scheme, (FRGS/1/2018/ STG01/UKM/02/16). The authors express gratitude to the Faculty of Science and Technology (FST) of Universiti Kebangsaan Malaysia (UKM), specifically, the Department of Chemical Sciences (JSK) and Polymer Research Centre (PORCE) for technical support and provided facilities.

6. References

Ahmad, H., Noor, A.M., Sabri, M.P.A., Ngteni, R. & Syed Hilmi, S.M.H. 2019. Mineral oil saturated hydrocarbon in crude palm oil-current status in Sime Darby palm oil mills. *Journal of Advanced Agricultural Technologies* 6(4): 299–303.

Albendea, P., Conchione, C., Menegoz Ursol, L. & Moret, S. 2024. A Study on Mineral Oil Hydrocarbons (MOH) Contamination in Pig Diets and Its Transfer to Back Fat and Loin Tissues. *Animals* 14(10): 1–16.

Ali, F. & Neha, K. 2024. HPLC and LC - MS in Analysis of Edible Oils and Fats. In Ahamad, J. & Nollet, L. M. L. (ed.). *Bioactive Compounds of Edible Oils and Fats*, pages 234–242. First Edit. Taylor & Francis Group.:

Andriukaitis, V. 2017. Commission Recommendation (EU) 2017/84: The monitoring of mineral oil hydrocarbons in food and in materials and articles intended to come into contact with food. *Official Journal of the European Union*, page.

Apedo, A. & Snow, N.H. 2019. Online LC–GC: The Ultimate "GC Connection." https://www.chromatographyonline.com/view/online-lc-gc-ultimate-gc-connection-0 [15 October 2023].

Bauwens, G., Pantó, S. & Purcaro, G. 2021. Mineral oil saturated and aromatic hydrocarbons quantification: Mono- and two-dimensional approaches. *Journal of Chromatography A* 1643(462044): 1–9.

Biedermann, M., Eicher, A., Altherr, T. & McCombie, G. 2022. Quantification of mineral oil aromatic hydrocarbons by number of aromatic rings via comprehensive two-dimensional gas chromatography: First results in food. *Journal of Chromatography Open 2* 100072: 1–14.

Biedermann, M., Fiselier, K. & Grob, K. 2009. Aromatic hydrocarbons of mineral oil origin in foods : method for determining the total concentration and first results. *Journal of Agricultural and Food Chemistry* 57: 8711–8721.

Biedermann, M. & Grob, K. 2009. Comprehensive two-dimensional GC after HPLC preseparation for the characterization of aromatic hydrocarbons of mineral oil origin in contaminated sunflower oil. *Journal of Separation Science* 32: 3726–3737.

Biedermann, M. & Grob, K. 2015. Comprehensive two-dimensional gas chromatography for characterizing mineral oils in foods and distinguishing them from synthetic hydrocarbons. *Journal of Chromatography A* 1375: 146–153.

Biedermann, M., Uematsu, Y. & Grob, K. 2011. Mineral oil contents in paper and board recycled to paperboard for food packaging. *Packaging Technology and Science* 24: 61–73.

Biopharma. (n.d.). The Ames test or bacterial reverse mutation test. https://www.eurofins.com.au/biopharma-services/genetic-toxicology/the-ames-test [16 July 2023].

Boogaard, P., Hedelin, A., Riley, A., Rushton, E. & Vaissiere, M. 2012. Use of the modified Ames test as an indicator of the carcinogenicity of residual aromatic extracts. Brussels.

Bratinova, S., Hoekstra, E., Emons, H., Hutzler, C., Kappenstein, O., Biedermann, M. & McCombie, G. 2020. The reliability of MOSH/MOAH data: a comment on a recently published article. *Journal of Consumer Protection and Food Safety* 15(3): 285–287.

Buijtenhuijs, D. & Van de Ven, B.M. 2019. Mineral Oils in food ; a review of occurrence and sources. Bilthoven.

Bunaciu, A.A., Fleschin, S. & Aboul-enein, H.Y. 2022. Determination of some edible oils adulteration with paraffin oil using infrared spectroscopy. *Pharmacia* 69(3): 827–832.

Cardoso, C.A.L., Caramão, E.B., de Castro, T.L.A. & Simionatto, E. 2023. Variation in the chemical composition of essential oils from Mangifera indica L. leaves by comprehensive two-dimensional gas chromatography. *Ecletica Quimica* 48(4): 27–36.

DOI:https//doi.org/10.22452/mjs.vol44no4.10
Malaysian Journal of Science 44(4): 102-119 (December 2025)

Carrillo, J.-C., Shen, H., Momin, F., Kral, O., Schnieder, H. & Kuhn, S. 2022. GTL synthetic paraffin oil shows low liver and tissue retention compared to mineral oil. *Food and Chemical Toxicology* 159: 112701.

Carrillo, J.C., van der Wiel, A., Danneels, D., Kral, O. & Boogaard, P.J. 2019. The selective determination of potentially carcinogenic polycyclic aromatic compounds in lubricant base oils by the DMSO extraction method IP346 and its correlation to mouse skin painting carcinogenicity assays. *Regulatory Toxicology and Pharmacology* 106: 316–333.

EFSA. 2012. Scientific opinion on mineral oil hydrocarbons in food. *EFSA Journal*, page.

EFSA, Arcella, D., Baert, K. & Binaglia, M. 2019. Rapid risk assessment on the possible risk for public health due to the contamination of infant formula and follow-on formula by mineral oil aromatic hydrocarbons (MOAH). *EFSA Supporting Publications*, page.

EFSA Panel, Schrenk, D., Bignami, M., Bodin, L., del Mazo, J., Grasl-Kraupp, B., Hogstrand, C., Hoogenboom, L., Leblanc, J.C., Nebbia, C.S., Nielsen, E., Ntzani, E., Petersen, A., Sand, S., Schwerdtle, T., Vleminckx, C., Wallace, H., Alexander, J., Goldbeck, C., Grob, K., Gómez Ruiz, J.Á., Mosbach-Schulz, O., Binaglia, M. & Chipman, J.K. 2023. Update of the risk assessment of mineral oil hydrocarbons in food. *EFSA Journal* 21(9): 1–143.

European Commission. 2022. Standing committee on plants, animals, food and feed section novel food and toxicological safety of the food chain.

Fang, X., Chen, Y., Gao, J., Run, Z., Chen, H., Shi, R., Li, Y., Zhang, H. & Liu, Y. 2023. Application of GC–TOF/MS and GC×GC–TOF/MS to Discriminate Coffee Products in Three States (Bean, Powder, and Brew). *Foods* 12(3123): 1–12.

Fengler, R. & Gruber, L. 2022. Migration of mineral oil hydrocarbons from contaminated paperboard into the food simulants Tenax and Sorb-Star—A comparison. *Packaging Technology and Science*: 603–620.

Finch, A., Eilers, G. & Harzke, F. 2006. Masking from mineral oil smell and scenting from mineral oils. Bremen (DE).

Fiorini, D., Paciaroni, A., Gigli, F. & Ballini, R. 2010. A versatile splitless injection GC-FID method for the determination of mineral oil paraffins in vegetable oils and dried fruit. *Food Control* 21: 1155–1160.

Fiselier, K. & Grob, K. 2009. Determination of mineral oil paraffins in foods by on-line HPLC – GC – FID : lowered detection limit ; contamination of sunflower seeds and oils. *European Food Research and Technology* 229: 679–688.

Flinn, R.A., Kehl, W.L., Schmid, B.K. & Stewart, M.M. 1965. Hydrogenation of mineral oils in the presence of amenor amount of a hydrogenating catalyst and a major amount of specific type of activated alumina.

Foodwatch. 2021. International tests of various food products for their contamination by mineral oil hydrocarbons (MOSH/MOAH).

Gamble, K.R. & Smith, D.W. 2009. Discrimination of ‘“ Odorless ”’ Mineral Oils Alone and as Diluents by Behaviorally Trained Mice. *Chemical Senses* 34: 559–563.

García-Cicourel, A.R., van de Velde, B., Roskam, G. & Janssen, H.-G. 2020. Supercritical fluid chromatography as a rapid single-step method for the determination of mineral oil saturated and aromatic hydrocarbons in purified mineral oils for food and cosmetics applications. *Journal of Chromatography A* 1614: 460713.

García-Cicourel, A.R., van de Velde, B., Verduin, J. & Janssen, H.G. 2019. Comprehensive off-line silver phase liquid chromatography x gas chromatography with flame ionization and vacuum ultraviolet detection for the detailed characterization of mineral oil aromatic hydrocarbons. *Journal of Chromatography A* 1607: 460391.

Gharbi, I., Moret, S., Chaari, O., Issaoui, M., Conte, L.S., Lucci, P. & Hammami, M. 2016. Evaluation of hydrocarbon contaminants in olives and virgin olive oils from Tunisia. *Food Control*, page. Elsevier Ltd.:

Gómez-Coca, R.B., Cert, R., Pérez-Camino, M.C. & Moreda, W. 2016. Determination of saturated aliphatic hydrocarbons in vegetable oils. *Grasas Y Aceites* 67(2): e127.

Hochegger, A., Moret, S., Geurts, L., Gude, T., Leitner, E., Mertens, B., O’Hagan, S., Poças, F., Simat, T.J. & Purcaro, G. 2021. Mineral oil risk assessment: knowledge gaps and roadmap. Outcome of a multi-stakeholders workshop. *Trends in Food Science and Technology* 113: 151–166.

Hochegger, A., Wagenhofer, R., Savic, S., Mayrhofer, E., Washuttl, M. & Leitner, E. 2022. Combination of multidimensional instrumental analysis and the Ames test for the toxicological evaluation of mineral oil aromatic hydrocarbons. *Journal of Agricultural and Food Chemistry* 70: 16401–16409.

Hoekstra, E., Bratinova, S. & (Editors). 2019. Guidance on sampling , analysis and data reporting for the monitoring of mineral oil hydrocarbons in food and food contact materials. Luxembourg.

DOI:https//doi.org/10.22452/mjs.vol44no4.10
Malaysian Journal of Science 44(4): 102-119 (December 2025)

IARC. 2012. Mineral oils, untreated or mildly treated: Evaluation of carcinogenic risks to humans, No. 100F. *IARC Monographs*: 179–196.

Institute for Publication. (n.d.). Mineral oil hydrocarbons MOSH / MOAH. Berlin.

Isola, A., Carrillo, J., Lemaire, P., Niemela, H. & Steneholm, A. 2023. Lack of human-relevant adversity of MOSH retained in tissues : Analysis of adversity and implications for regulatory assessment. *Regulatory Toxicology and Pharmacology* 137: 105284.

Jaén, J., Domeño, C., Alfaro, P. & Nerín, C. 2021. Atmospheric Solids Analysis Probe (ASAP) and Atmospheric Pressure Gas Chromatography (APGC) coupled to Quadrupole Time of Flight Mass Spectrometry (QTOF-MS) as alternative techniques to trace aromatic markers of mineral oils in food packaging. *Talanta* 227: 1–9.

Jaén, J., Domeño, C. & Nerín, C. 2022a. Development of an analytical method for the determination of mineral oil aromatic hydrocarbons (MOAH) from printing inks in food packaging. *Food Chemistry* 397: 1–9.

Jaén, J., Domeño, C. & Nerín, C. 2022b. Development of an analytical method for the determination of mineral oil aromatic hydrocarbons (MOAH) from printing inks in food packaging. *Food Chemistry* 397.

Jin, H. 2015. Dielectric strength and thermal conductivity of mineral oil based nanofluids. Delft Ubinersity of Technology, Netherlands,.

Jin, H., Andritsch, T., Tsekmes, I.A., Kochetov, R., Morshuis, P.H.F. & Smit, J.J. 2014. Properties of mineral oil based silica nanofluids. *IEEE Transactions on Dielectrics and Electrical Insulation* 21(3): 1100–1108.

Klaus, E.E., Tewksbury, E.J. & Fenske, M.R. 1962. Preparation , properties , and some applications of super-refined mineral oils. *ASLE Transactions* 5(1): 115–125.

Kojic, B.D., Dugic, P., Tatjana, B. & Dugic, G. 2019. Influence of the primary and secondary oxidation inhibors on the oxidation stability of the mineral base oils. *16th International Conference on Tribology Serbiatrib '19*, page 573–581.

Lachenmeier, D.W., Mildau, G., Krause, A., Marx, G., Walch, S.G., Hartwig, A. & Kuballa, T. 2017a. Evaluation of mineral oil saturated hydrocarbons (MOSH) and mineral oil aromatic hydrocarbons (MOAH) in pure mineral hydrocarbon-based cosmetics and cosmetic raw materials using 1H NMR spectroscopy [version 1; referees: 2 approved, 1 approved with reserva. *F1000Research* 6: 682.

Lachenmeier, D.W., Mildau, G., Krause, A., Marx, G., Walch, S.G., Hartwig, A. & Kuballa, T. 2017b. Evaluation of mineral oil saturated hydrocarbons (MOSH) and mineral oil aromatic hydrocarbons (MOAH) in pure mineral hydrocarbon-based cosmetics and cosmetic raw materials using 1H NMR spectroscopy. *F1000Research* 6.

Liao, R., Hao, J., Chen, G., Ma, Z. & Yang, L. 2011. A comparative study of physicochemical, dielectric and thermal properties of pressboard insulation impregnated with natural ester and mneral oil. *IEEE Transactions on Dielectrics and Electrical Insulation* 18(5): 1626–1637.

Liu, L., Huang, H., Wu, Y., Li, B. & Ouyang, J. 2017. Offline solid-phase extraction large-volume injection-Gas chromatography for the analysis of mineral oil-saturated Hydrocarbons in commercial vegetable oils. *Journal of Oleo Science*: 1–10.

Lommatzsch, M., Biedermann, M., Grob, K. & Simat, T.J. 2016. Analysis of saturated and aromatic hydrocarbons migrating from a polyolefin-based hot-melt adhesive into food. *Food Additives and Contaminants - Part A*: 473–488.

Lorenzini, R., Biedermann, M., Grob, K., Garbini, D., Barbanera, M. & Braschi, I. 2013. Migration kinetics of mineral oil hydrocarbons from recycled paperboard to dry food : monitoring of two real cases. *Food Additives & Contaminants: Part A* 30(4): 760–770.

Lorenzini, R., Fiselier, K., Biedermann, M., Barbanera, M., Braschi, I. & Grob, K. 2010. Saturated and aromatic mineral oil hydrocarbons from paperboard food packaging: estimation of long-term migration from contents in the paperboard and data on boxes from the market. *Food Additives and Contaminants* 27(12): 1765–1774.

Martin, D. 2008. Evaluation of the dielectric capability of ester based oils for power transformers based oils for power transformers. The University of Manchester,.

Matheson, A. 2023. A Modern Mineral Oil Hydrocarbon Analysis. https://doi.org/10.56530/lcgc.eu.do5379f3.

Moret, S., Scolaro, M., Barp, L., Purcaro, G. & Conte, L.S. 2016. Microwave assisted saponification (MAS) followed by on-line liquid chromatography (LC)-gas chromatography (GC) for high-throughput and high-sensitivity determination of mineral oil in different cereal-based foodstuffs. *Food Chemistry* 196: 50–57.

Müller, A., Jovalekic, M. & Tenbohlen, S. 2012. Solubility study of different gases in mineral and ester-based transformer oils. *2012 IEEE International Conference on Condition Monitoring and Diagnosis*, page 937–940. Bali.

Nestola, M. 2022. Automated workflow utilizing saponification and improved epoxidation for the sensitive determination of mineral oil saturated and aromatic hydrocarbons in edible oils

DOI:https//doi.org/10.22452/mjs.vol44no4.10
Malaysian Journal of Science 44(4): 102-119 (December 2025)

and fats. *Journal of Chromatography A* 1682: 463523.

Oellig, C. & Schwack, W. 2011. Planar solid phase extraction — A new clean-up concept in multi-residue analysis of pesticides by liquid chromatography – mass spectrometry. *Journal of Chromatography A* 1218: 6540–6547.

Oellig, C. & Schwack, W. 2014. Planar solid phase extraction clean-up and microliter-flow injection analysis – time-of-flight mass spectrometry for multi-residue screening of pesticides in food. *Journal of Chromatography A* 1351: 1–11.

Oppermann, U. & Leitner, E. 2017. Non-intentionally added substances in food and food contact materials - determination of mineral oil hydrocarbons by LC-GC Technique.

Otunga, G.N., Maiyoh, G.K., Macharia, B.N. & Tuei, V.C. 2019. Transformer mineral oil ingestion induces systemic sub-acute toxicity in Wistar rats. *Heliyon* 5: e02998.

Parkinson, L. 2022. EC sets limit on MOAH in foods. https://www.foodpackagingforum.org/news/ec-sets-limit-on-moah-in-foods [15 August 2023].

Patel, A., Guo, H. & Iglesias, P. 2018. Study of the lubricating ability of protic ionic liquid on an aluminium-steel contact. *Lubricants* 6(66): 1–13.

Pirow, R., Blume, A., Hellwig, N., Herzler, M., Huhse, B., Hutzler, C., Pfaff, K., Thierse, H.J., Tralau, T., Vieth, B. & Luch, A. 2019. Mineral oil in food, cosmetic products, and in products regulated by other legislations. Taylor and Francis Ltd.:

Polyakova, A., van Leeuwen, S. & Peters, R. 2022. Review on chromatographic and specific detection methodologies for unravelling the complexity of MOAH in foods. *Analytica Chimica Acta* 1234: 340098.

Purcaro, G. (n.d.). Excutive Summary : Main Sources of Moh Contamination and Entry Points Into the Cocoa Supply Chain. Gembloux.

Purcaro, G., Tranchida, P.Q., Barp, L., Moret, S., Conte, L.S. & Mondello, L. 2013. Detailed elucidation of hydrocarbon contamination in food products by using solid-phase extraction and comprehensive gas chromatography with dual detection. *Analytica Chimica Acta* 773: 97–104.

Rausch, M.K., Erikson, H., Tollefsen, G.E. & Kelly, T.W. 1981. White mineral oil made by two stage hydrogenation. United States.

Rawlings, A. V & Lombard, K.J. 2012. A review on the extensive skin benefits of mineral oil. *International Journal of Cosmetic Science* 34: 511–518.

Rossum, V., Gijsbertus & Johannes. 2022. Removal of unwanted mineral oil hydrocarbons.

Rouabeh, J., M'barki, L., Hammami, A., Jallouli, I. & Driss, A. 2019. Studies of different types of insulating oils and their mixtures as an alternative to mineral oil for cooling power transformers. *Heliyon* 5: e01159.

Ruiz, J.L.H., Liébanas, J.A., Vidal, J.L.M., Frenich, A.G. & González, R.R. 2021. Offline solid-phase extraction and separation of mineral oil saturated hydrocarbons and mineral oil aromatic hydrocarbons in edible oils, and analysis via gc with a flame ionization detector. *Foods* 10: 2026.

Sabrina, M. & Giorgia, P. 2022. Mineral Oil in food: State of the art. https://foodsafety4.eu/knowledge/articles/mineral-oil-in-food-state-of-the-art/.

Sdrigotti, N., Collard, M. & Purcaro, G. 2021. Evolution of hyphenated techniques for mineral oil analysis in food. *Journal of Separation Science* 44(1): 464–482.

Spohner, M. 2017. Study of dielectric properties of mineral oils and natural oils and methyl esters of natural oils. *19th IEEE International Conference on Dielectric Liquids, ICDL 2017*, page 1–4. Manchester, United Kingdom.

Srbinovska, A., Conchione, C., Lucci, P. & Moret, S. 2020. On-Line HP(LC)-GC-FID determination of hydrocarbon contaminants in fresh and packaged fish and fish products. *Journal of AOAC International* 0(0): 1–7.

Suwarno & Darma, I.S. 2008. Dielectric properties of mixtures between mineral oil and natural ester from palm oil. *WSEAS Transactions and Power Systems* 3(2): 37–46.

Toudja, T., Moulai, H., Nacer, A., Beldjilali, A., Khelfane, I. & Debche, A. 2014. Moisture and electrical discharges effect on naphthenic mineral oil properties. *IET Science, Measurement and Technology* 8(6): 588–594.

Tuei, V.C. 2023. Availability of vegetable edible oils and potential health implications in Kenya. *Open Access Library Journal* 10: e9756.

United States Pharmacopeial Convention. 2014. Safety data sheet : Mineral Oil. United States.

Wagner, M. & Oellig, C. 2019. Screening for mineral oil saturated and aromatic hydrocarbons in paper and cardboard directly by planar solid phase extraction and by its coupling to gas chromatography. *Journal of Chromatography A* 1588: 48–57.

Walaszek, Z., Hanausek, M. & Slaga, T.J. 2007. The role of skin painting in predicting lung cancer. *International Journal of Toxicology* 26: 345–351.

DOI:https//doi.org/10.22452/mjs.vol44no4.10
Malaysian Journal of Science 44(4): 102-119 (December 2025)

Weber, S., Schmidt, T., Schumacher, P., Kuballa, T., Mildau, G., Walch, S.G., Hartwig, A. & Lachenmeier, D.W. 2019. Quantification of mineral oil aromatic hydrocarbons (MOAH) in anhydrous cosmetics using 1H NMR. *Journal of Chemistry*: 10.

Weber, S., Schrag, K., Mildau, G., Kuballa, T., Walch, S.G. & Lachenmeier, D.W. 2018. Analytical methods for the determination of mineral oil saturated hydrocarbons (MOSH) and mineral oil aromatic hydrocarbons (MOAH)—A short review. *Analytical Chemistry Insights* 13: 1–16.

Wright, J. (n.d.). The fundamentals of mineral base oil refining. https://www.machinerylubrication.com/Read/28960/mineral-oil-refining [14 July 2023].

Wrona, M., Pezo, D. & Nerin, C. 2013. Rapid analytical procedure for determination of mineral oils in edible oil by GC-FID. *Food Chemistry* 141: 3993–3999.

Yuliastuti, E. 2010. Analysis of dielectric properties comparison between mineral oil and synthetic ester oil. Delft University of Technology,.

Zoccali, M., Barp, L., Beccaria, M., Sciarrone, D., Purcaro, G. & Mondello, L. 2016. Improvement of mineral oil saturated and aromatic hydrocarbons determination in edible oil by liquid-liquid-gas chromatography with dual detection. *Journal of Separation Science* 39: 623–631.

DOI:https//doi.org/10.22452/mjs.vol44no4.10
Malaysian Journal of Science 44(4): 102-119 (December 2025)